GEOLOGICAL & GEOCHRONOLOGICAL FRAMEWORK AND MINERALIZATION CHARACTERIZATION OF THE THORN PROPERTY, AND ASSOCIATED VOLCANOPLUTONIC COMPLEXES OF NORTHWESTERN BRITISH COLUMBIA, CANADA

by

ADAM THOMAS SIMMONS

Bachelor of Science (Honours), Queen's University, 2003

A THESIS SUBMITTED IN PARTIAL FULFILLMENT OF
THE REQUIREMENTS FOR THE DEGREE OF

MASTER OF SCIENCE

In

THE FACULTY OF GRADUATE STUDIES

(Geological Sciences)

THE UNIVERSITY OF BRITISH COLUMBIA
December 2005

Abstract

A geological investigation of Late Cretaceous volcanoplutonic rocks and associated hydrothermal systems was undertaken at the Thorn Property, northwestern British Columbia, Canada, to provide a geological framework for future research and exploration, and to characterize a newly recognized belt of Late Cretaceous volcanoplutonic rocks. Emphasis is placed on the Thorn Property in the belt because it contains the thickest sequence of Late Cretaceous volcanic strata in addition to containing a wide variety of hydrothermal alteration and mineralization.

Late Cretaceous volcanoplutonic rocks were emplaced into and onto rocks of the Stikine tectonostratigraphic terrane, as part of a continental arc. The Late Cretaceous volcanoplutonic rocks at the Thorn Property form part of the NNW-trending Late Cretaceous volcanoplutonic belt, which extends for at least 300 km from the Yukon Territory into northern British Columbia. Two distinct periods of magmatism have been recognized at the Thorn Property as part of the Late Cretaceous suites. The 87-93 Ma Thorn Suite comprises the oldest components of the belt and are the major host rocks for hydrothermal mineralizing systems. The younger 80-87 Ma Windy Table Suite was emplaced into, and unconformably deposited onto, rock of the Thorn Suite. Four sub-types of Windy Table intrusions are recognized and 1600 m of Windy Table volcanic strata was emplaced over a period of 6 million years in three phases from 80-86 Ma. The oldest phase in composed of welded, dacitic-andesitic lapilli tuffs, which is overlain by rhyolitic flow dome complexes and sporadically deposited variably welded dacitic to rhyolitic lapilli tuffs. Geochronology, field relationships and lead isotopic compositions of sulphides form mineralized systems and feldspar from intrusive rocks suites suggest that fluids for the mineralized systems were sourced from intrusive rocks of the Windy Table Suite.

Several styles of mineralization are present at the Thorn Property, including high-sulphidation mineral assemblage veins, polymetallic breccia-hosted replacement, porphyry Cu-Mo, skarn and base metal veins. Emphasis was placed on the high sulphidation mineral assemblage veins because they have the highest grade and tonnage potentials of all the systems and provide insights to the potential for high-sulphidation epithermal mineralization in the belt. These veins were deposited in a series of six NE-trending zones of brittle deformation in Thorn Suite rocks. Mineralogy and metal ratios indicate that the fluids for the mineralized vein systems were sourced to the SW, where the fluids may been focused along a previously developed NW-trending fault. Several lines of evidence suggest that the veins were deposited in the sub-epithermal environment at depths greater than 1600 m. Observed advanced argillic

alteration (pyrophyllite+dickite+diaspore) at the Thorn Property is characteristic of hot (>250°C) and potentially deep hydrothermal fluids. The distribution of metal ratios, alteration minerals and ore minerals suggests that as the fluids moved along zones of NE-trending brittle deformation from east to west and evolved from high-sulphidation, acidic fluids to more intermediate-sulphidation, neutral fluids with time, distance from source and/or greater fluid-wall rock interaction.

Field observations indicate that there is a spatial correlation between the presence of both Thorn Suite rocks and Windy Table Suite rocks and the presence of high-sulphidation systems. Two key components of this environment are the presence of non-reactive host rocks, such as the Thorn Suite and the presence of plutonic bodies which have potential to develop a large hydrothermal system (Windy Table Suite rocks). Future studies should focus more on the interaction of the high-sulphidation fluids with the overlying Windy Table volcanic strata to better evaluate the potential of widespread high-sulphidation epithermal systems in the Late Cretaceous volcanoplutonic belt of northwestern British Columbia.

Table of Contents

Chapter 1
General Introduction

Chapter 2
Geological and Geochronological Characterization of Cretaceous Magmatism in the Stikine Terrane with Emphasis on the Thorn Property and Surrounding Area, Northwest British Columbia, Canada

Chapter 3

Cretaceous Hydrothermal Mineralization of the Stikine Terrane with Emphasis on the Thorn Property and Surrounding Area, Northwest British Columbia, Canada

Chapter 4
Conclusions and Recommendations for Future Research

Appendices

List of Tables

Chapter 2

Chapter 3

Appendix I

Appendix II

Appendix III

List of Figures

Chapter 1

Chapter 2

Chapter 3

Appendix I

Plate 1

Acknowledgements

There are many people who deserve recognition for all the help that was given to me during this study and I am likely to forget a few herein and I apologize in advance if I've missed somebody.

Most importantly, during the second year of this study I was struck by a major illness and four people deserve extra recognition for stepping beyond their duties as friends to help me out in a time of need. My housemate Rob Carpenter helped me through the tough times at home and was always more than willing pick up things for me or even make meals. Additionally, he always made sure that I was going to the hospital and on time for all appointments even when I had trouble just making it into a cab. Claire Chamberlain housed me and comforted me for a period of time when I was downtown and unable to make it home for a few days. Claire's generosity during this time is greatly appreciated and I am forever indebted to her. Caroline Morisset always made sure that somebody was with me, acting as a co-ordinator for people to accompany to and from my various appointments. In addition to co-ordinating this effort, she also accompanied me to a couple of the appointments. Perhaps most important to me remaining positive during this time was the help that I received from Dianne Mitchinson. Dianne was with me during the critical times and always made sure that I made it to and from home safely. Dianne also accompanied me during what I consider my most critical/humiliating moment, perhaps of my life. These four people kept my spirits up, made sure that I was doing the right things, sent me home when I was trying to get work done at UBC, listened and made me feel comfortable during this time of need and I will remember this forever. True friends always come through when you need it most and these four stepped up to the plate. Thank you very much guys!

I would like to thank my supervisor, Dick Tosdal, whose input to this thesis was invaluable. During some down times, he always remained positive and encouraging about my project and spurred me on. Dick gave me a number of incredible opportunities, which include geological field trips and an introduction to mining and exploration companies in Vancouver and world-wide. These opportunities have enhanced my understanding of geological processes and created a network of contacts in the mining/geological world. Without Dick none of this would have happened. I'd also like to thank my committee members, Jim Mortensen and James Scoates, both of whom helped me with different

aspects of my research, but provided me with a basis for understanding of the various aspect, which allowed me to come to a number of conclusions in my thesis. Thomas Bissig and Shane Ebert, from UBC, both took a week out of there lives to come to the Thorn Property with me. The various discussions in the field were invaluable to my understanding of volcanological processes and hydrothermal systems. Additionally, there are a number of people who made significant contributions to my thesis and always kept me in check with my field observations and interpretations, in addition to reviewing my thesis, and the work herein. These people include Darcy Baker, Scott Parker and Henry Awmack from Equity Engineering Ltd., Mark Baknes, Rob Duncan and David Caulfield from Rimfire Mineral Corporation and Robert Brown from Cangold Ltd. Special thanks go out to David Caulfield and Henry Awmack for creating a number of opportunities for me and allowing me to flourish in the environment that they created at Rimfire/Equity. Additionally, Rimfire helped support this project financially, while Equity and Cangold allowed me to be part of their exploration teams, which allowed me to conduct my fieldwork for this thesis. Many conversations with Mitch Mihalynuk from the BCGS helped me in my understanding of regional tectonics, which allowed me to keep my project in the proper context.

My fellow peers at UBC helped out a great deal and were always there to help out with specific questions and listen when I needed to vent. These people include Alan Wainright, Claire Chamberlain, Dianne Mitchinson, Kiyoko Nakano, Sarah Gordee, Lyle Hanson, Rob Mackie and Julio Jurado. A special note should be made about my hard working officemate Julio, who often accompanied me on many consecutive nights of research, it's very difficult to pull these long nights off without somebody to talk to.

I would also like to thank the many sponsors of this project, which include MDRU, NSERC, SEG, Rimfire Minerals Corporation, BC & Yukon Chamber of Mines (Rock to Riches Program), Equity Engineering Limited and Cangold Limited. This project would have never been completed without the financial and logistical support of these sponsors.

Additionally, my family has always been patient with me. They don't quite understand why I remained in school to complete my M.Sc., but have always been the most supportive people during this time. My Mom, Dad, brothers Mark and Jason and cousin Don all helped me out in some way during this time. Thanks for the patience guys. Additionally, Amy Kerckhoff deserves special recognition for her kind and supportive

comments during this thesis. When things were going bad, she always had a way of making me happy again. I owe you big time!

Again, I apologize for those that I left out. Thank you all so much!

Chapter 1

General Introduction

Partially eroded remnants of a newly defined Late Cretaceous volcanoplutonic belt that has associated porphyry and epithermal alteration and mineralization extends over 300 km from the Golden Bear Mine, in British Columbia, northwest into the Yukon Territory (Figure 1-1). Two distinct magmatic suites characterize the arc: a) *ca.* 90 Ma Thorn Suite, and b) *ca.* 83 Ma Windy Table Suite (Simmons *et al.*, 2005a). These rocks were emplaced onto and into Upper Triassic Stuhini Group and Lower to Middle Jurassic Laberge Group rocks of the Stikine tectonostratigraphic terrane. High-sulphidation mineral assemblage veins and other hydrothermal deposits within the Late Cretaceous volcanoplutonic arc are associated with the Thorn and Windy Table Suites (Mihalynuk *et al.*, 2003; Baker, 2005; Simmons, 2004). The Thorn Property contains the widest range of hydrothermal systems and prior to this study was the best known example of a high-sulphidation epithermal style mineralization, similar to El Indio, and hosted within the Thorn Stock (Awmack, 2003). Deposit styles of the high-sulphidation epithermal class are highly variable and include base metal-rich and precious metal-rich varieties, which include structurally-controlled veins (Jannas *et al.*, 1990), disseminated-stockwork ores (Bissig *et al.*, 2002), auriferous breccias, vuggy quartz and massive sulphide bodies (Hedenquist *et al.*, 1998). At the Thorn Property, fault-controlled, steeply-dipping veins with high-sulphidation mineral assemblages represent the main focus of exploration on the property since 2000 (Awmack, 2000). Despite this recent exploration activity, there have been no detailed studies of the epithermal potential of the Thorn Property or the surrounding Late Cretaceous volcanoplutonic arc.

The Thorn Property contains six parallel northeast-trending, steeply-dipping, brittle fault zones, which contain high-sulphidation mineral assemblage veins that were emplaced after or during deformation of these zones (Lewis, 2002). These veins are hosted almost entirely within the Thorn Stock and to a lesser extent in the lower portions of the Windy Table volcanic rocks and pre-Cretaceous rocks (Awmack, 2000; Baker, in prep.). Approximately 1600 m of subhorizontal Windy Table volcanic strata overlie the known topographic high of the high-sulphidation assemblage veins. Prior to this study no stratigraphic or geochronologic studies had been carried out to determine if this style of mineralization is epithermal (occurring in the upper 1.5 km of the Earth's crust; Hedenquist *et al.*, 2000) or what the causative magmatic rock for producing the hydrothermal system was.

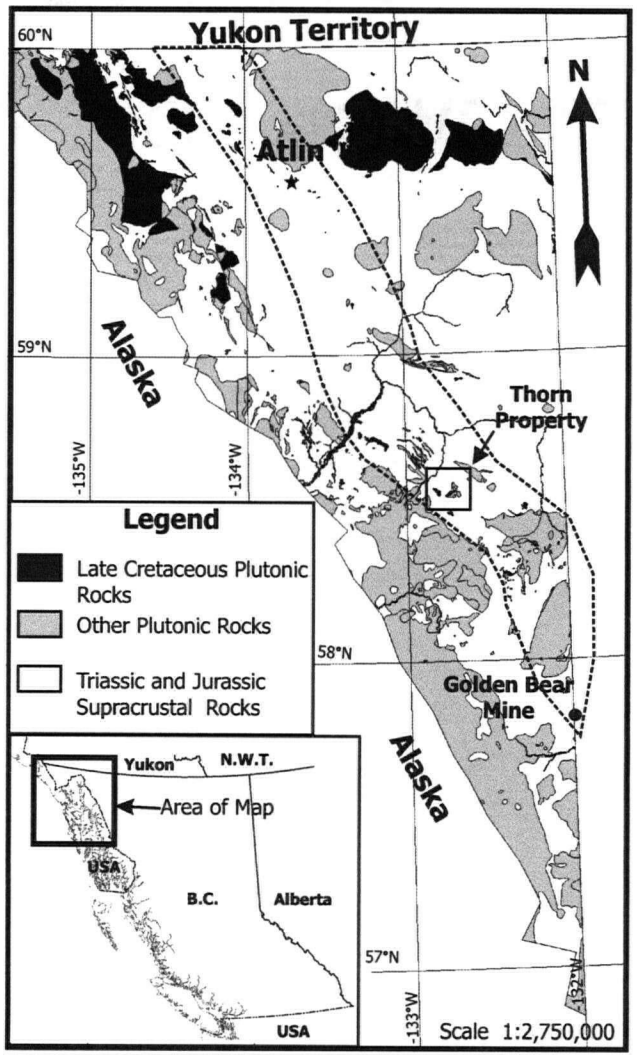

Figure 1-1: Location of project area highlighting the Late Cretaceous plutonic rocks of northwest British Columbia and the known extent of the NW B.C. Late Cretaceous volcanoplutonic belt. Area enclosed by dashed line represent the approximate spatial limits of the Late Cretaceous volcanoplutonic belt.

Objectives

This thesis defines the regional geological and geochronological framework of the Late Cretaceous arc in and along strike from the Thorn Property. Characterization of Late Cretaceous magmatic rocks and their associated hydrothermal systems in northwestern British Columbia is the second primary goal of this study. The project was designed to advance the understanding of the timing and styles of hydrothermal mineralization associated with Late Cretaceous magmatism and to develop a framework for future exploration of similar deposits in northwestern British Columbia. The project was supported by the Mineral Deposit Research Unit at the University of British Columbia, Rimfire Minerals Corporation, Cangold Limited and the Natural Sciences and Engineering Research Council of Canada (NSERC Discovery Grant to Richard Tosdal). Equity Engineering Limited provided logistical and financial support for three field seasons from 2003 to 2005. An NSERC Industrial Postgraduate Scholarship (IPS-A), Rocks to Riches Grant from the British Columbia and Yukon Chamber of Mines and a Society of Economic Geologists Student Research Grant provided additional funding.

The four main objectives of this thesis were to: 1) to establish a regional geologic framework of the Thorn Property, 2) to characterize the stratigraphy, timing, chemistry, evolution, origin and spatial extent of the NW B.C. Late Cretaceous volcanoplutonic belt, 3) to better understand the nature, timing and origin of hydrothermal alteration and mineralization within the Late Cretaceous volcanoplutonic belt and, 4) to assess the relationship between numerous styles of hydrothermal alteration and Late Cretaceous magmatic rocks. A major outcome of the study is a genetic and chronologic model for the high-sulphidation mineral assemblage veins at the Thorn Property.

Exploration History

Kennco Explorations (Western) Limited carried out the earliest known reported exploration on the Thorn property in 1959 during a regional exploration program. Kennco took a Cu-anomalous silt sample from the mouth of Camp Creek and followed it 1000 m upstream, where they took a "37-m chip sample across a silicified zone containing massive pyrite at a fault-controlled contact between chert breccia and volcanic fragmentals [which] assayed 0.34% Cu, 3.5 oz silver/ton and 0.04 oz gold/ton" (Barr, 1989).

The Julian Mining Company, the Canadian arm of Anaconda, staked the Thorn property in 1963. They carried out three field seasons of mapping and prospecting, discovering 17 mineral showings of three main types: quartz-pyrite-tetrahedrite-enargite veins; structurally-

controlled chalcopyrite-pyrite-quartz ± arsenopyrite veins and replacement zones and areas of widespread, low-grade disseminated chalcopyrite. Limited diamond drilling was carried out in 1963 (4 holes; 71 m) and 1965 (4 holes; 179 m) to evaluate quartz-barite-chalcopyrite-pyrite veins and a vuggy silica, disseminated enargite zone. Porphyry Cu-Mo style mineralization was discovered in 1964 and drilled in 1965 (8 holes; 889 m; Adamson, 1963, 1964, 1965a, 1965b).

In 1969, American Uranium Limited explored on two small claim groups: the Ink, which covered the Thorn enargite-pyrite-tetrahedrite veins near the mouth of Camp Creek and the Lin over the Cirque Zone. Mapping of the Ink claims identified altered quartz-feldspar porphyry of the Thorn Stock to extend at least 2500 m down La Jaune Creek from the mouth of Camp Creek, accompanied by Cu-bearing silt samples. On the Cirque Zone, American Uranium outlined a coincident Cu-Mo soil geochemical anomaly over an area 500 m in diameter (Sanguinetti, 1969).

The Thorn showings were re-staked as the Daisy claims in 1981 by J. R. Woodcock, who carried out limited silt sampling and collected rock samples for geochemical and petrographic analysis (Woodcock, 1982). In 1983, Inland Recovery Group Ltd. acquired the Daisy claims and carried out mapping, soil sampling and VLF-EM surveying near the junction of Camp and La Jaune creeks. Strong Ag-Au-Cu ± Zn soil geochemical anomalies were discovered along Camp Creek (Wallis, 1983; Woodcock, 1986).

In 1986, Inland Recovery and American Reserve Mining Corp. drilled eight holes from three drill sites within the soil geochemical anomaly extending west from the B Zone. Core was altered and variably mineralized throughout, but only the highest-grade sections were split and analyzed. The best intersection was reported as 2.77 m grading 3.78% Cu, 2.0 g/t Au and 153 g/t Ag, taken from hole 86-6 (Woodcock, 1987).

In 1989, the Daisy claims were optioned to Gulf International Minerals who carried out poorly documented chip sampling of some pyrite-enargite-tetrahedrite showings. No assays are available from this work and the claims were allowed to lapse. International Corona Corporation staked the Stress 1-3 claims adjacent and SW of the Daisy Claims and conducted three days of reconnaissance mapping and collected 41 rock samples in 1992 (Rye, 1992).

The Thorn showings were re-staked in 1993 as the Check-mate claim by Clive Aspinall. The following year, he split an additional 31 core samples from the 1986 drilling, commissioned petrographic analysis of six core specimens and a float boulder and re-interpreted the 1986 drill sections (Aspinall, 1994). Kohima Pacific Gold Corporation staked the Stuart 1-3 claims in 1997 and optioned the Check-mate claim in 1998. Kohima discovered the MP Vein near the mouth of

Camp Creek; this massive pyrite-enargite vein assayed 6.88% Cu and 179.0 g/t Ag across 0.5 m. An additional 11 core samples were taken from the 1986 drilling and 84 PIMA readings were taken from holes 86-1, 86-3 and 86-6, showing the predominance of illite, pyrophyllite and dickite in altered core (Poliquin and Poliquin, 1998).

Chevron Canada Limited staked the Outlaw 1-4 claims immediately southeast of Woodcock's Daisy claims in 1981. In 1982, Chevron ran soil lines up ridges and over a rough grid at 200 x 100 m spacing, indicating the presence of a strong Au-Ag-As-Sb-Cu-Pb soil geochemical anomaly over an area of 400 x 1,600 m (Brown and Shannon, 1982). The following year, a 50 x 50 m soil grid was sampled over the heart of the anomaly. Five trenches were blasted across an easterly-trending quartz-arsenopyrite-tourmaline vein, encountering only low gold and silver values (Walton, 1984). In 1987, four holes were drilled along one section from two sites within this clay-altered zone (Walton, 1987).

Glider Developments Inc. acquired the property in 1991 and laid out 12.4 line-km of soil grid over the heart of Chevron's soil geochemical anomaly. Vuggy quartz-pyrite-galena vein float from a clay-altered zone drilled by Chevron assayed up to 22.9 g/t Au (Cann and Lehtinen, 1991). Glider may also have drilled four holes on the Outlaw, but this work was never recorded and has not been confirmed.

Rimfire Minerals Corporation optioned the Check-mate and Stuart claims in February 2000, carried out an airborne magnetic/EM geophysical survey in July and staked the Thorn 1-7 claims in August to extend the property over the Outlaw soil geochemical anomaly, the Cirque Cu porphyry prospect and geophysical targets. Later fieldwork in 2000 focused on the high-sulphidation mineral assemblage veins within the Thorn Stock, resulting in the location and sampling of several previously reported zones and the discovery of several new showings. Soil samples were collected over an area measuring 1,500 x 1,600 m, on 25 x 100 m centres from lines trending 230° across the Thorn Stock. Several strong multi-element soil geochemical anomalies were defined, and only some of them could be explained by known mineralization. All remaining unsampled core from the 1986 diamond drilling was split and analyzed (Awmack, 2000).

In March 2002, First Au Strategies Corp. (now Cangold Limited) optioned the Thorn property from Rimfire and carried out three years of exploration (Awmack, 2003; Baker, 2003, 2005, in prep.). Exploration focused on locating the mineralized zones on the Julian claim, following up the soil geochemical anomalies defined in 2000. They also drilled several high-sulphidation mineral assemblage vein systems. Prospecting within a soil geochemical anomaly

resulted in discovery of the Oban breccia pipe, which contains matrix-hosted sphalerite and boulangerite. Subsequent work since then has evaluated: a) the Oban breccia and high-sulphidation mineral assemblage veins, and b) the potential for epithermal mineralization hosted in Windy Table volcanic strata.

In addition to the Thorn Property-specific exploration, largely reconnaissance regional exploration has occurred. Most exploration focussed on targeting porphyry deposits (e.g. White, 1970; Reid, 1987; Aspinall, 1991a, 1991b; Chapman, 1991). Only limited work has been carried out to evaluate other potential styles of hydrothermal alteration and mineralization (e.g. Lintott, 1981; Smith, 1989; Simmons, 2004).

Previous Work

The general geological framework and setting of high-sulphidation mineral assemblage veins at the Thorn Property and along the belt have included work from the British Columbia Geological Survey, a structural architecture study and a detailed petrographic study of high-sulphidation mineral assemblage veins and other style of mineralization. Relevant references include Mihalynuk *et al.* (2003), Lewis (2002), Lang and Thompson (2003), Baker and Simmons (2004) and Simmons *et al.* (2005b).

Two samples were collected for geochronology prior to the author beginning the project. One for U-Pb geochronology of Windy Table Suite strata and another for $^{40}Ar/^{39}Ar$ geochronology on sericite related to high-sulphidation mineral assemblage veins. Mitch Mihalynuk and Andrey Panteleyev collected these samples, respectively.

Methodology

A combination of detailed and regional geological mapping, petrography, geochronology, geochemistry and lead isotope geochemistry were integrated to understand Late Cretaceous continental arc evolution and distribution to constrain the nature and origin of several styles of hydrothermal alteration and mineralization present at the Thorn Property.

Fieldwork during 2003, 2004 and 2005 focussed on regional geological mapping to better constrain the geological framework of the Thorn Property and to better understand the distribution and importance of Late Cretaceous continental arc magmatism in the Stikine terrane of NW British Columbia. Detailed geological mapping of the Thorn Property was also undertaken to provide a revised geological map for the property and to better understand the relative age relationships of the various rock units and hydrothermal alteration. Samples were

collected specifically for geochronologic, petrographic, geochemical, fluid inclusion and lead isotope studies.

Observations of Late Cretaceous plutonic and volcanic rocks are based upon geological mapping. Observations of related hydrothermal systems are based on geological mapping as well as examination and logging of rock types, alteration, ore mineralogy and structure in drill core. Samples of drill core and mineralized hand samples were cut and prepared as polished thin sections and doubly-polished thin sections for petrography and fluid inclusion microthermometry, respectively. Mineralized samples that contained minerals that could not be readily identified by petrographic analyses were semi-quantitatively analyzed using the scanning electron microscope (SEM) to identify unknown mineralogy. A fluid inclusion study was attempted on high-sulphidation mineral assemblage veins, but was unsuccessful due to the extremely small sizes of fluid inclusions contained within quartz crystals.

A regional scale geochronologic study was conducted on intrusive and extrusive rocks, as well as hydrothermal alteration to develop a chronologic framework for events on the Thorn Property. Five samples were analysed by the U-Pb ID-TIMS method. These samples were analyzed by Richard Friedman at the Pacific Centre for Isotopic and Geochemical Research (PCIGR) at the University of British Columbia, Vancouver. Seventeen samples were analysed by using the U.S. Geological Survey's Sensitive High (Mass) Resolution Ion MicroProbe-Reverse Geometry (SHRIMP-RG) by Adam Simmons, Richard Tosdal, Alan Wainright and Claire Chamberlain at the Stanford University, Palo Alto, California. Joe Wooden and Frank Mazdab from the US Geological Survey directed activities while at Stanford University and helped with the interpretation of data. Six samples were analyzed for $^{40}Ar/^{39}Ar$ geochronology on altered samples by Tom Ullrich at the PCIGR, University of British Columbia, Vancouver.

Lead isotope compositions of sulphide minerals and feldspars from intrusive and volcanic rocks were analyzed to identify metal source and assess the degree of fluid wall-rock interaction during hydrothermal activity. Janet Gabites analyzed all Pb isotope samples at the PCIGR, University of British Columbia, Vancouver.

Samples taken for petrochemical analyses were analyzed for major, trace and rare earth elements at ALS Chemex Laboratories Limited in North Vancouver, Canada. Major elements and selected trace elements were determined by X-ray fluorescence spectrometry (XRF). Rare earth elements (REE) and remaining trace elements were determined by inductively coupled plasma mass spectrometry (ICP-MS).

Presentation

This thesis is presented in manuscript format, in accordance with the University of British Columbia guidelines. Results are presented as two individual research papers in Chapter 2 and Chapter 3. Both papers will be submitted for publication in the Canadian Journal of Earth Sciences. A previously published manuscript by the author is given in Appendix IV, which was published during the course of this thesis. Other supplementary information is provided in Appendices I-III. As these chapters are stand-alone papers, some repetition is unavoidable in order to provide clarity and context for each chapter.

Chapter 2

Geological and Geochronological Characterization of Late Cretaceous Continental Arc Magmatism in the Stikine Terrane: Thorn Property and Surrounding Area, Northwest British Columbia, Canada

Adam Simmons, Richard Tosdal, Darcy Baker and Richard Friedman

This chapter focuses on Late Cretaceous continental arc magmatic rocks and describes their regional distribution, age, and petrochemical characteristics. Late Cretaceous magmatic rocks are subdivided into three distinct suites based upon field mapping, geochemistry, petrography, and geochronology. Twenty-three new U-Pb ages are reported, mainly on Windy Table and Thorn Suite rocks, with lesser emphasis on pre- and post-Cretaceous magmatic rocks. This chapter also provides a tectonic history overview for northern Stikinia, based upon a literature review.

Chapter 3

Late Cretaceous Hydrothermal Mineralization of the Stikine Terrane: Thorn Property, Northwest British Columbia, Canada

Adam Simmons, Darcy Baker, Richard Tosdal, Tom Ullrich and Henry Awmack

This chapter provides a detailed overview of all styles of hydrothermal alteration and mineralization present at the Thorn Property. Particular emphasis is placed on structurally controlled high-sulphidation mineral assemblage veins and a polymetallic hydrothermal breccia hosted prospect, the Oban breccia. Descriptions of the alteration, ore mineralogy and vein textures are presented. The above combined with $^{40}Ar/^{39}Ar$ geochronology (six new ages

reported), lead isotopes and metal budgets and spatial zonation in the mineralized zones were used to confirm the source for hydrothermal fluids and to present a model of the Thorn Property.

Chapter 4

General Conclusions

This chapter outlines the overall conclusions of the research presented in chapters two and three. Exploration and future research are also discussed.

Appendices

Appendix I provides sample locations and sample descriptions of rocks used for U-Pb and $^{40}Ar/^{39}Ar$ geochronology. A report prepared by Richard Friedman at the PCIGR, UBC, discusses the detailed methodology and interpretation of 5 intrusive and extrusive rocks from the Thorn Property dated by the U-Pb ID-TIMS method. Similarly, a report is given on 17 intrusive and extrusive rocks from the Thorn Property and the surrounding area discussing the detailed methodology and interpretations for samples determined using the SHRIMP-RG at Stanford University, California. Tom Ullrich also provides a detailed $^{40}Ar/^{39}Ar$ geochronology method for six samples analysed at the PCIGR, UBC.

Appendix II provides sample location and descriptions for all samples collected during the course of this study.

Appendix III discusses the methodology, detection limits and duplicate analyzes (to test for precision) used for geochemical data. Samples were analysed at ALS Chemex Laboratories Ltd., North Vancouver.

Appendix IV provides a summary paper published in 2004 Geological Fieldwork. This paper summarizes fieldwork completed, preliminary geochronologic results, geochemical and petrographic characteristics of Late Cretaceous magmatic rocks and related hydrothermal alteration and mineralization. This paper was published as: Simmons, A.T., Tosdal, R.M.,

Baker, D.E.L., Friedman, R.M. and Ullrich, T.D. (2005): Late Cretaceous Volcano-Plutonic Arcs in Northwestern British Columbia: Implications for Porphyry and Epithermal Deposits; *in* Geological Fieldwork 2004, Grant, B. and Newell, J.M., Editors, *B.C. Ministry of Energy Mines and Petroleum Resources,* Paper RR15, Pages 347-360.

References

Adamson, R.S. (1963): Thorn Property Report, Taku Project; *Private report for Julian Mining Company Ltd.*, dated November 1963.

Adamson, R.S. (1964): Thorn Project; *Private report for Julian Mining Company Ltd.*, dated December 1964.

Adamson, R.S. (1965a): Thorn Project – 1965, Lower Zones; *Private report for Julian Mining Company Ltd.*, dated December 1965.

Adamson, R.S. (1965b): Thorn Project – 1965, Cirque Zone; *Private report for Julian Mining Company Ltd.*, dated December 1965.

Aspinall, N.C. (1991a): Geological and Geochemical Report on the Wahb Property, Mount Lester Jones Area, Tulsequah Region, *British Columbia Ministry of Energy and Mines,* Assessment Report #21,522.

Aspinall, N.C. (1991b): Geological and Geochemical work on the King Claims 2-6, 10-14, Atlin Mining Division, British Columbia, *British Columbia Ministry of Energy and Mines,* Assessment Report #21,530.

Aspinall, N.C. (1994): Assessment Report of 1994 Work on the Thorn-Sutlahine Au-Ag-Cu Property; British Columbia Ministry of Energy and Mines Assessment Report #23,612.

Awmack, H.J. (2000): 2000 Geological, Geochemical and Geophysical Report on the Thorn Property; *British Columbia Ministry of Energy and Mines,* Assessment Report #26,433.

Awmack, H.J. (2003): 2002 Geological, Geochemical and Diamond Drilling Report on the Thorn Property; *British Columbia Ministry of Energy and Mines,* Assessment Report #27,120.

Baker, D.E.L. (2003): 2003 Geological, Geochemical and Diamond Drilling Report on the Thorn Property; *British Columbia Ministry of Energy and Mines,* Assessment Report #27,379.

Baker, D.E.L. (2005): 2004 Geological, Geochemical, Geophysical and Diamond Drilling Report on the Thorn Property; *British Columbia Ministry of Energy and Mines,* Assessment Report #unassigned; to be released January, 2006.

Baker, D.E.L. (in prep.): 2005 Geological, Geochemical, Geophysical and Diamond Drilling Report on the Thorn Property; *British Columbia Ministry of Energy and Mines,* Assessment Report #unassigned, to be released January, 2007.

Baker, D.E.L. and Simmons, A. (2004): Thorn Ag-Au Prospect: New Mapping, New Ages, New Discovery; Presentation Abstract for the 2004 Mineral Exploration Roundup, *British Columbia & Yukon Camber of Mines,* Vancouver, British Columbia, Canada.

Barr, D.A. (1989): Geological Report on the Thorn Property; *Private Report for Shannon Energy Ltd.*, dated May 18, 1989.

Bissig, T., Clark, A.H., Lee, J.K.W. and Hodgson, C.J. (2002): Miocene landscape evolution in the Chilean flat-slab transect: uplift history and geomorphologic controls on epithermal processes in the El Indio-Pascua Au (-Ag, Cu) belt; *Economic Geology,* Volume 97, Pages 971-996.

Brown, D. and K. Shannon (1982): Geological and Geochemical Survey of Outlaw Claims 1-4; *British Columbia Ministry of Energy and Mines* Assessment Report #10,532.

Cann, R.M. and J. Lehtinen (1991): Geological and Geochemical Report on the Outlaw Claims; *British Columbia Ministry of Energy and Mines*, Assessment Report #21,756.

Chapman, J. (1991): Assessment Report on the Tulsequah D Project; *British Columbia Ministry of Energy and Mines*, Assessment Report #21,907.

Hedenquist, J.W., Arribas, A. and Reynolds, T.J. (1998): Evolution of an intrusion-centered hydrothermal system: Far Southeast-Lepanto porphyry and epithermal Cu-Au deposits, Philippines; *Economic Geology*, Volume 93, Pages 373-404.

Hedenquist, J.W., Arribas, A., Jr., and Gonzalez-Urien, E. (2000): Exploration for epithermal gold deposits; *Reviews in Economic Geology*, Volume 13, Pages 245-277.

Jannas, R.R., Beane, R.E., Ahler, B.A. and Brosnahan, D.R. (1990): Gold and copper mineralization at the El Indio deposit, Chile; *Journal of Geochemical Exploration*, Volume 36, Pages 233-266.

Lang, J.R. and A.. Thompson (2003): Thorn Property, British Columbia, Petrography and SEM Analysis of Eight Polished Thin Sections; *Private report for Rimfire Minerals Corporation and First Au Strategies Corp.*, dated January 17, 2003. *In* D.E.L. Baker (2003): 2003 Geological, Geochemical and Diamond Drilling Report on the Thorn Property.

Lewis, P. (2002): Structural Analysis of Au-Ag-Cu Mineralization in the Camp Creek area, Thorn Property; *Private report for Rimfire Minerals Corporation and First Au Strategies Corp.*, dated July 15, 2002. *In* H.J. Awmack (2003): 2002 Geological, Geochemical and Diamond Drilling Report on the Thorn Property.

Lintott, K.G. (1981): Assessment Report on Trenching and Drilling GO-1 Claim, *British Columbia Ministry of Energy and Mines* Assessment Report #9,495.

Mihalynuk, M.G., J. Mortensen, R. Friedman, A. Panteleyev and H.J. Awmack (2003): Cangold partnership: regional geologic setting and geochronology of high-sulphidation mineralization at the Thorn property, British Columbia; *Ministry of Energy and Mines,* Geofile 2003-10.

Poliquin, M.J. and J.D. Poliquin (1998): Geology and Hydrothermal Alteration Mineralogy of the Thorn Prospect; *British Columbia Ministry of Energy and Mines*, Assessment Report #25,725.

Reid, W. (1987): Geological and Geochemical Report, 1986, on the KS-1 and KS-2 Claim Blocks, *British Columbia Ministry of Energy and Mines*, Assessment Report #15,477.

Rye. K.A. (1992): Geological and geochemical report on the Thorn-Stress property; Stress 1, Stress 2 and Stress 3 mineral claims; *British Columbia Ministry of Energy and Mines,* Assessment Report #22,141.

Sanguinetti, M.H. (1969): Report on the Ink & Lin Claim Groups; *British Columbia Ministry of Energy and Mines*, Assessment Report #2,512.

Simmons, A.T. (2004): 2004 Geological and Geochemical, Report on the LJ and Sutlahine Properties; *British Columbia Ministry of Energy and Mines,* Assessment Report # unassigned, to be released December, 2005.

Simmons, A.T., Tosdal, R.M., Baker, D.E.L., Friedman, R.M. and Ullrich, T.D. (2005a): Late Cretaceous Volcano-Plutonic Arcs in Northwestern British Columbia: Implications for Porphyry and Epithermal Deposits; *in* Geological Fieldwork 2004, Grant, B. and Newell, J.M., Editors, *B.C. Ministry of Energy Mines and Petroleum Resources,* Paper RR15, pages 347-360.

Simmons, A.T., Tosdal, R.M. and Baker, D.E.L. (2005b): Thorn Au-Ag Prospect: A Geologic Framework for Late Cretaceous Porphyry-Epithermal Mineralization in Northwest British Columbia Canada; Oral Presentation Abstract for the 2005 GSN Conference, *Geological Society of Nevada.*

Smith, S.W. (1989): Assessment Report on the Geological and Geochemical Work on the Bryar Mineral Claim, Atlin Mining Division, British Columbia, *British Columbia Ministry of Energy and Mines* Assessment Report #19,326.

Wallis, J.E. (1983): Geology, Geochemistry, Geophysics of the Thorn Property; *British Columbia Ministry of Energy and Mines*, Assessment Report #11,923.

Walton, G. (1984): Geological, Geochemical and Physical Work, Outlaw 1-4 Claims; *British Columbia Ministry of Energy and Mines*, Assessment Report #12,654.

Walton, G. (1987): Tats Project, 1987 Summary Report; *British Columbia Ministry of Energy and Mines*, Assessment Report #16,726.

White, L.G. (1970): Geophysical Report on a Magnetometer Survey, Mad and Nut Claim Group, Atlin Mining Division, B.C., *British Columbia Ministry of Energy and Mines*, Assessment Report #2,537.

Woodcock, J.R. (1982): The Thorn Property; *British Columbia Ministry of Energy and Mines*, Assessment Report #10,243.

Woodcock, J.R. (1986): The Thorn Property; *Private report for American Reserve Mining Corporation*, dated January 24, 1986.

Woodcock, J.R. (1987): Drilling Report, Thorn Property; *British Columbia Ministry of Energy and Mines*, Assessment Report #15,897.

Chapter 2

Geological and Geochronological Characterization of Cretaceous Magmatism in the Stikine Terrane: Thorn Property and Surrounding Area, Northwest British Columbia, Canada

Abstract

The rocks on the Thorn property represent a remnant volcanic centre belonging to the Late Cretaceous volcanoplutonic arc of northwestern British Columbia. The Thorn property consists of 18 map claims covering approximately 14,857 ha (149 km^2) of mountainous terrain, approximately 130 km southeast of Atlin, B.C. The WNW-trending arc extends, at minimum, for 150 km from the Golden Bear Mine to the Yukon-British Columbia border and is constructed on top of the Paleozoic and early Mesozoic tectonostratigraphic terranes of the Stikine and Cache Creek Terranes. These terranes were accreted onto the western flank of North America at these latitudes (57°-60°) by at least 168 Ma, at which point the subduction zone was re-established to the west of the Stikine Terrane. Continental arc magmatism resumed in northwest B.C. by the latest Early Cretaceous (*ca.* 91 Ma) and continued episodically through to the Eocene (*ca.* 55 Ma).

The episodic Late Cretaceous to Eocene continental arc magmatism from theCoast Plutonic Belt can be subdivided based upon field relations, age, chemistry and texture. The oldest suite, the Thorn Suite, is characterized by a series of shallow level quartz-biotite-feldspar porphyritic quartz diorite stocks and dykes, which were emplaced from 92 Ma until 87 Ma. They are texturally distinct from other intrusive rocks in the arc, in that they contain 5-10%, 5-12 mm long, euhedral, prismatic biotite and 2-5% rounded quartz phenocrysts, which do not occur in other Late Cretaceous magmatic suites. No volcanic equivalents to these rocks are known in the mapped areas. The Thorn Suite consists of normal calc-alkaline arc magmas, that are slightly less evolved than younger magmas in the arc in terms of REE concentrations and trace element geochemistry.

The Windy Table Suite was emplaced from 86 Ma until 80 Ma in the current area of the Thorn property. Intrusive rocks have a wide range of textural variability including equigranular, aphanitic, variably developed porphyritic intrusions, granophyric and megacrystic. Although

porphyritic intrusions are the most common variety of Windy Table intrusions, they always lack well-developed biotite phenocrysts, rarely contain euhedral quartz phenocrysts and are dominantly monzonitic, making them readily distinguishable from the Thorn Suite intrusive rocks. These intrusions are considered to play an important mineralizing role throughout the Late Cretaceous volcanoplutonic arc in northwest British Columbia. Their lithogeochemistry suggests that they are slightly more evolved magmas than the Thorn Suite and that hornblende fractionation was more prevalent, possibly indicating that these magmas may have a greater capacity to produce large hydrothermal systems, because of an apparently greater availability of water. Volcanic equivalents of these rocks are sparsely scattered throughout the belt and generally do not exceed 200 m in thickness. The largest of the Windy Table volcanic centres is located at the Thorn Property where the subcircular volcanic sequences of outcrops have dimensions of 10 km across and a depositional thickness of at least 1.5 km. At the Thorn, the volcanic rocks are dominantly composed of variably welded dacitic lapilli tuffs with lesser rhyolite flows, volcaniclastic sandstones and conglomerates and sparse megabreccia units most commonly preserved at the edges of the volcanic centre. While the source area for the pyroclastic rocks is not known, textures indicate that these volcanic deposits are proximal to the eruptive centre.

Introduction

British Columbia (B.C.) has a rich history of exploration and mining of porphyry Cu (Mo-Au) deposits (e.g. Highland Valley, Gibraltar, Afton, Copper Mountain, Galore Creek). In contrast, other types of deposits that may form in the magmatic-hydrothermal system (e.g. epithermal, distal disseminated Au, etc.) have not been recognized to a great extent. Their apparent lack in B.C. is usually attributed to the deposits forming at high level and having a tendency to be amongst the first features to be eroded during mountain building processes in subduction and compressive tectonic environments, particularly when the deposits are as old as the Mesozoic. However, recent exploration in northwest and in the central interior of B.C. has found that favourable environments are present for porphyry-related deposits along a belt of Late Cretaceous magmatic rocks (e.g. Rimfire/Cangold's Thorn Au-Ag prospect, Barrick/Rimfire's Kizmet project, etc.), which is coincident with a belt of anomalous stream sediment geochemistry as identified by the British Columbia Geological Survey (Figure 2-1 & 2-2; GSC, 1988). Moreover, mineralization at the Thorn Property is associated with a previously unrecognized magmatic event in the northern Cordilleran. Understanding the geologic environment under which the magmatic rocks are spatially and temporally related to

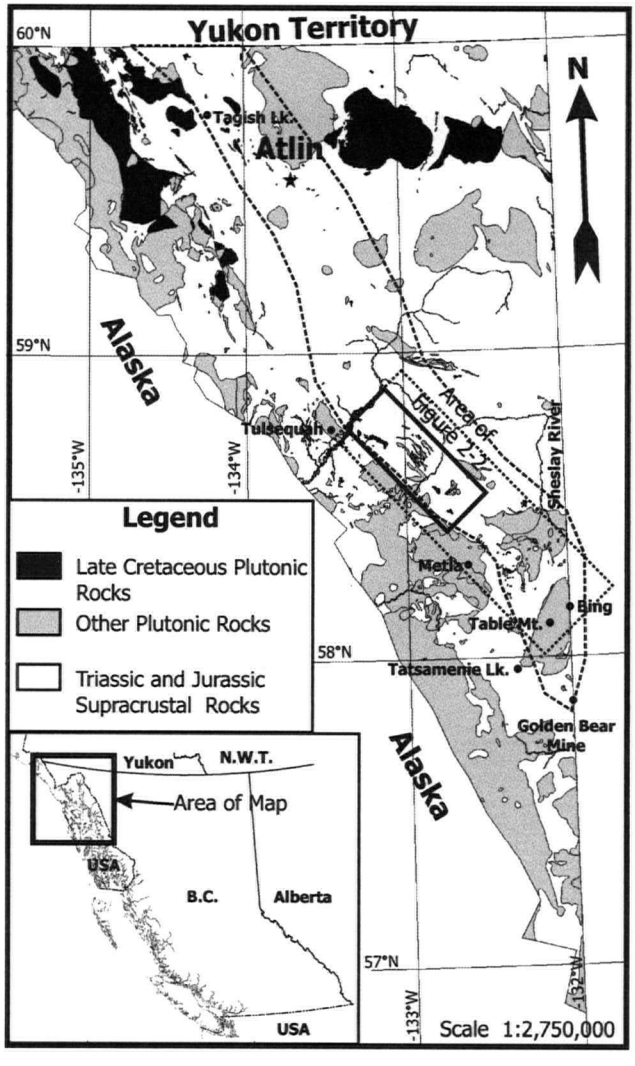

Figure 2-1: Location of study area highlighting the Late Cretaceous plutonic rocks of northwest British Columbia. Area enclosed by dashed line represents the approximate spatial extent of the Late Cretaceous volcanoplutonic belt. Area enclosed by dotted box represents the limits of the study area.

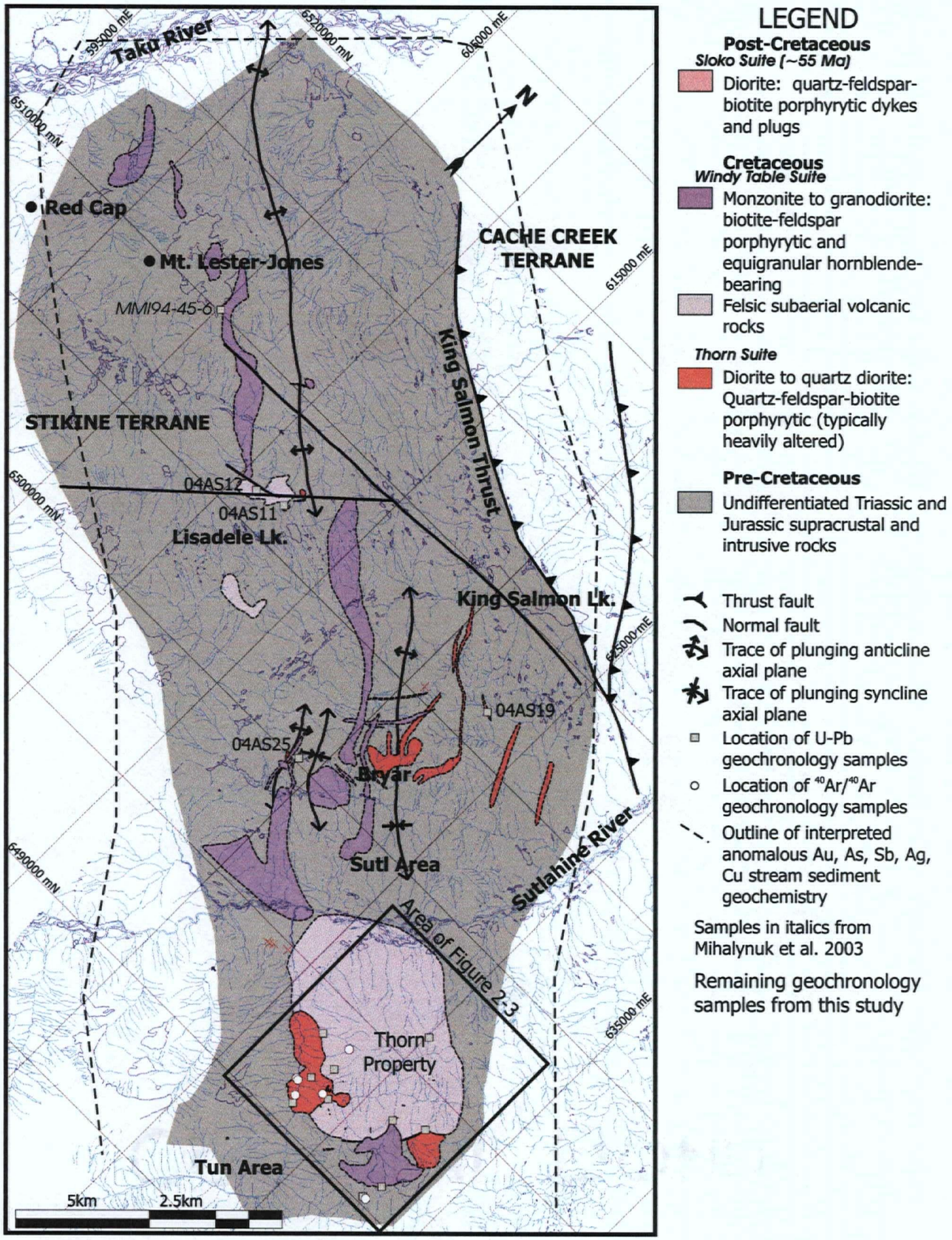

Figure 2-2: Regional map of the study area highlighting post accretionary magmatic rocks with geochronology sample locations and area of anomalous Au stream sediment geochemistry. Area of anaomalous geochemistry is also approximately is the extent of the Late Cretaceous volcanoplutonic belt.

mineralized and altered rocks as well as the subsequent erosional processes can have important implications upon how exploration for such deposits could be conducted. To further constrain the magmatic history surrounding the Thorn Property, a geochronological and geochemical study was undertaken in conjunction with bedrock mapping. Here, geochronological and geochemical results are presented for the major lithologic units in the study area as defined by Figure 2-2 and the Thorn Property (Figure 2-3). Details of mineralization and alteration will be presented in Chapter 3.

Porphyry Cu and epithermal deposits are spatially and temporally related to volcanic and plutonic rocks emplaced during the formation of long-lived magmatic arcs along convergent plate boundaries (e.g. Sillitoe, 1972; Sutherland-Brown, 1976; Titley, 1982; Sawkins, 1990; Bissig *et al.*, 2003). Recognizing the presence, types of deposits, and age of the mineralized volcanoplutonic complexes as well as their petrochemical characteristics in under-explored terranes is an important step toward identifying the metallogenic potential of a terrane as a means to aid exploration.

Regional Geological Context

Cretaceous and Tertiary magmatic rocks related to continental arc magmatism in western Canada and Alaska were emplaced into Paleozoic and Mesozoic volcanic arc rocks and related sedimentary rocks that were accreted onto the western margin of North America by at least the early Middle Jurassic in the northern Cordillera (Bacon, 1990; Hart *et al.*, 1995; Mihalynuk, 1999; Simmons *et al.*, 2005). The Stikine, Cache Creek and Quesnel tectonostratigraphic terranes underlie the region with Stikinia being the host terrane in the study area. These terranes are considered to represent a continuous ~1400 km long island arc developed outboard of western ancestral North America along a northwest-trending subduction zone during and prior to the Late Carboniferous (Mihalynuk *et al.*, 1994). A Late Permian to Late Triassic reconfiguration of the subduction zone followed the initial stage of collapse of the Slide Mountain basin during east-verging contraction (Nelson, 1993). The subduction zone was re-established outboard of Quesnellia and Stikinia by the Late Triassic, and the magmatic products are represented by the Stuhini and Nicola-Takla groups. Oroclinal bending of the terranes was also initiated during this time, in response to the collision of the Cache Creek plateau with Quesnellia and Stikinia (Mihalynuk *et al.*, 1994).

Extensive arc volcanism and plutonism dominated Stikinia and Quesnellia in the Upper Triassic. Generally, the Triassic volcanic rock sequences are very similar, grading from subalkaline volcanic rocks (Stuhini and Nicola-Takla Groups, respectively) in the south to

volcaniclastic sedimentary rocks (Lewes River Group and Nazcha Formation, respectively) in the north (Gabrielse, 1969). Arc-derived sedimentary rocks dominate the Late Triassic arc near the proposed oroclinal hinge, whereas arc volcanic rocks dominate elsewhere along the arc (Gabrielse, 1969). This time period represents the closure of the Cache Creek Ocean due to the oroclinal bending of the Stikinia-Quesnellia arc. Monger *et al.* (1991) and Jackson (1992) provide evidence for the linkage of Stikinia and Cache Creek terranes at this time while the linkage between Cache Creek and Quesnellia (albeit in southern British Columbia) is provided by Monger (1984).

Lower to Middle Jurassic Laberge Group clastic sedimentary rocks were deposited on Upper Triassic Stuhini Group rocks throughout the region. Mihalynuk (1999) proposed that these sedimentary rocks recorded dissection of the Stuhini arc at the hinge zone of the oroclinal bend. South of the hinge zone, continued subduction under Stikinia and Quesnellia resulted in voluminous calc-alkaline Hazelton Group volcanism. Nixon *et al.* (1993) established that Quesnellia was emplaced against the western margin of North America by 186 Ma. Locally, clastic sedimentary rocks are composed of detritus from older Laberge Group strata, indicating that rapid uplift occurred in limited areas. This basin cannibalization may represent the initiation of the Whitehorse Trough collapse (Mihalynuk, 1999). Southwest-verging thrust faults play an important role in the development of the arc at this time. For example, the southwest verging movement of the King Salmon Thrust (Thorstad and Gabrielse, 1986) allowed for the emplacement of the Laberge Group and the formation of the clastic foredeep of the proto-Bowser Basin, which began in the latest Toarcian to Aalenian time (Ricketts, *et al.*, 1992; Mihalynuk, 1999).

Prior to the Middle Jurassic the Stikine, Quesnel and Cache Creek terranes were discrete tectonic elements separated by subduction or collision zones. Oroclinal collapse initiated the thrusting of Quesnellia over western North America and trusting of Cache Creek over Stikinia. Mihalynuk (1999) estimates shortening in excess of 50% some 100 km to the north of the study area in the Tagish Lake vicinity. The Cache Creek and Stikine terranes are stitched together by 172 Ma by the undeformed Fourth of July batholith (Mihalynuk and Smith, 1992). Metamorphic cooling of the terrane is recorded by muscovite cooling ages from the Boundary Ranges metamorphic suite giving a $^{40}Ar/^{39}Ar$ plateau age of 172 Ma (Smith and Mihalynuk, 1992). Sedimentation in the Laberge Basin ceased by the latest Middle Jurassic and a period of tectonic quiescence followed this period, marking the beginning of a magmatic lull, which lasted some 50 million years.

By the Cretaceous, magmatism and strike slip deformation dominated the tectonics of the Northern Cordilleran. Magmatism resumed in the latest Early Cretaceous with the onset of the Whitehorse Magmatic Epoch, which lasted from approximately 111 Ma (Hart, 1995) until 100 Ma (Mihalynuk, 1999). The following 15 millions years were relatively quiescent regionally; however, Thorn Suite rocks were deposited and emplaced during this time and are the dominant host rocks at the Thorn Property. Windy Table Suite rocks were emplaced following the emplacement of Thorn Suite Magmatism. The onset of Windy Table volcanism is variable along the northeast trending belt, but had begun by at least 86 Ma at the Thorn Property (Simmons *et al.*, 2005b). Volcanic rocks of this age are generally flat lying, but may be tilted adjacent to steeply dipping normal faults.

Following another magmatic hiatus, magmatism resumed from 59 – 53 Ma (Mihalynuk, 1999) as part of the Sloko Suite. These intermediate to felsic magmatic rocks are represented by voluminous eruptions of volcanic rocks with coeval semi-circular granitic plutons, which mark the roots of Sloko-age volcanoes in the Coast Belt (Mihalynuk, 1999). North-northeast to north-northwest trending porphyritic quartz diorite dyke swarms may have fed Sloko volcanic rocks.

Geological Setting of the Study Area

The Thorn Property is located on the western margin of the Stikine tectonostratigraphic terrane, where the Coast geomorphologic belt meets the Intermontane geomorphologic belt, as defined by Wheeler and McFeely (1987). Three distinct periods of magmatism postdate the amalgamation of Stikinia, Cache Creek and Quesnellia and their accretion onto the western flank of North America. These magmatic bodies are emplaced into and deposited onto Upper Triassic subaqueous mafic volcanic rocks and associated marine sedimentary rocks (Stuhini Group) and Lower to Middle Jurassic clastic sedimentary rocks (Laberge Group), both of which are referred to as basement rocks below. Stuhini Group rocks are the oldest rocks mapped in the study area and are unconformably overlain by the Laberge Group at a shallow angle, east of the Outlaw Zone (Simmons *et al.*, 2005a; see Figure 2-6). The basement rocks were deformed during the amalgamation of Stikinia, Cache Creek and Quesnellia and their subsequent accretion onto the western flank of North America. Deformation during this period is characterized by regional sub-greenschist metamorphism, northwest-trending upright, open to closed folds and northwest-trending trust faults. The Fourth of July Suite plutonic rocks intruded into the basement rocks by 168 Ma, and cut deformed Mesozoic rocks, indicating that amalgamation and accretion had ceased prior to these intrusions. North of the project area, in

the Tagish Lake vicinity, Mihalynuk (1999) demonstrated that *ca.* 172 Ma Fourth of July Suite Plutons cut deformed Mesozoic rocks.

A series of felsic pyroclastic rocks and igneous intrusions were emplaced episodically during the Late Cretaceous and are separated into two distinct periods: Thorn Suite (93-88 Ma) and Windy Table Suite (86-80 Ma). Eocene magmatism has not been recognized on the Thorn Property, but has been reported approximately 10 km directly north by Simmons (2005).

Late Cretaceous magmatism in the study area is part of the Coast Batholith, which is a series of continental arcs that were emplaced into the same geographic location along a NNW-trending belt from *ca.* 120 Ma to *ca.* 55 Ma. Previous attempts (e.g. Brew and Morrell, 1983; Monger, 1984) have been made to subdivide the Coast Batholith in northern B.C. and southern Yukon with limited success. This study proposes geologic, geochemical and textural discriminates, which can serve as a basis for subdividing the Coast Batholith in the Golden Bear Mine, King Salmon Lake and Taku River areas. Traditionally, the Late Cretaceous component of the Coast Batholith has been viewed as insignificant, and many of the voluminous volcanic centres were assumed to be of Sloko magmatic ages (e.g. Souther, 1971), which have associated epithermal mineralization in southern Yukon (e.g. Mt. Skukum, Engineer Mine). However, recent work by Mihalynuk *et al.* (1999 & 2003) and Simmons *et al.* (2004, 2005a, b) have begun to define a distinctive NNW-trending Late Cretaceous volcano-plutonic arc, which extends from at least the Golden Bear Mine area to the B.C.-Yukon border. The Late Cretaceous portion of the Coast Batholith has limited E-W spatial distribution with an estimated maximum width of 20 km at these latitudes. These magmatic rocks spatially overlap with Eocene Sloko magmatic rocks in the project area, however there is a general trend of younging magmatic towards the west, possibly supporting the slab rollback theory proposed by Brew and Morrell (1983).

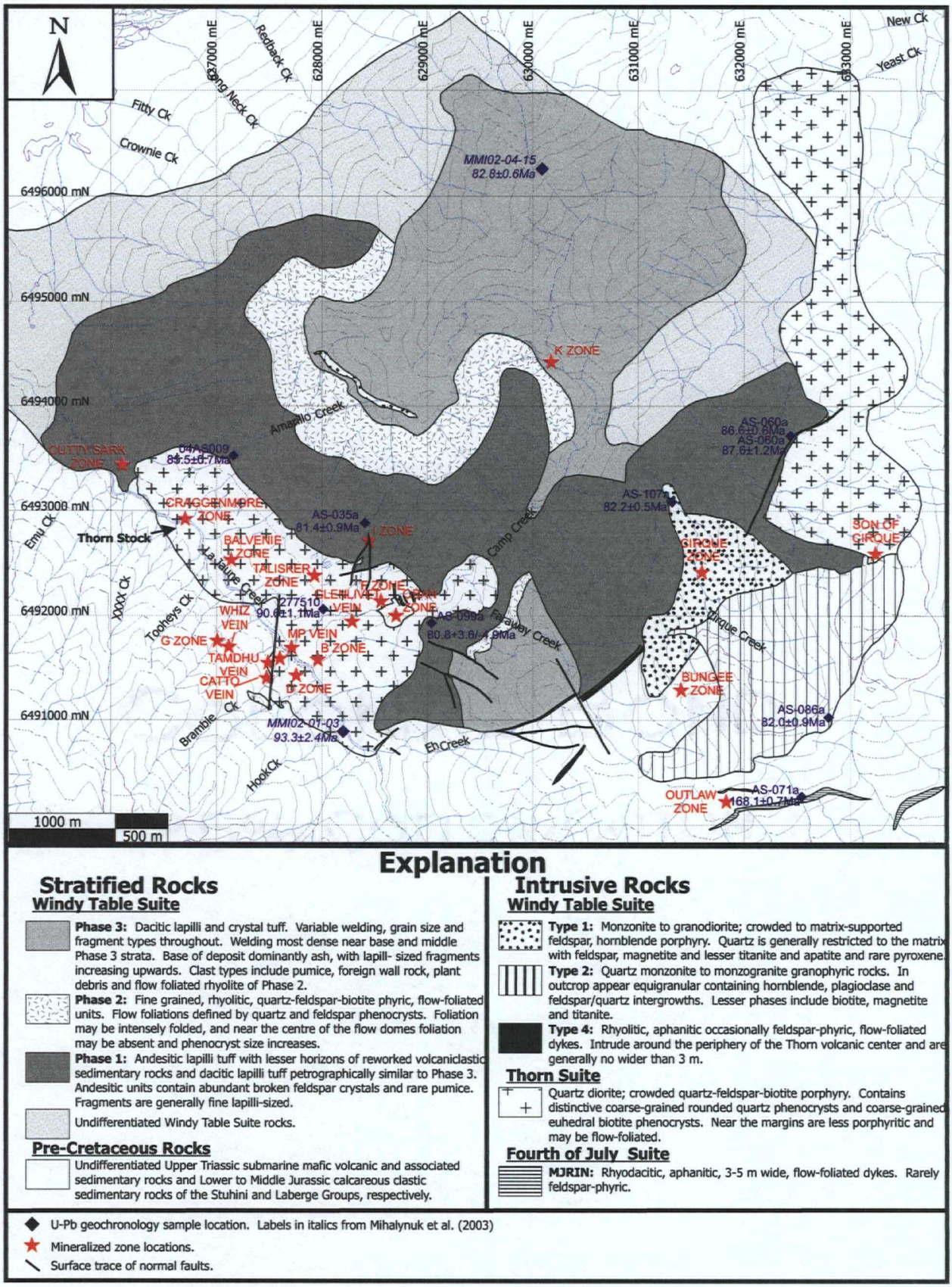

Explanation

Stratified Rocks

Windy Table Suite

Phase 3: Dacitic lapilli and crystal tuff. Variable welding, grain size and fragment types throughout. Welding most dense near base and middle Phase 3 strata. Base of deposit dominantly ash, with lapill- sized fragments increasing upwards. Clast types include pumice, foreign wall rock, plant debris and flow foliated rhyolite of Phase 2.

Phase 2: Fine grained, rhyolitic, quartz-feldspar-biotite phyric, flow-foliated units. Flow foliations defined by quartz and feldspar phenocrysts. Foliation may be intensely folded, and near the centre of the flow domes foliation may be absent and phenocryst size increases.

Phase 1: Andesitic lapilli tuff with lesser horizons of reworked volcaniclastic sedimentary rocks and dacitic lapilli tuff petrographically similar to Phase 3. Andesitic units contain abundant broken feldspar crystals and rare pumice. Fragments are generally fine lapilli-sized.

Undifferentiated Windy Table Suite rocks.

Pre-Cretaceous Rocks

Undifferentiated Upper Triassic submarine mafic volcanic and associated sedimentary rocks and Lower to Middle Jurassic calcareous clastic sedimentary rocks of the Stuhini and Laberge Groups, respectively.

Intrusive Rocks

Windy Table Suite

Type 1: Monzonite to granodiorite; crowded to matrix-supported feldspar, hornblende porphyry. Quartz is generally restricted to the matrix with feldspar, magnetite and lesser titanite and apatite and rare pyroxene.

Type 2: Quartz monzonite to monzogranite granophyric rocks. In outcrop appear equigranular containing hornblende, plagioclase and feldspar/quartz intergrowths. Lesser phases include biotite, magnetite and titanite.

Type 4: Rhyolitic, aphanitic occasionally feldspar-phyric, flow-foliated dykes. Intrude around the periphery of the Thorn volcanic center and are generally no wider than 3 m.

Thorn Suite

Quartz diorite; crowded quartz-feldspar-biotite porphyry. Contains distinctive coarse-grained rounded quartz phenocrysts and coarse-grained euhedral biotite phenocrysts. Near the margins are less porphyritic and may be flow-foliated.

Fourth of July Suite

MJRIN: Rhyodacitic, aphanitic, 3-5 m wide, flow-foliated dykes. Rarely feldspar-phyric.

- U-Pb geochronology sample location. Labels in italics from Mihalynuk et al. (2003)
- Mineralized zone locations.
- Surface trace of normal faults.

Figure 2-3: Simplified geology of the Thorn Property and locations of samples collected for U-Pb geochronology & ages, and locations of mineralized zones.

Triassic and Jurassic Supracrustal Rocks

The Upper Triassic Stuhini Group and the Lower to Middle Jurassic Laberge Group predominantly underlie the study area. These rocks form the basement rocks to the Cretaceous and later magmatic events.

Stuhini Group

Stuhini Group strata form a northwesterly-trending belt from the Golden Bear Mine area to the Tulsequah area where the strata were named by Kerr (1948) after Stuhini Creek. These strata continue to the north through the Tagish Lake area (Mihalynuk, 1999) and are correlative to the Lewis River Group further north (Wheeler, 1961 and Hart *et al.*, 1989).

A wide range of rock types including basic to intermediate subalkaline flows, pyroclastic rocks and related sedimentary rocks characterize the Stuhini Group (Mihalynuk 1999). The Stuhini Group may be divided in the study area into a sequence dominated by sub-marine volcanic rocks and a sequence dominated by clastic sedimentary rocks and lesser carbonate rocks. Near the Thorn Property (Figure 2-3), submarine mafic volcanic strata are overlain by sedimentary strata (Simmons *et al.*, 2003; Baker, 2003) and are similar to the section described by Mihalynuk (1999) at Willison Bay, approximately 90 km north of the study area.

On the Thorn Property, the Stuhini Group consists of submarine mafic volcanic rocks at the base, which changes up stratigraphic section to include increasing amounts of intercalated siltstones and conglomerates. South of the Thorn Property in the Metla area, an andesitic lapilli and crystal tuff originally thought to belong to part of the Windy Table Group rocks, yielded a U-Pb Sensitive High Resolution Ion Micro Probe Reverse Geometry (SHRIMP-RG; zircon) age of 249 ± 6.4 Ma (Figure 2-5a; Table 2-2; 04AS-21), based on weighted mean of the spot analyzes (Appendix I). It is unclear if this age represents Paleozoic basement rocks similar to those of the Wann River Orthogneiss (Currie, 1990) or if it is Stuhini Group rock with a slightly older age than the accepted range for Stuhini Group rocks. If this age does represent Stuhini Group volcanic rocks it may represent the first age on volcanic rocks from this group, and certainly would be the first known date of a Stuhini Group volcanic rock north of the Iskut River area near the Eskay Creek Mine, some 400 km south of the project area.

The Stuhini Group locally contains significant quantities of intrusive rocks, commonly associated with pyroclastic rocks correlative in age. South of the Thorn Property in the Bing area near the Sheslay River, two U-Pb zircon ages on subvolcanic intrusive rocks were obtained using SHRIMP-RG as part of this study. A strongly foliated gabbro containing large plagioclase

crystals (2mm to 15mm) and interstitial hornblende yielded an SHRIMP-RG age of 214.2 ± 2.4 Ma (Figure 2-5c; Table 2-2; 04AS-27), while an equigranular granodiorite located approximately 5 km north of the foliated gabbro yielded a U-Pb zircon SHRIMP-RG age of 219.2 ± 3.5 Ma. Mihalynuk (1999) interpreted the foliated gabbroic rocks as subvolcanic intrusions. All U-Pb ages from intrusive rocks from this study are considered to be crystallization ages.

Sinwa Formation

The upper part of the Stuhini Group contains the Sinwa Formation and can be traced discontinuously throughout the study area (Souther, 1971; Figure 2-3). The Sinwa Formation ranges in thickness from 5-20 m and unconformably overlies Stuhini Group clastic sedimentary rocks on the Thorn Property (Simmons *et al.*, 2005a).

It comprises two main rock types: lower limestone and upper clastic sedimentary rocks. Dolomitization, skarnification and recrystallization of limestone are widespread. Local boulder conglomerate units containing volcanic and intrusive rocks may correlate with the "Limestone Boulder Conglomerate" of Mihalynuk (1999), which separates Upper Triassic Stuhini Group strata from Pliensbachian argillites of the Laberge Group in the Kirtland and Moon Lake areas, north of the study area.

Laberge Group

The Laberge Group extends from the Dease Lake area in the south to the Yukon in the north, well outside the northwest British Columbia volcanoplutonic belt on Figure 2-1, and is the major map unit in the study area. Souther (1971) estimated the thickness of the Laberge Group in the region to be 3100 m, although others have estimated the thickness to be as much as 5000 m (e.g., Bultman 1979). The Laberge Group comprises boulder to cobble conglomerates (mafic volcanic clasts > intrusive clasts and intrusive clasts > mafic volcanic clasts), immature sandstones and siltstones, wackes, and argillites, all of which are generally calcareous. Correlation of individual sequences is difficult due to rapid lateral facies changes and lack of marker horizons. On the Thorn Property, Laberge Group rocks unconformably overlie rocks of the Stuhini Group at a low angle. These strata are thought to be an overlap assemblage linking terranes by the Early Jurassic (Wheeler *et al.*, 1991, Mihalynuk 1999).

Pre-Cretaceous Magmatic Rocks

Fourth of July Suite (Middle Jurassic)

Jurassic plutons are common in the Coast Batholith to the northwest of the study area where they in part form the Fourth of July Plutonic Suite of Mihalynuk (1999). They are sparsely observed southeast of the Taku River. During this study several Fourth of July Suite intrusions has been recognized in one location at the Thorn Property and dated at 168.1±0.7 Ma (AS-071a, Table 2-2; Figure 2-6A) by U-Pb zircon (TIMS) geochronology (Appendix I). Intrusions of this age on the Thorn Property are 3-5 m wide, fine-grained, aphanitic rhyodacite dykes, which intrude into Stuhini Group rocks at the Outlaw prospect (Figure 2-3). The 168.1±0.7 Ma age from the rhyodacite dyke at the Outlaw is, furthermore, not a common age for Jurassic magmatism regionally. However, biotite cooling ages from the Fourth of July Plutonic Suite can be as young as 164 Ma (e.g. Roots & Parrish, 1988), which suggests the potential for plutonic rocks of similar age lying to the west of the study area. Fourth of July-aged intrusions have important tectonic implications, as they apparently record the age of amalgamation and accretion of the Stikine, Cache Creek and Quesnel Terranes.

Cretaceous Magmatic Rocks

The immense Coast Plutonic Complex is a NNW-trending magmatic arc on the west coast of North America resulting from the subduction of oceanic crust, west of the current location of Stikinia, since the Late Jurassic. On the eastern flank of the Coast Plutonic Complex in the northern Cordilleran, magmatism after the accretion of the Stikine Terrane began at about 120 Ma (Mihalynuk, 1999; Currie, 1994; Bultman, 1979) and continued until the Eocene. In the area between Golden Bear Mine and the Taku River (Figure 2-2; 2-3), magmatism began at *ca.* 90 Ma, with the last major period of magmatism *ca.* 55 Ma.

In the study area, three distinct short-lived periods of Cretaceous and Tertiary magmatism are documented based on relative geological relations, geochronology and geochemistry. These intruded and erupted through older rocks including the Fourth of July Suite, Stuhini Group and Laberge Group rocks. The oldest Cretaceous Suite (*ca.* 93-88 Ma) Thorn Suite is volumetrically the least extensive and only contains plutonic rocks. The volumetrically most important is the *ca.* 86-80 Ma Windy Table Magmatic Suite, which contains both plutonic rocks and their extrusive equivalents. These rocks are most commonly associated with hydrothermally altered rocks. The youngest magmatic event is the *ca.* 58-54 Ma Sloko Suite, which contains only plutonic rocks in the study area, however extrusive equivalents are

known throughout the northern Cordilleran (e.g., Mihalynuk, 1999). Geochronological support for these suites are given in Tables 2-1, 2 and Figures 2-4, 5, 6.

Thorn Suite Magmatism (93-88 Ma)

Intrusive rocks of the Thorn Suite are not widely recognized in the Canadian Cordilleran, therefore their spatial distribution, genesis and importance is not well understood. Examples of Thorn Suite rocks occur at the Thorn Property (Mihalynuk *et al.*, 2003; Simmons *et al.*, 2005), and in the Racine Lake area, approximately 90 km north of the study area (Bultman, 1979). The Thorn Stock on the Thorn Property is the host to a significant high-sulphidation mineral assemblage Au-Ag-Cu showing. The 3.5 km by 1.5 km stock intrudes at the intersection of two major lineaments striking NW and E that are defined by magnetic and resistivity lows (Awmack, 2003). These lineaments underlie La Jaune and Camp creeks along which the stock is elongate in the NW and to a lesser extent in the E directions (Figure 2-3). No significant surficial expression of these lineaments can be mapped, but presumably they are associated with the accretion of Stikinia onto the western flank of North America.

The stock forms a topographic low and forms cliffs along fractures surfaces. Less altered stock forms dark grey-green outcrops, which locally have well-developed columnar jointing (Figure 2-7a; Baker, 2003). The Thorn Stock is quartz-plagioclase-biotite porphyritic quartz diorite. The stock may contain as much as 10%, large (up to 1 cm across), rounded quartz phenocrysts and up to 15% euhedral biotite phenocrysts, which form prisms up to 2 cm in length. These porphyritic textures, along with a generally high degree of alteration make Thorn Suite intrusions unique from other Late Cretaceous in the region. Marginal phases of the stock are fine-grained feldspar phyric and flow-banded. Hydrous phases are biotite and lesser hornblende. Common accessory minerals include magnetite, apatite and zircon.

Pervasive sericite-chlorite-carbonate alteration of these rocks has destroyed most microscopic and macroscopic textures, with the most notable textural destruction occurring in the matrix of the stock. Plagioclase phenocrysts are sericite-chlorite altered, but still show remnant albite twinning and occasionally in the largest of phenocrysts the cores of the crystals may be partly preserved as unaltered plagioclase (Figure 2-7B). Embayed quartz phenocrysts are common (Figure 2-7B) and show that quartz was partly resorbed and was out of equilibrium with the surrounding melt. Biotite occurs as replacement of hornblende and as euhedral biotite books, both of which have been later altered to sericite and magnetite (Figure 2-7B).

Table 2-1: U-Pb SHRIMP-RG zircon analytical data for samples from the study area

Sample Spot	^{206}Pb [1] %	U (ppm)	Th (ppm)	$^{232}Th/^{238}U$	^{206}Pb [2] (ppm)	$^{206}Pb/^{238}U$ [2]	1σ %	$^{207}Pb/^{206}Pb$ [2]	1σ %	Apparent Age $^{206}Pb/^{238}U$ [3]	(Ma, 1σ)
					Thorn Suite						
277510 (Quartz Diorite)											
AS510-1	0.20	1334	113	0.09	14.80	0.01286	0.88	.0478	3.3	82.37	(0.73)
AS510-2	0.30	715	63	0.09	8.08	0.01315	0.97	.0508	2.9	83.91	(0.82)
AS510-3	0.29	1042	161	0.16	12.20	0.01366	0.91	.0500	2.8	87.24	(0.79)
AS510-4	0.79	914	97	0.11	10.80	0.01356	1.10	.0458	9.8	87.03	(0.83)
AS510-5	0.21	1036	142	0.14	12.30	0.01372	1.10	.0467	4.3	87.94	(0.93)
AS510-6	0.12	1701	267	0.16	20.70	0.01420	0.84	.0495	2.2	90.71	(0.77)
AS510-7	0.52	504	130	0.27	6.04	0.01397	1.30	.0534	10.6	88.83	(0.95)
AS510-8	0.00	1421	190	0.14	17.40	0.01419	0.87	.0468	2.7	90.96	(0.79)
AS510-9	0.00	1767	1017	0.59	21.60	0.01424	0.86	.0483	3.5	91.07	(0.76)
AS510-10	0.06	1485	173	0.12	17.90	0.01392	1.10	.0441	4.4	89.54	(0.99)
AS510-11	0.26	669	182	0.28	8.16	0.01421	0.97	.0507	2.8	90.61	(0.89)
AS510-12	0.11	711	69	0.10	8.32	0.01348	1.00	.0404	9.0	87.12	(0.85)
AS510-13	0.30	544	49	0.09	6.09	0.01295	1.00	.0445	5.3	83.25	(0.87)
AS510-14	4.78	400	46	0.12	5.20	0.01489	1.60	.0730	13.0	92.30	(1.20)
AS060a (Quartz Diorite)											
AS60-1	0.26	629	154	0.25	8.16	0.01509	1.20	.0491	7.4	96.40	(1.10)
AS60-2	0.37	641	119	0.19	7.59	0.01376	1.00	.0500	4.4	87.87	(0.89)
AS60-3	0.16	1247	309	0.26	14.6	0.01355	0.89	.0465	3.3	86.93	(0.77)
AS60-4	0.00	414	72	0.18	5.01	0.01395	1.20	.0402	8.5	90.20	(1.00)
AS60-5	0.43	357	51	0.15	4.08	0.01309	1.20	.0394	8.1	84.71	(10.00)
AS60-6	0.60	1143	237	0.21	13.3	0.01342	0.93	.0482	5.6	85.91	(0.80)
AS60-7	0.24	1325	233	0.18	15.9	0.01401	0.89	.0496	3.9	89.46	(0.78)
AS60-8	0.23	1174	232	0.20	13.6	0.01335	1.20	.0428	7.7	85.99	(0.96)
AS60-9	0.17	1098	206	0.19	12.9	0.01367	0.91	.0480	3.5	87.49	(0.79)
AS60-10	0.41	1409	411	0.30	16.5	0.01362	0.89	.0491	3.8	87.08	(0.76)
AS60-11	0.17	1427	419	0.30	17.0	0.01382	0.87	.0484	2.8	88.40	(0.76)
AS60-12	0.15	1159	179	0.16	13.8	0.01375	0.91	.0442	4.7	88.42	(0.79)
					Windy Table Suite						
04AS009 (Weakly welded crytal, lapilli tuff)											
4AS9B-1	0.16	387	269	0.72	4.90	0.01460	1.00	.0421	8.1	94.13	(0.92)
4AS9B-2	0.07	259	35	0.14	2.90	0.01288	1.20	.0398	7.3	83.30	(1.10)
4AS9B-3	0.06	237	42	0.18	2.67	0.01317	1.30	.0488	4.7	84.20	(1.10)
4AS9B-4	0.17	353	106	0.31	4.04	0.01315	1.40	.0393	19.5	85.08	(0.92)
4AS9B-5	0.00	473	52	0.11	5.43	0.01337	0.94	.0478	3.3	85.60	(0.82)
4AS9B-6	0.00	212	52	0.26	2.36	0.01307	4.10	.0528	4.7	83.10	(3.40)
4AS9B-7	0.05	285	77	0.28	3.27	0.01350	1.20	.0561	4.2	85.60	(1.00)
4AS9B-8	0.32	396	103	0.27	5.53	0.01623	1.20	.0486	10.6	103.70	(1.10)
4AS9B-9	0.00	435	146	0.35	5.06	0.01349	1.00	.0454	7.0	86.65	(0.86)
4AS9B-10	0.30	264	55	0.21	3.17	0.01379	1.30	.0401	13.1	89.10	(1.10)
4AS9B-11	0.76	186	89	0.49	2.05	0.01256	1.70	.0350	23.1	81.70	(1.20)
4AS9B-12	0.08	280	115	0.42	3.21	0.01345	1.20	.0538	4.1	85.40	(1.00)
4AS9B-13	0.01	739	91	0.13	8.99	0.01421	0.79	.0499	3.4	90.70	(0.71)
4AS9B-14	0.11	305	82	0.28	3.46	0.01324	1.10	.0512	4.1	84.44	(0.99)
4AS9B-15	0.18	1466	281	0.20	16.80	0.013356	0.63	.0481	2.2	85.50	(0.54)
4AS9B-16	0.00	1584	357	0.23	18.40	0.013525	0.61	.0480	2.2	86.57	(0.53)
4AS9B-17	0.59	243	94	0.40	2.77	0.01298	2.00	.0362	20.1	84.40	(1.50)
04AS003 (Feldspar porphyritic quartz monzonite)											
AS-03-1	0.23	396	287	0.75	4.2	0.012236	1.31	.0494	6.9	78.22	(1.07)
AS-03-2	-0.41	289	227	0.81	3.2	0.012803	1.47	.0444	8.2	82.35	(1.26)
AS-03-3	0.13	1540	639	0.43	18.0	0.013604	0.68	.0488	3.5	86.99	(0.62)
AS-03-4	-0.28	1194	490	0.42	13.2	0.012887	0.75	.0454	4.0	82.78	(0.65)
AS-03-5	-0.27	324	212	0.67	3.7	0.013169	3.32	.0456	9.4	84.56	(2.83)
AS-03-6	-0.21	1119	436	0.40	12.8	0.013285	1.86	.0460	4.0	85.25	(1.59)
AS-03-7	-0.06	458	354	0.80	5.1	0.013051	1.29	.0472	6.2	83.64	(1.12)
AS-03-8	0.19	873	444	0.53	9.0	0.012048	0.94	.0490	5.3	77.06	(0.77)
AS-03-9	-0.08	394	213	0.56	4.2	0.012456	1.31	.0469	7.3	79.87	(1.10)
AS-03-10	37.64	213	148	0.72	3.2	0.017556	2.16	.3458	21.3	70.19	(11.79)
AS-03-11	0.44	298	232	0.80	3.0	0.011559	1.66	.0510	8.6	73.76	(1.29)
AS-03-12	0.00	158	84	0.55	1.7	0.012378	2.09	.0476	11.2	79.30	(1.73)
AS-03-13	-0.24	385	266	0.71	4.0	0.012215	1.27	.0457	6.8	78.45	(1.04)

[1] Common lead
[2] Atomic ratios of radiogenic Pb
[3] $^{206}Pb/^{238}U$ age using ^{207}Pb to correct for common lead

Table 2-1: Continued

Sample Spot Name	^{206}Pb [1] %	U (ppm)	Th (ppm)	$\frac{^{232}Th}{^{238}U}$	^{206}Pb [2] (ppm)	$\frac{^{206}Pb}{^{238}U}$ [2]	1σ %	$\frac{^{207}Pb}{^{206}Pb}$ [2]	1σ %	Apparent Age $^{206}Pb/^{238}U$ [3]	(Ma, 1σ)
AS086a (Granophyric granodiorite)											
AS86-1	0.03	452	322	0.73	4.93	0.01270	1.10	.0479	3.8	81.30	(0.91)
AS86-2	0.26	1261	765	0.63	14.00	0.01284	0.90	.0466	3.8	82.33	(0.73)
AS86-3	0.22	1068	914	0.88	11.70	0.01269	0.92	.0482	3.7	81.25	(0.75)
AS86-4	0.31	539	400	0.77	5.97	0.01261	1.30	.0329	20.8	82.27	(0.87)
AS86-5	0.22	510	353	0.72	5.63	0.01263	1.10	.0353	7.5	82.13	(0.88)
AS86-6	0.90	352	245	0.72	3.87	0.01264	1.30	.0446	12.8	81.30	(0.99)
AS86-7	0.05	1588	1680	1.09	17.70	0.01298	0.86	.0493	2.3	82.95	(0.72)
AS86-8	0.23	294	158	0.56	3.26	0.01302	1.30	.0562	7.8	82.50	(1.00)
AS86-9	0.20	260	124	0.49	2.73	0.01224	1.30	.0492	4.9	78.30	(1.00)
AS86-10	0.37	903	741	0.85	9.97	0.01282	0.96	.0487	4.3	82.01	(0.77)
AS035a (Densely welded lithic poor lapilli tuff)											
35A-1	2.95	542	218	0.42	6.12	.012723	1.52	.0452	18.0	81.75	(1.08)
35A-2	0.11	1268	1448	1.18	13.98	.012811	1.37	.0474	2.2	82.08	(1.12)
35A-3	0.38	302	169	0.58	3.28	.012481	1.47	.0422	11.9	80.50	(1.11)
35A-4	0.64	259	110	0.44	2.70	.012053	1.45	.0478	6.4	77.21	(1.12)
35A-5	1.18	213	74	0.36	2.55	.013641	2.04	.0388	28.4	88.32	(1.43)
35A-6	32.36	307	125	0.42	4.87	.012493	8.69	.3043	6.6	80.07	(5.79)
35A-7	11.81	320	146	0.47	4.41	.014083	3.65	.0446	57.6	90.51	(2.82)
35A-8	4.85	1938	795	0.42	21.36	.012286	1.20	.0524	14.1	78.24	(1.04)
35A-9	27.37	543	187	0.36	5.68	.009122	4.58	.0711	67.5	56.77	(2.85)
35A-10	20.25	542	208	0.40	9.84	.015716	4.63	.2090	3.0	107.65	(3.88)
35A-11	14.46	511	232	0.47	6.81	.013263	2.66	.0471	52.3	85.00	(2.24)
35A-12	36.53	612	299	0.50	9.69	.012276	8.20	.0850	94.6	74.96	(5.68)
35A-13	0.00	270	141	0.54	2.92	.012423	1.44	.0377	9.9	80.58	(1.14)
35A-14	17.01	481	276	0.59	4.16	.008531	3.31	.0645	46.4	53.56	(1.62)
35A-15	0.43	1007	932	0.96	11.03	.012694	1.11	.0479	3.0	81.29	(0.91)
35A-16	4.33	314	125	0.41	3.82	.013550	2.01	.0478	26.6	86.76	(1.43)
35A-17	3.14	1153	499	0.45	13.16	.012942	1.26	.0522	11.6	82.42	(0.97)
35A-18	0.40	483	232	0.50	5.39	.012864	1.33	.0443	10.5	82.75	(1.02)
35A-19	-0.04	1482	1221	0.85	17.09	.013399	1.08	.0464	2.1	85.94	(0.93)
35A-20	0.34	851	585	0.71	9.68	.013212	1.12	.0485	2.7	84.52	(0.95)
35A-21	-0.27	554	266	0.50	5.86	.012363	1.20	.0490	5.0	79.06	(0.93)
35A-22	0.19	859	550	0.66	9.44	.012735	1.42	.0462	3.0	81.73	(1.16)
Regional Samples Collected Outside of the Thorn Property											
Unknown Magmatic Suite											
04-AS21 (Andesitic lapilli tuff)											
AS21-1	-0.10	53	19	0.37	10.3	0.039089	2.51	.0504	1.79	247.42	(6.34)
AS21-2	0.09	921	308	0.35	3.3	0.035994	0.92	.0502	28.48	227.76	(2.11)
AS21-3	-1.04	28	12	0.47	16.1	0.040201	3.78	.0430	0.95	256.67	(9.82)
AS21-4	0.50	151	104	0.71	6.0	0.038944	1.42	.0551	5.05	245.07	(3.59)
AS21-5	0.22	342	47	0.14	10.3	0.034581	1.00	.0462	10.17	218.67	(2.26)
AS21-6	-0.82	36	21	0.60	18.6	0.035379	3.01	.0441	1.09	225.93	(7.10)
Stuhini Group											
04-AS28 (Granodiotrite)											
AS28-1	-0.82	81	25	0.32	8.2	0.034867	1.71	.0440	2.42	222.73	(3.90)
AS28-2	0.36	157	78	0.51	5.7	0.033951	2.16	.0533	4.59	214.47	(4.66)
AS28-3	0.09	53	15	0.30	11.4	0.035598	3.14	.0514	1.62	225.28	(7.19)
AS28-4	-0.22	181	83	0.47	6.2	0.036346	1.20	.0490	5.66	230.64	(2.86)
AS28-5	-0.64	86	38	0.45	9.8	0.034686	1.74	.0454	2.56	221.20	(4.00)
AS28-6	-0.76	67	23	0.35	9.2	0.032001	1.91	.0441	1.85	204.59	(4.01)
AS28-7	-0.06	64	21	0.34	9.7	0.031169	2.32	.0496	1.70	197.98	(4.69)
AS28-8	0.12	105	33	0.32	6.2	0.027758	1.34	.0505	2.51	176.30	(2.45)
AS28-9	-0.73	84	22	0.27	8.4	0.033438	1.80	.0445	2.40	213.56	(3.93)
AS28-10	-0.17	132	69	0.54	6.3	0.034381	1.74	.0491	3.91	218.28	(3.85)
AS28-11	0.03	247	59	0.25	4.6	0.033255	1.05	.0506	7.07	210.82	(2.28)
AS28-12	0.03	181	41	0.24	5.4	0.032675	1.22	.0505	5.09	207.20	(2.59)

[1] Common lead
[2] Atomic ratios of radiogenic Pb
[3] $^{206}Pb/^{238}U$ age using ^{207}Pb to correct for common lead

Table 2-1: Continued

Sample Spot Name	^{206}Pb [1] %	U (ppm)	Th (ppm)	$^{232}Th/^{238}U$	^{206}Pb [2] (ppm)	$^{206}Pb/^{238}U$ [2]	1σ %	$^{207}Pb/^{206}Pb$ [2]	1σ %	Apparent Age $^{206}Pb/^{238}U$ [3]	(Ma, 1σ)
04-AS27 (Gabbro)											
AS27-1	-0.54	144	40	0.29	4.41	0.035548	1.47	.0399	13.8	226.37	(3.41)
AS27-2	0.52	240	71	0.31	7.30	0.035465	1.05	.0548	4.5	223.51	(2.43)
AS27-3	-0.07	149	36	0.25	4.54	0.035564	1.28	.0501	5.6	225.42	(2.96)
AS27-4	0.09	722	125	0.18	21.67	0.034941	0.61	.0513	2.5	221.21	(1.37)
AS27-5	-0.45	356	67	0.19	9.54	0.031154	1.02	.0465	4.6	198.65	(2.07)
AS27-6	0.08	128	44	0.36	3.75	0.034126	1.65	.0511	7.1	216.15	(3.66)
AS27-7	-0.23	192	78	0.42	5.68	0.034425	1.33	.0487	6.1	218.67	(2.99)
AS27-8	0.33	195	96	0.51	5.57	0.033281	1.49	.0477	10.7	210.36	(3.23)
AS27-9	0.11	276	87	0.32	8.06	0.033933	1.59	.0513	6.1	214.88	(3.47)
AS27-10	0.18	420	236	0.58	12.26	0.034005	0.93	.0519	4.0	215.19	(2.05)
AS27-11	0.55	129	66	0.53	3.76	0.033849	1.59	.0548	7.0	213.42	(3.51)
AS27-12	0.19	161	55	0.35	4.60	0.033184	1.28	.0518	5.5	210.06	(2.77)
				Unknown Suite							
04-AS20 (Lithic rich lapilli tuff)											
AS20-1	0.02	440	173	0.41	11.13	0.029431	0.92	.0474	5.8	186.95	(1.78)
AS20-2	0.86	1043	262	0.26	12.47	0.013920	0.89	.0511	5.1	88.35	(0.82)
AS20-3	0.03	591	95	0.17	7.14	0.014057	1.17	.0481	5.4	89.96	(1.09)
AS20-4	-0.05	2038	580	0.29	25.19	0.014384	0.61	.0464	3.3	92.10	(0.58)
AS20-5	0.20	353	225	0.66	8.63	0.028447	1.02	.0513	7.7	180.46	(2.03)
AS20-6	-0.24	558	140	0.26	13.66	0.028512	0.81	.0478	3.8	181.65	(1.52)
AS20-7	-0.20	517	469	0.94	12.88	0.029011	0.92	.0461	5.1	184.71	(1.73)
				Windy Table Suite							
04AS12 (Monzonite)											
4AS12-1	0.00	1009	114	0.12	11.50	0.013331	0.56	.0507	4.4	85.04	(0.45)
4AS12-2	0.00	1233	179	0.15	14.10	0.013270	1.70	.0424	5.4	85.50	(1.50)
4AS12-3	0.00	728	79	0.11	8.57	0.013730	1.40	.0495	2.6	87.70	(1.30)
4AS12-4	0.14	1097	100	0.09	13.00	0.013801	0.50	.0506	3.0	88.05	(0.44)
4AS12-5	0.00	716	213	0.31	8.42	0.013735	0.61	.0495	4.2	87.74	(0.52)
4AS12-6	0.22	841	84	0.10	9.90	0.013652	0.55	.0470	3.4	87.50	(0.49)
4AS12-7	0.22	942	93	0.10	11.20	0.013803	0.51	.0491	2.4	88.23	(0.46)
4AS12-8	0.17	388	106	0.28	4.53	0.013590	2.80	.0490	8.2	86.90	(2.40)
4AS12-9	0.18	1067	155	0.15	12.40	0.013494	0.49	.0502	2.2	86.14	(0.44)
4AS12-10	0.18	1281	166	0.13	15.30	0.013864	0.50	.0493	2.2	88.59	(0.46)
04-AS22 (Flow-foliated dacite)											
AS22-1	-0.31	335	106	0.33	3.99	0.013846	1.52	.0453	7.3	88.92	(1.39)
AS22-2	-0.20	467	190	0.42	5.42	0.013521	1.18	.0407	11.7	86.76	(1.06)
AS22-3	0.09	284	135	0.49	3.29	0.013477	1.97	.0484	7.8	86.22	(1.74)
AS22-4	-0.44	143	36	0.26	4.24	0.034451	1.48	.0470	6.8	219.29	(3.33)
AS22-5	-1.14	293	108	0.38	3.26	0.012956	1.49	.0386	8.9	83.92	(1.30)
AS22-6	1.07	247	96	0.40	2.64	0.012446	2.27	.0561	8.0	78.89	(1.85)
AS22-7	-1.12	136	42	0.32	1.65	0.014095	2.09	.0389	12.4	91.24	(1.97)
AS22-8	-0.06	269	128	0.49	2.89	0.012522	1.57	.0472	8.5	80.27	(1.32)
AS22-9	0.07	597	230	0.40	6.97	0.013592	1.01	.0442	8.6	86.97	(0.92)
AS22-10	-0.16	128	36	0.29	1.29	0.011749	2.29	.0238	71.5	75.41	(1.80)
AS22-11	0.01	428	208	0.50	4.56	0.012420	1.24	.0477	6.6	79.56	(1.03)
AS22-12	0.28	387	149	0.40	4.12	0.012401	1.34	.0498	7.1	79.23	(1.12)
04AS25 (Plagioclase megacrystic monzonite)											
4AS25-1	0.05	652	268	0.42	7.53	0.013426	0.63	.0478	3.7	85.97	(0.54)
4AS25-2	0.00	250	132	0.54	2.89	0.013650	1.30	.0595	11.4	86.10	(0.87)
4AS25-3	0.71	165	65	0.41	1.90	0.013070	1.40	.0303	26.7	85.50	(1.10)
4AS25-4	0.00	151	46	0.31	1.73	0.013320	1.30	.0438	6.5	85.70	(1.10)
4AS25-5	0.00	1140	389	0.35	13.50	0.013790	0.50	.0444	4.2	88.66	(0.42)
4AS25-6	0.32	744	295	0.41	8.48	0.013194	0.69	.0455	7.2	84.73	(0.51)
4AS25-7	0.16	508	130	0.26	5.77	0.013290	0.81	.0526	7.2	84.60	(0.61)
4AS25-8	0.07	1188	441	0.38	13.90	0.013549	0.50	.0444	4.2	87.12	(0.42)
4AS25-9	0.01	815	257	0.33	9.44	0.013392	0.55	.0426	3.3	86.31	(0.49)

[1] Common lead
[2] Atomic ratios of radiogenic Pb
[3] $^{206}Pb/^{238}U$ age using ^{207}Pb to correct for common lead

Table 2-1: Continued

Sample Spot Name	^{206}Pb [1] %	U (ppm)	Th (ppm)	$^{232}Th/^{238}U$	^{206}Pb [2] (ppm)	$^{206}Pb/^{238}U$ [2]	1σ %	$^{207}Pb/^{206}Pb$ [2]	1σ %	Apparent Age $^{206}Pb/^{238}U$ [3]	(Ma, 1σ)
04-AS23 (Diorite)											
AS23-1	-0.47	360	171	0.49	3.96	0.012794	1.31	.0303	32.8	82.33	(1.12)
AS23-2	-0.03	501	147	0.30	14.72	0.034198	0.83	.0502	5.0	216.83	(1.89)
AS23-3	0.74	205	71	0.36	2.20	0.012501	1.80	.0535	9.0	79.49	(1.51)
AS23-4	0.65	332	142	0.44	3.69	0.012965	1.86	.0453	14.0	82.51	(1.57)
AS23-5	0.02	485	203	0.43	5.27	0.012645	1.20	.0359	24.6	80.99	(1.01)
AS23-6	-0.04	86	40	0.48	2.51	0.033827	1.97	.0373	26.7	214.55	(4.36)
AS23-7	-0.21	182	57	0.32	3.43	0.021906	1.55	.0472	7.8	139.98	(2.25)
AS23-8	-1.12	311	140	0.47	3.51	0.013125	1.39	.0388	8.7	84.99	(1.24)
AS23-9	0.43	239	88	0.38	2.56	0.012472	1.65	.0510	8.5	79.56	(1.38)
AS23-10	1.28	214	68	0.33	2.40	0.013045	1.93	.0578	8.5	82.49	(1.67)
AS23-11	-0.24	613	477	0.80	6.85	0.013015	1.78	.0458	5.5	83.56	(1.51)
AS23-12	-0.27	246	81	0.34	2.82	0.013353	1.56	.0456	8.3	85.74	(1.40)
AS23-13	-0.54	457	228	0.51	4.94	0.012568	1.27	.0434	7.0	80.94	(1.07)
04-AS29 (Quartz monzonite)											
AS29-1	-0.11	1103	270	0.25	11.95	0.012605	0.79	.0467	4.1	80.84	(0.66)
AS29-2	2.13	1146	258	0.23	12.27	0.012466	1.87	.0476	14.3	78.18	(1.51)
AS29-3	-0.08	1188	467	0.41	12.87	0.012613	0.71	.0430	6.0	80.87	(0.60)
AS29-4	5.40	4983	1052	0.22	56.08	0.013100	0.43	.0529	13.6	79.40	(0.67)
AS29-5	-0.06	3248	992	0.32	36.80	0.013186	0.78	.0472	2.3	84.50	(0.67)
AS29-6	0.12	2143	1481	0.71	23.28	0.012647	0.60	.0486	2.8	80.91	(0.51)
AS29-7	-0.02	1886	651	0.36	21.47	0.013251	0.65	.0463	3.6	84.87	(0.57)
AS29-8	0.71	3120	1521	0.50	35.47	0.013235	0.99	.0450	6.4	84.16	(0.85)
AS29-9	0.12	588	126	0.22	6.43	0.012735	1.11	.0486	5.9	81.48	(0.95)
AS29-10	-0.02	3391	1751	0.53	36.89	0.012666	0.53	.0466	2.8	81.15	(0.45)
AS29-11	0.31	3680	620	0.17	40.26	0.012735	0.50	.0492	2.8	81.32	(0.42)
AS29-12	0.14	2294	637	0.29	25.26	0.012817	1.10	.0488	2.8	81.99	(0.91)
Sloko Group											
04AS11 (Diorite porphyry)											
4AS11-1	0.40	265	80	0.31	1.74	0.007530	3.1	.0370	20.0	49.00	(1.50)
4AS11-2	0.47	206	67	0.34	1.66	0.009540	1.6	.0675	5.7	59.64	(0.97)
4AS11-3	0.15	658	360	0.56	4.82	0.008461	1.0	.0422	7.0	54.65	(0.54)
4AS11-4	0.00	587	236	0.42	4.44	0.008870	1.5	.0497	6.2	56.72	(0.83)
4AS11-5	0.58	319	123	0.40	2.31	0.008270	1.4	.0341	12.7	53.94	(0.75)
4AS11-6	0.00	289	106	0.38	2.15	0.008630	1.9	.0460	23.7	55.48	(0.77)
4AS11-7	0.28	394	127	0.33	2.91	0.008510	1.3	.0397	11.1	55.11	(0.67)
4AS11-8	0.50	183	59	0.33	1.42	0.008810	2.0	.0325	30.3	57.61	(0.98)
4AS11-9	0.00	183	47	0.26	1.37	0.008640	2.0	.0381	25.6	56.10	(0.95)
4AS11-10	0.25	525	175	0.34	4.00	0.008860	1.5	.0491	3.7	56.71	(0.88)
4AS11-11	0.16	366	98	0.28	2.77	0.008780	1.3	.0475	8.4	56.32	(0.70)
4AS11-12	0.00	339	124	0.38	2.41	0.008190	2.2	.0376	19.7	53.20	(1.10)
04AS19 (Diorite porphyry)											
4AS19-1	0.04	1053	410	0.40	8.56	0.009515	0.65	.0518	5.7	60.69	(0.35)
4AS19-2	0.72	131	52	0.41	1.03	0.009360	2.30	.0683	18.5	58.40	(1.10)
4AS19-3	0.78	219	69	0.32	1.67	0.008810	1.50	.0476	10.5	56.49	(0.84)
4AS19-4	0.53	312	151	0.50	2.31	0.008440	1.20	.0365	16.7	54.89	(0.60)
4AS19-5	0.29	283	84	0.31	2.19	0.009084	1.10	.0578	6.2	57.51	(0.67)
4AS19-6	1.04	313	143	0.47	2.36	0.008410	1.90	.0216	62.9	55.72	(0.63)
4AS19-7	0.00	464	262	0.58	3.63	0.009021	0.90	.0403	9.1	58.40	(0.51)
4AS19-8	0.05	679	230	0.35	5.04	0.008504	0.72	.0355	7.3	55.39	(0.41)
4AS19-9	1.01	239	80	0.35	2.03	0.009960	1.30	.0602	6.7	62.87	(0.81)

[1] Common lead
[2] Atomic ratios of radiogenic Pb
[3] $^{206}Pb/^{238}U$ age using ^{207}Pb to correct for common lead

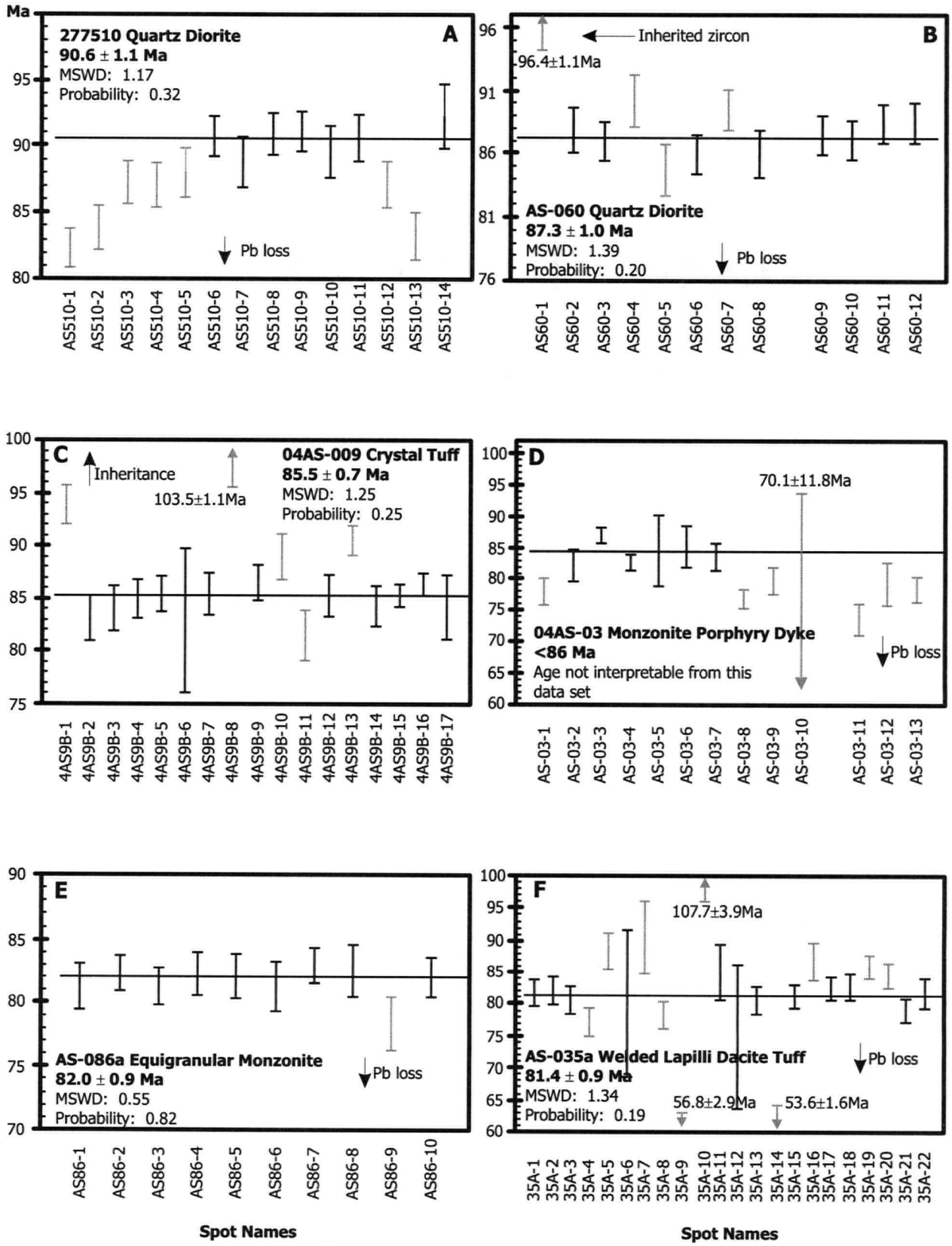

Figure 2-4: Weighted mean $^{206}Pb/^{238}U$ age plots for samples from the Thorn Property. U-Pb ages of intrusive and extrusive rocks from the Thorn Property. Errors bars given at 2σ values. Grey point data rejected in calculation due to either interpreted Pb loss or inheritance. "Point data" represent individual ablated and ionized points from separate zircons on a grain mount. **Zircons were the mineral analyzed for all samples in the geochronology shown above.**

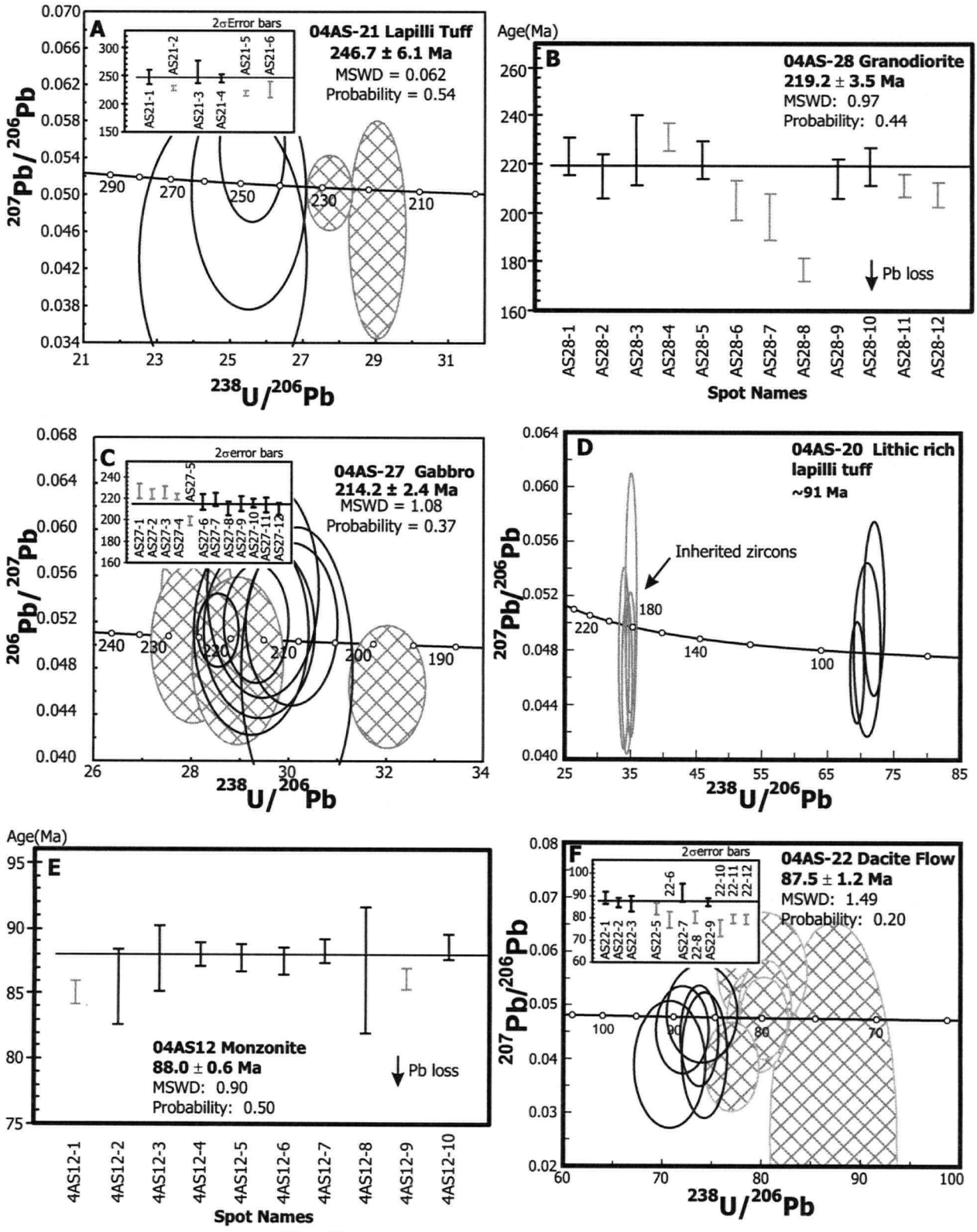

Figure 2-5: Weighted mean $^{206}Pb/^{238}U$ age plots for samples from intrusive and extrusive rocks from the region surrounding the Thorn Property. Ages are determined by weighted mean. Grey spot data are rejected due to either Pb loss or inheritance. Tera-Waserburg concordia plots are shown for comparison between concordia and weighted mean ages. All errors at 2σ values. Tera-Wasserburg plots are $^{207}Pb/^{206}Pb$ vs. $^{238}U/^{206}Pb$. "Point data" represent individual ablated and ionized points from separate zircons on a grain mount. **Zircons were the mineral analyzed for all samples in the geochronology shown above.**

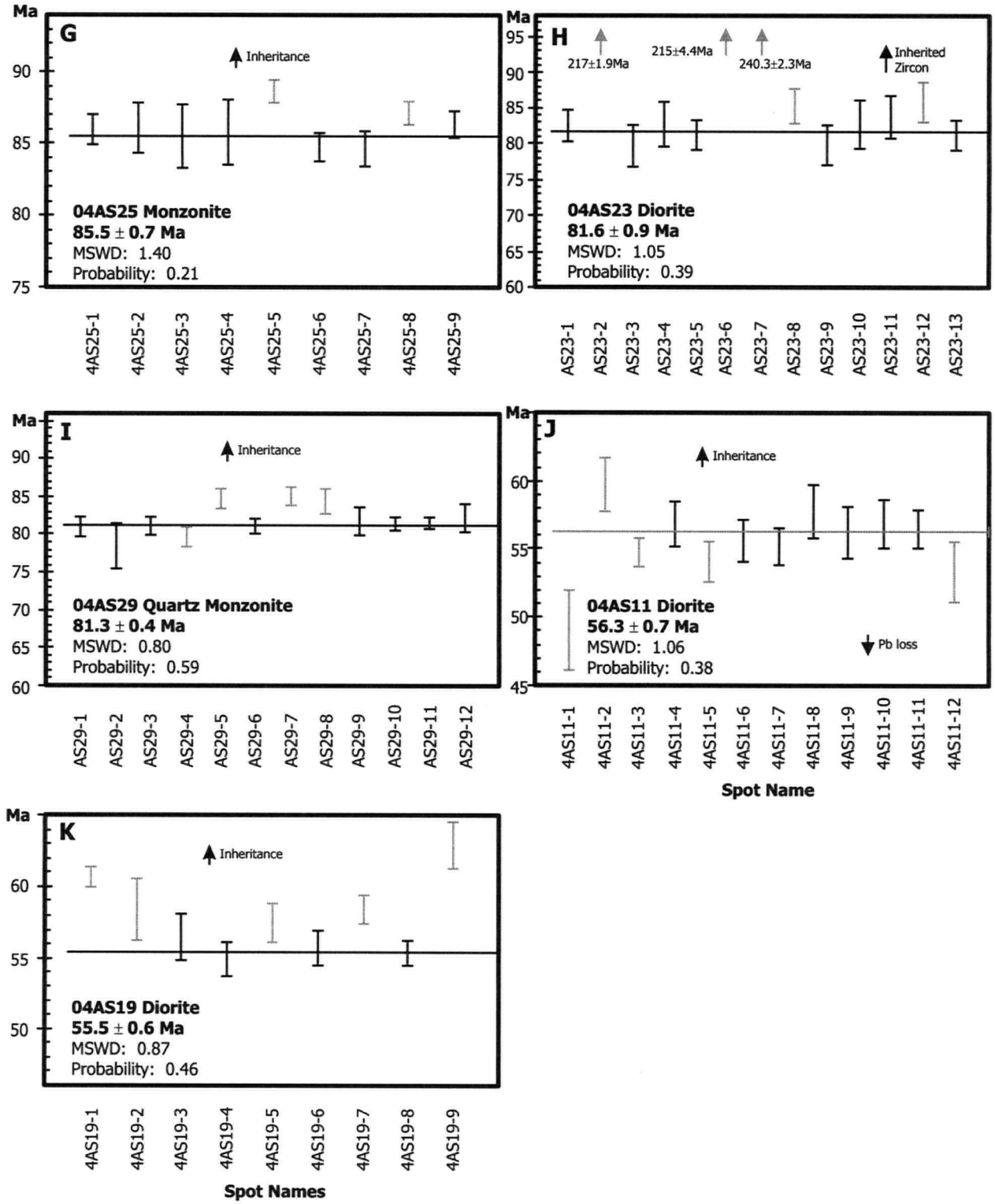

Figure 2-5: Weighted mean $^{206}Pb/^{238}U$ age plots for samples from intrusive and extrusive rocks from the region surrounding the Thorn Property. Ages are determined by weighted mean. Grey spot data are rejected due to either Pb loss or inheritance. Tera-Waserburg concordia plots are shown for comparison between concordia and weighted mean ages. All errors at 2σ values. Tera-Wasserburg plots are $^{207}Pb/^{206}Pb$ vs. $^{238}U/^{206}Pb$. "Point data" represent individual ablated and ionized points from separate zircons on a grain mount. **Zircons were the mineral analyzed for all samples in the geochronology shown above.**

Table 2-2: U-Pb ID-TIMS zircon analytical data for samples from the Thorn Property

Sample Fraction[1]	Wt. (mg)	U[2] (ppm)	Pb*[3] (ppm)	$^{206}Pb/^{204}Pb$[4]	Pb[5] (pg)	^{208}Pb[3] %	Isotopic Ratios (1σ, %)[6] $^{206}Pb/^{238}U$	$^{207}Pb/^{235}U$	$^{207}Pb/^{206}Pb$	Apparent Age (2σ, %)[6] $^{206}Pb/^{238}U$	$^{207}Pb/^{235}U$	$^{207}Pb/^{206}Pb$
Fourth of July Suite												
AS-071a (Rhyodacite dyke)												
A	0.012	256	6.9	1406	4	11.8	0.02645 (0.14)	0.1807 (0.46)	0.04956 (0.41)	168.3 (0.5)	168.7 (1.4)	174 (19)
B	0.011	617	16.6	2372	5	11.7	0.02639 (0.12)	0.1799 (0.29)	0.04944 (0.22)	167.9 (0.4)	167.9 (0.9)	169 (10)
C	0.014	396	10.6	2632	3	12.0	0.02597 (0.11)	0.1770 (0.31)	0.04942 (0.26)	165.3 (0.4)	165.5 (1.0)	168 (12)
D	0.017	265	7.0	751	10	11.3	0.02598 (0.14)	0.1777 (0.44)	0.04960 (0.37)	165.3 (0.5)	166.1 (1.4)	176 (18)
Thorn Suite												
AS-060a (Quartz diorite)												
B	0.108	718	9.5	22229	3	6.4	0.01372 (0.13)	0.0919 (0.18)	0.04860 (0.10)	87.8 (0.2)	89.3 (0.3)	128.8 (4.9)
C	0.272	436	5.6	178	636	5.8	0.01353 (0.33)	0.0897 (1.5)	0.04810 (1.3)	86.6 (0.6)	87.3 (2.5)	104 (62/64)
D	0.362	677	8.8	6470	32	5.5	0.01356 (0.09)	0.0895 (0.21)	0.04786 (0.15)	86.8 (0.2)	86.9 (0.4)	92.1 (7.3)
Windy Table Suite												
AS-107a (Quartz monzonite porphyry)												
A	0.047	378	5.0	623	24	13.5	0.01279 (0.17)	0.0841 (0.50)	0.04766 (0.41)	81.9 (0.3)	82.0 (0.8)	83 (19)
B	0.059	261	3.4	1029	12	13.1	0.01270 (0.12)	0.0838 (0.36)	0.04784 (0.29)	81.4 (0.2)	81.7 (0.6)	92 (14)
C	0.066	204	2.7	781	14	13.9	0.01286 (0.14)	0.0847 (0.40)	0.04776 (0.33)	82.4 (0.2)	82.5 (0.6)	87 (16)
D	0.050	427	5.6	1563	11	8.7	0.01321 (0.14)	0.0871 (0.28)	0.04785 (0.22)	84.6 (0.2)	84.8 (0.5)	92 (10)
AS-099a (Flow foliated rhyolite)												
A	0.006	499	7.6	915	3	11.2	0.01504 (0.65)	0.1087 (1.7)	0.05245 (1.5)	96.2 (1.2)	104.8 (3.4)	305 (66/68)
B	0.010	314	5.6	56	95	8.1	0.01789 (1.4)	0.1390 (4.6)	0.05634 (3.9)	114.3 (3.2)	132 (12)	466 (163/182)
C	0.008	587	8.3	573	8	8.2	0.01437 (0.15)	0.0955 (0.62)	0.04821 (0.55)	92.0 (0.3)	92.6 (1.1)	110 (26)
D	0.008	853	11	652	9	9.5	0.01278 (0.30)	0.0846 (1.6)	0.04801 (1.5)	81.9 (0.5)	82.5 (2.5)	100 (69/72)
AS-035a (Welded lapilli dacite tuff)												
B	0.012	431	6.5	1117	4	15	0.01427 (0.20)	0.0951 (0.62)	0.04834 (0.55)	91.3 (0.4)	92.2 (1.1)	116 (26)
C	0.013	441	5.8	565	8	15.6	0.01224 (0.28)	0.0836 (0.75)	0.04953 (0.69)	78.4 (0.4)	81.5 (1.2)	173 (32)
D	0.007	328	4.5	754	2	14.7	0.01289 (0.35)	0.0842 (1.9)	0.04740 (1.8)	82.6 (0.6)	82.1 (3.0)	69 (84/89)

[1] Zircon fraction identifier
Zircons are non-magnetic on a Frantz magnetic separator at field strength of 1.8 A with: m5=magnetic at side slope 5°, m2=magnetic at side slope 2°, n2=non-magnetic at side slope 2°, n1=non-magnetic at side slope 1°
Grain size: vc=>134 µm, c=<134 µm and >104 µm, m=<104 µm and >74 µm, f=<74 µm
Air abraded fractions are marked with s=strong, m=medium, n=non-abraded
Grain shape: el=elongate, eq=equant, eu=euhedral, p=prismatic, s=stubby, su=subhedral, an=anhedral, ta=tabular, ti=tips or n=needles
[2] U blank correction of 1 pg ± 20%; U fractionation corrections were measured for each run with a double ^{233}U-^{235}U spike (about 0.005/amu)
[3] Radiogenic Pb
[4] Measured ratio corrected for spike and Pb fractionation of 0.0037/amu ± 20% (Daly collector) which was determined by repeated analysis of NBS Pb 981 standard
[5] Total common Pb in analysis based on blank isotopic composition
[6] Corrected for blank Pb, U and common Pb. Common Pb corrections based on Stacey and Kramers (1975) model Pb at the age of the rock or the $^{207}Pb/^{206}Pb$ age of the rock

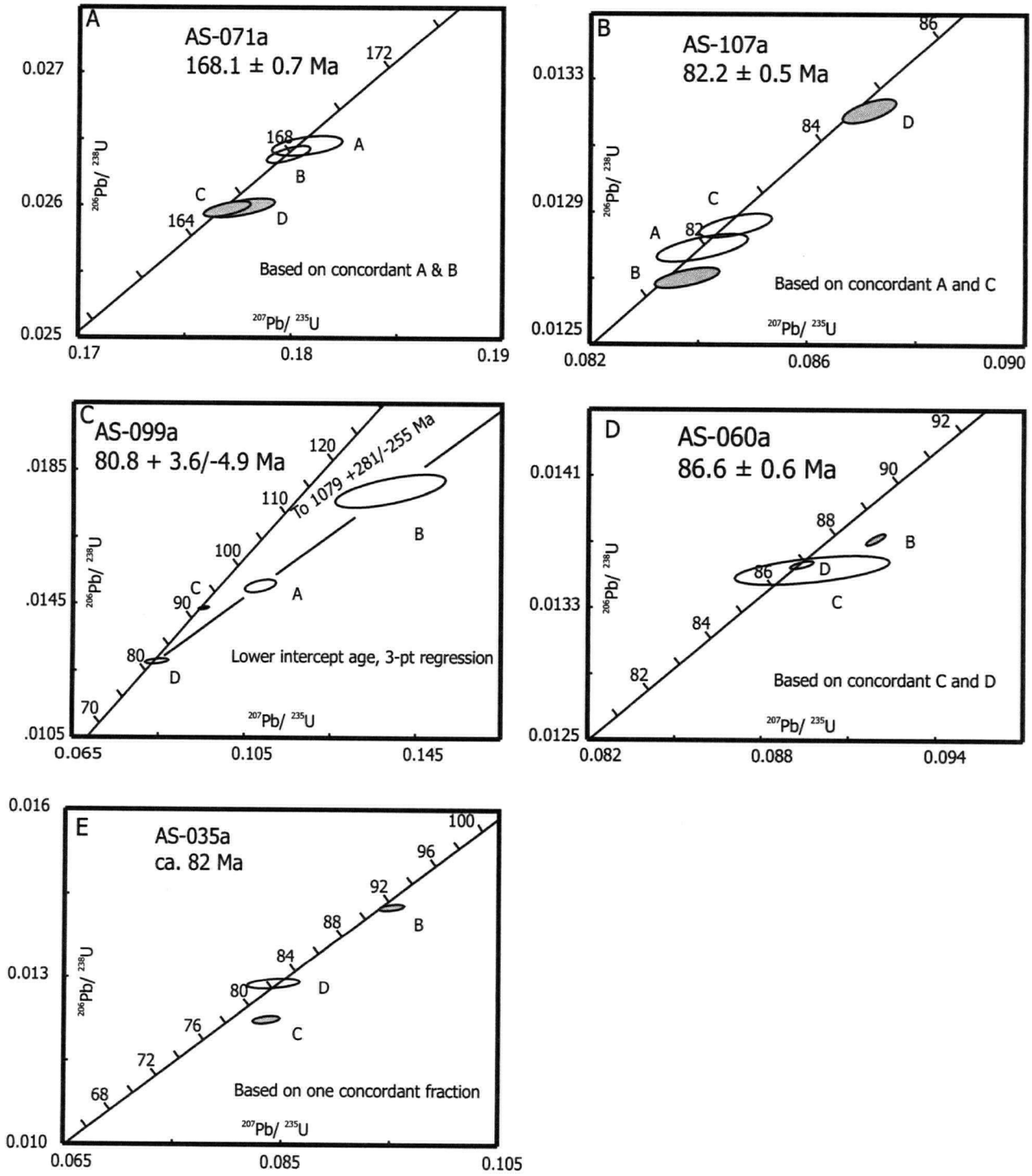

Figure 2-6: U/Pb concordia plots for intrusive and extrusive rock from the Thorn Property. Zircon for these samples were analyzed by the ID-TIMS method. Open boxes and closed boxes denote fractions used and rejected for the age calculation. Refer to appendix 1 for the interpretations.

Several other small Thorn Stock-like intrusive rocks have been mapped and sampled between the Golden Bear Mine and Taku River. However, assigning plutonic rocks to particular periods of magmatic activity is difficult, as similar lithologies are known to intrude as part of the Tertiary Sloko magmatic epoch (Mihalynuk, 1999; Simmons *et al.*, 2005). Sloko intrusive rocks that appear similar may only be distinguished from Thorn Suite visually by containing only up to 2% quartz phenocrysts (always less than 3 mm across) and by their relatively fresh nature containing unaltered plagioclase phenocrysts. In the study area, only three ages have been reported as age-equivalent to the Thorn Suite. Mihalynuk *et al.* (2003) reports a U-Pb TIMS zircon age of 93.3 ± 2.4 Ma for the Thorn Stock; a U-Pb SHRIMP-RG zircon age of 90.6 ± 1.1 Ma, as part of this study confirms this age (Figures 2-3, 2-4A; Appendix I). This new age should is interpreted as a minimum age because the sample has experienced significant Pb loss (Figure 2-4A), but is still within error of the age reported by Mihalynuk *et al.* (2003). Other related intrusions include a texturally similar, slightly smaller stock, located 4 km to the NE of the Thorn Stock with a U-Pb SHRIMP-RG zircon age of 87.6 ± 1.2 Ma and a U-Pb TIMS zircon age of 86.6 ± 0.6 Ma (Figure 2-4B and 2-6D; Appendix I).

Windy Table Suite Magmatism (86-80 Ma)

On the Thorn Property the onset of the Windy Table Suite is recorded by an U-Pb SHRIMP-RG zircon age of 85.5 ± 0.7 Ma (Figures 2-3, 2-4C) on the basal unit of approximately 1.5 km of largely pyroclastic sequence of stratigraphy, which unconformably overlie the Thorn Stock (Figure 2-8A). However, elsewhere along the volcanoplutonic belt there are plutons slightly older than the onset of Windy Table volcanism on the Thorn Property. These plutons occur north of the Thorn Property in the Mt. Lester Jones area and southeast of the Thorn Property in the Inklin River area and yield U-Pb SHRIMP-RG zircon ages of 88.0 ± 0.6 Ma and 87.7 ± 1.1 Ma (Figures 2-2, 2-5E & 2-5F), respectively. These plutons, while close in age to the Thorn Suite rocks, are texturally distinct form the Thorn Suite, and compositionally are more closely related to the Windy Table Suite. Thus, it can be expected that the onset of Windy Table magmatism regionally is variable. Volcanic rocks at the Thorn Property are intruded by several small co-magmatic plutons, which contain a wide variety of textures and are generally more monzonitic or granitic than the Thorn Suite plutons.

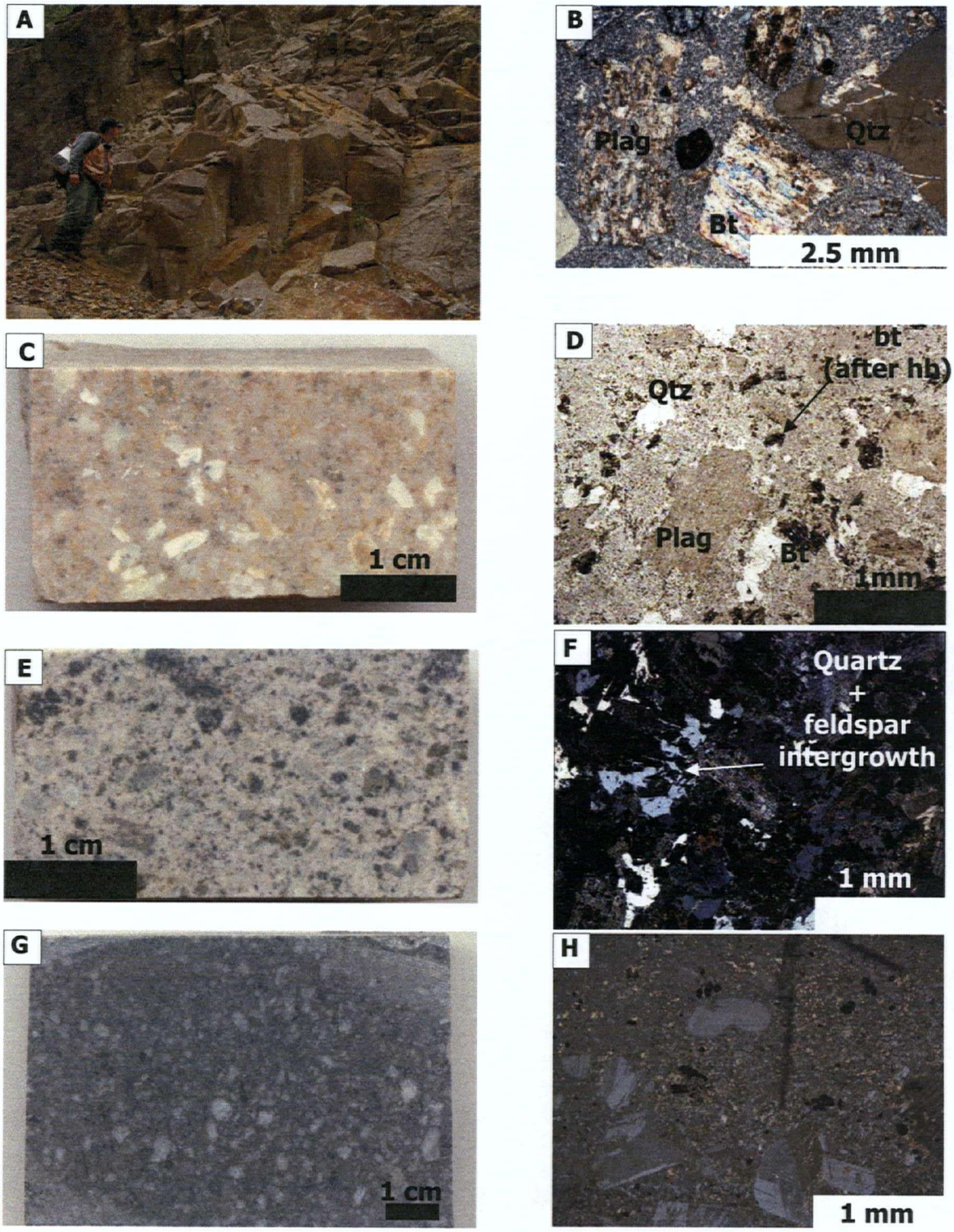

Figure 2-7: Photos and photomicrographs of plutonic textures from igneous rocks in the study area. A) columnar jointing in the Thorn Stock; B) photomicrograph of Thorn Stock with altered biotite and plagioclase and embayed quartz phenocrysts in fine grained sericite/chlorite matrix (crossed polars); C) Type 1 Windy Table intrusion from the Cirque with large plagioclase phenocrysts; D) photomicrograph of C) with irregular quartz, and biotite after hornblende in fine sericite matrix; E) Type 2 Windy Table intrusion from the Cirque; F) photomicrograph of E) showing the granophyric texture (crossed polars); G) Sloko intrusive rock with plagioclase, biotite and quartz phenocrysts; H) photomicrograph of G) showing unaltered plagioclase and quartz phenocrysts in a fine-grained plagioclase-sericite matrix. Qtz=quartz, Plag=plagioclase feldspar, bt=biotite, hb=hornblende

Volcanic Rocks

Cretaceous subaerial volcanic and sedimentary rocks are rare but important strata throughout the northern Canadian Cordilleran (Mihalynuk, 1999). Plutonic equivalents of these strata are more common (see below). In the study area, these strata form three volcanic centres at Lisadele Lake, the Thorn Property and the Metla Property (approximately 20 km SE of Thorn; Figure 2-1), each is separated by 10-20 km, and are generally only a couple of hundred metres thick, except at the Thorn Property, where the thickest sequence of Windy Table Suite volcanic strata are preserved. These volcanic deposits overlie Stuhini Group rocks in the Tun and Sutl areas. Together, these volcanic and plutonic rocks are part of a northwesterly trending magmatic belt with associated hydrothermal alteration and mineralization.

Historically, these strata were mapped as Tertiary Sloko Group volcanic rocks (*ca.* 55 Ma) by Souther (1971) in the Tulsequah map area. However, Mihalynuk *et al.* (2003) reported a U-Pb zircon age of 82.8 ± 0.6 Ma from a rhyolite breccia on the Thorn Property (Figure 2-3), which suggests that the Sloko Group mapped by Souther (1971) likely includes significant Late Cretaceous volcanic rocks. Subsequent mapping and U-Pb geochronology (summarized in Figures 2-4; 2-5; 2-6) has confirmed the ages and extended the belt of Late Cretaceous volcanic rocks north and south of the Thorn Property. These rocks are considered correlative to the Windy Table Suite volcanic rocks described by Mihalynuk (1999) in the Tagish Lake area (Figure 2-1).

The best known preserved section of these strata is located at the Thorn Property. Here, approximately 1600 m of subaerial volcanic and related sedimentary rocks are preserved. The Thorn volcanic sequence is characterized by flat-lying strata, except around the margins, where the contact between older strata and Late Cretaceous volcanic rocks is steeply faulted, causing local rotation and tilting of volcanic stratigraphy. This faulted margin is continuous along the eastern contact and forms a curvilinear trace across the geologic map (Figure 2-3). Spatially limited outcroppings of megabreccia (boulder sized fragments of surrounding Triassic and Jurassic country rocks with lesser felsic volcanic rocks, contained in an glassy, ±welded, ash matrix) are present near the fault trace, implying that the fault trace may mark the outer limit of the eruptive centre. Along La Jaune Creek, the Thorn Stock and Windy Table volcanic rocks are faulted against Stuhini Group rocks, which rise some 3000 m topographically above the known base of the Windy Table volcanic strata and some 1000 m above the topographically highest outcrops of Windy Table strata (Figure 2-3). Three distinct periods of volcanism are

present at the Thorn: 1) Phase 1, which includes the basal stratigraphy and is composed mainly of andesitic to dacitic pyroclastic rocks with lesser reworked volcaniclastic rocks, 2) Phase 2, which overlies Phase 1 and is composed of a rhyolite flow dome complex, and 3) Phase 3, which overlies Phase 2 and is composed of a thick sequence of dacitic pyroclastic rocks (Figure 2-3).

The basal contact of the Windy Table Suite volcanic rocks crops out for several tens of metres in Amarillo Creek at the Thorn Property (Figure 2-3, 2-8A). Here, the basal contact is a monomictic clast-supported, cobble to boulder conglomerate. Clasts are typically rounded and composed of quartz-feldspar-biotite porphyritic diorite to quartz diorite similar to the underlying Thorn Stock. The conglomerate matrix is made up of coarse- to fine-sand sized detritus, chiefly composed of diorite, rounded quartz, broken biotite and subrounded feldspar, which have been replaced by sericite.

Above the basal conglomerate is a 120 m succession composed dominantly of dacitic to andesitic lapilli tuffs with lesser flows and volcaniclastic rocks, which comprises the lower strata of Phase 1 (Figure 2-3, 2-9). Individual beds do can not be traced for more than 10's metres along strike due to a lack of marker horizons and probable rapid lateral facies changes. Tuffs are unwelded to weakly welded and commonly contain plant and wood debris. In Amarillo Creek, a 15-80 cm lithic-poor, weakly welded, dacitic crystal tuff directly overlies the basal conglomerate (Figure 2-8B). This tuff has a U-Pb SHRIMP-RG zircon age of 85.5 ± 0.7 Ma (Figures 2-3, 2-4C; Appendix I). This age marks the onset of Windy Table volcanism on the Thorn Property. Flow-foliated rocks in Amarillo Creek are steeply dipping and cut through the tuffaceous stratigraphy. These units may have served as feeder units to extrusive flow domes some 300 m up section where the flow foliated units have more of a horizontal geometry with convoluted flow folds. Similar flow-foliated units in Faraway Creek have a U-Pb TIMS zircon age of 80.8 +3.6/-4.9 Ma (Figures 2-3, 2-6C; Appendix I)). Stratigraphically above the tuff-dominated strata is a 80 m section of volcaniclastic-dominated strata with lesser tuffs (Figure 2-9). Individual beds are poorly sorted, can be difficult to distinguish, and are laterally discontinuous due to intense post depositional block faulting and overburden. Typically, clasts are volcanic rocks with lesser sedimentary rocks and intrusive rocks. Clasts are subrounded to rounded, and range in size from boulder to fine sand. A 360 m-section dominated by dacitic lapilli tuff overlies the volcaniclastic rocks (Figure 2-9). This section is texturally similar to the lowermost sequence of tuffs. Approximately 15 m above the volcaniclastic sequence is a 5 m thick feldspar phenocrystic trachyte flow, which yielded a U-Pb SHRIMP-RG zircon age of 81.4 ± 0.9 Ma (AS-035a, Figure 2-4F).

Stratigraphically above the tuff and volcaniclastic dominated sequence of Phase 1 is a 340 m thick section of flows, domes, and intrusive rocks of Phase 2. At the headwaters of Amarillo Creek is series of vertical dykes, which are inferred to be feeders to the extrusive lavas, as well as domes (Figure 2-9). Here, the domes and dykes are flow-foliated. Foliation is generally flat-lying, but is locally intensely folded (syn-magmatic) and steeply dipping in the feeder dykes. Overall, the lava-dominated section is characterized by fine-grained, dacitic quartz-feldspar-biotite phyric flow foliated units (Figure 2-8E) at the base that upsection become coarser grained quartz-feldspar phenocrystic coherent rhyolite (Figure 2-8G). Flow foliations are defined by aligned, rounded, microscopic (no larger than 10 μm) quartz (with lesser chlorite) clots separated by wider zones of very fine-grained sericite-chlorite altered matrix (Figure 2-8f). Biotite and feldspar form sparse anhedral phenocrysts up to 1 mm, both are sericite altered, but biotite tends to be fresher than feldspar (Figure 2-8F). Coherent units are very distinct with the dominant phenocrysts being up to 20% rounded quartz (not embayed as in the intrusions around the Thorn), with lesser and finer grained feldspar in a fine-grained pervasive sericite chlorite altered matrix (Figure 2-8H). Minor tuffs and volcanic rocks are intercalated with the lavas. Similar flow foliated units in Faraway Creek have a U-Pb TIMS zircon age of 80.8 +3.6/-4.9 Ma (Figures 2-3, 2-6C). An ^{40}Ar-^{39}Ar cooling age on coarse muscovite (closure temperature ~ 350°C) of 83.1 ± 1.8 Ma (Simmons, 2005) was obtained from a trachyandesite sill intruding the strata about 215 m up from the base of this sequence.

Poorly outcropping pyroclastic strata compose another 900 m that extends to the current top of the volcanic sequence as part of Phase 3 (Figure 2-9). Strata from this interval are variably welded lapilli-block and ash tuffs with variable amounts of crystal components. Limited mapping through this interval show that dense welding occurs near the base of this unit and is separated from the lavas at its base by dark grey ash tuff, which is at least 15 m thick. Upwards through this sequence welding generally decreases with patches of intensely welded tuff. This unit contains variable amounts of lithic, juvenile and crystal fragments throughout. Lithic fragments are rare throughout the 900 m sequence (up to 10% locally) and are most commonly flow foliated dacitic rocks, of Phase 2, and other fine-grained volcanic rocks (Figure 2-8B). Pumice fragments, up to 1 cm long, are relatively common, becoming more flattened where welded (Figure 2-8B). Close to the top of the volcanic sequence, Mihalynuk (2003) reported an U-Pb (zircon) age of 82.8 ± 0.6 Ma (Figure 2-3; 2-9) for a rhyolite.

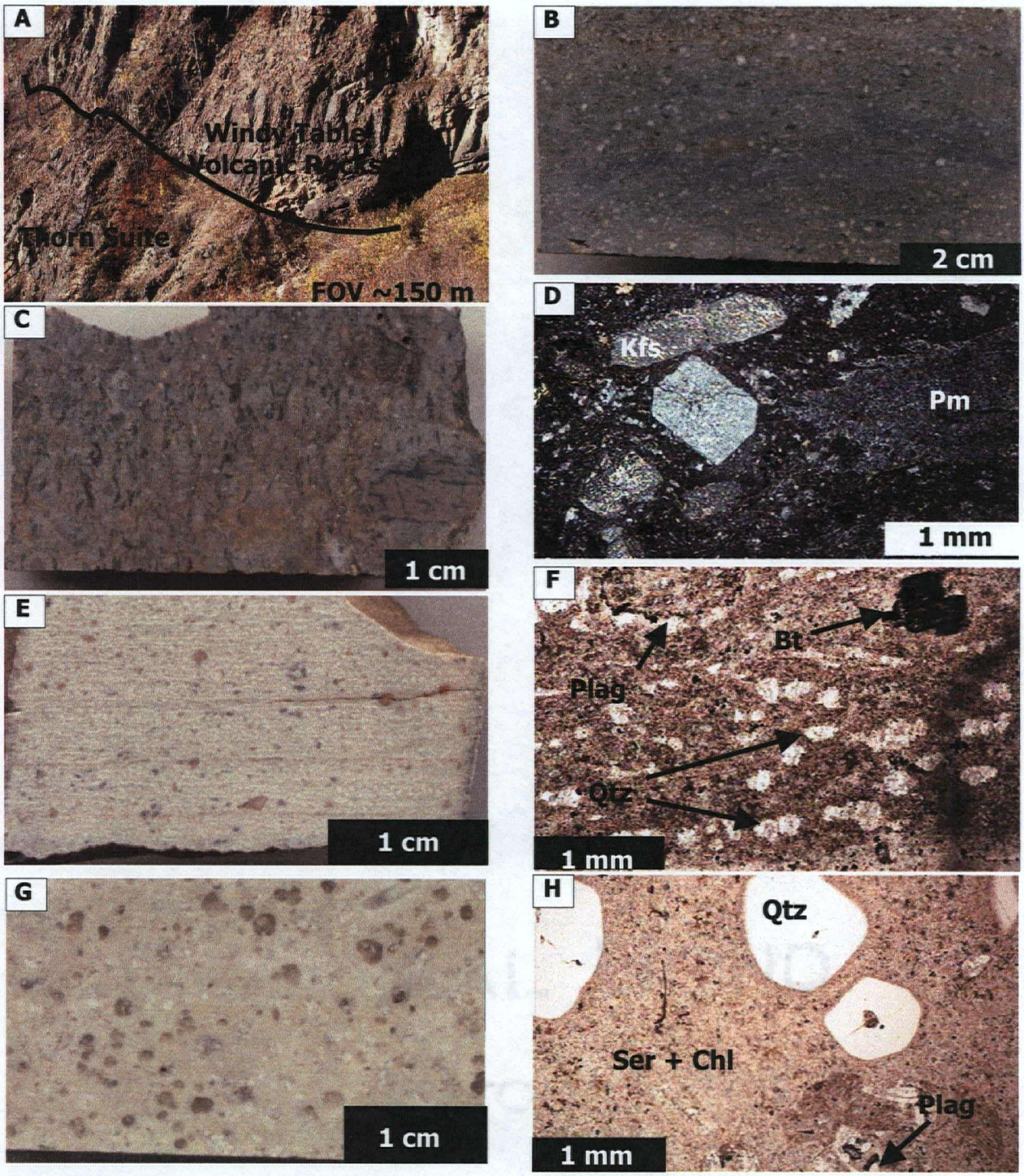

Figure 2-8: Photos and photomicrographs showing volcanic facies variations from Windy Table volcanic rocks. A) Unconformable contact between the Thorn Stock and the overlying Windy Table volcanic rocks. B) Sample 04AS-009 of slightly welded crystal tuff with feldspar fragments visible, unit is part of Phase 1 volcanism directly above the unconformity; C) part of Phase 3 volcanism showing lapilli-sized lithic fragments of flow foliated dacite and fine lapilli-sized fiamme in a moderate to densely welded tuff (crossed polars); D) photomicrograph of C) with pumice fragment and K-feldspar crystals; E) Sample AS-099a, part of Phase 2 volcanism, showing flow foliated rhyolite; F) photomicrograph of E) with fine quartz defining flow foliation with sparse biotite and plagioclase phenocrysts; G) Coherent rocks at core of rhyolite dome with large quartz phenocrysts; H) photomicrograph of G) showing quartz and plagioclase phenocrysts in a fine sericite matrix. Qtz=quartz, Chl=chlorite, Plag= plagioclase feldspar, Ser=sericite, Bt=biotite, Pm=pumice, Kfs=potassium feldspar.

Subvolcanic Intrusive Rocks

The common Windy Table Suite plutonic rocks comprise four different compositional and textural types of intrusions, Types 1 to 4. Type 1 is a biotite-bearing, porphyritic diorite to monzonite that contains conspicuous feldspar phenocrysts. These rocks have associated hydrothermal systems throughout the region. Examples include the 83.8±0.2Ma (MMI94-45-6, Figure 2-2) Mount Lester Jones Porphyry (Mihalynuk *et al.*, 2003), the 87.3±0.9Ma (MMI94-9-4, Figure 2-2) Red Cap Porphyry (Mihalynuk *et al.*, 2003) and the 82.2±0.2Ma (Figure 2-6B) Cirque Monzonite. Type 2 is a biotite-hornblende-bearing, medium-grained, granophyric, monzonite to granodiorite. Examples of these include the 82.0 ± 0.9 Ma monzonite (Figure 2-4E; Appendix I) and the 81.3 ± 0.4 Ma Table Mountain Quartz Monzonite (Figures 2-1, 2-5I; Appendix I). Other examples of this intrusive suite were mapped in the Bryar area and Lisadele Lake area (Figure 2-2). Type 3 intrusions are plagioclase megacrystic dykes and sills. These intrusions are spatially limited to the Sutl area where a U-Pb SHRIMP zircon age of 85.5 ± 0.7 Ma was determined (Figures 2-2, 2-5G; Appendix I). The least prevalent intrusive rocks of the Windy Table Suite are fine-grained, aphanitic trachytic dykes, which crop out on the Thorn Property and form Type 4 intrusions. These rocks could represent subvolcanic equivalents or feeders to the trachytic flows in the Windy Table Volcanic Rocks.

Type 1 intrusive rocks are the most common in the Late Cretaceous volcanoplutonic belt. These rocks range from monzonite to quartz monzonite with rare granodiorite and diorite and are porphyritic. They are characterized by dyke and sill complexes, and less common as small stocks and plutons. Individual dykes may be up to 50 m wide. One of these dykes cuts through the Thorn Stock near the B-zone, which has U-Pb SHRIMP zircon data which suggests that it is less than 86 Ma, but a definitive age could not be determined form the data acquired for this rock (Figure 2-4D). In areas where Windy Table volcanic centres are present, Type 1 intrusive rocks commonly are stocks up to 2 km across. Porphyries may range from crowded to matrix-supported with plagioclase being the dominant phenocrystic phase, while biotite and hornblende are less common. Biotite generally forms irregularly-shaped clots rather than euhedral crystals (Figure 2-7C-D). The matrix is fine grained and equigranular consisting of a combination of fine-grained quartz, K-feldspar and magnetite. Common accessory phases include titanite, apatite, zircon and magnetite with lesser or rare pyroxene. These intrusions commonly have associated weak porphyry Cu-Mo-(Au) mineralization.

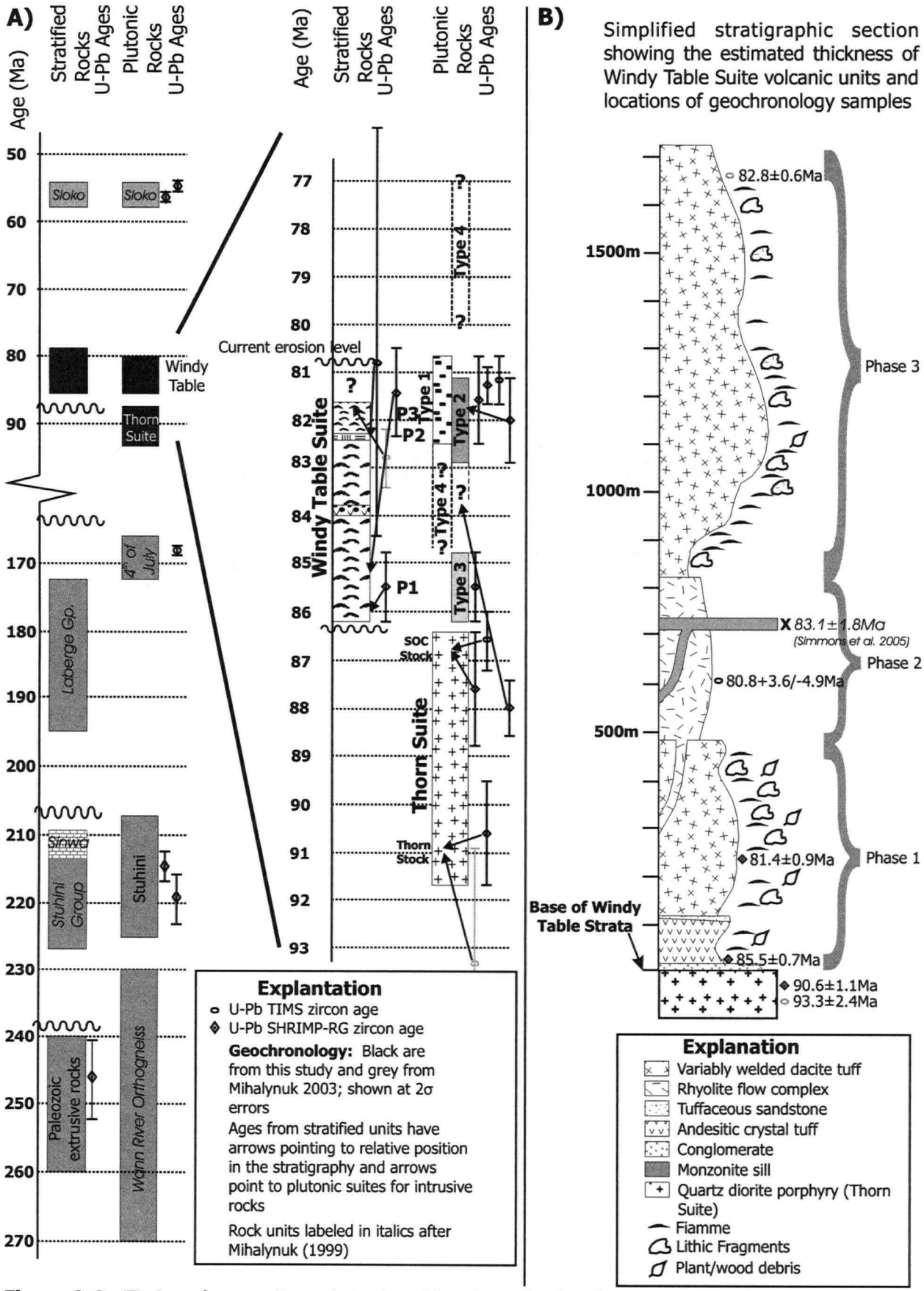

Figure 2-9: Timing of map units and stratigraphic column for the Thorn Property with emphasis on Late Cretaceous magmatic rocks. A) Stratigraphic units plotted against geologic time scale; and B) Stratigraphic section through the Windy Table Suite volcanic rocks.

Type 2 Windy Table intrusive rocks are less common than, but spatially associated with Type 1 intrusions. At the Thorn, in the Cirque area, they appear to be a slightly later phase than the main Type 1 porphyritic Cirque monzonite. Type 2 intrusions always form large stocks and intrusive complexes. At Table Mountain, east of Tatsamenie Lake, these intrusions form a large intrusive complex with Type 1 intrusions and are at least 20 km across. In outcrop, they weather to a salt-and-pepper texture. They appear to be equigranular rocks in hand specimen, but in thin section always have granophyric textures (Figure 2-7E-F). These rocks range from quartz monzonite to monzogranite. Major mineral phases include hornblende, plagioclase and K-feldspar/quartz intergrowths in varying amounts. Common accessory phases include biotite, titanite and magnetite.

Type 3 and 4 Windy Table intrusions are less common and volumetrically less important than Types 1 and 2. Type 3 intrusions are only known in the Sutl area where they form narrow north-trending dykes (Figure 2-2). They characteristically contain megacrystic plagioclase up to 3 cm long. The megacrysts are contained in a matrix, which would otherwise be described as plagioclase-quartz porphyry with lesser hornblende in a matrix of fine-grained quartz and K-feldspar. Type 4 intrusions occur only as narrow felsic dykes, in and around Windy Table Suite volcanic centres. These dykes most commonly intrude around the edges of the volcanic centre, however may also be found intruding basal units of the volcanic strata described above. Absolute ages have not been determined for these dykes because no zircon or titanite could be recovered from the samples. However, relative age relations suggest that they are part of the Windy Table suite magmatism.

Sloko Suite Magmatism (58-54 Ma)

Souther (1971) mapped abundant early Tertiary Sloko plutonic and volcanic rocks along the Late Cretaceous volcanoplutonic belt from the Golden Bear area to the Tulsequah area. Between this study and Mihalynuk *et al.* (2003), only two locations are known where unequivocal Sloko plutonic rocks crop out. Both examples are plagioclase-biotite porphyritic diorite in the Lisadele Lake area and the Sutl area, where they intrude into Laberge Group clastic sedimentary rocks. These rocks yielded U-Pb SHRIMP zircon ages of 56.3 ± 0.7 Ma and 55.5 ± 0.6 Ma respectively (Figure 2-5J-K). The petrologic similarity of this rock and the Thorn Stock make it very difficult to unequivocally distinguish the two rock suites in the field. One criteria used to distinguish the two is that Sloko Suite rocks generally contain less quartz and are rarely unaltered.

Mafic Dykes

Mafic dykes are present in the study area. The most prominent set trends between 035° and 050°, and are generally fine-grained, massive, strongly magnetic, basaltic and no wider than 2-5 m. Calcite-filled amygdaloidal basalt, and coarser grained gabbroic dykes are less common. The absolute ages of these dykes are not known, nor is it known how many types and orientations of dykes are present in the study area. However, these dykes cross-cut every major rock unit and mineralized systems in the study area and are not altered. Therefore these dykes are considered to have been emplaced post mineralization, which post dates the youngest known Windy Table strata at 81.4 ± 0.9 Ma (Sample AS-035a; Figure 2-4D). Oliver (1996) mapped similar dykes near the Golden Bear Mine, where they are *ca.* 15 Ma and geochemically similar to the "Level Mountain Basalt".

Lithogeochemistry

Forty-two samples of Late Cretaceous to Tertiary igneous rocks, as well as four pre-Cretaceous igneous rocks and older constituents of the coast batholith were analyzed for major and trace elements to determine geochemical distinctions between the magmatic rock suites. The least altered samples were selected for this study.

Results

All samples were analyzed for major elements oxide and trace element concentrations at ALS Chemex Laboratories Limited in North Vancouver, Canada (Table 2-3). Major elements and selected trace elements were determined by X-ray fluorescence spectrometry (XRF). Rare earth elements (REE) and remaining trace elements were determined by inductively coupled plasma mass spectrometry (ICP-MS).

Major Element Geochemistry

Using major element geochemistry to classify rocks at the Thorn Property is problematic due to high degrees of acid leaching and alteration, which results in a net loss of CaO and Na_2O and potential increases in K_2O, Al_2O_3 and SiO_2. Nonetheless in order to build criteria to distinguish these rocks from each other and varying degrees of alteration, representative rock units judged to be in their least altered states were analyzed. High degrees of variation in K_20 and Na_2O with respect to silica indicate that some of the major elements were at least in part mobile during post emplacement processes, such as alteration (e.g. Figure 2-10A & C). However, trends which reflect fractionation processes are still present (e.g. Figure 2-10D, E-H).

Table 2-3: Geochemistry of Rocks from the study area

		Stuhini Group				4th of July		Thorn Plutonic Suite		
Sample		AS70a	AS70a2	04AS27	04AS28	AS71a	AS71a2	277510	277540	AS68b
SiO_2	wt%	47.31	47.21	56.8	63.5	73.55	73.68	58.87	60.89	61.93
TiO_2	wt%	0.94	0.93	0.79	0.45	0.51	0.56	0.44	0.38	0.47
Al_2O_3	wt%	17.58	17.6	18.7	17.85	14.75	14.9	16.13	15.54	15.79
Fe_2O_3	wt%	10.56	10.43	4.24	3.74	2.55	2.5	4.43	3.63	4.36
FeO	wt%	6.29	6.21	2.52	2.23	2.12	1.61	3.15	1.74	2.96
MnO	wt%	0.17	0.16	0.06	0.07	0.03	0.02	0.16	0.41	0.08
MgO	wt%	4.71	4.61	3.43	0.88	0.93	0.89	2.64	2.48	1.55
CaO	wt%	5.79	6.04	6.73	3.3	0.08	0.06	4.69	3.92	3.89
Cr_2O_3	wt%	0.02	0.02	0.01	0.01	0.02	0.01	0.01	0.01	0.01
Na_2O	wt%	4.15	4.12	6.29	5.56	0.09	0.06	2.38	1.24	3.2
K_2O	wt%	1.07	1.14	0.86	3.12	3.58	3.7	2.12	3.08	2.31
BaO	wt%	0.04	0.04	0.04	0.15	0.08	0.10	0.17	0.13	0.26
P_2O_5	wt%	0.19	0.19	0.33	0.15	0.04	0.03	0.19	0.16	0.19
LOI	wt%	7.01	6.89	1.53	1.73	2.97	2.79	7.04	6.31	4.26
Total	wt%	*99.58*	*99.41*	*99.9*	*100.5*	*99.19*	*99.29*	*99.35*	*98.2*	*98.39*
Ba	ppm	199.5	239.0	337.0	1595.0	653.0	807.0	1540.0	1115.0	2510.0
Co	ppm	33.5	32.5	11.5	8.7	3.7	3.8	10.5	5.6	7.9
Cr	ppm	120.0	120.0	60.0	100.0	190.0	110.0	80.0	110.0	90.0
Cs	ppm	12.7	17.5	1.2	2.6	12.1	5.9	6.4	5.2	7.8
Cu	ppm	132.0	132.0	47.0	15.0	6.0	------	20.0	------	27.0
Ga	ppm	16.0	16.0	22.0	23.0	16.0	17.0	18.0	17.0	19.0
Hf	ppm	2.0	1.0	5.0	3.0	5.0	4.0	3.0	3.0	3.0
Mo	ppm	------	------	2.0	3.0	2.0	4.0	------	------	3.0
Nb	ppm	2.0	2.0	6.0	8.0	5.0	5.0	6.0	7.0	7.0
Ni	ppm	33.0	33.0	19.0	12.0	12.0	11.0	11.0	8.0	9.0
Pb	ppm	5.0	7.0	16.0	9.0	6.0	6.0	17.0	15.0	22.0
Rb	ppm	46.3	52.2	23.5	83.4	88.8	99.4	45.2	80.1	86.6
Sn	ppm	1.0	1.0	2.0	1.0	2.0	2.0	------	------	2.0
Sr	ppm	529.0	538.0	896.0	818.0	34.6	35.4	740.0	213.0	807.0
Ta	ppm	------	------	0.5	------	------	------	------	0.5	0.5
Th	ppm	1.0	1.0	4.0	4.0	4.0	4.0	8.0	7.0	9.0
Tl	ppm	------	------	------	------	0.5	0.6	------	1.4	0.6
U	ppm	0.7	0.6	2.0	1.7	1.1	1.1	6.2	4.4	5.2
V	ppm	366.0	353.0	201.0	80.0	50.0	54.0	95.0	62.0	87.0
W	ppm	1.0	1.0	4.0	2.0	1.0	2.0	1.0	1.0	1.0
Y	ppm	15.9	16.8	20.1	15.0	48.5	30.4	14.0	12.4	13.0
Zn	ppm	74.0	72.0	46.0	46.0	34.0	31.0	71.0	47.0	486.0
Zr	ppm	45.9	44.1	166.0	133.0	146.5	138.0	92.1	95.4	117.5
La	ppm	5.1	5.0	9.7	14.0	22.5	17.2	24.3	21.7	25.4
Ce	ppm	12.1	12.0	21.4	32.9	42.8	38.9	44.6	41.0	46.4
Pr	ppm	1.7	1.7	2.7	3.0	5.9	4.4	4.8	4.5	5.2
Nd	ppm	7.9	8.2	13.1	13.2	26.0	18.2	18.4	17.1	20.5
Sm	ppm	2.3	2.4	3.1	3.3	6.5	4.3	3.3	3.0	3.6
Eu	ppm	0.7	0.8	0.8	1.1	1.3	0.9	0.8	0.9	1.0
Gd	ppm	2.6	2.7	3.4	2.9	7.0	4.4	3.0	2.8	3.2
Tb	ppm	0.5	0.5	0.5	0.4	1.3	0.8	0.4	0.4	0.4
Dy	ppm	2.8	2.9	3.5	2.4	7.9	5.0	2.3	2.1	2.3
Ho	ppm	0.6	0.6	0.7	0.5	1.7	1.1	0.4	0.4	0.4
Er	ppm	1.7	1.8	2.2	1.5	5.1	3.2	1.3	1.3	1.3
Tm	ppm	0.3	0.3	0.3	0.2	0.8	0.5	0.2	0.2	0.2
Yb	ppm	1.7	1.7	2.1	1.4	5.1	3.5	1.3	1.2	1.3
Lu	ppm	0.3	0.3	0.3	0.2	0.9	0.6	0.2	0.2	0.2

Major oxide concentrations from XRF; all others by ICP-MS, from ALS Chemex, North Vancouver, B.C.

Table 2-3: Continued

		Thorn Suite		Windy Table Volcanic Rocks							
Sample		4AS12	AS60a	AS16a	AS17a	AS20a	AS33a	AS34a	AS35a	AS52a	AS56a
SiO_2	wt%	60.9	60.9	72.75	64.39	54.17	59.8	64.98	71.99	74.04	76.19
TiO_2	wt%	0.43	0.48	0.37	0.38	0.69	0.63	0.42	0.15	0.16	0.07
Al_2O_3	wt%	17.25	16.09	14.86	14.8	14.64	16.49	16.11	13.94	13.91	12.54
Fe_2O_3	wt%	4.42	4.35	2.05	3.02	6.53	6.22	3.07	1.66	1.1	1.06
FeO	wt%	4.18	3.28	0.64	1.54	4.89	3.80	0.96	0.64	0.39	0.39
MnO	wt%	0.1	0.13	0.02	0.09	0.16	0.07	0.07	0.08	0.02	0.02
MgO	wt%	1.5	1.48	0.42	0.82	3.73	1.24	0.3	0.2	0.14	0.11
CaO	wt%	3.1	4.68	0.24	3.06	5.83	3.54	2.63	1.23	0.48	0.06
Cr_2O_3	wt%	------	0.01	0.02	0.02	0.02	0.01	0.01	0.03	0.01	0.02
Na_2O	wt%	4.14	2.8	1.76	2.93	2.62	2.27	2.91	3.07	2.58	2.43
K_2O	wt%	2.7	2.28	3.53	4.62	2.88	2.59	4.59	3.92	5.67	5.6
BaO	wt%	0.22	0.21	0.07	0.14	0.11	0.27	0.21	0.12	0.16	0.06
P_2O_5	wt%	0.19	0.2	0.15	0.18	0.26	0.25	0.16	0.04	0.04	0.02
LOI	wt%	3.21	5.95	3.03	5.16	7.70	6.35	3.50	2.75	1.42	1.34
Total	wt%	*98.3*	*98.86*	*99.28*	*99.63*	*99.38*	*99.78*	*99.02*	*99.2*	*99.74*	*99.53*
Ba	ppm	2110.0	2050.0	495.0	1265.0	993.0	2580.0	1890.0	1040.0	1435.0	410.0
Co	ppm	8.7	6.9	4.1	6.4	23.5	12.2	5.9	1.4	0.9	0.8
Cr	ppm	50.0	70.0	150.0	160.0	140.0	70.0	90.0	210.0	100.0	190.0
Cs	ppm	3.0	8.0	5.9	8.5	10.8	15.0	5.2	3.5	5.8	2.1
Cu	ppm	10.0	5.0	6.0	18.0	60.0	36.0	15.0	------	9.0	------
Ga	ppm	22.0	18.0	17.0	16.0	16.0	17.0	17.0	14.0	13.0	14.0
Hf	ppm	3.0	3.0	4.0	4.0	3.0	4.0	5.0	4.0	4.0	4.0
Mo	ppm	2.0	2.0	5.0	6.0	5.0	------	5.0	2.0	7.0	4.0
Nb	ppm	7.0	6.0	9.0	15.0	9.0	9.0	14.0	12.0	19.0	31.0
Ni	ppm	10.0	7.0	10.0	12.0	32.0	13.0	10.0	7.0	6.0	7.0
Pb	ppm	18.0	15.0	10.0	19.0	12.0	14.0	18.0	20.0	12.0	23.0
Rb	ppm	67.8	72.0	117.0	160.0	80.7	88.0	136.0	112.5	141.5	191.0
Sn	ppm	1.0	1.0	------	1.0	------	------	------	------	------	2.0
Sr	ppm	1290.0	811.0	58.0	353.0	405.0	538.0	551.0	179.5	156.5	76.5
Ta	ppm	0.5	------	0.7	1.2	0.7	0.6	1.2	1.0	1.5	2.6
Th	ppm	8.0	9.0	11.0	18.0	8.0	8.0	15.0	15.0	17.0	27.0
Tl	ppm	------	------	------	------	------	------	0.5	------	0.7	0.9
U	ppm	3.8	5.2	5.0	6.5	4.0	3.5	8.7	5.7	6.8	8.8
V	ppm	94.0	86.0	40.0	51.0	174.0	119.0	58.0	9.0	9.0	2.5
W	ppm	16.0	2.0	3.0	3.0	2.0	1.0	3.0	2.0	2.0	5.0
Y	ppm	15.6	13.8	8.6	12.2	17.2	15.2	16.8	11.1	11.6	29.8
Zn	ppm	57.0	49.0	35.0	47.0	63.0	84.0	50.0	42.0	29.0	26.0
Zr	ppm	104.0	102.5	146.5	147.0	106.0	119.5	167.0	145.0	127.5	81.2
La	ppm	26.6	25.6	29.5	30.6	19.6	25.1	30.2	29.4	33.9	20.3
Ce	ppm	46.8	46.4	53.1	53.8	37.2	46.7	55.2	49.6	56.5	44.4
Pr	ppm	5.0	5.3	5.4	5.3	4.0	5.1	5.7	4.7	5.6	5.1
Nd	ppm	20.7	20.6	19.1	18.3	15.6	19.0	20.5	15.1	17.2	18.3
Sm	ppm	3.7	3.6	2.9	3.0	3.2	3.6	3.8	2.3	2.7	4.6
Eu	ppm	1.2	1.0	0.6	0.7	0.9	0.9	0.9	0.5	0.5	0.2
Gd	ppm	3.5	3.3	2.6	3.0	3.2	3.4	3.6	2.4	2.7	4.4
Tb	ppm	0.5	0.5	0.3	0.4	0.5	0.5	0.5	0.3	0.4	0.8
Dy	ppm	2.6	2.4	1.5	2.2	2.9	2.7	2.8	1.7	1.8	4.6
Ho	ppm	0.5	0.5	0.3	0.4	0.6	0.5	0.5	0.3	0.4	0.9
Er	ppm	1.5	1.4	0.9	1.2	1.7	1.6	1.7	1.1	1.1	2.9
Tm	ppm	0.2	0.2	0.1	0.2	0.3	0.2	0.2	0.2	0.2	0.4
Yb	ppm	1.4	1.4	0.8	1.3	1.6	1.4	1.7	1.2	1.2	3.0
Lu	ppm	0.2	0.2	0.1	0.2	0.3	0.2	0.3	0.2	0.2	0.5

Major oxide concentrations from XRF; all others by ICP-MS, from ALS Chemex, North Vancouver, B.C.

Table 2-3: Continued

		Windy Table Volcanic Rocks						Windy Table Intrusive Rocks			
Sample		AS58a	AS61a	4AS9	4AS13	4AS20	4AS29	AS63a	AS66a	AS68e	AS86a
SiO_2	wt%	76.06	55.48	61.4	63.1	43.3	81.9	70.44	65.99	64.51	59.85
TiO_2	wt%	0.07	0.58	0.56	0.47	0.25	0.06	0.25	0.5	0.55	0.74
Al_2O_3	wt%	12.59	13.91	18.1	15.85	4.51	10.55	14.8	14.95	15.21	16.46
Fe_2O_3	wt%	1.31	5.22	4.49	4.61	6.14	0.71	1.85	3.43	4.11	6.17
FeO	wt%	0.84	3.80	4.23	4.29	7.20	0.66	1.03	2.44	2.89	3.80
MnO	wt%	0.06	0.31	0.12	0.11	0.1	------	0.06	0.1	0.1	0.12
MgO	wt%	0.12	3.8	1.4	1.68	12.25	0.09	0.62	1.4	1.78	2.78
CaO	wt%	0.47	6.69	3.15	3.41	8.75	0.03	1.5	2.47	2.71	4.58
Cr_2O_3	wt%	0.04	0.03	------	0.01	0.14	0.01	0.02	0.02	0.02	0.03
Na_2O	wt%	1.86	2.57	4.45	3.95	0.05	1.1	3.01	3.61	3.78	3.61
K_2O	wt%	4.79	2.62	1.48	2.95	1.27	2.31	4.37	4.39	4.4	3.58
BaO	wt%	0.03	0.11	0.16	0.20	------	0.06	0.19	0.12	0.13	0.14
P_2O_5	wt%	0.01	0.25	0.17	0.18	------	------	0.07	0.18	0.23	0.35
LOI	wt%	2.16	7.62	4.31	2.78	23.40	1.85	2.05	2.14	1.78	1.44
Total	wt%	*99.58*	*99.22*	*99.9*	*99.4*	*100.00*	*98.7*	*99.27*	*99.34*	*99.37*	*99.93*
Ba	ppm	102.5	841.0	1560.0	1580.0	26.0	572.0	1700.0	1045.0	1120.0	1295.0
Co	ppm	0.9	15.1	13.8	8.4	47.3	0.6	2.6	8.0	8.5	15.9
Cr	ppm	310.0	240.0	40.0	60.0	1120.0	100.0	210.0	160.0	160.0	240.0
Cs	ppm	3.7	8.6	17.6	7.2	25.6	4.2	5.8	6.7	8.6	3.1
Cu	ppm	------	26.0	16.0	12.0	56.0	27.0	24.0	14.0	13.0	37.0
Ga	ppm	16.0	15.0	22.0	19.0	6.0	14.0	16.0	16.0	17.0	18.0
Hf	ppm	4.0	3.0	4.0	3.0	1.0	4.0	5.0	6.0	6.0	5.0
Mo	ppm	2.0	4.0	3.0	2.0	------	4.0	9.0	8.0	8.0	4.0
Nb	ppm	24.0	9.0	11.0	9.0	1.0	19.0	17.0	18.0	19.0	15.0
Ni	ppm	9.0	53.0	20.0	9.0	505.0	8.0	9.0	12.0	16.0	22.0
Pb	ppm	17.0	99.0	27.0	20.0	2.5	26.0	28.0	20.0	21.0	19.0
Rb	ppm	175.0	81.2	37.4	80.5	66.9	104.5	132.0	165.5	174.0	110.5
Sn	ppm	1.0	1.0	1.0	1.0	1.0	1.0	1.0	1.0	2.0	2.0
Sr	ppm	63.8	590.0	1120.0	706.0	181.0	44.6	281.0	389.0	469.0	681.0
Ta	ppm	2.0	0.6	0.7	0.7	------	2.6	1.2	1.5	1.5	1.0
Th	ppm	22.0	6.0	7.0	12.0	0.5	37.0	14.0	20.0	18.0	10.0
Tl	ppm	0.5	------	------	------	0.9	0.6	0.8	0.7	0.8	------
U	ppm	3.2	2.6	14.2	4.1	0.3	7.6	3.7	8.6	6.8	3.5
V	ppm	2.5	104.0	112.0	89.0	107.0	5.0	23.0	63.0	78.0	120.0
W	ppm	3.0	1.0	4.0	10.0	3.0	3.0	3.0	3.0	3.0	3.0
Y	ppm	30.7	15.2	15.6	15.6	5.5	14.6	13.2	15.6	15.8	16.8
Zn	ppm	63.0	308.0	136.0	64.0	38.0	18.0	37.0	46.0	56.0	67.0
Zr	ppm	88.0	105.5	134.0	96.4	18.0	91.6	181.0	187.0	214.0	167.5
La	ppm	19.4	20.1	29.4	23.8	2.5	32.0	34.5	31.4	33.6	29.8
Ce	ppm	43.3	36.7	54.1	36.4	4.7	56.1	58.0	55.9	61.1	54.1
Pr	ppm	5.1	4.2	4.9	4.2	0.6	5.3	5.8	5.8	6.4	6.0
Nd	ppm	18.6	15.7	19.2	17.1	2.9	19.4	19.5	20.1	22.6	22.5
Sm	ppm	4.9	3.2	4.0	3.1	0.7	3.2	3.1	3.5	4.0	4.1
Eu	ppm	0.2	0.9	1.4	0.9	0.3	0.3	0.7	0.8	0.9	1.1
Gd	ppm	4.5	3.1	3.5	3.1	0.8	3.1	3.0	3.4	3.7	4.1
Tb	ppm	0.8	0.5	0.5	0.4	0.1	0.4	0.4	0.5	0.5	0.6
Dy	ppm	4.8	2.7	2.7	2.6	0.8	2.1	2.1	2.6	2.8	3.2
Ho	ppm	1.0	0.5	0.5	0.5	0.2	0.4	0.4	0.5	0.6	0.6
Er	ppm	3.1	1.5	1.6	1.6	0.5	1.3	1.3	1.5	1.6	1.7
Tm	ppm	0.5	0.2	0.2	0.2	0.1	0.2	0.2	0.2	0.2	0.2
Yb	ppm	3.2	1.4	1.5	1.6	0.5	1.4	1.4	1.7	1.6	1.6
Lu	ppm	0.5	0.2	0.2	0.2	0.1	0.2	0.3	0.3	0.3	0.3

Major oxide concentrations from XRF; all others by ICP-MS, from ALS Chemex, North Vancouver, B.C.

Table 2-3: Continued

		Windy Table Intrusive Rocks						Felsic Dykes (post mineral)		
Sample		AS107a	AS107a2	4AS25	4AS03	4AS22	4AS23	277515	AS21a	AS64a
SiO_2	wt%	68.01	67.75	65.7	65.8	64.3	63.1	80.78	78.82	77.15
TiO_2	wt%	0.39	0.39	0.4	0.37	0.27	0.4	0.02	0.04	0.06
Al_2O_3	wt%	15.02	15.07	15.45	14.35	15.85	16.5	11.68	13.33	12.37
Fe_2O_3	wt%	1.33	1.32	1.86	3.23	3.02	4.16	0.53	0.57	0.95
FeO	wt%	0.71	0.84	1.75	3.06	2.86	3.86	0.32	0.45	0.51
MnO	wt%	0.02	0.02	0.04	0.07	0.12	0.12	0.02	0.02	0.04
MgO	wt%	0.57	0.61	1.78	1	0.85	1.4	0.18	0.18	0.16
CaO	wt%	2.28	2.33	2.33	3.84	3.1	3.33	0.03	0.05	0.39
Cr_2O_3	wt%	0.03	0.04	0.01	0.01	0.01	0.01	0.02	0.03	0.02
Na_2O	wt%	3.01	3.02	4.12	3.88	3.25	4.28	1.75	1.15	3.92
K_2O	wt%	4.83	4.85	3.82	2.23	3.63	3.25	2.14	2.8	1.33
BaO	wt%	0.14	0.15	0.17	0.05	0.21	0.21	0.02	0.04	0.04
P_2O_5	wt%	0.17	0.17	0.18	0.13	0.15	0.24	0.01	0.01	0.02
LOI	wt%	3.84	3.68	2.80	4.79	5.51	2.56	2.17	2.60	1.91
Total	wt%	*99.66*	*99.43*	*98.7*	*99.8*	*100.5*	*99.6*	*99.37*	*99.64*	*98.39*
Ba	ppm	1245.0	1350.0	1745.0	516.0	1485.0	1770.0	41.4	191.0	161.5
Co	ppm	2.4	2.0	2.0	7.4	3.6	7.7	0.6	0.8	0.6
Cr	ppm	260.0	290.0	70.0	70.0	60.0	80.0	170.0	210.0	210.0
Cs	ppm	6.1	6.2	4.8	3.5	1.9	2.1	33.0	56.3	1.6
Cu	ppm	58.0	23.0	6.0	12.0	7.0	15.0	19.0	8.0	------
Ga	ppm	15.0	14.0	18.0	18.0	17.0	19.0	20.0	21.0	16.0
Hf	ppm	5.0	5.0	3.0	4.0	4.0	4.0	3.0	4.0	5.0
Mo	ppm	7.0	5.0	3.0	4.0	5.0	4.0	2.0	2.0	2.0
Nb	ppm	15.0	15.0	10.0	10.0	13.0	12.0	16.0	23.0	36.0
Ni	ppm	12.0	12.0	10.0	11.0	8.0	10.0	7.0	8.0	7.0
Pb	ppm	25.0	21.0	16.0	18.0	11.0	20.0	15.0	26.0	15.0
Rb	ppm	195.5	185.5	197.0	90.7	93.0	81.9	165.0	189.5	74.3
Sn	ppm	2.0	2.0	1.0	1.0	1.0	1.0	2.0	2.0	4.0
Sr	ppm	210.0	212.0	376.0	281.0	584.0	657.0	34.6	36.5	285.0
Ta	ppm	1.3	1.3	1.0	0.8	0.8	0.7	2.1	2.7	3.1
Th	ppm	18.0	18.0	16.0	14.0	11.0	9.0	15.0	20.0	26.0
Tl	ppm	1.0	0.9	1.1	0.5	------	------	0.7	0.7	------
U	ppm	6.4	6.2	4.7	5.5	3.9	3.4	13.1	23.6	10.0
V	ppm	46.0	44.0	90.0	61.0	31.0	69.0	2.5	2.5	2.5
W	ppm	7.0	6.0	79.0	4.0	2.0	3.0	3.0	2.0	1.0
Y	ppm	13.0	13.2	13.2	12.4	12.6	14.4	7.1	13.6	43.0
Zn	ppm	38.0	34.0	33.0	99.0	48.0	72.0	29.0	109.0	26.0
Zr	ppm	168.0	173.5	116.5	142.0	148.0	137.0	32.6	48.0	76.0
La	ppm	28.7	28.4	14.2	23.9	31.2	30.5	7.1	7.3	9.0
Ce	ppm	48.5	48.8	22.1	41.4	44.0	45.1	13.0	15.0	22.1
Pr	ppm	5.0	5.0	2.1	4.3	5.2	5.1	1.4	1.8	3.2
Nd	ppm	17.5	17.4	8.9	17.0	20.0	20.7	4.8	6.2	13.7
Sm	ppm	3.0	3.1	1.7	2.9	2.7	3.2	0.9	1.5	4.9
Eu	ppm	0.7	0.7	0.8	0.7	0.8	1.0	0.1	0.2	0.1
Gd	ppm	2.8	2.9	2.1	2.9	3.0	3.3	0.9	1.5	5.2
Tb	ppm	0.4	0.4	0.3	0.4	0.4	0.4	0.2	0.3	1.1
Dy	ppm	2.3	2.1	1.8	1.8	2.0	2.4	0.9	1.6	6.6
Ho	ppm	0.4	0.5	0.4	0.4	0.4	0.5	0.2	0.4	1.4
Er	ppm	1.3	1.3	1.1	1.0	1.2	1.5	0.7	1.2	4.3
Tm	ppm	0.2	0.2	0.2	0.2	0.2	0.2	0.1	0.2	0.6
Yb	ppm	1.3	1.3	1.2	1.0	1.3	1.4	0.8	1.4	4.4
Lu	ppm	0.2	0.3	0.2	0.2	0.2	0.2	0.1	0.3	0.7

Major oxide concentrations from XRF; all others by ICP-MS, from ALS Chemex, North Vancouver, B.C.

Table 2-3: Continued

		Sloko Intrusive Rocks	Mafic Dykes (post-Cretaceous)					
Sample		4AS11	277522	277532	AS18a	AS18a2	AS24a	AS42a
SiO_2	wt%	58.1	62.13	40.16	57.14	57.48	50.23	51.39
TiO_2	wt%	0.6	0.66	1.29	0.73	0.75	1.28	1.6
Al_2O_3	wt%	16.35	16.55	14.09	15.87	15.93	15.91	15.16
Fe_2O_3	wt%	5.69	4.62	6.45	4.98	5	9.08	8.58
FeO	wt%	5.66	2.64	5.02	3.41	2.96	5.72	4.18
MnO	wt%	0.12	0.12	0.37	0.09	0.08	0.1	0.16
MgO	wt%	2.54	1.31	4.49	2	1.86	6.55	3.53
CaO	wt%	6.36	2.76	10.44	4.61	4.62	6.37	5.97
Cr_2O_3	wt%	------	0.02	0.02	0.02	0.02	0.03	0.04
Na_2O	wt%	3.26	3.6	1.76	2.88	2.72	2.66	3.07
K_2O	wt%	1.04	2.34	2.63	3.6	3.62	0.37	2.31
BaO	wt%	0.08	0.2	0.05	0.2	0.2	0.08	0.17
P_2O_5	wt%	0.21	0.32	0.51	0.19	0.19	0.42	0.81
LOI	wt%	4.73	4.43	17.15	7.47	6.87	6.61	6.46
Total	wt%	*99.4*	*99.13*	*99.55*	*99.84*	*99.4*	*99.78*	*99.31*
Ba	ppm	888.0	1800.0	467.0	1805.0	1820.0	578.0	1670.0
Co	ppm	14.6	11.7	23.6	11.1	11.4	33.5	17.6
Cr	ppm	50.0	110.0	130.0	120.0	120.0	200.0	90.0
Cs	ppm	2.0	11.5	33.0	22.6	21.3	7.3	3.1
Cu	ppm	18.0	27.0	24.0	17.0	19.0	36.0	15.0
Ga	ppm	21.0	18.0	16.0	18.0	18.0	17.0	18.0
Hf	ppm	2.0	5.0	4.0	4.0	4.0	3.0	5.0
Mo	ppm	4.0	------	------	2.0	2.0	2.0	3.0
Nb	ppm	8.0	13.0	12.0	5.0	5.0	9.0	19.0
Ni	ppm	11.0	19.0	40.0	13.0	15.0	103.0	19.0
Pb	ppm	12.0	19.0	11.0	14.0	16.0	10.0	23.0
Rb	ppm	27.6	59.2	100.0	105.5	107.0	6.2	27.7
Sn	ppm	1.0	------	1.0	1.0	1.0	------	1.0
Sr	ppm	871.0	577.0	1505.0	601.0	618.0	862.0	738.0
Ta	ppm	0.6	0.8	0.6	------	------	0.5	0.9
Th	ppm	8.0	10.0	4.0	10.0	10.0	3.0	3.0
Tl	ppm	------	0.6	0.6	------	------	------	------
U	ppm	4.3	3.5	1.3	3.2	3.2	1.1	1.2
V	ppm	146.0	92.0	162.0	104.0	106.0	188.0	165.0
W	ppm	2.0	2.0	2.0	1.0	1.0	2.0	1.0
Y	ppm	20.7	13.9	24.2	12.7	13.0	21.4	31.6
Zn	ppm	81.0	66.0	86.0	72.0	68.0	97.0	100.0
Zr	ppm	86.1	157.0	154.0	126.5	126.5	119.0	197.0
La	ppm	20.6	30.3	30.7	20.2	20.4	21.6	44.6
Ce	ppm	40.2	57.2	65.5	38.6	38.6	45.5	93.8
Pr	ppm	3.9	6.1	7.7	4.2	4.3	5.3	10.9
Nd	ppm	17.7	22.1	30.4	15.6	15.6	21.2	42.3
Sm	ppm	4.0	4.0	6.0	3.1	3.1	4.4	8.0
Eu	ppm	1.2	1.0	1.7	0.9	0.9	1.3	2.2
Gd	ppm	4.1	3.6	5.9	3.0	3.1	4.4	7.7
Tb	ppm	0.6	0.5	0.8	0.4	0.4	0.7	1.1
Dy	ppm	3.2	2.5	4.3	2.4	2.2	3.7	5.7
Ho	ppm	0.7	0.5	0.8	0.5	0.5	0.8	1.1
Er	ppm	1.9	1.4	2.3	1.3	1.3	2.3	3.1
Tm	ppm	0.3	0.2	0.3	0.2	0.2	0.3	0.4
Yb	ppm	1.8	1.2	2.1	1.2	1.2	2.1	2.8
Lu	ppm	0.3	0.2	0.3	0.2	0.2	0.3	0.4

Major oxide concentrations from XRF; all others by ICP-MS, from ALS Chemex, North Vancouver, B.C.

The Late Cretaceous and Tertiary rock suites, as well as pre-Cretaceous rocks have high-K to medium-K calc-alkaline compositions (Figure 2-10A). The Late Cretaceous and Tertiary units are largely intermediate in composition (59 – 78 wt.% SiO_2) while older rocks, particularly the Stuhini Group, are more mafic in composition (<65 wt.% SiO_2). Mafic dykes and felsic dykes have SiO_2 compositions of 48 – 65% and 74 – 78%, respectively (Figure 2-10A). Felsic dykes likely represent high silica rhyolites. Aside from the Stuhini Group rocks, all magmatic rocks are medium to high-K calc-alkaline rocks in the K_2O vs. SiO_2 diagram (Figure 2-10A). In detail Thorn Suite rocks tend to be medium-K calc-alkaline, whereas the Windy Table Suite rocks tend to be high-K calc-alkaline (Figure 2-10A). Most rocks are weakly peraluminous aside from the Stuhini Group rocks and the late mafic dykes (Figure 2-10B). Moreover, Windy Table Suite intrusions fall for the most part on the boundary between peraluminous and metaluminous, whereas Thorn Suite intrusions are always weakly peraluminous (Figure 2-10B). Minor mobility of elements is event in the Cretaceous rocks suites, particularly with CaO, K_2O and Na_2O, where there are significantly different compositions over a narrow range in silica compositions (Figure 2-10A, C, D). This affect is likey due to alteration and is difficult to explain via fractionation form the magma. The weak peraluminous nature of Late Cretaceous Magmatic rocks in the northwestern Cordillera has also been well documented by Ballantyne and Littlejohn (1982) and Mihalynuk (1999).

Decreasing CaO with increasing SiO_2 for all rocks shows that plagioclase played an important role during the formation of the magmatic systems. The decreasing trends in with increasing SiO_2, for MgO, TiO_2 and P_2O_5 reflect fractionation by pyroxene, titanite, apatite, zircon and/or monazite, respectively (Figures 2-10F, G, H). These trends are typical of a fractionating melt in an arc environment (e.g. Bissig *et al.*, 2003; Mihalynuk, 1999).

Trace and Rare Earth Element Geochemistry

Trace element abundances in igneous rocks can be used to provide constraints for tectonic setting, protoliths and conditions of generation and evolution of magmas. These elements are relatively immobile compared to major elements making them particularly useful in areas where rocks are pervasively and extensively altered, as is the case in the study area. Concentrations of these elements may reflect fractionation of minerals, in which they are major components, both at the site of partial melting where the magmas are generated and/or in the ensuing magma chambers, in addition to providing information on the chemical compositions of the source rocks. The discussion below emphasizes selected elements commonly used to characterize the origins of magmas.

Classifying rocks using immobile elements is important in rocks that have been altered. Figures 2-11A & B show examples of rock discriminations using both alkalis and immobile elements vs. silica. Using the alkalis vs. silica discrimination diagram of LeBas *et al.* (1986) shows that Late Cretaceous intrusive and volcanic rocks evolve from diorite through granodiorite to granite, whereas the discrimination diagram using immobile elements of Winchester and Floyd (1977) shows these rocks evolving from diorite through monzonite through syenite (Figure 2-10). Petrographic analyses of these rocks show that the discrimination using immobile elements is more accurate. For example, the Thorn Stock contains plagioclase only as the feldspar component, yet plots as a granodiorite using alkalis. However, using immobile elements is not completely correct. For example the Thorn Stock contains up to 5-8% rounded quartz phenocrysts and thus has been called quartz diorite rather than a diorite as it plots on the immobile element discrimination diagram.

The Ba/La ratios from Late Cretaceous magmatic rocks from the study area exceed 20 (Figures 2-10C, D), except in the case of high-silica rhyolite units, which record high alkaline earth concentrations, suggestive of an arc rather than a back arc setting (e.g. Kay et al. 1994; Sasso and Clark, 1998; Bissig et al., 2003). Differences in Sr abundances are particularly important between intrusive rocks of the Windy Table Suite and the Thorn Suite, as Thorn Suite rocks are distinctively enriched in Sr, though there is minor overlap in the two suites (Figure 2-11E). The same trend is also present in the Rb/Sr ratio, where Windy Table intrusive rocks have marginally, but consistently higher values, indicating that these rocks are more evolved than the Thorn Suite intrusions (Figure 2-11F).

Rare earth element concentrations in rocks have been widely and effectively used as petrogenetic indicators in similar tectonic environments to the Canadian northern Cordilleran (e.g. Kay et al. 1991; Bissig et al. 2003). These elements behave similarly to other trace elements, in that their concentrations may reflect fractionation of minerals, and may provide information on the generation and evolution of magma, as well as the composition of the source rocks. Heavy-REE (HREE) partition into garnet and hornblende, whereas the middle-REE (Gd-Er: MREE) most readily partition into hornblende. REE concentrations with concave-up chondrite-normalized patterns are therefore considered to indicate hornblende fractionation (Bissig *et al.*, 2003). Light-REE (LREE) are the most incompatible elements in the REE series and are therefore concentrated in later stages of magmatism relative to the MREE and HREE. Eu, when present in its divalent state, behaves similarly to Sr and substitutes readily for Ca^{2+} into feldspar, because they have similar ionic radii and charge. However in oxidizing magmas where Eu^{3+} is the dominant Eu species, only minor Eu fractionation would be expected.

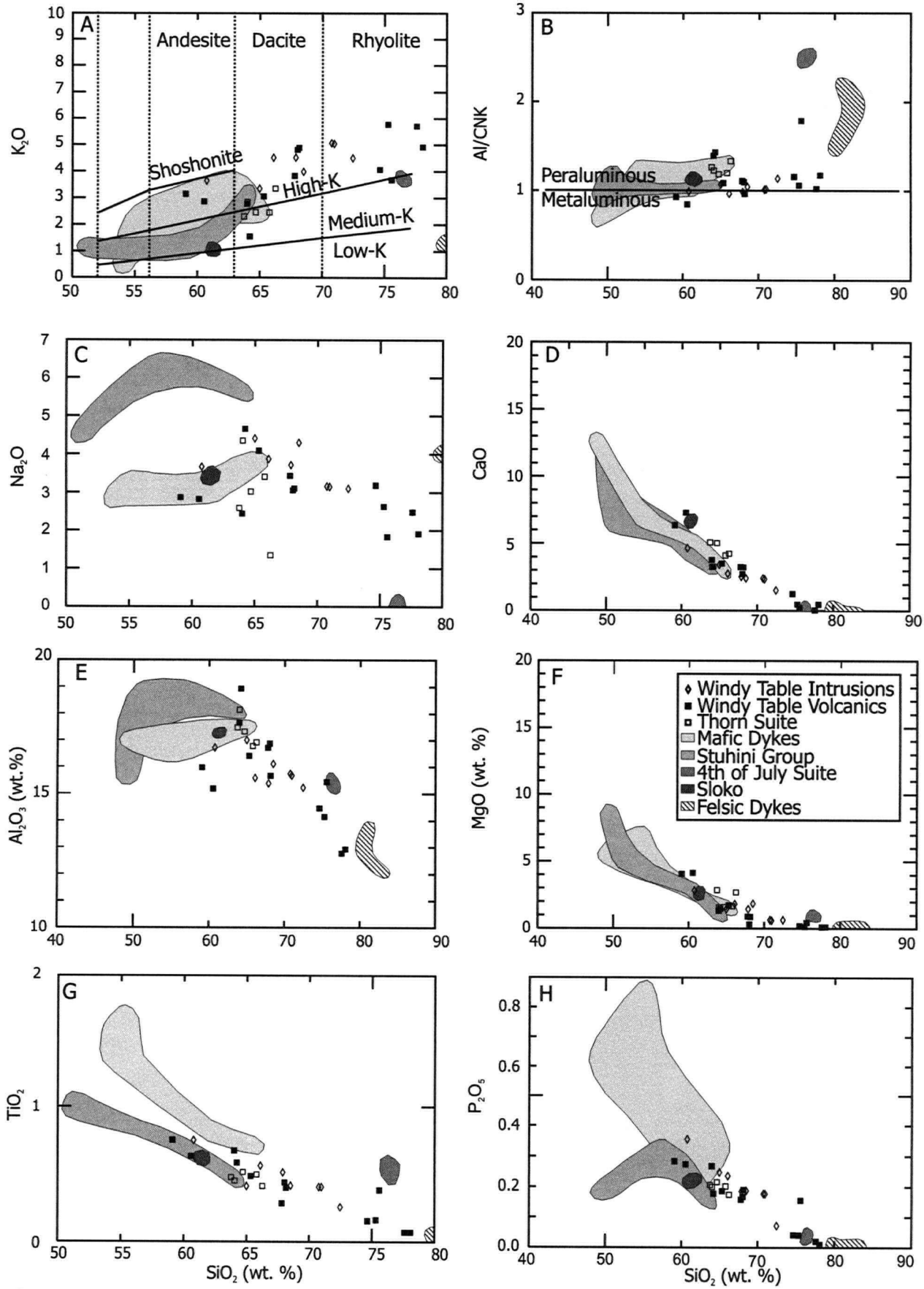

Figure 2-10: Harker-type plots for major elements versus SiO_2 and aluminum satuartion indecies versus SiO_2 of Peccerillo and Taylor (1976). Shaded areas based on data from this study.

The individual units of the Late Cretaceous volcanoplutonic belt in the study area have distinctive chondrite-normalized REE characteristics (Figure 2-12) and are distinct from pre-Cretaceous rocks of the Stuhini Group and Fourth of July Suite. These older rocks exhibit relatively flat REE patterns with the latter having higher overall concentrations of all REE and a negative Eu anomaly. The Stuhini Group sample (AS-070a; Figure 2-12A) was taken from a sub-aqueous massive basaltic flow, which typically yield flat relatively enriched REE patterns, because their magmas is derived from the partial melting of the upper mantle. Mihalynuk (1999) documents Fourth of July Suite rocks and suggested that these magmas display similar chemistry to mature volcanic arcs (Figure 2-12B). Sample AS-071a does not display similar chemistry. The high SiO_2 concentration of this rock suggests that it was a late stage intrusive rock that may partially crystallized in vapour phase, this relatively evolved state may explain the differences in REE concentrations (Figure 2-12B).

Subtle but important distinctions in chondrite-normalized REE patterns can be made between Late Cretaceous magmatic suites (Figure 2-12). The Thorn Suite rocks have typical mature continental arc patterns with unfractionated HREE and MREE and a minor negative to absent Eu anomaly (Figure 2-12C; Kay *et al.* 1991). In Figures 2-12D & E, the younger Windy Table Suite rocks are separated into their extrusive and intrusive component (Figures 2-12D & E). The Windy Table intrusions are distinct from the Thorn Suite rocks in that they have overall slightly more elevated LREE concentrations, have a slightly more pronounced negative Eu anomaly (though still only minor), and a slight concave up MREE to HREE pattern (Figure 2-12E). One sample from the Windy Table intrusive suite (04AS25(1); Figure 2-12E) has lower concentrations of LREE and MREE and a positive Eu anomaly; this sample is a plagioclase megacrystic rock and the pattern can be explained by the addition of the megacrystic plagioclase. La/Sm and La/Yb ratios are generally higher in Windy Table rocks, particularly with the La/Sm ratio, suggesting that Windy Table magmas are generally more evolved than their Thorn Suite counterparts (Figure 2-11G). Additionally, the extended trace element chondrite normalized patterns for all Cretaceous rocks show a Nb and Ta depletion, indicating that these rocks formed in an arc environment (Figure 2-11H). Windy Table Suite volcanic rocks display similar REE pattern to their intrusive equivalents, with a less pronounced to absent MREE and HREE fractionation pattern and more irregularities. Two samples (AS-058a and AS-056a) display enriched HREE and large negative Eu anomalies and are more similar to the Type 4 Windy Table Intrusions (Figure 2-12D). These samples are siliceous flow-foliated dykes, which geochemically resemble high-silica rhyolite (Figure 2-10A & B). Their relatively flat REE signature may be due either fractionation by late stage accessory minerals crystallizing in the

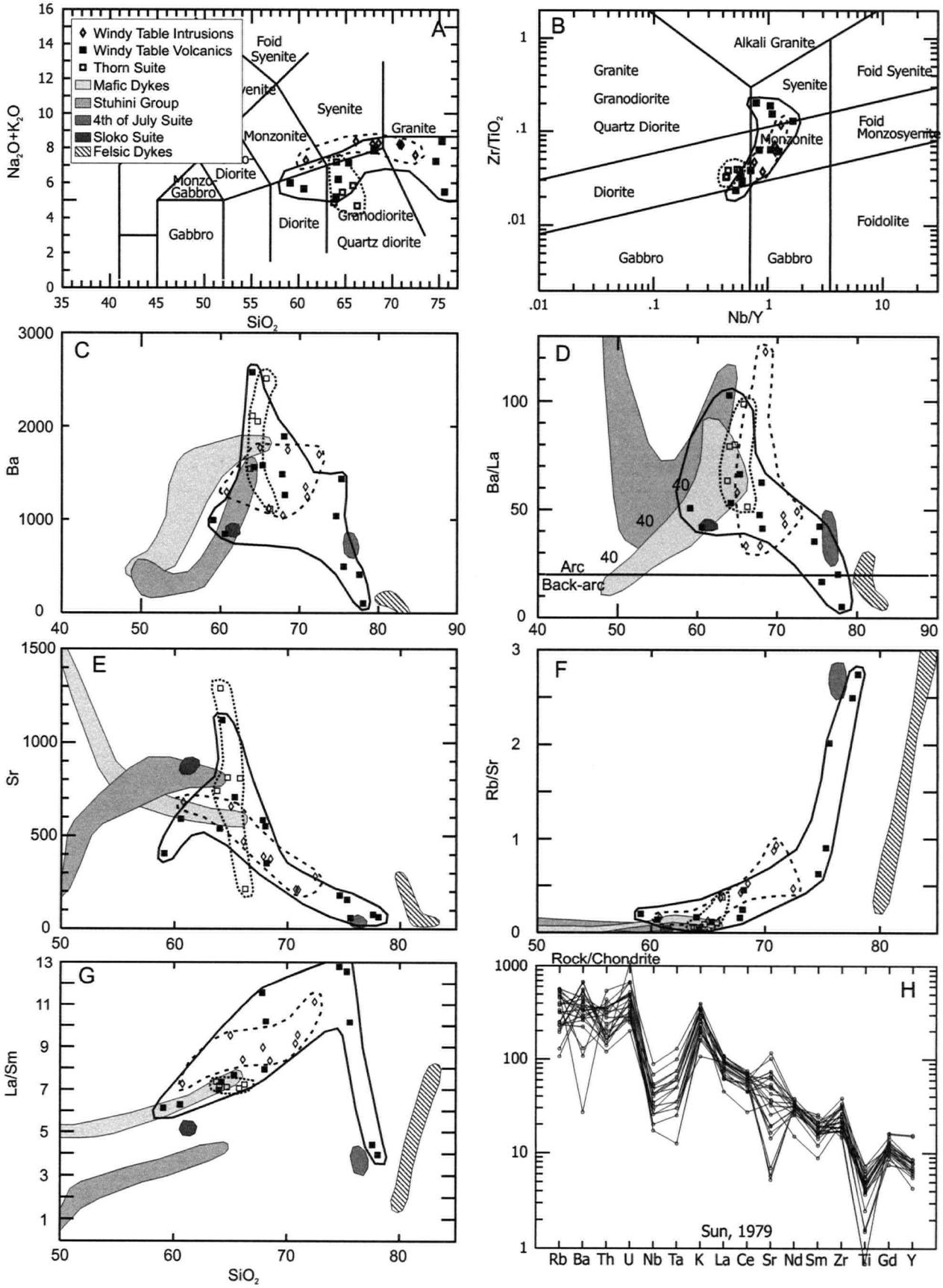

Figure 2-11: Trace and REE Geochemistry of Late Cretaceous Magmatic Rocks. Areas enclosed by solid, dashed and dotted lines correspond to the respective fields for Windy Table volcanic rocks, Windy Table intrusive rocks and Thorn Suite rocks. H shows chondrite-normalized extended trace element patterns of all Cretaceous rocks.

dykes or by contamination by older Triassic rocks, which they intrude, the cause of the large negative Eu anomaly is not known. One sample (AS-016a; Figure 2-12D) has lower concentrations of HREE; it is unknown why this sample has this REE pattern. The irregularity of Windy Table volcanic rocks may be explained by the presence of the lithic fragments, which affect the overall REE pattern. A second possible explanation is that the volcanic stratigraphy is more complex than originally thought and may contain several distinctive periods of pyroclastic deposition, which have distinct chemistry.

Sloko Group intrusive rocks are geochemically distinct from Thorn Suite rocks, having flatter REE patterns and increased concentrations of MREE and HREE (Figure 2-12G). This pattern suggests that Sloko rocks are less evolved than Thorn Suite rocks, perhaps a reflection of their slightly more basic composition. Type 4 Windy Table Suite intrusive rocks have a relatively flat REE pattern with large negative Eu anomalies and may be both relatively enriched or depleted in REE (Figure 2-12H). Mafic Dykes have similar REE patterns to the Thorn Suite intrusions, but generally contain high concentrations of all rare earth elements.

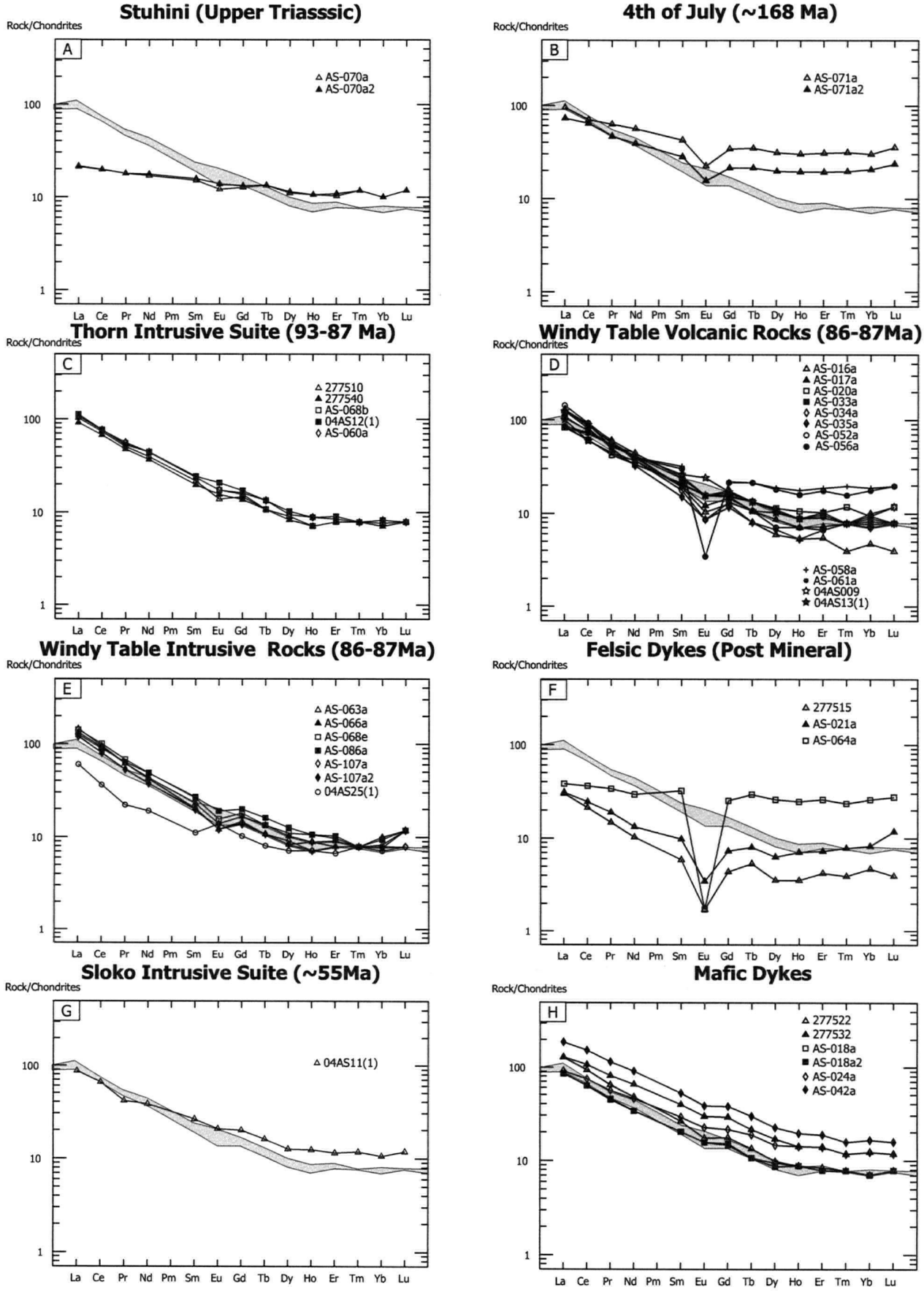

Figure 2-12: Rare Earth Element Geochemistry of samples from the Thorn and surrounding area, divided into Suites and ages of rocks. Grey outline of Thorn Suite Intrusive rocks. Plots after Sun and McDonough, 1989.

Discussion

Prior to this study, the significance, spatial distribution and relation to hydrothermal systems to Late Cretaceous magmatism in the northwest Cordilleran was unknown. Moreover, Late Cretaceous magmatism, particularly from 93-80 Ma was generally regarded as a volumetrically insignificant component of the Coast Plutonic Complex. Many of these magmatic centres were previously mapped as Tertiary Sloko Group rocks. Work at the Thorn Property has demonstrated that the metaluminous, calc-alkaline melts of the Windy Table Group are coeval with significant hydrothermal systems.

The magmatic centre located at the Thorn Property is part of a newly recognized NNW-trending continental magmatic arc, which extends from at least the Golden Bear Mine to the Tagish Lake area, a distance of approximately 300 km. Magmatism along this continental arc occurred from 93 Ma to 80 Ma. These magmatic rocks can be separated into two distinct periods of magmatism, the 93-87 Ma Thorn Magmatic Suite and the 86-80 Ma Windy Table Magmatic Suite.

Late Cretaceous magmatism in the Coast Plutonic Belt of the Canadian Cordilleran plays an important role in the development of significant hydrothermal systems in the study area. Understanding the timing, geochemical nature and structural architecture of the map units is a critical step in developing exploration guidelines for ore deposits. At the Thorn Property, magmatic events are constrained to four distinct periods after the accretion of Stikinia onto the western flank of North America. Furthermore, Late Cretaceous magmatic rocks, a rarity in the Coast Plutonic Complex, are both host of, and contemporaneous with, high-sulphidation mineral assemblage veins. Figure 2-13 shows the unmixing ages for all zircons taken as part of this study, apart from the Fourth of July Suite. Unmixing ages are generated using Isoplot 3.00 (Ludwig, 2003), which includes partial implementation of the Sambridge and Compston (1994) "mixture modeling" method for deconvoluting a suite of data obtained on single-crystal samples that contain multiple age components. The peaks displayed in Figure 2-13 correspond to the *ca.* 93-87 Ma Thorn Suite (host of the high-sulphidation veins), and the *ca.* 86-80 Ma Windy Table Suite (contemporaneous with high-sulphidation veins). Additionally, the Windy Table Suite can be separated into two distinctive events, an early *ca.* 87 Ma event, likely corresponding to Phase 1 volcanism and Types 2 and 3 plutonism, and a later event at *ca.* 82 Ma, corresponding to Phases 2 and 3 volcanism and Type 1 plutonism (Figure 2-13).

Several lines of evidence suggest that Windy Table volcanic rocks were deposited in a volcanotectonic depression, though only limited mapping of these rocks was carried out

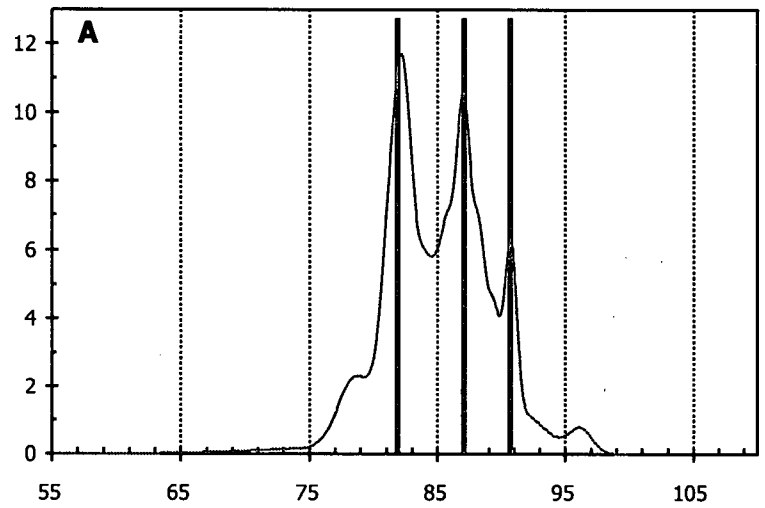

Age	±2σ	Fraction	±2σ
81.88	0.29	0.45	0.17
87.04	0.3	0.38	0.16
90.68	0.35	0.17	---

relative misfit = 0.217

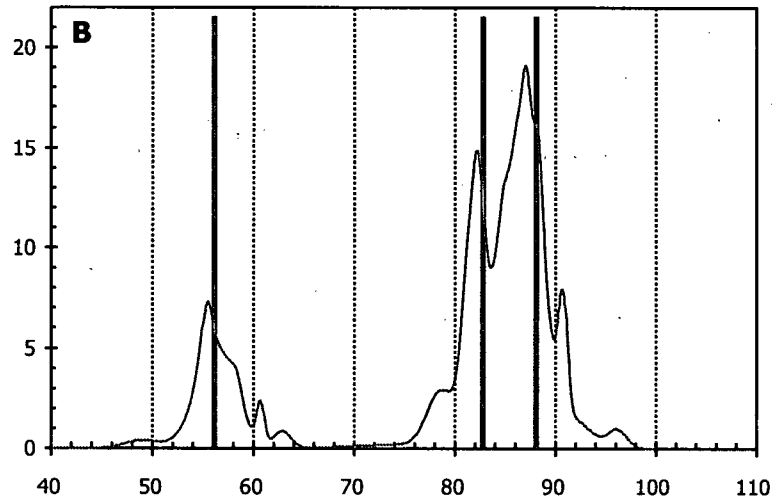

Age	±2σ	fraction	±2σ
56.06	0.43	0.16	0.08
82.8	0.25	0.32	0.11
88.13	0.17	0.45	---

relative misfit = 552.124

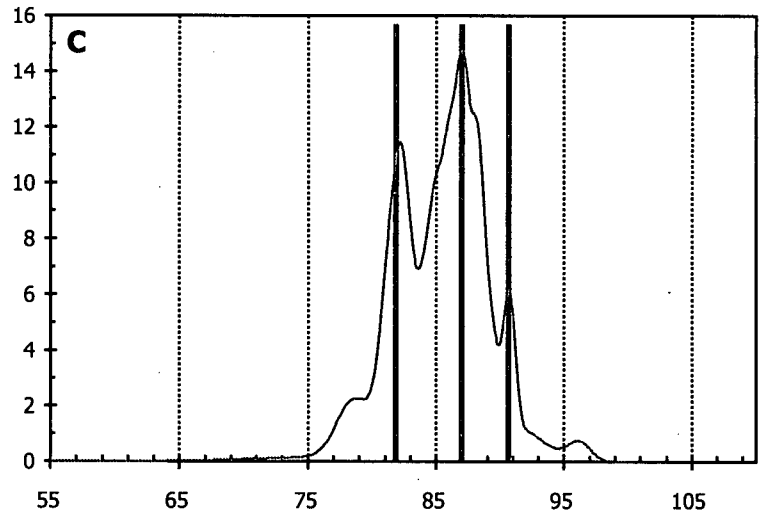

Age	±2σ	fraction	±2σ
81.84	0.28	0.33	0.13
86.954	0.19	0.54	0.16
90.68	0.36	0.13	---

relative misfit = 0.266

Figure 2-13: Unmixing diagram based on Sambridge and Compston (1994) for A) all Late Cretaceous zircons taken regionally , B) all post-Jurassic zircons taken regionally and C) all Late Cretaceous zircons from the Thorn Property. Method for unmixing is taken from Sambridge and Compston (1994) whose "mixture modeling" method deconvolutes a suite of dates obtained on single crystal samples that contain multiple age components.

during this study. One important piece of information which supports this is that the basal unit of the volcanic strata is that it is composed of sedimentary rocks, which contain dominant clasts comprised of Triassic and Jurassic basement rocks. This unit is only exposed in one location were it is only approximately 2 m thick. However, along La Jaune Creek no sedimentary rocks composed of basement rocks are known. This is explained by post-depositional block faulting, described by Lewis (2002), in which movement NE of La Jaune Creek was down, thus putting higher-level strata in fault contact with Triassic strata. Development of the paleodepression is marked by the exhumation of the Thorn Stock, which was exhumed over 4-5 million years (Figure 2-9), fronm the time of emplacement of the Thorn Stock. Secondly, extensive megabreccia composed of both Windy Table rocks and Stuhini Groups rocks are located at the Cutty Sark Zone and to a lesser extent in Faraway Creek. Both of these locations are at or near the mapped limits of Windy Table strata and indicate that the surrounding walls were oversteepened producing the megabreccia units at the Cutty Sark Zone and Faraway Creek. Thirdly, approximately 1600 m of volcanic stratigraphy, composed mainly of variably welded pyroclastic rock of Phase 1 and 3 are exposed in Amarillo Creek. Lipman (2000) suggests that thick sequences of pyroclastic rocks, such these, are usually attributed to fill deposits of a paleodepression or a caldera. Additionally, arcuate faults bounding the volcanic rocks particularly on the eastern contact between Windy Table rocks and older rocks are suggestive of a caldera-forming environment, in which Thorn Suite rocks are evidence of precollapse volcanism, Phase 1 Windy Table rocks are initial depression fill deposits, Phase 2 Windy Table volcanism represents resurgent deposits, and Phase 3 filled the remainder of the caldera due to post-collapse caldera-related events.

Extrusive and intrusive rocks of the Late Cretaceous volcanoplutonic belt are weakly peraluminous to weakly metaluminous calc-alkaline suites, characteristic of continental magmatic arcs. Thorn Suite shows no negative Eu anomalies and have moderate to high Sr concentrations. Additionally HREE concentrations suggest that neither garnet or hornblende was present in the residuum or hornblende fractionation did not play a significant role in Thorn Suite magmas. In contrast, minor negative Eu anomalies combined with slightly convex-upward HREE patterns in Windy Table Group rocks indicate that Windy Table magmas may have experienced slight plagioclase fractionation from the melt and that hornblende was an important phase in the residuum or hornblende fractionation out of the melt played a more important role in Windy Table rocks. Additionally, higher La/Sm ratios in Windy Table Suite rocks indicate that they are more evolved that the Thorn Suite rocks, as LREE are fractionated

by accessory phases such as zircon and apatite, which are more common in evolved melts (Krauskopf and Bird, 1995).

The Windy Table Suite rocks form the volumetric majority of all magmatic rocks in the area between the Thorn and Tulsequah mine. The Thorn Suite rocks have a distinctive petrochemical signature in which hornblende played an important role as either residuum or as a fractionating phase during the genesis of these magmas. The relatively steep LREE to MREE signature of these rocks suggest that they are more evolved than rocks that predate them. This relatively evolved nature may play an important role in the formation of large hydrothermal systems along the belt. These rocks are potentially important source rocks for mineralizing fluids at the Thorn Property and their extrusive rocks may play an important role as host for the mineralizing system.

Conclusions

A NNW-trending Late Cretaceous volcanoplutonic belt forms part of the Coast Plutonic Complex and is comprised of the 93-87 Ma Thorn Suite and the 86-80 Ma Windy Table Suite. These rocks were emplaced onto and into Late Triassic and Middle Jurassic rocks of the Stikine Terrane. The Thorn Suite rocks were exhumed over a period of 4-5 million years upon which a thin sequence of locally derived sedimentary rocks and breccia were deposited. Approximately 1600 m of Windy Table Strata overlie the Thorn Stock. The Windy Table Suite rocks were deposited in a volcanotectonic depression. Three distinct phases of volcanism are noted in the Windy Table strata. Phase 1 represents the initial pyroclastic fill deposits in the paleodepression and Phase 2 represents resurgent flow dome complexes. Subsidence features in the volcanic deposit are obscured by later Phase 3 pyroclastic rocks, which overlie Phases 1 and 2, and also by post depositional block faulting. The Windy Table Suite also includes numerous small intrusive complexes, which are subdivided regionally into 4 distinct types based upon petrologic and geochemical characteristics. These intrusions are the apparent source rocks for mineralizing fluids and are contemporaneous whith hydrothermal alteration. Locating similar environments in the in the Late Cretaceous belt that contain Windy Table and Thorn Suite rocks could be critical to evaluating the potential for developing a mineralized system.

References

Awmack, H.J. (2003): 2002 Geological, Geochemical and Diamond Drilling Report on the Thorn Property; *British Columbia Ministry of Energy and Mines,* Assessment Report #27,120.

Bacon, C.R., Foster, H.L. and Smith, J.G. (1990): Rhyolitic Calderas of the Yukon-Tanana terrane, East Central Alaska: Volcanic Remnants of a Mid-Cretaceous Magmatic Arc; *Journal of Geophysical Research*, Volume 95, Number B13, pages 21,451-21,461.

Baker, D.E.L. (2003): 2003 Geological, Geochemical and Diamond Drilling Report on the Thorn Property; *British Columbia Ministry of Energy and Mines,* Assessment Report #27,120.

Ballantyne, S.B. and Littlejohn, A.L. (1982): Uranium mineralization and lithogeochemistry of the Surprise Lake batholith, Atlin, British Columbia; *in* Uranium in Granites, Maurice, Y.T. (editor); *Geological Survey of Canada*, Paper 81-23, pages 145-155.

Bissig, T., Clark, A.H., Lee, J.K.W. and von Quadt, A. (2003): Petrogenetic and Metallogenic Responses to Miocene Slab Flattening: New Constraints from El Indio-Pascua Au-Ag-Cu belt, Chile/Argentina; *Mineralium Deposita,* Volume 38, pages 844-862.

Brew, D.A. and Morrell, R.P. (1983): Intrusive rocks and Plutonic Belts of southeastern Alaska; *Geological Society of America,* Memoir 159, pages 171-193.

Bultman, T.R. (1979): Geology and tectonic history of the Whitehorse Trough west of Atlin; unpublished Ph.D. thesis, *Yale University,* 284 pages.

Currie, L.D. (1990): Metamorphic Rocks in the Florence Range, Coast Mountains, Northwestern British Columbia (104M/8); *in* Geological Fieldwork 1989, *B.C. Ministry of Energy, Mines, and Petroleum Resources*, Paper 1990-1, pages 197-203.

Currie, L.D. (1994): The Geology and Mid-Jurassic amalgamation of Tracy Arm Terrane and Stikinia of northwest British Columbia, unpublished Ph.D. thesis, *Carleton University*, 385 pages.

Geological Survey of Canada (1988): *National Geochemical Reconnaissance 1:250,000 Map Series (Tulsequah)*; Open File 1647.

Gabrielse, H. (1969): Geology of the Jennings River map-area, British Columbia (104-O); *Geological Survey of Canada*, Paper 68-55, 37 pages.

Hart, C.J.R., Pelletier, K.S., Hunt, J. and Fingland, M. (1989): Geological map of Carcross (105D/2) and part of Robinson (105D/7) map areas; *Indian and Northern Affairs Canada,* Open File Map 1989-1.

Hart, C.J.R. (1995): Magmatic and tectonic evolution of the Intermontane Superterrane and the Coast Plutonic Complex in southern Yukon Territory; unpublished M.Sc. thesis, *The University of British Columbia*, 198 pages.

Jackson, J.L. (1992): Tectonic Analysis of the Nisling, Northern Stikine and Northern Cache Creek Terranes, Yukon and British Columbia; unpublished Ph.D. thesis; *University of Arizona*, Tucson, 200 pages.

Kay, S.M., Mpodozis, C., Ramos, V.A. and Munizaga, F. (1991): Magma source variations for mid-late Tertiary Magmatic Rocks associated with a shallowing subduction zone and thickening crust in the central Andes (28-33°S). In: Harmon R.S., Rapela, C. (eds) Andean Magmatism and its tectonic setting; *Geological Society of America Special Paper 265,* Littleton, Colorado, pages 113-137.

Kay, S.M., Mpodozis, C., Tittler, A. and Cornejo, P. (1991): Tertiary magmatic evolution of the Maricunga Mineral Belt in Chile; *International Geology Reviews*, volume 36, pages 1079-1112.

Kerr, F.A. (1948): Taku River map area, British Columbia; *Geological Survey of Canada,* Memoir 248.

Krauskopf, K.B. and Bird D.K. (1995):Introduction To Geochemistry, Third Edition, *WBC/McGraw-Hill*, New York; Chapter 20: Distribution of the Elements, pages 534-558.

LeBas, M.J., LeMaitre, R.W., Streckeisen, A., and Zanettin, B. (1986): A chemical classification of volcanic rocks based on the total alkali silica diagram; *Journal of Petrology*, volume 27, pages 745-750.

Lewis, P. (2002): Structural Analysis of Au-Ag-Cu Mineralization in the Camp Creek area, Thorn Property; *Private report for Rimfire Minerals Corporation and First Au Strategies Corp.,*

dated July 15, 2002. *In* H.J. Awmack (2003): 2002 Geological, Geochemical and Diamond Drilling Report on the Thorn Property.

Lipman, P.W. (2000): Calderas; *in* Encyclopedia of Volcanoes, Sigurdsson, H., editor, *Academic Press*, San Diego, California, USA, Pages 643-662.

Ludwig, K.R. (2003): IsoplotEx v. 3.0, *Berkeley Geochronology Center*, Special Publication Number 4, 71 Pages.

Mihalynuk M.G. and Smith, M.T. (1992): Highlights of 1991 mapping in the Atlin-west map area (104N/12); *in* Geological Fieldwork 1991, Grant, B. and Newell, J.H., editors, *B.C. Ministry of Energy Mines and Petroleum Resources,* Paper 1992-1, pages 221-227.

Mihalynuk, M.G., Nelson, J. and Diakow, L. (1994): Cache Creek Terrane entrapment: oroclinal paradox within the Canadian Cordillera; *Tectonics*, Volume 13, pages 575-595.

Mihalynuk, M.G. (1999): Geology and Mineral Resources of the Tagish Lake Area, B.C.; *Ministry of Energy and Mines*, Bulletin 105.

Mihalynuk, M.G., J. Mortensen, R. Friedman, A. Panteleyev and H.J. Awmack (2003): Cangold partnership: regional geologic setting and geochronology of high-sulphidation mineralization at the Thorn property. British Columbia; *Ministry of Energy and Mines,* Geofile 2003-10.

Monger, J.W.H. (1984): Cordilleran Tectonics: A Canadian Perspective; *Bulletin de la Société Géologique de France*, Series 7, Volume 26, pages 197-324.

Monger, J.W.H., Wheeler, J.O., Tipper, H.W., Gabrielse, H., Harms, T., Struik, L.C., Campbell, R.B., Dodds, C.J., Gehrels, G.E. and O'Brien, J. (1991): Cordilleran Terranes; *in* Geology of the Cordilleran orogen in Canada, Gabrielse, H. and Yorath, C.J. editors, *Geological Survey of Canada*, Geology of Canada, Volume 4, pages 281-327.

Nixon, G.T., Archibald, D.A. and Heaman, L.M. (1993): ^{40}Ar-^{39}Ar and U-Pb geochronometry of the Polaris Alaskan-Type complex, British Columbia: Precise timing of Quesnellia-North America interaction; *Geological Association of Canada – Mineralogical Society of Canada*, Annual Meeting, Program and Abstracts, page A76.

Oliver, J. L. (1996): Geology of Stikine Assemblage Rocks in the Bearskin (Muddy) and Tatsamenie Lake District, 104K/1 and 104K/8, Northwestern British Columbia, Canada and Characteristics of Gold Mineralization, Golden Bear Mine: Northwestern British Columbia: *Queen's University*, Unpublished Ph.D. thesis, 242 pages.

Peccerillo, A. and Taylor, S.R. (1976): Geochemistry of Eocene calc-alkaline volcanic rocks form the Kastamonu area, northern Turkey, *Contributions to Mineralogy and Petrology*, Volume 58, pages 63-81.

Ricketts, D.B., Evenchick, C.A., Anderson, R.G. and Murphy D.C. (1992): Bowser Basin, northern British Columbia: Constrains on the initial timing of subsidence and Stikinia-North America interactions; *Geology*, Volume 20, pages 1119-1122.

Roots, C. F. and Parrish, R. R., 1988, Age of the Mount Harper volcanic complex, southern Ogilvie Mountains, Yukon. In Radiogenic Age and Isotopic Studies, Report 2. Geological Survey of Canada Paper 88-2, pp. 29-36

Sambridge, M.S. and Compston, W. (1994): Mixture modeling of multi-component data sets with application to Ion-Probe Zircon Ages; *Earth and Planetary Science Letters*, volume 128, pages 373-390.

Sasso, A.M. and Clark, A.H. (1998): The Farallón Negro Group, Northwest Argentina: magmatic hydrothermal and tectonic evolution and implications for Cu-Au metallogeny in the Andean back-arc; *Society of Economic Geology Newsletters*, Volume 34, pages 18-18.

Sawkins, F.J., 1990, Metal Deposits In Relation To Plate Tectonics, 2nd edn.: Berlin, Springer-Verlag, 461 p.

Sillitoe, R.H. (1972): Relation of metal provinces in western Americas to subduction of oceanic lithosphere: *Geological Society of America Bulletin*, v. 83, p. 813–818.

Simmons, A.T., Tosdal, R., Mortensen, J., Baker, D. and Baknes, M. (2004): Geologic Framework and temporal and spatial distribution of Cretaceous Epithermal Systems in northwest British Columbia; Poster Abstract for the Mineral Exploration Roundup, *British Columbia & Yukon Chamber of Mines.*

Simmons, A.T., Tosdal, R.M., Baker, D.E.L., Friedman, R.M. and Ullrich, T.D. (2005a): Late Cretaceous Volcano-Plutonic Arcs in Northwestern British Columbia: Implications for Porphyry and Epithermal Deposits; *in* Geological Fieldwork 2004, Grant, B. and Newell, J.M., Editors, *B.C. Ministry of Energy Mines and Petroleum Resources,* Paper RR15, pages 347-360.

Simmons, A.T., Tosdal, R.M. and Baker, D.E.L. (2005b): Thorn Au-Ag Prospect: A Geologic Framework for Late Cretaceous Porphyry-Epithermal Mineralization in Northwest British Columbia Canada; Oral Presentation Abstract for the 2005 GSN Conference, *Geological Society of Nevada.*

Smith, M.T. and Mihalynuk, M.G. (1992): Tulsequah Glacier: Maple Leaf (104K); *in* Exploration in British Columbia 1991, *B.C. Ministry of Energy, Mines, and Petroleum Resources*, pages 133-142.

Souther, J.G. (1971): Geology and Mineral Deposits of the Tulsequah map-area, British Columbia; *Geological Survey of Canada,* Memoir 362, 84 pages.

Stacey, J.S. and Kramers, J.D. (1975): Approximation of terrestrial lead isotope evolution by a two-stage model; *Earth and Planetary Science Letters*, Volume 26, pages 207-221.

Sun, S.-s, Nesbit, R.W. and Sharaskin, A.Y., (1979): Geochemical characteristics of mid-ocean ridge basaltsl; *Earth and Planetary Science Letters*, Volume 35, pages 429-448.

Sun, S.S. and McDonough, W.F. (1989): Chemical and isotopic systematics of oceanic basalts: Implications for mantle composition and processes; *in* Magmatism In The Ocean Basins, *Geological Society of London*, Special Publication 42, pages 313-345.

Sutherland Brown, A., ed., 1976, Porphyry deposits of the Canadian Cordillera; *Canadian Institute of Mining and Metallurgy*, Special Volume 15, 510 p.

Thorstad, L.E., and Gabrielse, H. (1986): The Upper Triassic Kutcho Formation, Cassiar Mountains, north-central British Columbia; *Geological Survey of Canada*, Paper 86-16, 53 pages.

Titley, S.R., ed., 1982, Advances In Geology Of The Porphyry Copper Deposits, Southwestern North America: Tucson, University of Arizona Press, 560 p.

Wheeler, J.O. (1961): Whitehorse map-area, Yukon Territory, (105D); *Geological Survey of Canada,* Memoir 312, 156 pages.

Wheeler, J.O. and McFeely, P. (1987): Tectonic Assemblage Map of the Canadian Cordillera, *Geological Survey of Canada*, Open File 1565.

Wheeler, J.O., Brookfield, A.J., Gabrielse, H., Monger, J.W.H., Tipper, H.W. and Woodsworth, G.J. (1991): Terrane map of the Canadian Cordillera; *Geological Survey of Canada,* Map 1713A, scale 1:2 000 000.

Winchester, J.A. and Floyd, P.A. (1977): Geochemical discrimination of different magma series and their differentiation products using immobile elements; *Chemical Geology*, Volume 20, pages 325-343.

Chapter 3

Late Cretaceous Hydrothermal Mineralization of the Stikine Terrane: Thorn Property, Northwest British Columbia, Canada

Abstract

Structurally-controlled high-sulphidation mineral assemblage veins and a polymetallic breccia-hosted deposit (Oban breccia) are the most important styles of mineralization present on the Thorn Property. Other styles of mineralization include porphyry Cu-Mo, Zn-Fe skarn and quartz-carbonate-arsenopyrite-stibnite veins. Both the veins and the breccia are hosted in *ca.* 91 Ma quartz-plagioclase-biotite porphyritic quartz diorite of the Thorn Suite. The veins are temporally related to the later stages of the *ca.* 82 Ma Windy Suite rocks, while the breccia-hosted deposit predates Windy Table suite rocks.

The Oban breccia is a magmatic-hydrothermal breccia, which is host to polymetallic Ag-Pb-Zn-(Au-Cu) mineralization and is located within the Thorn Stock. The breccia is clast-supported, consisting of rounded cobbles and boulders of Thorn Stock and rare Triassic Stuhini Group and/or Jurassic Laberge Group rocks. Crustiformally-banded boulangerite, sphalerite and pyrite make up the majority of ore minerals and replace the sand-sized broken feldspar-quartz (with rare euhedral biotite) to rock flour matrix of the breccia. The clast-supported nature of the breccia limits the grade of the mineralized breccia. Sericite, carbonate, and quartz alteration are characteristic of the breccia.

Structurally-controlled veins contain minerals and mineral assemblages characteristic of a high-sulphidation system, including enargite + pyrite, pyrophyllite, diaspore and alunite. Alteration and mineralization are controlled by steeply-dipping NE-trending normal faults, which occur in six parallel and distinct zones along La Jaune Creek. Higher Cu/Zn and As/Sb ratios indicate that auriferous fluids were sourced in the SW of the vein systems. In the up-dip and NE directions as well as with time, fluids evolved from high-sulphidation and acid to intermediate sulphidation and neutral. Approximately 1600 m of older Windy Table volcanic strata overlie the known tops of the younger high-sulphidation mineral assemblage vein systems suggesting that the veins formed at sub-epithermal depths.

Pb isotopic compositions of feldspar from magmatic rocks and sulphides suggest that the Windy Table suite rocks are the likely sources for the auriferous fluids. No or little fluid-wall rock interaction took place during the deposition of the ore minerals. Additionally, the Pb isotopic compositions for sulphides in mineralized rocks as well as feldspar from igneous rocks fall between known Pb isotopic compositions for mineralized rocks from the pre-Cretaceous and Tertiary of the Stikine Terrane, indicating that the Pb source for mineralized rocks at the Thorn are part of a single evolving system for the Stikine terrane.

Introduction

The linkage between hydrothermal systems and magmatic events is well-documented (e.g. Sillitoe, 1972; Sutherland-Brown, 1976; Titley, 1982; Sawkins, 1990; Bissig *et al.*, 2003). However, in the Canadian northern Cordilleran linkages between mineralizing systems and the rocks that sourced the mineralizing fluids, have been poorly demonstrated. The Late Cretaceous magmatic events of the Thorn and the Windy Table Suites (Chapter 2) have been only recently been described (e.g. Mihalynuk, 1999; Simmons *et al.*, 2005). These rocks form a Late Cretaceous volcanoplutonic arc, which extends at least 300 km from the Golden Bear Mine in the southeast to the Tagish Lake area in the northwest (Figure 3-1). Hydrothermal systems with spatial correlation to the Late Cretaceous volcanoplutonic belt have been recognized in the past, but their timing and origin was not well understood (e.g. Golden Bear, Thorn, Red Cap, Bing). Understanding the timing, style and the pre-depositional environment of mineralized systems in relation to their host and source rocks is an important step in developing exploration models and exploration concepts with reasonable spatial constraints.

The Late Cretaceous volcanoplutonic arc is a northwest-trending belt comprised of two major components; the older Thorn Suite diorite porphyry intrusions and the younger Windy Table dacitic pyroclastic rocks, associated rhyolite flow domes and subvolcanic intrusions (Chapter 2). Volcanic remnants are periodically preserved along the belt and separated by 10-20 km. At the Thorn Property, the volcanic centre is preserved in a volcanic-tectonic depression in which the pyroclastic rocks have a preserved estimated thickness of 1600 m. Two significant periods of hydrothermal activity have been recognized at the Thorn Property. The oldest occurs prior to the onset of Windy Table magmatism and after the emplacement of the Thorn Stock, during which time the Thorn Stock was exhumed. The youngest of the two systems, and perhaps the more important of the two, occurred during the waning stages of Windy Table volcanism and is hosted in the Thorn stock at the base of the Windy Table strata.

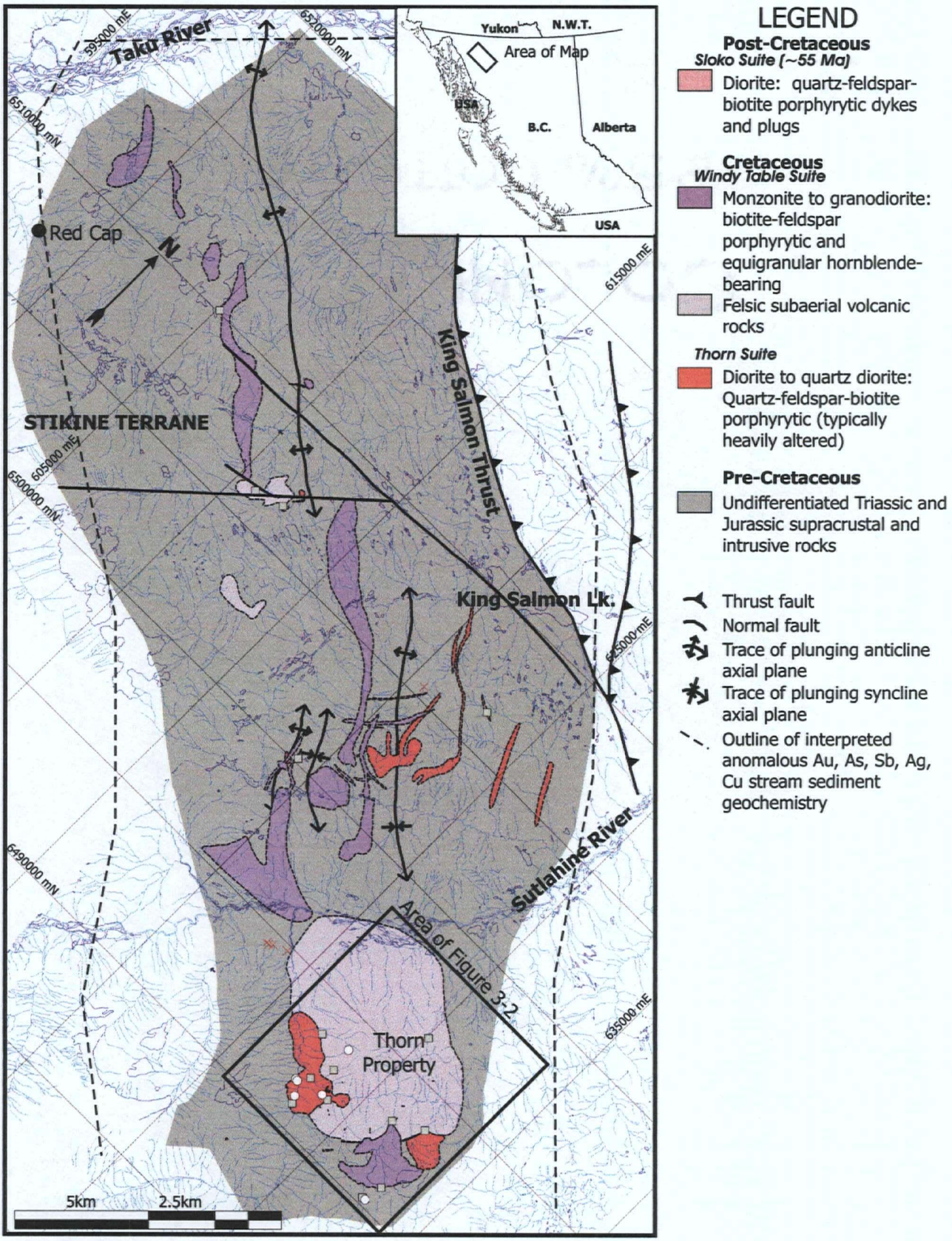

Figure 3-1: Regional map of the study area highlighting post accretionary magmatic rocks and the area of anomalous Au stream sediment geochemistry. Area of anaomalous geochemistry is also the approximate extent of the Late Cretaceous volcanoplutonic belt.

The objectives of this paper are to:

1) demonstrate the linkage between Late Cretaceous magmatism and hydrothermal systems at the Thorn Property.
2) document the styles and types of mineralizing systems at the Thorn Property; and discuss exploration techniques.
3) discuss metal zonations and alteration and their implications for fluid evolution in high-sulphidation systems.
4) discuss timing, structure and stratigraphy as important pre-mineralizing events to the formation of magmatic-hydrothermal mineralization and alteration at the Thorn Property.
5) compare other systems world-wide to put the mineralizing system the Thorn Property into perspective.

Geological Framework of the Thorn Property

The Thorn Property is located in northwest British Columbia in the Stikine tectonostratigraphic terrane, which represents an exotic volcanic arc developed outboard of western North America during the late Paleozoic through to the mid-Jurassic and was accreted onto North America at these latitudes by 172 Ma (Mihalynuk and Smith, 1992; Smith and Mihalynuk 1992). At the Thorn Property the Stikine arc is composed of the Stuhini and Laberge Groups, which comprise the host rocks for Late Cretaceous magmatism and related mineralizing events (Figure 3-2; Simmons *et al.*, 2005; Chapter 2). The Stuhini Group is an island arc sequence formed on top of the Paleozoic Stikine Assemblage rocks and is represented by a thick sequence of submarine massive andesite and pillow basalt with intercalated siltstone, overlain by increasing amounts of deep submarine clastic sedimentary rocks that shallow upwards with increasing amounts of thin limestone beds (Awmack, 2003; Baker, 2003; Simmons *et al.*, 2005). The top of the Stuhini Group is marked by the 5-20 m thick limestone unit known as the Sinwa Formation (Souther, 1971). Laberge Group rocks unconformably overlie the Stuhini Group rocks and are composed of approximately 3.5–5 km of calcareous clastic sedimentary rocks including sandstone, conglomerate and shale (Bultman, 1979).

Following the accretion of the Stikine arc a subduction zone was re-established west of the current location of Stikinia. Magmatism related to this subduction is recorded in three events at the Thorn Property beginning with the 93-88 Ma Thorn Suite followed by the 86-80 Ma Windy Table Suite and the 58-54 Ma Sloko Suite (Chapter 2). Together, the Thorn and

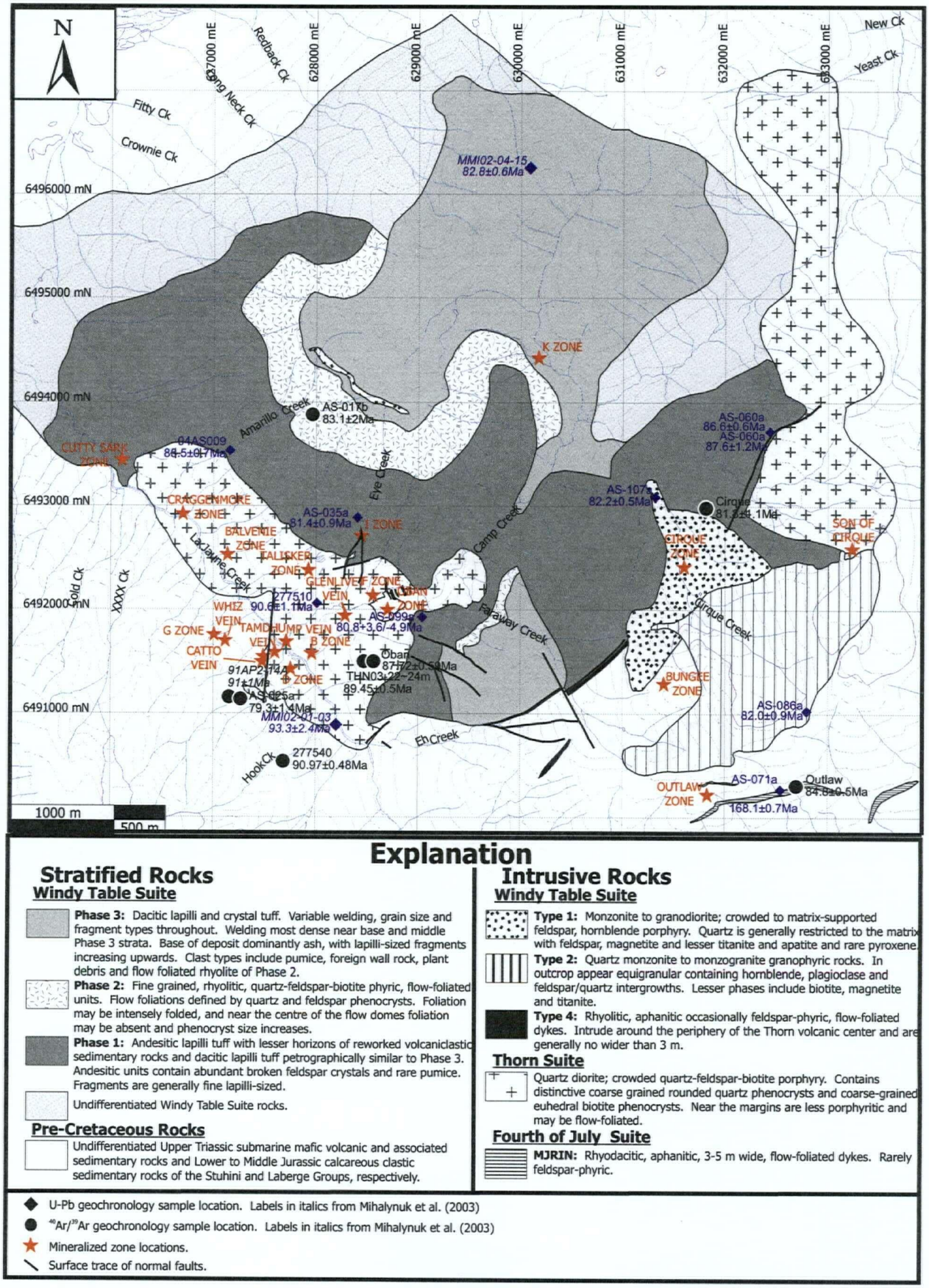

Explanation

Stratified Rocks

Windy Table Suite

Phase 3: Dacitic lapilli and crystal tuff. Variable welding, grain size and fragment types throughout. Welding most dense near base and middle Phase 3 strata. Base of deposit dominantly ash, with lapilli-sized fragments increasing upwards. Clast types include pumice, foreign wall rock, plant debris and flow foliated rhyolite of Phase 2.

Phase 2: Fine grained, rhyolitic, quartz-feldspar-biotite phyric, flow-foliated units. Flow foliations defined by quartz and feldspar phenocrysts. Foliation may be intensely folded, and near the centre of the flow domes foliation may be absent and phenocryst size increases.

Phase 1: Andesitic lapilli tuff with lesser horizons of reworked volcaniclastic sedimentary rocks and dacitic lapilli tuff petrographically similar to Phase 3. Andesitic units contain abundant broken feldspar crystals and rare pumice. Fragments are generally fine lapilli-sized.

Undifferentiated Windy Table Suite rocks.

Pre-Cretaceous Rocks

Undifferentiated Upper Triassic submarine mafic volcanic and associated sedimentary rocks and Lower to Middle Jurassic calcareous clastic sedimentary rocks of the Stuhini and Laberge Groups, respectively.

Intrusive Rocks

Windy Table Suite

Type 1: Monzonite to granodiorite; crowded to matrix-supported feldspar, hornblende porphyry. Quartz is generally restricted to the matrix with feldspar, magnetite and lesser titanite and apatite and rare pyroxene.

Type 2: Quartz monzonite to monzogranite granophyric rocks. In outcrop appear equigranular containing hornblende, plagioclase and feldspar/quartz intergrowths. Lesser phases include biotite, magnetite and titanite.

Type 4: Rhyolitic, aphanitic occasionally feldspar-phyric, flow-foliated dykes. Intrude around the periphery of the Thorn volcanic center and are generally no wider than 3 m.

Thorn Suite

Quartz diorite; crowded quartz-feldspar-biotite porphyry. Contains distinctive coarse grained rounded quartz phenocrysts and coarse-grained euhedral biotite phenocrysts. Near the margins are less porphyritic and may be flow-foliated.

Fourth of July Suite

MJRIN: Rhyodacitic, aphanitic, 3-5 m wide, flow-foliated dykes. Rarely feldspar-phyric.

- U-Pb geochronology sample location. Labels in italics from Mihalynuk et al. (2003)
- $^{40}Ar/^{39}Ar$ geochronology sample location. Labels in italics from Mihalynuk et al. (2003)
- Mineralized zone locations.
- Surface trace of normal faults.

Figure 3-2: Simplified geology of the Thorn Property and locations of samples collected for U-Pb and $^{40}Ar/^{39}Ar$ geochronology, interpreted ages, and locations of mineralized zones.

Windy Table Suites comprise the Late Cretaceous volcanoplutonic belt, which extends for at least 300 km from the Golden Bear Mine to the BC-Yukon border (Simmons *et al.*, 2005).

The Thorn Suite rocks are typified by the "Thorn Stock", which is a quartz-plagioclase-biotite porphyritic quartz diorite. Large (>1 cm) euhedral biotite phenocrysts and rounded quartz phenocrysts are diagnostic of this rock type in the Late Cretaceous volcanoplutonic belt. The stock is elongate in two directions; with the major axis trending northwest and the minor axis trending east-west. These directions correspond to two major regional lineaments that are likely related to the accretion of Stikinia onto Cache Creek, based upon their NNW-orientation (Figure 3-2). The stock has reported U-Pb zircon ages of 90.6 ± 1.1 Ma and 93.3 ± 2.4 Ma (Chapter 2 and Mihalynuk *et al.*, 2003) and is the major host unit for quartz-enargite-tetrahedrite-pyrite veins and the Oban breccia-hosted, matrix replacement boulangerite-sphalerite-pyrite-chalcopyrite mineralized systems.

The Windy Table rocks are divided into intrusive and extrusive rocks. The intrusive rocks can be divided into four sub-types based upon textures and composition. The following is meant only as a brief description of these sub-types, Chapter 2 provides a concise overview of these units and reasons why they are subdivided. Type 1 intrusions are characterized by the Cirque Porphyry, which is a variably porphyritic quartz monzonite containing feldspar, biotite and hornblende phenocrysts with quartz in the matrix, and fine grained feldspar and minor titanite (Figure 2-3). These intrusions are constrained mainly to the later stages of the Windy Table Suite (Chapter 2). Type 2 rocks are microgranophyric quartz monzonite to monzogranite and contain feldspar-quartz intergrowths, as well as hornblende and biotite. These intrusions are slightly older than Type 1 intrusions, and are less common (Chapter 2). Type 3 intrusions, which occur 2 km north of the Thorn Property, are characterized by megacrystic plagioclase in an otherwise feldspar-quartz porphyritic rock. These rocks are defined by flatter chondrite-normalized REE patterns and a large positive Eu anomaly and characterize the early stages of the Windy Table Suite (Chapter 2). Type 4 rocks occur as several narrow felsic flow-foliated dykes and crosscut all of the above intrusive types. These rocks are aphanitic, typically highly sericite-altered, K-feldspar bearing rhyodacites (Chapter 2).

The Windy Table Suite extrusive rocks unconformably overlie the Thorn Stock and cover the majority of the map area on the Thorn Property (Figure 3-2). The volcanic strata form a greater than 5 km-wide volcanic sequence with curvilinear fault contacts. These faults mark the boundaries of the volcanic-tectonic depression, possibly of a caldera, in which the volcanic srata has been preserved. All volcanic strata broadly dip shallowly to the northeast away from

the fault at La Jaune Creek. Although not the type locality for Windy Table Suite volcanic rocks (see Mihalynuk, 1999), the volcanic centre at the Thorn Property represents the thickest sequence of these strata, estimated to be approximately 1600 m thick (Figure 3-3; Simmons *et al.*, 2005). The sequence of strata can be subdivided into three distinct periods of volcanic activity. Phase 1 of the volcanic strata, forming the base of the Windy Table Suite sequence here are approximately 560 m thick, composed of unwelded to slightly welded, dacitic to andesitic, crystal and lapilli tuffs with lesser volcaniclastic rocks (Chapter 2). This phase of volcanism is constrained by the age of the lowermost strata of Phase 1 which has a U-Pb zircon age of 85.5 ± 0.7 Ma and is overlain by Phase 2 volcanic rocks dated at 80.8 +3.6/-4.9 Ma (Chapter 2). Phase 2 volcanism is characterized by approximately 340 m of flow-foliated rhyolitic flow domes and shallow-level intrusions (Figure 3-3). Phase 3 volcanic rocks overlie the flow domes and are composed of approximately 900 m of viably welded dacitic tuffs. Timing of this stage of volcanism is document by Mihalynuk *et al.* (2003), who reports a U-Pb TIMS zircon age of 82.8 ± 0.6 Ma near the top of Phase 3 volcanic strata, indicating that 900 m of strata were deposited in a very short time span (Figure 3-3).

The Sloko Suite rocks intruded the area regionally, although none have been observed on the Thorn Property (Simmons *et al.*, 2005). The Sloko Suite rocks are similar to the Thorn Suite rocks, but are generally unaltered and contain less quartz. Although not present on the Thorn Property, the Sloko Suite rocks are important geochronologically as there is resetting of the $^{40}Ar/^{39}Ar$ systematics in the alteration assemblages associated with mineralized rocks at the Thorn Property (Appendix 1).

Mineralizing Events

At the Thorn Property, two distinct periods of hydrothermal activity are evident based on geochronologic results and stratigraphic relationships. These periods are separated into "pre-Windy Table hydrothermal alteration and mineralization" and "Windy Table-associated alteration and mineralization". Pre-Windy Table hydrothermal activity is represented by the Oban breccia, located on the southeast side of Camp Creek. The breccia is hosted entirely within the Thorn Stock (Figure 3-2). This period of hydrothermal activity is constrained by two $^{40}Ar/^{39}Ar$ ages to between 90 Ma and 87.1 Ma (Figure 3-3). The Oban breccia is an Ag-Au-Pb-Zn- (Cu) deposit hosted in a magmatic-hydrothermal breccia (Baker, 2003). A second hydrothermal event, which is coeval with Windy Table Suite rocks, occurred between 85.3 Ma and 77.9 Ma (Figure 3-3). Hydrothermal mineralization temporally and spatially related to Windy Table rocks includes structurally-controlled enargite-tetrahedrite veins, weak porphyry Cu-Mo and Fe-Zn-Ag

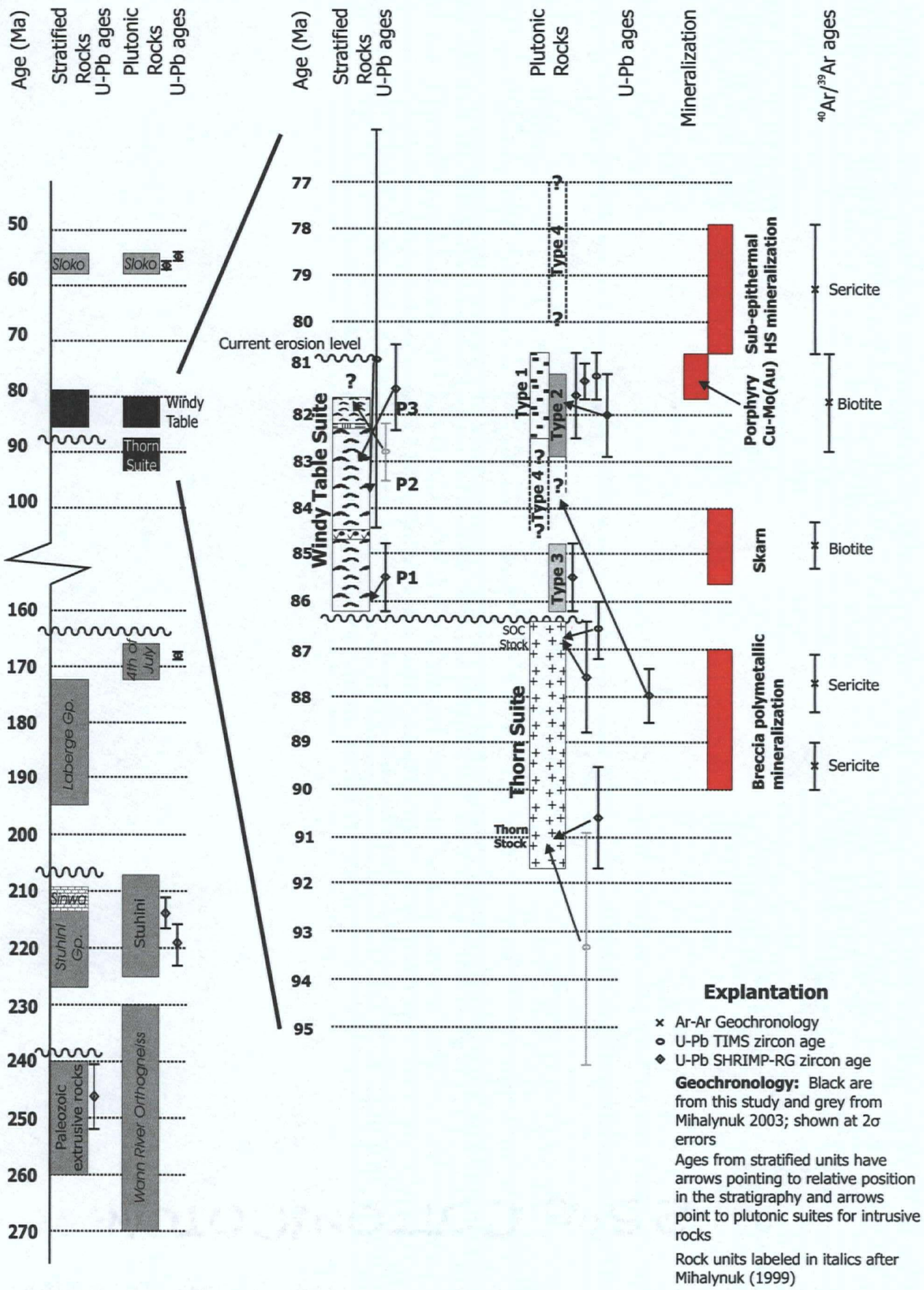

Figure 3-3: Stratigraphic column for rocks from the Thorn Property with emphasis on Late Cretaceous magmatic rocks and timing of related hydrothermal alteration. Errors are given at 2σ levels.

skarn. The Windy Table-associated hydrothermal event is more widespread on the Thorn Property (Figure 3-2). Appendix 1 provides a concise overview of the interpretation of $^{40}Ar/^{39}Ar$ ages and results.

Pre-Windy Table Hydrothermal Systems

Hydrothermal systems predating the Windy Table Suite rocks in the Late Cretaceous are rare throughout the north Cordilleran (Mihalynuk, 1999). The beginning of the Windy Table Suite is constrained to 85.5 ± 0.7 Ma (Chapter 2) and thus any hydrothermally altered rock predating this is referred to as pre-Windy Table. On the Thorn Property, the Oban breccia fits this criterion and is constrained by two $^{40}Ar/^{39}Ar$ sericite ages presented below.

Oban Breccia

The Oban breccia forms a broadly circular body approximately 300 m in diameter within the Thorn Stock near its northeast extent, south of Camp Creek (Figure 3-2). The Oban breccia is interpreted as a magmatic-hydrothermal breccia formed from fluid streaming above a crystallizing pluton, presumably beneath the Thorn Stock. Baker (2003) compared the characteristics of the Oban breccia with generalized characteristics of known magmatic-hydrothermal breccias worldwide (Sillitoe, 1985) determining a clear magmatic-hydrothermal origin. These characteristics are summarized in Table 3-1.

The Oban breccia consists of pervasively altered breccia comprised of pebble to metre-scale, typically rounded to sub-rounded fragments, predominately of the Thorn Stock quartz diorite porphyry (Figure 3-4A). Other fragments include aphanitic, felsic volcanic units and black argillite, likely from overlying Stuhini and Laberge Group rocks. The matrix to this fragment framework varies from medium- grained, broken feldspar-quartz to fine-grained, dark grey rock flour. Both matrix types are interpreted to be the products of grinding and milling of the Thorn Stock during fragmentation (Figure 3-4B). The breccia is clast-supported containing approximately 85% clasts and 15% matrix. Mineralization in the breccia is irregular and is limited to a 40 m x 40 m zone within the core of the breccia. Locally the matrix is comprised of massive pyrite-sphalerite-boulangerite. In these zones porphyry fragments show evidence of reaction with sulphide-depositing fluid (i.e., irregular, cuspate fragment-sulphide contacts) indicating that the sulphide zone formed by matrix replacement.

Controls on the distribution of mineralization in the Oban breccia are difficult to determine. Two factors need to be considered: (a) the distribution of the breccia body, and (b) the distribution of sulphides within it. The distribution of breccia outcrops, although obscured

Table 3-1: Comparison of Oban Breccia with generalized characteristics of magmatic-hydrothermal breccias.

Characteristic	Magmatic Hydrothermal Breccias (non-porphyry systems)[1]	Oban Breccia
Morphology	Roughly circular or ovoid pipes. Several pipes show decreased brecciation inward and downward	Apparently circular
Inclination	Subvertical (<15°)	?
Horizontal	Generally 50-300 m, but up to 900 x 1300 m	Minimum 300 m diameter
Vertical extent	Several times greater than maximum horizontal dimension; >725 m in 4 districts	Minimum 220 m (Baker, 2003)
Tops/Bottoms	Bottoms irregular but grossly flat, with breccia terminating abruptly against less altered intrusive or country rocks. Topped by domed or altered rocks.	Unknown
Reached paleosurface?	Not likely	Localized argillite fragments possibly from overlying sedimentary rocks
Clusters?	Occur alone or in clusters of up to 200	Only known example
Structure	Regional structures play little part in localizing pipes	No apparent structural control
Relation to intrusive rocks	Commonly in upper parts or immediately above stocks or plutons	Within 70 m of contact with Windy Table strata; in columnar jointed Thorn Stock
Coeval intrusive activity	Fine grained porphyritic intrusive rock as dykes, fragments and partly disaggregated bodies in breccia	Unrecognized
Fragments	Angular to subrounded from a few centimetres to a few metres. Upper parts of some pipes have tabular fragments. Spheroidal clasts may have concentric onion-like fracturing.	Rounded to subrounded, rare angular fragments.
Matrix	Generally absent. Rock flour in pipes more milling.	Granular to silt-sized rock flour matrix common.
Vertical displacement	Small: commonly 25-125 m downward displacement. Local jigsaw textures. Little mixing of rock types where wall rocks are variable.	Little mixing of rock types
Contacts	Abrupt, 1-5 m of closely spaced vertical fractures; or gradational.	Gradational between massive and fractured porphyry to breccia
Alteration & mineralization	All breccias underwent alteration and open-spaced filling, >50% ore bearing in a cluster.	Widespread but variable alteration between fragments
Alteration type	Sericite most common, tourmaline, chlorite, silica common; K-feldspar, propylitic, calc-calc-silicate in a few.	
Mineralization	Metal zonation common	Pb-Zn-Ag-(Cu) out to Zn-Pb-(Au)

[1] generalized characteristics summarized by Sillitoe (1985)

by till cover, suggests that the body has a circular outcrop pattern of about 300 m in diameter. Additionally, three outcrops of magmatic-hydrothermal breccia were mapped within the F Zone, across Camp Creek from the Oban zone (Figure 3-2). These outcrops may be portions of the main Oban breccia that became isolated during incision of Camp Creek. If so, the northern contact of the breccia dips southward which would imply that the pipe has a southward plunge. Additionally, breccia outcrops within the F Zone locally show steep contacts characterized by a gradient of fracture intensity between breccia and massive porphyry. These observations also support a pipe-like geometry for the breccia.

A major zone of pyrite-sphalerite-boulangerite has been intersected in several drill holes in three sections across the Oban breccia. These intersections indicate that within the pipe-like breccia body, the mineralized zone is tabular, dips steeply to the west and trends NNE. The true width of this zone varies from 14–26 m. A generally lower-grade zone up to 25 m wide flanks this mineralized core. Massive sulphide from this style of mineralization may grade up to 3.48 g/t Au, 6149 g/t Ag, 42.97 % Pb and 3.45% Zn (Awmack, 2003). However, because

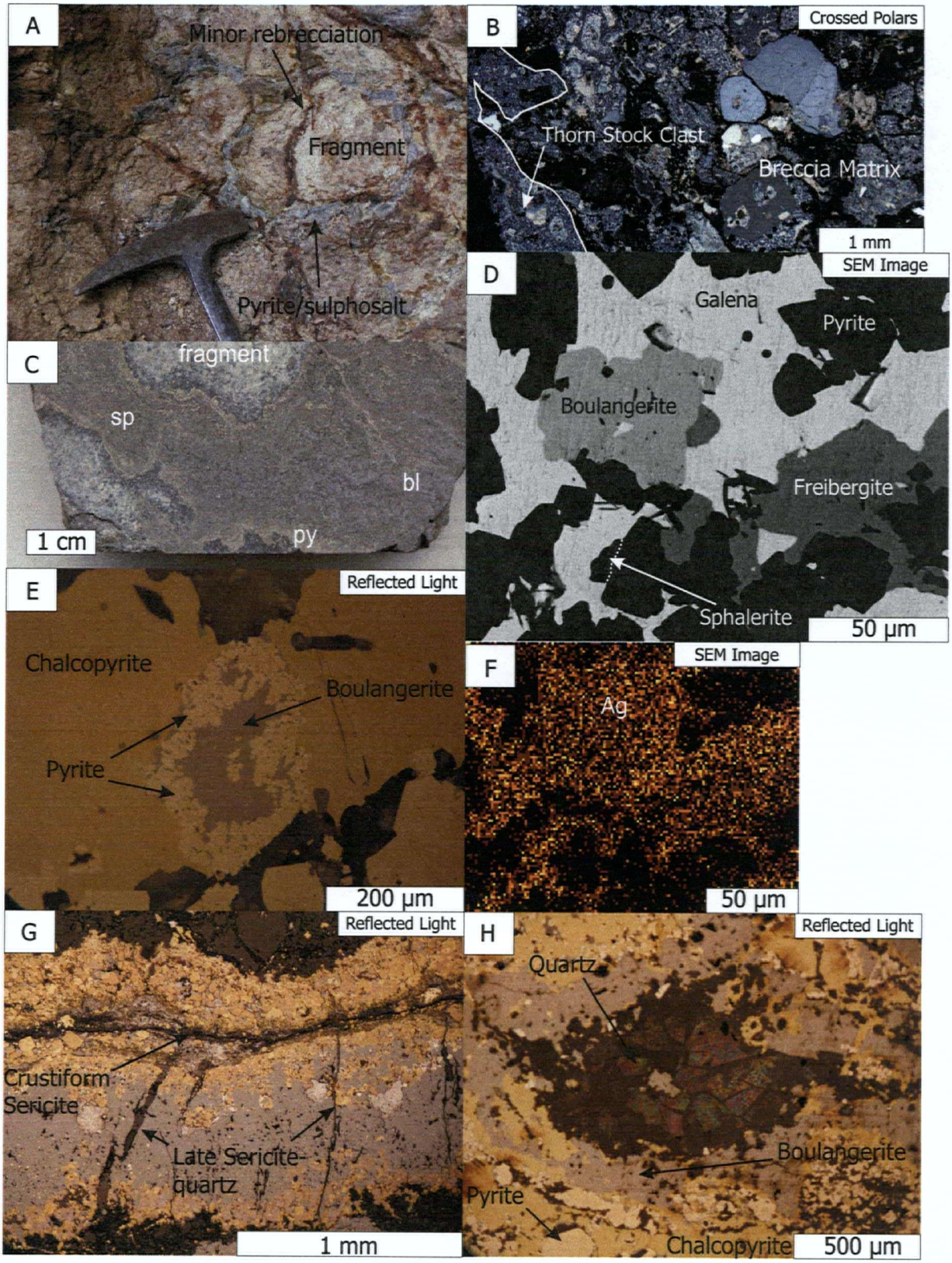

Figure 3-4: Photographs, photomicrographs and images of Oban breccia textures, mineralization and alteration. A) Sulphides and sulphosalts surrounding fragments, replacing matrix and minor re-brecciation of Oban breccia fragment, B) Milled matrix of unmineralized breccia, composed of milled smaller fragments of Thorn Stock as well as feldspar and quartz from Thorn Stock, with minor sericite, C) Crustiform banding of boulangerite (bl), sphalerite (sp) and pyrite (py), D) Mineral overgrowths and replacement showing relative timing of (oldest to youngest) galena, boulagerite, sphalerite, freibergite and pyrite, E) chalcopyrite replacement by pyrite and boulangerite, F) Same image as D, scanning for Ag peaks, showing that Ag is richest in early sulphides, especially in boulangerite and freibergite, G) Early sericite as part of the crustiform assemblage and later quartz sericite veinlets cutting crustiform assemblages, and E) Late open-space filling by quartz.

auriferous fluids replace the matrix of the breccia and the breccia is dominantly clast-supported, the grade becomes highly diluted. Typical intersections include: 38.6 m of 1.22 g/t Au and 188 g/t Ag (THN03-19; Figure 3-2; Baker, 2003), 40.7 m of 0.83 g/t Au and 119 g/t Ag (THN03-21; Figure 3-2) and 30.6 m of 62 g/t Ag (THN03-22; Baker 2003). Within these broader intersections higher-grade intersections such as 14.0 m of 1.97 g/t Au and 190 g/t Ag (THN03-19) were yeilded (Figure 3-2; Baker, 2003).

The mineralized trend is manifest in sulphide content (and metal grades) and possibly in a distinct breccia facies (fragment-supported, rock flour-rich). No secondary planar features–such as veins or faults, are present suggesting that a specific type of breccia was preferentially mineralized. Surface examination of outcrops was unable to provide mappable breccia facies. Instead, breccia characteristics such as fragment size and abundance change over short distances within single outcrops. Therefore, the control and extent of mineralized Oban breccia has yet to be discovered and it is unlikely that such facies could be followed through drilling.

Ore Mineralogy

Ore minerals are crustiform-banded and replace the matrix of the breccia. In hand specimen, sphalerite, boulangerite and pyrite bands are most common (Figure 3-4C). However, sericite, chalcopyrite, and cassiterite have also been identified as part of the banded ore assemblage. Other ore minerals observed in thin section or on the scanning electron microscope (SEM) are galena, freibergite, arsenopyrite, hematite and cassiterite (arsenopyrite, hematite and cassiterite from Lang and Thompson, 2003). Re-brecciation of the Oban breccia occured with the introduction of the auriferous fluid, but is rare throughout the mineralized zone, indicating that the event during which ore minerals precipitated was relatively subdued. Chalcopyrite and cassiterite are constrained to a narrow central zone in the mineralized area and may represent the earliest fluid phases that precipitated Cu- and Sn-rich minerals. Pb- and Zn-rich sulphides and sulphosalts were deposited peripheral to the Cu-Zn zone, probably from cooler fluids.

Pyrite is present as fine-grained anhedral masses, commonly contained within other ore minerals or as coarse-grained (>0.5 mm) euhedral pyrite, which overgrows and cross-cuts most other ore minerals (Figure 3-4D). Early sulphide phases include galena and boulangerite, both of which are replaced and overgrown by younger freibergite and sphalerite (Figure 3-4D). During the early sulphide stage, galena is replaced by boulangerite. During the sulphide stage, most freibergite is later than sphalerite, but is also commonly intergrown with sphalerite (Figure 3-4D). Arsenopyrite is commonly associated with, and intergrown with, late pyrite, while

cassiterite occurs as inclusions in early stage sulphides (Lang and Thompson, 2003). Additionally, chalcopyrite and cassiterite occur as intergrowths, which are overgrown by later Pb-bearing mineral phases in the core of the system (Figure 3-4E). The distribution of chalcopyrite and cassiterite, while potentially important remains unknown.

Understanding the distribution and zoning of ore minerals within the mineralized body is important because particular ore minerals are associated with precious metals such as Ag and Au. In the Oban breccia, Ag is more important than Au (in terms of concentration and value), although weak Au does carry into the wall rock. Observations from drill core show that a typical mineralized section through the Oban breccia would grade from a chalcopyrite-pyrite core outwards to a boulangerite-sphalerite-pyrite zone grading outwards to a pyrite-only shell. Observations from the SEM suggest that the most Ag-rich minerals are freibergite and boulangerite (Figure 3-4F). Thus the zonation of minerals in drill core is consistent with an Ag-rich core coincident with the boulangerite-sphalerite-pyrite zone contained within a low-grade Au shell coincident with the pyrite only outer zone of the mineralized Oban breccia.

Alteration Mineralogy

Alteration of the Oban breccia is characterized by carbonate-sericite-quartz coincident with the most intensely mineralized breccia. The intense alteration grades outwards away from the mineralized zone to chlorite-carbonate (±sericite) assemblages. Both the matrix and clasts of the breccia are pervasively altered. Sericite occurs in two texturally distinct forms: a) as late veins with quartz that cross-cut crustiform banding or euhedral laths disseminated throughout breccia; and b) as part of the crustiform assemblage either associated with pyrite-rich bands or as separate massive sericite bands (Figure 3-4G). Post-sulphide euhedral disseminated sericite has a $^{40}Ar/^{39}Ar$ plateau age of 87.72 ± 0.59 Ma (THN03-22; Figure 3-5A; Table 3-1; Appendix I), while massive sericite from the crustiform assemblage has and $^{40}Ar/^{39}Ar$ plateau age of 89.45 ± 0.50 Ma (Oban; Figure 3-5B; Table 3-2; Appendix I). The closure temperature of sericite is not well constrained, but is accepted to be approximately 350 ± 50°C (Hanes, 1991), which is well below the temperature of sulphide deposition. Therefore, sericite is considered to have cooled instantaneously below its closure temperature. However, the small grain size of sericite causes increased potential for Ar-loss during post-depositional processes (e.g., other magmatic and hydrothermal events). Appendix I shows four samples which have undergone post depositional Ar-loss due to heating during the *ca.* 55 Ma Sloko magmatic event. Carbonate (mainly ankerite with lesser calcite) and quartz are mainly constrained spatially to the sphalerite-boulangerite rich zones and appear to have precipitated in open space (Figure 3-4H).

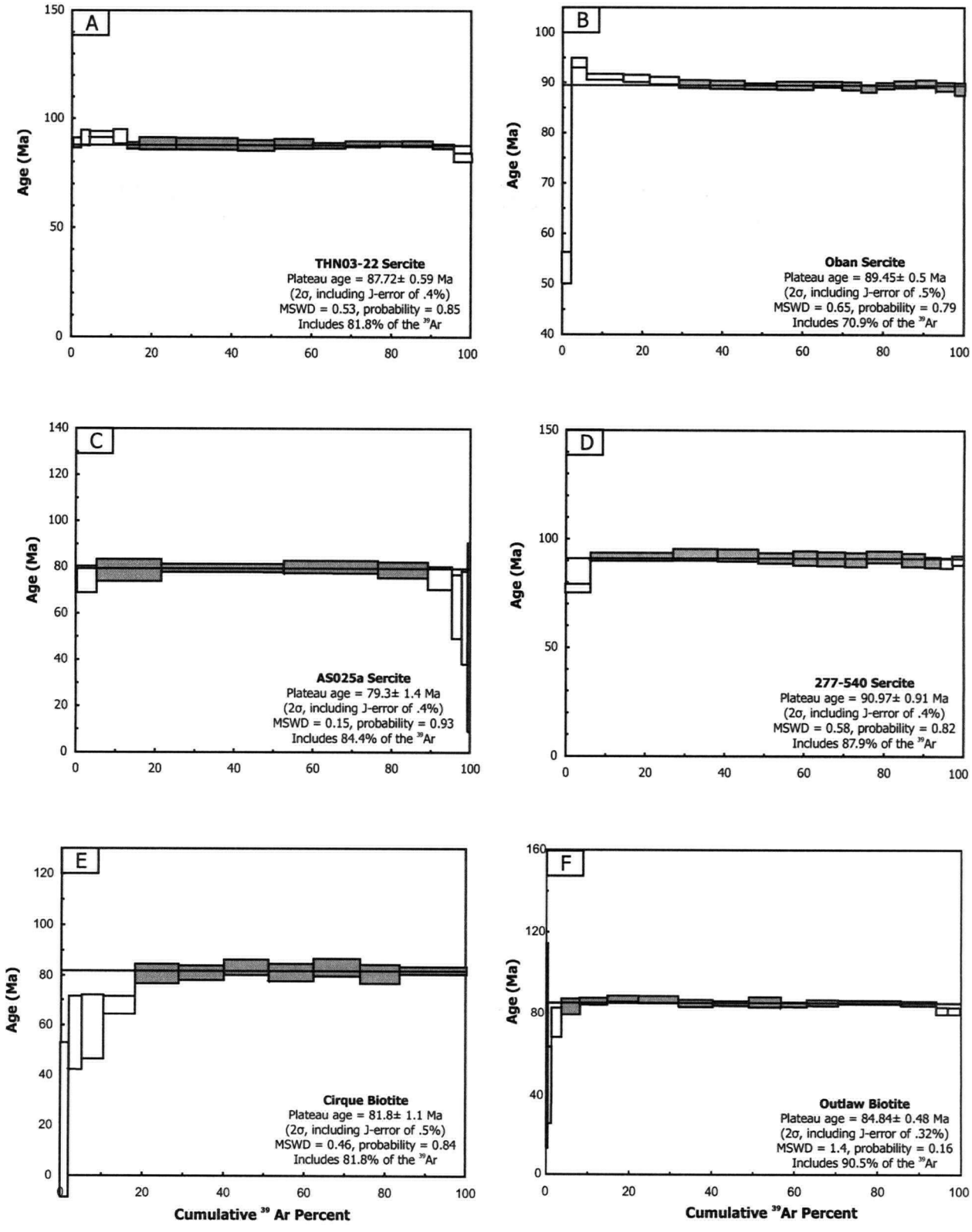

Figure 3-5: $^{40}Ar/^{39}Ar$ geochronology of alteration from the Thorn Property. Plateau steps are filled, and open boxes are rejected. Errors in box heights given at 2σ. Inverse isochrons shown in Appendix I.

Table 3-2: $^{40}Ar/^{39}Ar$ results from alteration mineralogy associated with mineralized zones

Laser Power(%)	Isotope Ratios $^{40}Ar/^{39}Ar$	$^{38}Ar/^{39}Ar$	$^{37}Ar/^{39}Ar$	$^{36}Ar/^{39}Ar$	Ca/K	Cl/K	$\%^{40}Ar$ atm	f ^{39}Ar	$^{40}Ar^*/^{39}ArK$	Age
		Sample=**Oban**		Mineral=**Sericite**						
2	7.363±0.006	0.016±0.056	0.010±0.066	0.015±0.043	0.095	0	57.52	2.27	3.131±0.186	53.16±3.11
2.2	6.068±0.007	0.013±0.038	0.009±0.065	0.002±0.090	0.092	0	7.88	3.83	5.600±0.059	94.00±0.96
2.4	5.801±0.005	0.013±0.017	0.009±0.020	0.001±0.063	0.088	0	6.62	9.07	5.427±0.036	91.16±0.59
2.5	5.942±0.007	0.0130.030	0.009±0.043	0.002±0.040	0.085	0	9.16	6.51	5.408±0.044	90.85±0.73
2.6	5.760±0.007	0.013±0.020	0.009±0.033	0.001±0.065	0.092	0	6.72	7.4	5.383±0.047	90.44±0.77
2.7	5.669±0.006	0.013±0.024	0.010±0.017	0.001±0.108	0.098	0	5.94	7.7	5.342±0.050	89.76±0.82
2.8	5.681±0.008	0.013±0.023	0.009±0.034	0.001±0.054	0.091	0	6.3	8.57	5.333±0.049	89.62±0.80
2.9	5.626±0.005	0.013±0.022	0.009±0.024	0.001±0.075	0.083	0	5.7	7.96	5.31± 0.03	89.32±0.61
3	5.599±0.008	0.013±0.029	0.009±0.028	0.001±0.064	0.083	0	5.15	9.05	5.320±0.050	89.41±0.82
3.1	5.607±0.005	0.012±0.022	0.012±0.037	0.001±0.072	0.111	0	5.01	7.14	5.336±0.036	89.67±0.59
3.2	5.634±0.006	0.013±0.032	0.017±0.033	0.001±0.109	0.164	0	5.83	4.69	5.316±0.051	89.34±0.83
3.3	5.660±0.005	0.013±0.041	0.016±0.026	0.001±0.100	0.154	0	6.79	3.78	5.286±0.047	88.84±0.77
3.5	5.631±0.005	0.013±0.029	0.016±0.021	0.001±0.087	0.158	0	5.68	4.39	5.321±0.039	89.42±0.63
3.8	5.623±0.005	0.013±0.031	0.029±0.018	0.001±0.106	0.284	0	5.28	5.45	5.336±0.042	89.67±0.68
4.1	5.642±0.005	0.013±0.035	0.029±0.022	0.001±0.125	0.282	0	5.41	4.96	5.347±0.048	89.85±0.79
4.4	5.634±0.006	0.013±0.036	0.052±0.016	0.001±0.125	0.505	0	5.95	4.64	5.309±0.055	89.23±0.90
4.8	5.710±0.005	0.013±0.029	0.062±0.017	0.002±0.149	0.601	0	7.73	2.57	5.279±0.075	88.73±1.23
Total/Avg.	**5.753±0.001**	**0.013±0.003**	**0.034±0.002**	**0.002±0.009**		**0**		**100**	**5.329±0.007**	
J=0.009550±0.000014										
Volume 39ArK =3803.24										
Integrated Date =89.14±0.26										
		Sample=**THN03-22**		Mineral=**Sericite**						
1.8	25.01± 0.01	0.018±0.109	0.274±0.013	0.025±0.058	0.328	0	18.42	2.01	18.000±0.471	88.53±2.26
2	38.033±0.013	0.025±0.068	0.245±0.017	0.068±0.036	0.028	-.001	47.71	2.2	18.484±0.758	90.85±3.63
2.1	23.835±0.009	0.016±0.059	0.093±0.010	0.018±0.044	0.139	0	17.61	5.95	18.831±0.292	92.51±1.40
2.2	37.305±0.019	0.025±0.075	0.163±0.018	0.065±0.029	0.35	0	47.74	3.46	18.613±0.702	91.46±3.36
2.3	22.856±0.009	0.019±0.122	0.184±0.009	0.018±0.046	0.304	0	15.11	3.04	17.751±0.302	87.33±1.45
2.5	21.522±0.029	0.016±0.077	0.062±0.024	0.013±0.033	0.129	0	14.11	9.16	17.944±0.596	88.26±2.86
2.7	21.371±0.027	0.016±0.024	0.037±0.023	0.012±0.048	0.075	0	14.71	15.41	17.916±0.565	88.12±2.71
2.8	22.404±0.024	0.017±0.042	0.061±0.021	0.016±0.042	0.099	0	18.41	9.07	17.761±0.514	87.37±2.47
2.9	22.172±0.023	0.015±0.051	0.057±0.020	0.015±0.025	0.067	0	16.88	9.75	17.938±0.461	88.23±2.22
3	22.288±0.010	0.016±0.062	0.068±0.012	0.016±0.037	0.08	0	17.68	8.16	17.763±0.276	87.38±1.33
3.1	22.325±0.011	0.016±0.066	0.064±0.012	0.016±0.035	0.087	0	17.37	8.62	17.894±0.282	88.01±1.35
3.2	23.253±0.008	0.017±0.068	0.098±0.010	0.019±0.032	0.138	0	19.23	5.66	17.948±0.237	88.27±1.14
3.4	22.054±0.012	0.016±0.058	0.072±0.011	0.015±0.038	0.099	0	15.73	7.66	17.946±0.289	88.26±1.39
3.6	22.845±0.007	0.019±0.077	0.106±0.014	0.018±0.033	0.141	0	18.63	5.23	17.679±0.219	86.98±1.05
4	22.599±0.011	0.020±0.068	0.121±0.013	0.021±0.057	0.219	0	21.95	4.63	16.647±0.403	82.02±1.94
Total/Avg.	**22.353±0.003**	**0.016±0.009**	**0.067±0.003**	**0.015±0.006**		**0**		**100**	**17.871±0.069**	**88.11±0.35**
J =0.002794±0.000008										
Volume 39ArK =481.41										
Integrated Date =88.11±0.70										
		Sample=**AS025a**		Mineral=**Sericite**						
1.8	48.756±0.015	0.056±0.078	0.238±0.025	0.119±0.033	0.539	0.005	67.89	4.92	15.061±1.202	74.34± 5.81
2	40.761±0.024	0.037±0.058	0.073±0.018	0.086±0.025	0.214	0.002	60.42	16.36	15.918±0.993	78.48±4.79
2.2	21.672±0.017	0.018±0.070	0.038±0.019	0.020±0.029	0.111	0	24.72	31.19	16.096±0.375	79.34±1.81
2.4	21.701±0.027	0.016±0.085	0.049±0.024	0.020±0.039	0.116	0	24.04	24.04	16.195±0.570	79.81±2.75
2.7	26.002±0.025	0.021±0.071	0.092±0.021	0.036±0.046	0.195	0	36.98	12.77	15.927±0.721	78.52±3.48
3.1	34.786±0.026	0.025±0.050	0.191±0.022	0.070±0.038	0.423	0	54.3	6.13	15.204±1.037	75.03±5.01
3.5	58.102±0.030	0.038±0.156	0.466±0.030	0.162±0.057	1.088	-.001	76.72	2.51	12.679±2.846	62.78±13.85
4	127.418±0.029	0.108±0.053	0.792±0.029	0.408±0.040	1.839	0.005	90.41	1.47	11.672±4.140	57.87±20.20
4.5	186.190±0.033	0.168±0.120	1.945±0.033	0.631±0.054	5.498	0.011	94.25	0.6	9.967±8.342	49.54±40.89
Total/Avg.	**30.207±0.005**	**0.026±0.014**	**0.143±0.004**	**0.049±0.007**		**0.003**		**100**	**16.064±0.149**	**77.79± 0.73**
J =0.002793±0.000008										
Volume 39ArK =137.62										
Integrated Date =77.79±1.45										
		Sample=**277540**		Mineral=**Sericite**						
1.8	19.002±0.023	0.019±0.076	0.083±0.023	0.012±0.038	0.184	0	16	6.31	15.566±0.416	76.88±2.01
2	19.940±0.019	0.015±0.054	0.030±0.018	0.005±0.048	0.272	0	6.25	20.82	18.577±0.384	91.39±1.84
2.1	20.975±0.027	0.015±0.027	0.049±0.021	0.008±0.046	0.179	0	9.4	11.2	18.776±0.555	92.34±2.66
2.2	21.016±0.028	0.015±0.053	0.055±0.026	0.008±0.045	0.264	0	9.67	10.2	18.734±0.576	92.14±2.76
2.3	21.256±0.023	0.016±0.025	0.062±0.020	0.010±0.065	0.228	0	11.7	8.81	18.482±0.499	90.93±2.39
2.4	22.345±0.033	0.016±0.100	0.086±0.023	0.014±0.049	0.16	0	15.57	6.05	18.458±0.706	90.82±3.39
2.5	21.501±0.033	0.015±0.063	0.074±0.026	0.011±0.067	0.113	0	12.82	7	18.382±0.697	90.45±3.34
2.6	22.240±0.034	0.016±0.069	0.096±0.027	0.014±0.036	0.156	0	15.56	5.43	18.322±0.696	90.16±3.34
2.8	21.043±0.027	0.015±0.097	0.059±0.022	0.009±0.058	0.073	0	10.18	8.74	18.605±0.559	91.52±2.68
3	22.050±0.029	0.018±0.036	0.091±0.025	0.013±0.045	0.155	0	15	5.69	18.303±0.625	90.07±3.00
3.2	22.663±0.014	0.020±0.064	0.133±0.019	0.016±0.089	0.249	0	17.39	3.93	18.096±0.517	89.08±2.48
3.5	24.060±0.017	0.023±0.072	0.178±0.013	0.021±0.045	0.41	0.001	21.84	2.95	18.014±0.490	88.68±2.36
4	23.668±0.012	0.029±0.095	0.185±0.017	0.019±0.065	0.483	0.002	19.32	2.87	18.255±0.452	89.84±2.17
Total/Avg.	**20.811±0.004**	**0.016±0.010**	**0.116±0.003**	**0.008±0.009**		**0**		**100**	**18.510±0.081**	**90.17±0.40**
J =0.002797±0.000006										
Volume 39ArK =459.57										
Integrated Date =90.17±0.80										

Volumes are 1E-13 cm3 NPT
Neutron flux monitors: 28.02 Ma FCs (Renne et al., 1998)
Isotope production ratios: $(^{40}Ar/^{39}Ar)K=0.0302$, $(^{37}Ar/^{39}Ar)Ca=1416.4306$, $(^{36}Ar/^{39}Ar)Ca=0.3952$,
Ca/K=1.83($^{37}ArCa/^{39}ArK$).
*=Radiogenic ^{40}Ar

Table 3-2: Continued

Laser Power(%)	Isotope Ratios $^{40}Ar/^{39}Ar$	$^{38}Ar/^{39}Ar$	$^{37}Ar/^{39}Ar$	$^{36}Ar/^{39}Ar$	Ca/K	Cl/K	$\%^{40}Ar$ atm	f ^{39}Ar	$^{40}Ar^*/^{39}ArK$	Age
		Sample=**Cirque**		Mineral=**Biotite**						
2	51.23±0.013	0.053±0.107	0.417±0.034	0.171±0.037	4.024	0.002	97.47	2.03	1.294±1.804	22.18±30.72
2.2	19.235±.010	0.025±0.105	0.722±0.016	0.055±0.054	6.968	0	82.63	3.19	3.349±0.869	56.82±14.52
2.4	20.849±.012	0.026±0.075	0.767±0.022	0.060±0.044	7.407	0	83.28	5.28	3.493±0.771	59.23±12.85
2.6	7.494±0.008	0.016±0.071	0.490±0.018	0.012±0.057	4.729	0	46.6	7.67	4.010±0.212	67.83±3.52
2.8	5.933±0.009	0.015±0.054	0.155±0.027	0.004±0.189	1.498	0	19.55	10.7	4.782±0.235	80.61±3.87
3	5.702±0.010	0.014±0.100	0.190±0.024	0.003±0.172	1.834	0	15.83	11.21	4.809±0.174	81.04±2.87
3.2	5.786±0.009	0.016±0.060	0.362±0.017	0.003±0.185	3.494	0	14.74	11.03	4.944±0.185	83.27±3.05
3.4	5.696±0.007	0.015±0.057	0.125±0.031	0.003±0.223	1.203	0	15.61	11.05	4.815±0.212	81.16±3.49
3.7	5.505±0.007	0.015±0.093	0.106±0.021	0.002±0.339	1.026	0	10.48	11.47	4.937±0.213	83.16±3.50
4	5.594±0.008	0.015±0.116	0.234±0.016	0.003±0.248	2.258	0	14.7	9.78	4.781±0.227	80.59±3.74
4.3	5.386±0.007	0.016±0.078	0.726±0.015	0.003±0.111	7.014	0	9.95	16.58	4.863±0.091	81.93±1.49
Total/Avg.	**7.967±0.001**	**0.017±0.013**	**0.774±0.002**	**0.012±0.012**		**0**		**100**	**4.850±0.043**	
J =0.009555±0.000014										
Volume 39ArK =309.73										
Integrated Date =77.50±1.44										
		Sample=**Outlaw**		Mineral=**Biotite**						
1.8	258.904±0.019	0.442±0.036	0.097±0.035	0.851±0.027	0.045	0.062	97.51	0.39	6.352±5.224	63.28±51.14
2	43.348±0.028	0.250±0.033	0.038±0.088	0.132±0.052	0.004	0.049	89.6	0.94	4.352±1.947	43.60±19.27
2.2	26.418±0.018	0.229±0.019	0.017±0.042	0.064±0.036	0.013	0.047	70.79	2.3	7.534±0.761	74.81±7.40
2.4	12.374±0.032	0.191±0.034	0.009±0.056	0.014±0.043	0.008	0.04	30.83	4.53	8.347±0.394	82.70±3.82
2.6	10.393±0.014	0.191±0.018	0.006±0.091	0.006±0.056	0.008	0.041	15.19	6.65	8.629±0.167	85.43±1.62
2.8	10.195±0.014	0.195±0.019	0.005±0.265	0.005±0.059	0	0.042	12.53	7.54	8.745±0.158	86.55±1.53
3	9.797±0.016	0.199±0.015	0.004±0.070	0.004±0.107	0.002	0.042	9.61	9.64	8.708±0.184	86.20±1.78
3.2	9.628±0.015	0.201±0.018	0.006±0.074	0.004±0.095	0.013	0.043	9.82	8.31	8.518±0.170	84.36±1.65
3.4	9.562±0.011	0.201±0.014	0.005±0.034	0.003±0.063	0.006	0.043	9.2	8.86	8.525±0.120	84.42±1.16
3.6	9.797±0.026	0.201±0.023	0.004±0.290	0.004±0.066	0	0.043	10.61	7.66	8.584±0.263	85.00±2.55
3.8	9.855±0.010	0.202±0.015	0.007±0.082	0.005±0.062	0.01	0.043	12.11	6.17	8.460±0.123	83.80±1.19
4	9.779±0.014	0.196±0.016	0.006±0.396	0.004±0.028	0.016	0.042	10.77	7.53	8.551±0.136	84.68±1.31
4.3	9.232±0.009	0.190±0.012	0.002±0.222	0.002±0.041	0	0.041	5.64	15.1	8.598±0.083	85.14±0.80
4.5	9.419±0.009	0.174±0.014	0.005±0.095	0.003±0.065	0.006	0.037	7.75	8.53	8.525±0.102	84.43±0.98
4.7	10.867±0.013	0.163±0.018	0.014±0.028	0.009±0.060	0.011	0.034	21.69	2.8	8.158±0.194	80.88±1.88
5.5	10.420±0.008	0.157±0.021	0.012±0.050	0.008±0.072	0.005	0.033	18.59	3.05	8.145±0.177	80.74±1.72
Total/Avg.	**11.353±0.002**	**0.195±0.002**	**0.003±0.041**	**0.010±0.007**		**0.043**		**100**	**8.546±0.029**	**83.98± 0.31**
J =0.005620±0.000018										
Volume 39ArK =1343.71										
Integrated Date =83.98±0.62										

Volumes are 1E-13 cm3 NPT
Neutron flux monitors: 28.02 Ma FCs (Renne et al., 1998)
Isotope production ratios: $(^{40}Ar/^{39}Ar)K=0.0302$, $(^{37}Ar/^{39}Ar)Ca=1416.4306$, $(^{36}Ar/^{39}Ar)Ca=0.3952$, $Ca/K=1.83(^{37}ArCa/^{39}ArK)$.
*=Radiogenic ^{40}Ar

Paragenetic Sequence

Figure 3-4 shows the paragenetic sequence for the Oban breccia, which was is based on petrographic descriptions and SEM analyses from 11 thin sections. From this sequence it is evident that the there are three stages of mineralization present: a) an early chalcopyrite, pyrite, cassiterite and arsenopyrite phase; b) main-stage galena, boulangerite, sphalerite and freibergite and; c) late stage dominated by pyrite. The main-stage is accompanied by open-space quartz, carbonate alteration, while late-stage pyrite is closely associated with crustiform sericite. Post-mineral sericite quartz veins crosscut all stages of mineralization.

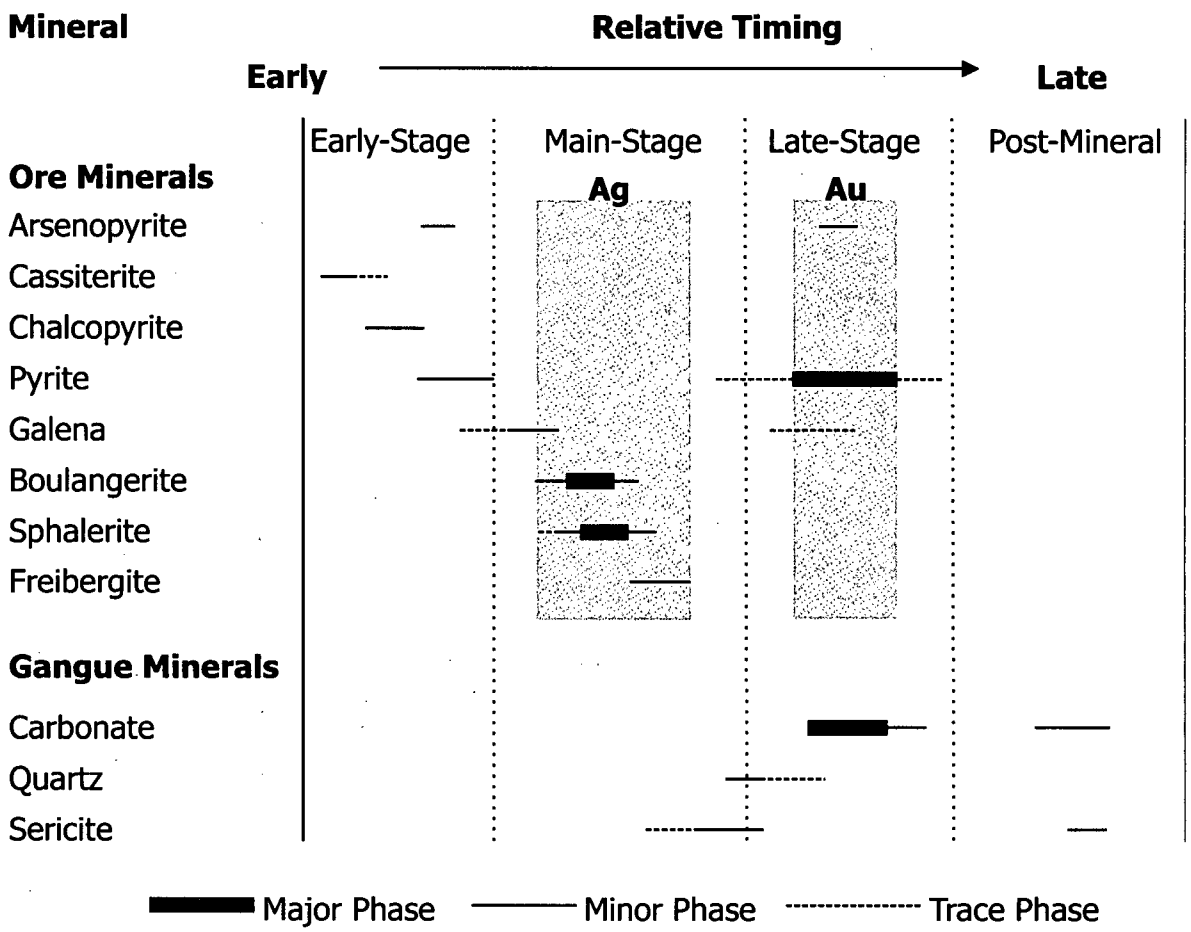

Figure 3-6: Interpreted paragenetic sequence of ore and alteration mineralogy from the Oban breccia. Shaded Ag and Au zones are interpreted from correlation of assay data with main ore minerals present. Low-grade Au extends outwards from the main mineralized zone along with crustiform pyrite, while high-grade Ag is most commonly associated with boulangerite, freibergite and galena of the "main stage".

Mineralized Systems Associated With Windy Table Magmatism

Windy Table-associated hydrothermal systems are defined below as hydrothermal alteration and mineralization whose textures suggest that their relative timing is younger than the initial deposition of Windy Table rocks. On the Thorn Property, four styles of mineralization fit these criteria: a) enargite-tetrahedrite veins, b) porphyry Cu-Mo, c) skarn and, d) quartz-stibnite-arsenopyrite veins. Emphasis herein is placed upon the enargite veins because they are potentially the most important style of mineralization at the Thorn Property in terms of grade, tonnage potential, and for understanding the potential for Late Cretaceous epithermal Au-Ag-Cu systems in northwestern British Columbia.

Enargite Veins

The structural architecture prior to the deposition of the enargite veins plays an important role in the deposition, distribution and continuity of hyrdothermally altered and mineralized zones. The orientation of altered zones associated with enargite veins at the Thorn Property are controlled by at least six NE-trending, planar fracture/fault meshes that cut the Thorn Stock. Brittle deformation occurred prior to and during hydrothermal alteration (Lewis, 2002). The best exposure of one of these zones is in the NE-trending Camp Creek, which is eroded along one of the deformed, altered and mineralized corridors (Figure 3-7A). Other corridors are exposed along La Jaune Creek. From south to north along La Jaune Creek, these corridors correspond to the B-Zone, Camp Creek Corridor, Talisker/I-Zone, Balvenie Zone and Craggenmore Zone. Extensive glacial till has covered most of these zones, which limits mapping of altered zones and their continuity. However, Induced Polarization (IP) suggests that altered and mineralized zones continue NE away from La Jaune Creek at least until the contact of the Thorn Stock and Windy Table strata (~1500 m). Acidic hydrothermal fluids used these deformed zones as fluid pathways along which the surrounding rocks were altered to the advanced argillic stage (pyrophyllite-dickite-diaspore), creating steeply-dipping planar altered zones up to 100 m thick (Figure 3-7B).

Later auriferous fluids used the same structures and precipitated a high-sulphidation mineral assemblage in veins and ore shoots in the altered zones. Veins in these corridors are discontinuous and range in width from mm-scale to approximately 3 m. However, in most high-grade zones, vein complexes of up to 4.5 m thick dominate, rather than the grade being controlled by one individual vein. A shell of lower grade rock in which enargite and tetrahedrite

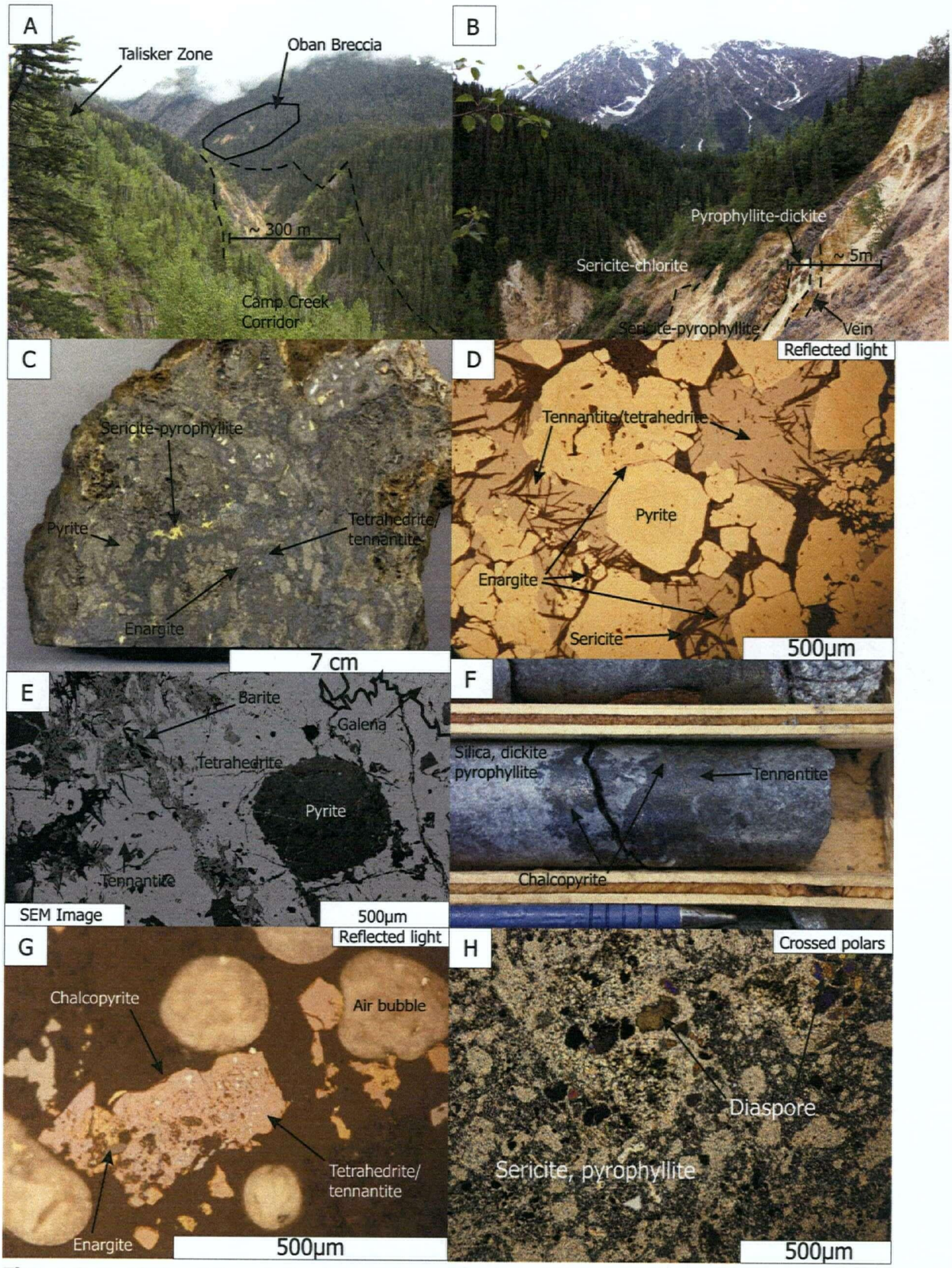

Figure 3-7: Photographs, photomicrographs and images of high-sulphidation (HS) mineral assemblage veins. A) Shows the scale and distribution of mineralized zone in Camp creek (looking NE), B) alteration zonation around HS mineral assemblage veins, C) pyrite brecciated by enargite/ tetrahedrite (en/tt), D) zoned pyrite crosscut by en/tt, E) tt, overgrowing and replacing tenanntite (tn), F) chalcopyrite replacing and overgrowing tn/tt, G) galena replacing tn and tt, and h) sericite replacing diaspore.

are disseminated flanks the high-grade zones. At the Talisker zone, two drill holes (Figure 3-2) intersected high-grade zones of 3.6 m of 4.48 g/t Au and 65.3 g/t Ag and 4.2 m of 4.44 g/t Au, 407.9 g/t Ag and 2.95% Cu contained within larger low-grade intercepts of 56.1 m of 1.27 g/t Au and 16.7 g/t Ag and 43.9 m of 0.76 g/t Au, 48.9 g/t Ag and 0.36% Cu, respectively (Baker 2005).

Lack of outcrop in the lower portions of the Windy Table volcanic strata does not permit proper evaluation of the continuity of planar altered and mineralized zones into these strata along strike of known enargite vein occurrences. At the I-Zone, where Windy Table strata and the Thorn Stock are fault contacted, vein assemblages and advanced argillic alteration are noted in the Windy Table strata (Lewis, 2002; Awmack, 2003).

The Thorn Stock was exhumed between 93-85.5 Ma and approximately 1600 m of Windy Table Group volcanic strata were deposited on top of the exposed stock (Figure 3-3, Chapter 2). It is unclear how the enargite veins are manifested at the Thorn Stock-Windy Table strata contact, because the unconformable contact is covered by overburden in areas where the mineralized and altered zones would intersect the Windy Table strata. However, further up-section several intensely silicified and kaolinite-altered zones are along strike and up-dip and parallel to the underlying enargite veins. The kaolinite-altered zones could represent higher-level parts of the hydrothermal system that precipitated the underlying enargite veins, which only exhibit weakly anomalous Au-Ag-As-Sb values. At El Indio, Chile, this unconformable contact was important in the ore-forming environment as it provided a competency contrast, which allowed for local "blow-outs" or widening of brittly deformed zones, which created wider ore-forming environments (Jannas, 1999). Hydrothermally altered and mineralized rocks at El Indio only extend for a maximum of 50 m above the unconformity, however zones of anomalous Ag-Au-Cu-As-Sb are present above known veins in the Escabroso Group (Jannas, 1990; Bissig *et al.*, 2003). The silicified zones above the enargite veins in the Windy Table Group at the Thorn Property may be expressions of the hydrothermal system at shallower level positions.

Ore Mineralogy

The concept of high, intermediate and low sulphidation is a subject of much debate and currently lacks a set of terminology that separates genetic from non-genetic terms. Einaudi *et al.* (2003) discuss this topic in detail. For the purposes of consistency with current terminology, the enargite veins at the Thorn Property are referred to as a "high-sulphidation mineral assemblage" rather than as a "high-sulphidation deposit". A mineral assemblage is defined as

groupings of minerals that occur in direct contact and that do not display evidence of reaction with one another (Barton *et al.*, 1963). Moreover, the concept of sulphidation state of fluid is defined by Barton (1970), where the frame of reference is temperature and the fugacity of sulphur. From this concept, Einaudi *et al.* (2003) introduced divisions in sulphidation states based on mineral reactions common in porphyry-copper deposits, porphyry-related veins and epithermal precious-metal deposits. These divisions are termed "very low", "low", "intermediate", "high" and "very high". The most important of these boundaries pertaining to this study is the division between high and intermediate sulphidation where the mineral reaction chalcopyrite (intermediate) = bornite + pyrite (high), which approximately coincides with tennantite = enargite (Einaudi *et al.*, 2003). At the Thorn Property, an early crystallizing ore assemblage in the structurally controlled veins described above consists of pyrite + enargite, which may be termed a "high-sulphidation mineral assemblage" (Figure 3-7C, D).

The high-sulphidation mineral assemblage veins display highly variable textures ranging from massive to semi-massive sulphide/sulphosalt at the core of the systems to disseminated sulphide/sulphosalt outboard of the cores (Figure 3-7B, C, E). Other textures include framboidal ores at the north end of the F-Zone, open space-filling ores at the B-Zone and sheeted veins at the I-Zone. The cores of semi-massive to massive sulphide are dominated by pyrite, enargite, tetrahedrite and tennantite, with lesser galena (Ag- and non-Ag-rich varieties), sphalerite, chalcopyrite, pyrargyrite, Au/Ag tellurides and cassiterite, all of which have been confirmed by SEM. Additional minerals discussed below but recognized by other workers include native Au, electrum, argentite and polybasite (Lang and Thompson, 2003). Massive cores of the systems form in previously altered, steeply-dipping, planar sheets as discontinuous pods of massive/semi-massive sulphide, termed ore shoots. Individual ores shoots plunge steeply along the planar altered zones and the continuity from one ore shoot to the next likely reflects the auriferous fluid flux for a given area on the Thorn Property. The subject of ore continuity is explored further below.

Pyrite occurs as several different forms in the veins throughout the property, but it is most commonly formed as euhedral, coarse grains that are growth banded. This variety also forms earliest in the paragenetic sequence for ore minerals at most locations and is closely associated with late-stage quartz. Late fine-grained varieties are intergrown with sulphosalts or as discrete pyrite-sericite veins, which crosscut all sulphide mineral assemblages. The main Cu-bearing phases include tennantite, enargite and tetrahedrite (from most to least abundant property-wide), these phases postdate the main quartz and are most commonly associated with sericite, pyrophyllite, dickite, and diaspore alteration. However, enargite is overgrown and

replaced by tennantite and tetrahedrite at the southern Glenlivet vein and the Tamdhu vein (Figure 3-7D). Additionally, tennantite is replaced by tetrahedrite by most veins in the northwest parts of the F-Zone (e.g. Jim Beam vein; Figure 3-7F). This trend from higher to lower sulphidation assemblage minerals is noted in other structurally controlled high-sulphidation mineral assemblage veins (e.g. El Indio, Chile; Jannas, 1990 and Lepanto, Philippines; Hedenquist *et al.*, 1998). Additionally, the remaining Cu-bearing phase, chalcopyrite, occurs as volumetrically important phases in the topographically highest potions of the veins systems (e.g. Talisker Zone drill hole THN05-37; Baker, in prep.), and overgrows all other Cu-bearing phases (Figure 3-7e).

Base metal sulphides occur mainly as inclusions and intergrowths with early forming Cu-bearing phases, particularly tennantite/tetrahedrite. These minerals include galena and sphalerite. Two varieties of galena were observed using the SEM: a) Ag-rich galena, and b) Ag-poor galena. The Ag-rich variety was found to always overgrow and replace non-Ag galena. Sphalerite commonly overgrows sphalerite. Additionally, cassiterite appears to have precipitated during the early stages of Cu-bearing sulphide and before sphalerite.

Au/Ag tellurides and pyrargyrite overgrow and replace tennantite/tetrahedrite phases and are most commonly associated with chalcopyrite (confirmed by SEM on samples from the Glenlivet vein; Figure 3-2, 7G). Polybasite, argentite and native gold/electrum were reported by Lang and Thompson (2003). From their descriptions polybasite and argentite most likely precipitated during the waning stages of tennantite/tetrahedrite precipitation, whereas native Au/electrum precipitated with interpreted low temperature open space-filling radiating quartz ± sericite and pyrophyllite (Lang and Thompson, 2003).

Alteration Mineralogy

Alteration mineralogy in hydrothermal systems may give insights to temperature and depth of formation, hydrothermal fluid composition, pH conditions, etc. (e.g. Einaudi *et al.*, 2003; Hedenquist *et al.*, 2000; Henley and Ellis, 1983; Reyes, 1990; Simmons and Browne, 2000). Structurally controlled, altered, steeply-dipping, planar zones coincident with high-sulphidation mineral assemblage veins occur prior to and during ore mineralogy deposition. On an outcrop scale, there is a general zonation outwards from a quartz, diaspore core to a pyrophyllite, dickite, sericite (± diaspore, rutile) zone to a sericite zone with increasing amounts of chlorite outwards from the mineralized area (Figure 3-7B).

Quartz occurs mainly as an early phase prior to the deposition of all ore minerals (with exception of minor overlap with early pyrite). It occurs in three distinct periods during the

paragenesis of the high-sulphidation assemblage veins. The earliest phase is highly variable in terms of grain size and is largely re-crystallized to finer grained quartz with undulose extinction and 120° intergranular contacts. It is unclear what proportion of quartz was added during this stage. A second stage of quartz occurs as open-space filling vuggy quartz, which is most prevalent at the B-zone, but occurs as a minor component in most other veins. This stage of quartz is overgrown by early stage pyrite and other ore minerals. Late- to post-ore mineral quartz (with sericite veins) crosscuts all ore minerals. Diaspore and rutile are less common and occur with early stage quartz. Quartz, diaspore-dominated zones lie at the core of the vein systems and are typically less than 4 m wide.

Outboard of the quartz core, a zone of pyrophyllite, dickite, sericite, (± diaspore, rutile) occurs for approximately 5 m (Figure 3-7B). Typically, pyrophyllite, sericite and dickite occur together and replace early-stage quartz, but are overgrown by vuggy silica (Figure 3-7H). Pyrophyllite is the earliest phase and is largely replaced by sericite and dickite. Early pyrite is brecciated by this alteration suite and occurs with Cu-bearing mineral phases and other sulphides after early pyrite (Lang and Thompson, 2003). This assemblage of alteration minerals is important for many reasons. Most importantly the pyrophyllite, diaspore assemblage is indicative of a high-sulphidation environment (White and Hedenquist, 1995). Pyrophyllite is an important mineral in these types of systems because it can precipitate in two distinct environments: 1) at low temperatures if supersaturated with respect to quartz (pyrophyllite, chalcedony assemblages), and 2) at high temperatures if at quartz saturation (~300°C; pyrophyllite, dickite/kaolinite assemblages; Hedenquist and White, 2005). The alteration assemblage at the Thorn Property consists of pyrophyllite, diaspore, dickite, rutile and sericite, which corresponds to temperatures of formation of approximately 250°C (Henley and Ellis, 1983). At the Balvenie zone, natroalunite was recognized by PIMA (Baker, in prep.). This location is higher topographically than the majority of analysed samples and is considered to be farther from the source of fluids, which explains the presence of lower temperature assemblages such as natroalunite. Additionally, an $^{40}Ar/^{39}Ar$ age plateau of 79.3 ± 1.4 Ma was obtained on sericite from this alteration assemblage (Table 3-1; Figure 3-5C; Appendix I), limiting the age of alteration to be associated with late Windy Table Suite. Sericite is considered to have precipitated below its closure temperature of ~350°C (Hanes, 1991), because the temperature of precipitation of the above ore and alteration minerals is approximately 250-300°C, and provides the best timing for alterations associated with high-sulphidation mineralization. Conversely, Mihalynuk *et al.*, (2003), report a $^{40}Ar/^{39}Ar$ age of 91.0 ± 1.0 Ma. However, this sample was taken from 1986 drill core of "most intensely sericite

altered" stock and had no textural relation to any ore mineralogy, and is not considered to be the age of alteration associated with high-sulphidation mineral assemblage veins. This is supported by a $^{40}Ar/^{39}Ar$ age of 90.97 ± 0.91 Ma on a sample of sericite from the "least altered" Thorn Stock well away from any mineralized zone (Figure 3-5D). This age is considered to be the initial background alteration, possibly associated with the crystallization of the Thorn Stock.

Outboard of the pyrophyllite dominated zone, there is a widespread zone of sericite, chlorite alteration with chlorite alteration increasing away from the core of the system. This alteration is coincident with pyrite alteration and extends well beyond known mineralized zones. Post/late stage pyrite, barite, and carbonate veins crosscut all other alteration phases. Plumbojarosite occurs as a common phase late during the oxidation of the ore assemblage (Lang and Thompson, 2003).

Metal Ratio Zonations

Fluid evolution in epithermal systems is well-documented in both high (Jannas, 1995) and low (Wurst, 2004) sulphidation systems. Ratios of particular metals are used to distinguish between proximal and distal signatures relative to the source area. In the case of most magmatic-hydrothermal systems, Cu and As are more proximal to the source relative to Zn and Sb. In the case of high and intermediate sulphidation systems, this is particularly useful because the amount of relative Cu vs. Zn depends upon the presence of enargite vs. tennantite/tetrahedrite vs. chalcopyrite and the amount of As vs. Sb depends upon the presence of As-bearing phases such as enargite and tennantite vs. tetrahedrite.

Proper analyses of these ratios require a large database of mineralized rocks, in order to determine if any metal zonations are present. At the Thorn Property, a large enough drill hole database does not exist to create adequate long sections. The best example of a whole vein system exposed at surface is the Camp Creek corridor. The Camp Creek corridor is a continuous mineralized zone, which extends for approximately 1500 m (Figure 3-8A, B). Additionally, only samples considered to be mineralized (>0.4 g/t Au) and in place were used. Eighty-seven samples were analyzed as part of five exploration programs from 2000 to 2005 by Equity Engineering Limited at ACME Analytical Laboratories and ALS Chemex Laboratories (Awmack, 2000, 2003; Baker, 2003, 2005, in prep.). Results of these analyses are presented in Table 3-3 and Figure 3-8A, B. The respective metal ratios were grouped based upon "natural breaks" using MapInfo. The "Natural Break" algorithm is based on the procedure described by Jenks and Caspall (1971). The algorithm uses the average of each range to distribute the data more evenly across the ranges. It distributes the values so that the average of each range is as

Table 3-3: As/Sb and Cu/Zn ratios for high-sulphidation assemblage veins

Sample	Easting	Northing	As/Sb	Cu/Zn
129059	627686	6491690	4.4	4.0
206602	627895	6491853	0.4	0.1
206608	627894	6491845	1.3	129.9
206611	628157	6491970	1.1	21.5
206614	627880	6491595	0.5	0.8
206615	627859	6491591	0.5	1.4
206616	627906	6491603	1.4	3.5
206632	627547	6491610	3.4	33.1
206633	627557	6491609	2.7	1.2
206634	627609	6491598	0.6	9.1
206636	627524	6491636	180.1	2.7
206637	627521	6491624	5.0	8.2
206649	628681	6492225	1.1	7.1
206651	628673	6492225	0.3	0.1
206652	628686	6492214	0.8	12.2
206654	628556	6492205	0.5	0.2
206655	628546	6492155	0.4	1.6
206656	628558	6492149	0.4	2.7
206657	628574	6492156	0.8	3.5
206658	628511	6492128	0.5	7.2
206659	628888	6492203	1.2	0.0
206661	628742	6492278	8.8	0.9
206662	628619	6492213	0.9	24.8
206663	628247	6492024	0.9	1.3
206802	627776	6491846	2.0	5.8
206806	627958	6491872	4.1	0.4
206807	627958	6491872	1.7	1.6
206811	627860	6491588	0.9	3.3
206815	627643	6491609	1.0	14.1
206817	627638	6491612	2.1	76.8
206818	627638	6491612	0.9	113.9
206820	627505	6491721	1.3	27.2
206824	627509	6491580	2.4	50.6
206826	627489	6491566	0.4	6.9
206827	627489	6491566	0.5	2.7
206828	627489	6491560	5.1	11.3
206830	627453	6491531	352.5	0.1
206831	627551	6491407	4.4	15.2
206843	627781	6491555	3.1	10.9
209611	628655	6492217	0.4	7.1
209612	628805	6492221	0.9	0.0
209613	628451	6492104	1.5	14.6
209614	628502	6492162	1.2	7.2
209616	628435	6492097	1.4	41.7
209617	628435	6492089	1.1	13.5
209618	628320	6491962	1.7	16.9
209619	628481	6492140	0.5	6.0
209620	628309	6491946	1.9	83.7
209621	628284	6492028	0.6	3.2
209622	628275	6492031	0.6	0.4
209623	628572	6492243	0.8	0.3
209624	628579	6492242	0.5	1.4
209625	628702	6492245	1.0	10.3
209626	628733	6492266	42.6	1.6
277539	627742	6491573	0.7	6.3
277543	628362	6492009	0.6	11.7
277555	628301	6491995	0.8	0.2
277556	628610	6492232	1.5	0.1
277557	628611	6492234	0.8	12.6
277654	627893	6491920	0.4	100.0
277655	627898	6491920	2.4	15.6
277656	628021	6492053	0.5	1.0
277657	628151	6492063	1.8	3.8
277658	628183	6492095	1.4	11.4
277659	628165	6492077	1.0	3.7
277660	628229	6492102	1.2	3.5
277661	628218	6492064	1.0	0.4
277662	628441	6492153	1.8	0.1
277667	628323	6492005	1.3	1.0
277671	628304	6491982	5.0	0.1
277675	628857	6492253	4.0	0.0
278001	628042	6491627	0.7	27.2
279994	628183	6491961	2.1	20.3
3390	627918	6491863	0.9	6.0
3393	627736	6491579	2.5	2.5
129057	627686	6491690	4.0	20.1
277702	628318	6491960	1.0	8.8
277703	628314	6491966	1.6	15.0
277705	628327	6491975	1.0	7.8
277707	628445	6492095	1.6	7.3
277708	628444	6492096	1.0	4.6
277710	628441	6492099	1.2	32.3
277712	628438	6492087	1.0	8.2
277714	628431	6492097	1.0	4.9
276494	627895	6491864	2.9	71.5
276491	628183	6491961	1.0	7.7
276493	627895	6491864	1.4	55.1

Sample locations are given in UTM for NAD83, Zone 8.
Samples used for metal ratio analyses all contain high-sulphidation assemblage mineralization are considered to be mineralized (i.e. contain >0.4g/t Au).

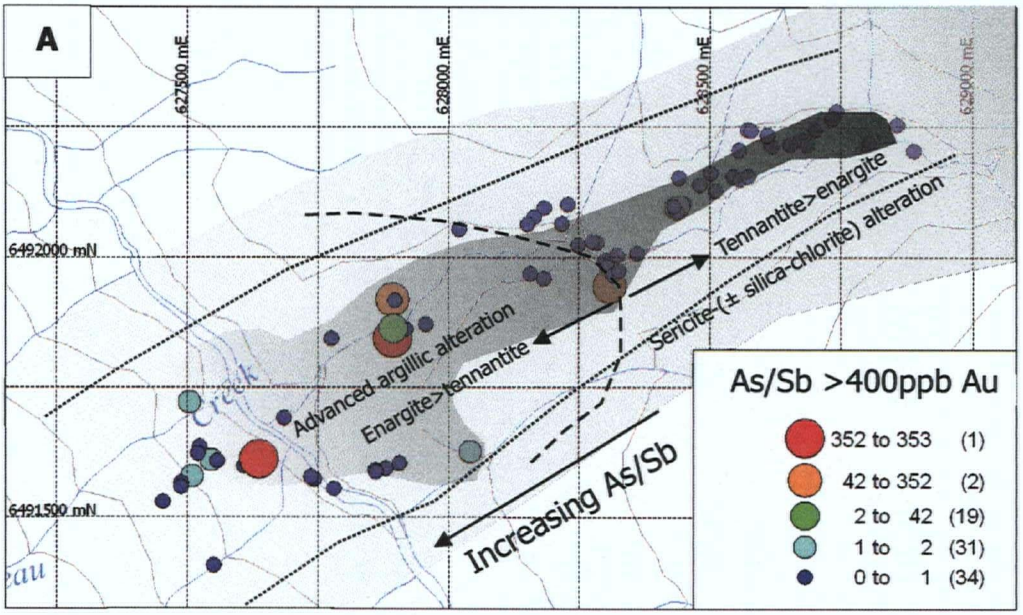

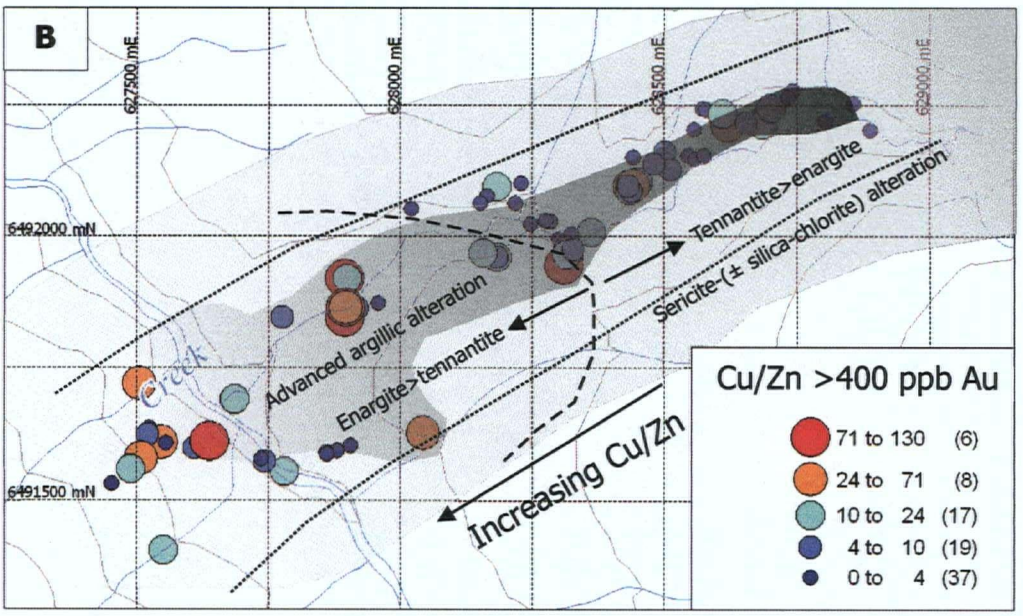

Figure 3-8: Metal zonations in the Camp Creek structural corridor: a) As/Sb ratios for mineralized samples, b) Cu/Zn ratios for mineralized samples. Both show the approximate limits of advanced argillic alteration as well as enargite>tennantite/ tetrahedrite and tennantite/tetrahedrite>enargite zones. Area enclosed by dotted line marks the approximate limits of the Camp Creek structural corridor. Note also that advanced argillic alteration widens closer to La Jaune Creek.

close as possible to each of the range values in that range. This ensures that the ranges are well represented by their averages, and that data values within each of the ranges are fairly close together.

Both the Cu/Zn and As/Sb ratios decrease towards the northeast along the Camp Creek structural corridor (Figure 3-8A, B). These decreases are coincident with two distinct zonations in the ore mineralogy of the veins: a) enargite > tennantite in the southwest and b) tennantite > enargite in the northeast. Additionally, there is a zone of tennantite > chalcopyrite, which is not present at the topographic level of the Camp Creek corridor, which is outboard of the tennantite > enargite zone (e.g. Talisker Zone drill hole THN05-37; Figure 3-2; Baker, in prep.). High Cu/Zn and As/Sb ratios coupled with higher concentrations of enargite in the southwest indicate that the source/up-temperature direction is in the area La Jaune Creek. Large enough data sets are not present to properly evaluate the other parallel high-sulphidation mineral assemblage vein complexes.

Paragenetic Sequence

The above are general descriptions of minerals and their textural relationships. However, there are highly variable textures and mineralogy depending on the showing and where it located with respect to the source area of the hydrothermal fluids. Figure 3-9 shows the paragenetic sequence for high-sulphidation mineral assemblage veins. This paragenetic sequence was generated from petrographic descriptions and SEM analyses from 37 thin sections. Additional information on minerals not recognized as part of this study are provided by Lang and Thompson (2003). During the early stages of hydrothermal activity, pervasive quartz alteration is accompanied by diaspore and lesser rutile alteration (Figure 3-9). Widespread, but low amounts of pyrite alteration is present during the waning stages of the early stage. At the beginning of the main stage alteration and mineralization, pyrophyllite and sericite alteration dominate with lesser vuggy quartz and barite and rare alunite. Additionally, PIMA has recognized dickite in most hand specimens that are pyrophyllite altered, but it was not confirmed in thin section. The alteration mineral assemblage of pyrophyllite-diaspore-dickite-rutile provides very tight constrains on the temperature of formation to a minimum of 250°C, and is most common in deeper parts of acid-sulphate/high-sulphidation systems (Hedenquist *et al.*, 1996). Widespread late chlorite with lesser carbonate alteration are distal alteration products of the system. Late stage quartz-pyrite and barite veins crosscut all alteration and mineralization. Additional minerals recorded by PIMA as part of the distal/lower temperature alteration include kaolinite and smectite (Baker, in prep.). This sequence of

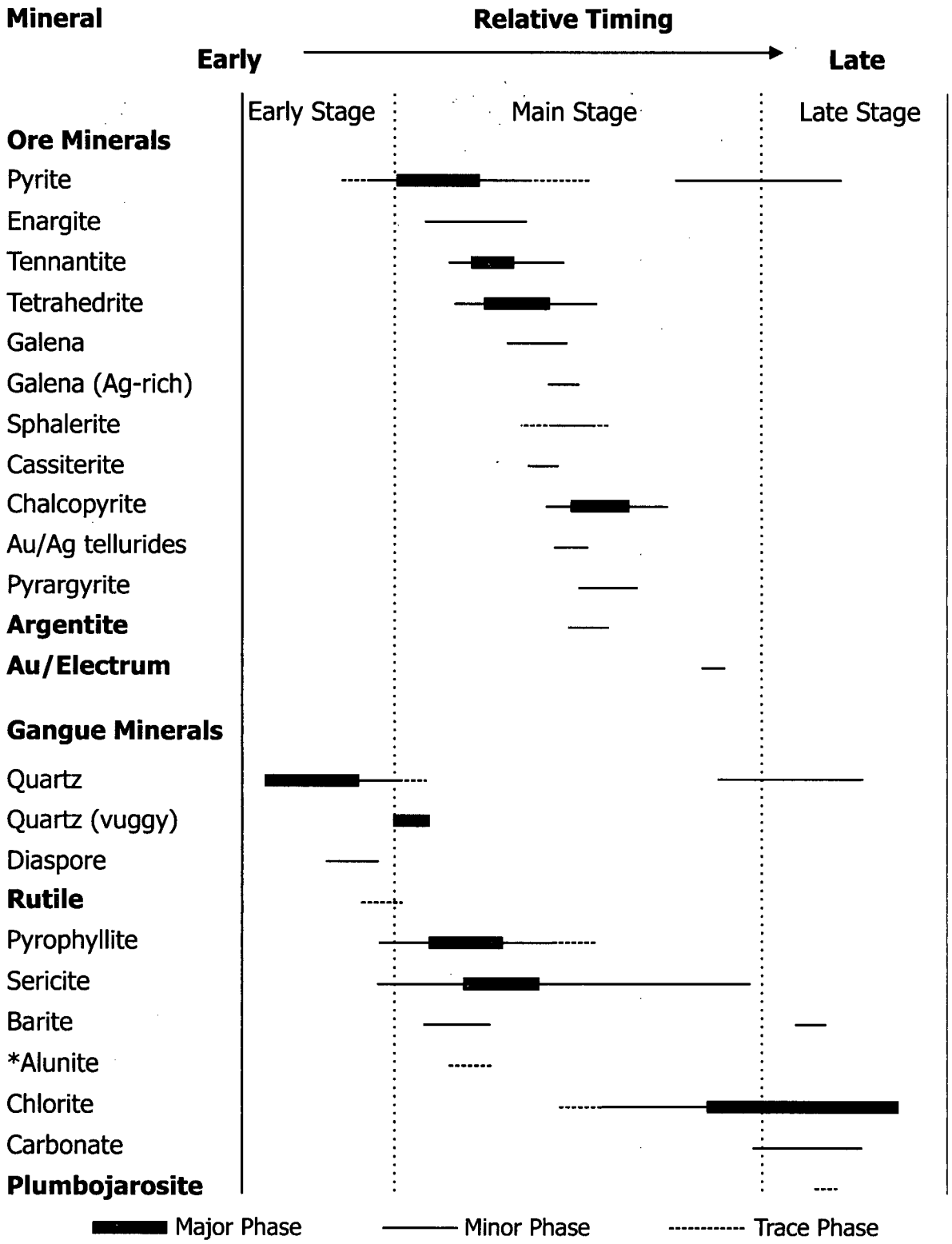

* Not recognized in thin section; recognized by PIMA analysis
Bold from Lang and Thompson (2003)

Figure 3-9: Interpreted paragenetic sequence of ore and alteration mineralogy from high-sulphidation mineral assemblage veins. Based on petrographic and SEM analyses on 37 thin sections taken from different showings across the Thorn Property. The paragenesis shows a typical progression from high sulphidation acidic fluids to lower sulphidation and more neutral fluids.

alteration minerals shows decreasing temperature and acidity with time and/or distance from source (greater fluid rock interaction).

Early main stage sulphide deposition is dominated by pyrite. The pyrite is coarse-grained and growth-zoned. All Cu-bearing mineral phases overgrow and replace pyrite and each other. From earliest to latest, the precipitating Cu-bearing mineral phases are: enargite, tennantite, tetrahedrite and chalcopyrite. This progression in Cu-bearing mineral phases shows a fluid evolution from high-sulphidation mineral assemblages to intermediate-sulphidation mineral assemblages. Base metal phases such as galena and sphalerite in addition to cassiterite are intergrown with and included in the dominant Cu-bearing mineral phases at a given location. In addition to native Au/electrum, pyrargyrite and argentite were sulphides that precipitated late in the paragenesis. Lang and Thompson (2003) report very late native Au in open-space filling low temperature quartz-pyrophyllite.

Other Mineralizing Styles

Hydrothermal systems associated with Windy Table magmatic rocks are dynamic and widespread. These include weak porphyry Cu-Mo at the Cirque Zone, Zn-Fe (± Ag-Au) skarn at the Outlaw and Bungee zones approximately 1 km southeast of the Windy Table volcanic rocks. Arsenopyrite-stibnite-barite-quartz-carbonate veins are also widespread. Each of these types are briefly outlined below.

Porphyry Cu-Mo

Weak porphyry Cu-Mo mineralization at the Cirque zone is located approximately 2500 m NE of and 250 m topographically above the closest high-sulphidation mineral assemblage vein (Figure 3-2). Thin (1 mm-8 cm) structurally controlled quartz vein sets with subhorizontal and subvertical vein orientations characterize the mineralized zones at the Cirque (Simmons *et al.*, 2005). Ore minerals occur as disseminations in the host rock and in the quartz veins. Vein mineralogy includes quartz-pyrite-chalcopyrite-molybdenite with lesser feldspar and rare sulphosalt. Where veining is most intense, biotite-sericite alteration dominates and is overprinted by clay alteration. A broader zone of chlorite alteration flanks the biotite zone. A $^{40}Ar/^{39}Ar$ plateau age of 81.1 ±1.1 Ma was obtained on fine grained, shreddy-looking biotite from the potassically altered quartz monzonite host rock (Figure 3-5E; Table 3-1; Appendix I). It is unlikely that the hydrothermal system at the Cirque zone was the feeder to higher level mineralization in the Camp Creek area for two reasons: 1) absolute ages from both systems are distinct, and 2) the porphyry system at the Cirque is located topographically higher than the high-sulphidation mineral assemblage veins and it is unlikely that fluids migrated downwards.

The source of the fluids for the high-sulphidation mineral assemblage veins could either be from a similar stock to those at the Cirque emplaced at slightly deeper levels or from the plutons in the Cirque area, which may have been moved down relative to the veins by post-depositional normal faulting.

Skarn

A strong Au-As-Sb-Ag-Pb-Zn soil geochemical anomaly covers 400 x 2,000 m of alpine terrain approximately five kilometres southeast of the Thorn high-sulphidation mineral assemblage veins and three kilometres south of the Cirque Zone (Figure 3-2). This area is underlain by calcareous siltstone, sandstone, conglomerate, chert and minor limestone of the Upper Triassic Stuhini Group. The clastic sedimentary rocks have been thermally metamorphosed to hornfels by a biotite-hornblende monzogranite stock (Windy Table intrusion Type 2; Chapter 2), which intrudes them to the north (Figure 3-2). Highly fractured and altered felsic dykes, belonging to the Jurassic Fourth of July Suite, intrude the Stuhini Group rocks as a series of subparallel E-W trending sills (Chapter 2) in the Outlaw area. Quartz-carbonate-base metal sulphide-arsenopyrite replacement or veins occur adjacent to Fourth of July Suite sills (Walton, 1987). Four holes were drilled along a single section by Chevron, in a 75 x 200 m zone of clay alteration (the "Clay Zone"), with quartz-galena-arsenopyrite-pyrite veins; their best intersection assayed 8.3 g/t Au across 0.95 m (Walton, 1987). An $^{40}Ar/^{39}Ar$ plateau age of 84.84 ± 0.48 Ma was determined for biotite from one of the Fourth of July Suite sills in the "Clay-Zone" and is interpreted to be the age of alteration associated with skarn and hornfels formation in the Stuhini Group rocks (Figure 3-5F; Table 3-1). Calc-silicate alteration, such as garnet and diopside are widespread, but is most commonly weakly to moderately distributed throughout the Outlaw Zone.

Other skarn bodies are noted at the Bungee Zone (Figure 3-2, Awmack, 2003). The Bungee Zone consists of two zones of semi-massive to massive pyrrhotite with minor quartz and epidote, which lie along the upper and lower contacts of the Sinwa Formation. Pyrrhotite is hosted within the adjacent argillite units presumably of the Stuhini and Laberge Groups, apparently as a skarn or replacement. Both pyrrhotite bodies dip moderately to the south; the upper one appears to be 10-20 m thick and the lower one about 2 m thick. Limited work on these bodies show weak precious metal mineralization accompanied by weak Zn mineralization of up to 0.95 % (Awmack, 2000).

Quartz-Carbonate-Chalcopyrite-Stibnite-Arsenopyrite Veins

Several quartz-carbonate-chalcopyrite-barite-stibnite-arsenopyrite veins occur on the property and are always hosted in older Stuhini and Laberge Group rocks, with the exception of the K-zone in Windy Table volcanic rocks (Awmack, 2000). At the G zone, a quartz-carbonate-sulphide vein in Gee Creek lies within an erratically mineralized fault zone, which strikes 103°/48°S, cutting through argillite and pillow basalt of the Stuhini Group. Several similar but narrower quartz-carbonate-sulphide veins, including those at the E zone, are present 400 m south of the G zone at the contact between the Stuhini Group rocks and the Thorn Stock. Veins at the E-zone are along strike of high-sulphidation mineral assemblage veins at the Tamdhu Zone (Awmack, 2003). This style of mineralization may be the result of acid sulphate mineralization contacting a reactive rock with abundant carbonate. Thus could be a rock buffered equivalent of the veins in the Camp Creek corridor.

Pb Isotope Geochemistry

A lead isotope study was undertaken to help provide a framework to evaluate potential magma sources for Late Cretaceous hydrothermal systems at the Thorn Property. Two plagioclase feldspar separates from Type 2 Windy Table intrusive rocks and Thorn Suite intrusive rocks were analyzed for their lead isotopic compositions, in addition to six sulphide mineral separates, including two from each of the Oban breccia base metal matrix replacement, high-sulphidation assemblage veins and the Cirque Cu-Mo porphyry. Plagioclase feldspar and sulphide lead isotopic compositions are commonly interpreted as initial values because little uranium is incorporated in these minerals, which limits change in isotopic composition through time-integrated growth.

Methodology

Lead isotopic compositions were determined using a modified VG54R thermal ionization mass spectrometer at the Pacific Centre for Isotopic and Geochemical Research (PCIGR) Laboratory at the University of British Columbia, Vancouver. Measured isotopic compositions were corrected for instrumental mass fractionation of 0.15% per mass unit based on replicate analyses of NBS SRM981 and the recommended values of Thirlwall (2000).

Results from the magmatic and mineralized rocks are reported in Table 3-4 and plotted on $^{208}Pb/^{204}Pb$ vs. $^{206}Pb/^{204}Pb$ and $^{207}Pb/^{204}Pb$ vs. $^{206}Pb/^{204}Pb$ covariation diagrams (Figure 3-10). The Pb isotopic growth curve of Stacey and Kramers (1975) has been plotted on the figure for isotopic reference. Lead isotopic compositions are plotted for various VMS deposits in Stikinia

and Cache Creek Terranes, which formed mainly during the Jurassic and Triassic (Childe, 1997) and for Jurassic and Tertiary mineralization in the Stewart mining camp (Alldrick, 1991). No Pb isotopic data is available for Jurassic Laberge Group rocks or the Triassic Stuhini Group. Values reported by Childe (1997) for Triassic and Jurassic VMS deposits are meant to serve as approximations for volcanic rocks of the same age in Stikinia.

Results

The Thorn and Windy Table intrusive suites form the oldest and youngest suites comprising the NW British Columbia volcanoplutonic belt (Chapter 2), and have two distinct lead isotopic compositions (Figure 3-10A, B). The Windy Table Suite has less radiogenic and heterogeneous Pb isotopic compositions ($^{206}Pb/^{204}Pb$ = 19.005 to 19.558, $^{208}Pb/^{204}Pb$ = 38.49 to 39.10, $^{207}Pb/^{204}Pb$ = 15.592 to 15.626). Whereas, the Thorn Suite has considerably more radiogenic Pb compositions, compared to their Windy Table intrusive counterparts ($^{206}Pb/^{204}Pb$ = 19.488, $^{208}Pb/^{204}Pb$ = 39.017, $^{207}Pb/^{204}Pb$ = 15.632), though only one sample was analyzed. Both the Thorn Suite rock and Sample AS-035a from the Windy Table Suite are moderately to highly sericite altered and the anomalous value may reflect the hydrothermal alteration of the feldspars. Additional analyzes will be carried out to better constrain the Pb isotopic compositions of the Thorn Suite.

From the petrographic analyses above, native Au and electrum are not important phases in either the Oban breccia or high-sulphidation mineral assemblage veins. Precious metals are considered to form in other sulphide minerals as either part of the mineral structure or as refractory Au and Ag. Therefore, the Pb isotopic composition of the sulphides are presumably of the ore-forming fluid and can be used to identify metal sources of the various mineralizing types, in addition to assessing the degree of fluid-wall rock interaction (Tosdal *et al.*, 1999). Lead isotopic compositions for sulphide minerals are most similar to the Windy Table suite intrusive rocks, with somewhat more radiogenic lead isotopic composition. These samples overlap somewhat with the Tertiary cluster of Alldrick (1991), but are distinctively more radiogenic than older VMS deposits in NW B.C. reported by Childe and Alldrick (Figure 3-10A, B).

Sulphide samples from the Oban breccia, Cirque porphyry Cu-Mo and high-sulphidation mineral assemblage veins have similar Pb isotopic compositions, which for the most part plot within error of each other. This cluster of sulphide minerals is slightly more radiogenic than the Windy Table intrusive rock sample, but is again within error of each other. The strong over lap between the Windy Table intrusive rock and the sulphide cluster suggest that the source for

auriferous fluids were Windy Table suite intrusions. The more radiogenic nature of the sulphide minerals may reflect wall rock interaction with the hydrothermal fluid farther away from the fluid source. However, no Pb isotopic data for the surrounding Stuhini and Laberge Group rocks is available. As an alternative, sulphide Pb isotopic compositions, given by Alldrick (1990) and Childe (1997), for VMS deposits in Stikinia and Cache Creek, which range in age from Paleozoic to Jurassic in NW B.C. are used as approximations for similar-aged volcanic and sedimentary strata of the Stuhini and Laberge Groups. Assuming this is accurate, the less radiogenic Pb isotopic compositions of sulphide from the earlier VMS deposits preclude either the Stuhini or Laberge Group rocks from contributing Pb to the bulk of the sulphides in all of the mineralizing systems at the Thorn Property. Furthermore, the lack of Tertiary rocks present at the Thorn Property eliminate potential Tertiary sources of Pb, such as the *ca.* 55 Ma Sloko magmatic suite.

Although there is only a limited data set, every style of mineralization shows a progression from less radiogenic, paragenetically earlier sulphide phases to more radiogenic, paragenetically later sulphide phases. That is, at the Cirque from molybdenite to chalcopyrite, in the Oban breccia from boulangerite to pyrite and in high-sulphidation mineral assemblage veins from enargite to tetrahedrite. It is unclear at this point how important this is as, due to the small data set and most of the sulphide Pb isotopic compositions being within error of one another. However, this effect may be explained by greater wall rock interaction with late stage fluids, though no potential source of Pb has been identified.

Pb isotopic compositions presented in Figure 3-10A, B are consistent with the conclusions of Childe (1997), whereby there is an overall evolution from less to more radiogenic Pb isotopic compositions over time in the Stikine Terrane. The Late Devonian Forrest Kerr pluton, which intrudes Stikinia (Alldrick, 1991; Childe, 1997), provides data for the oldest rocks in this trend. The Tulsequah Chief, Granduc and Eskay Creek deposits formed within the Paleozoic Stikine Assemblage, Upper Triassic Stuhini Group and Lower to Middle Jurassic Hazelton Group, respectively and provide Pb isotopic data for Pb evolution in Stikinia from Mississippian to the Middle Jurassic. Galena from the Stewart Mining Camp provides Pb isotopic compositions for the Tertiary. Pb isotopic compositions provided as part of this study fall directly on the Pb isotopic evolution path for the Stikine terrane plotting between the Tertiary data of Alldrick (1991) and the pre-Cretaceous ores of Childe (1997).

Table 3-4: Lead isotopic compositions of feldspar mineral separates of Late Cretaceous magmatic rocks and sulphide separates of related Late Cretaceous hydrothermal mineralization

Sample[1]	Location	Rock Type[2]	Mineral[3]	$^{206}Pb/^{204}Pb$	Error%	$^{207}Pb/^{204}Pb$	Error%	$^{208}Pb/^{204}Pb$	Error%	$^{207}Pb/^{206}Pb$	Error%	$^{208}Pb/^{206}Pb$	Error%
Thorn Suite													
277510	Thorn Stock	qtz-pl-bt diorite porphyry	pl	19.488	0.479	15.632	0.467	39.01	0.52	0.802	0.119	2.002	0.203
Windy Table Suite													
AS-035a	Eye Creek	lt-poor welded dacite	kf	19.558	0.053	15.626	0.071	39.10	0.09	0.799	0.023	1.999	0.044
AS-086a	Cirque	bt-hbl monzogranite	fs	19.005	0.044	15.592	0.066	38.49	0.08	0.820	0.022	2.025	0.043
Oban Breccia													
Oban	Oban	Massive Sulphide	bl	19.074	0.061	15.621	0.068	38.55	0.11	0.819	0.043	2.021	0.067
Oban	Oban	Massive Sulphide	py	19.099	0.045	15.649	0.066	38.66	0.08	0.819	0.023	2.024	0.044
High-sulphidation Assemblage veins													
Glen	F-Zone	Massive Sulphide	en	19.072	0.044	15.600	0.065	38.52	0.08	0.818	0.022	2.020	0.043
Glen	F-Zone	Massive Sulphide	tt	19.096	0.047	15.638	0.066	38.62	0.09	0.819	0.025	2.023	0.046
Porphyry Cu-Mo													
Cirque	Cirque	Qtz-vein	cp	19.155	0.108	15.701	0.111	38.83	0.19	0.819	0.049	2.027	0.096
Cirque	Cirque	Qtz-vein	mo	19.030	0.048	15.626	0.066	38.56	0.09	0.821	0.027	2.027	0.046

1. All analysis by Janet Gabites at the PCIGR Laboratory, University of British Columbia, Vancouver.
   All ratios corrected for isotopic fractionation (0.15% per atomic mass unit), based on repeated analyses of NBS SRM981 lead standard.
2. qtz = quartz, pl = plagioclase feldspar, bt= biotite, lt = lithic, hbl = hornblende
3. Minerals analyzed: pl = plagioclase feldspar, kf = potassium feldspar, fs = feldspar undifferentiated, bl = boulangerite, py = pyrite, en = enargite, tt = tetrahedrite/tennantite, cp = chalcopyrite, mo = molybdenite
   Uncertainties are obtained by numerically propagating all mass fractionation and analytical uncertainties through the calculations and are presented at the 2σ level.

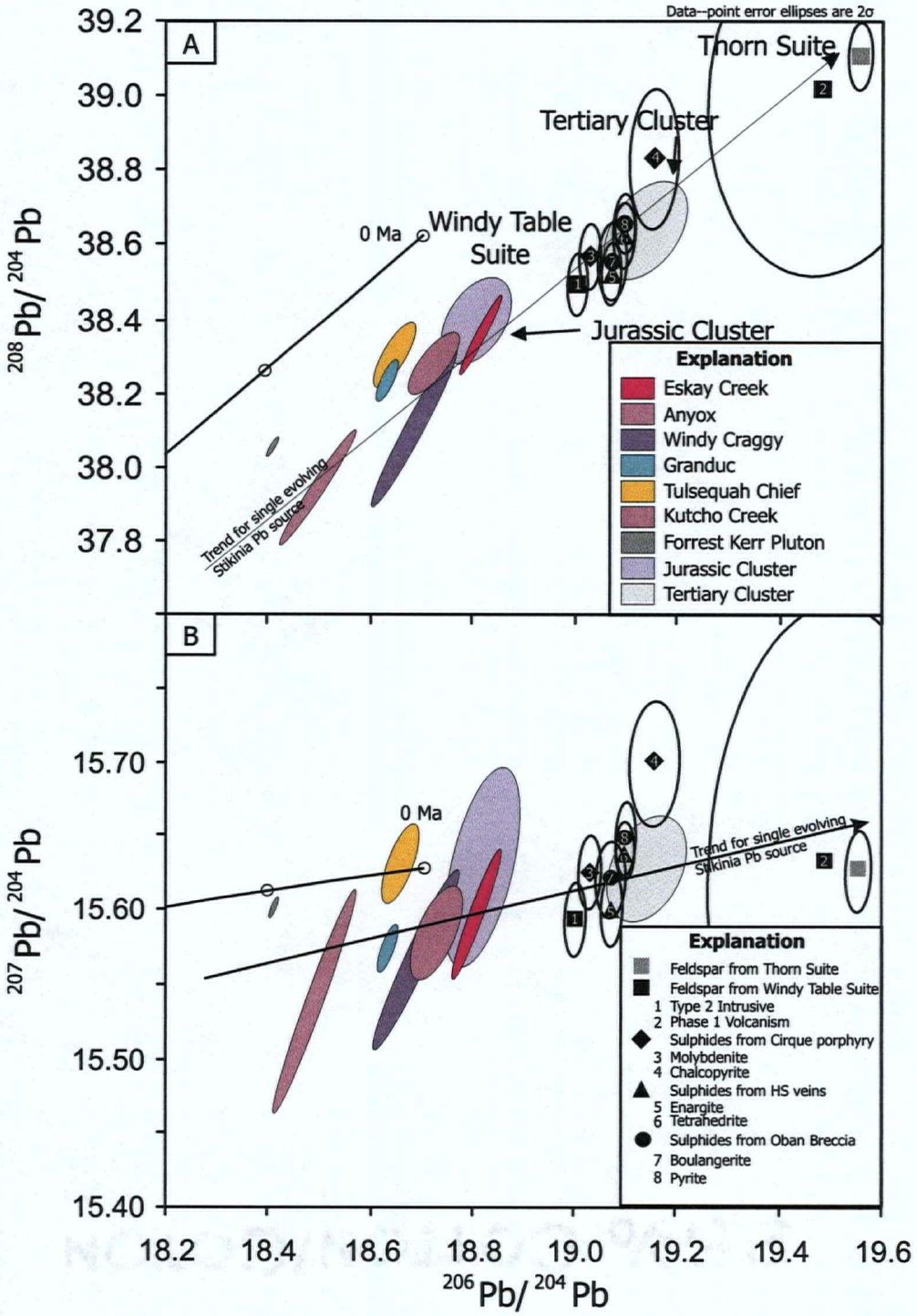

Figure 3-10: A) $^{208}Pb/^{204}Pb$ vs. $^{206}Pb/^{204}Pb$ diagram and B) $^{207}Pb/^{204}Pb$ vs. $^{206}Pb/^{204}Pb$ diagram. The Pb isotopic growth curve of Stacey & Kramers (1975) is shown in both diagrams for reference. The Jurassic and Tertiary clusters of mineralized rocks from the Stewart Mining Camp are after Alldrick (1990). All other VMS fields provided above are after Childe (1997).

Discussion

Field relationships, geochronology and lead isotopic compositions of sulphides and feldspars all suggest that magmatic rocks of the NW B.C. Late Cretaceous volcanoplutonic belt produced large hydrothermal systems, which are responsible for several styles of mineralization noted at the Thorn Property. The major host rock for the most prospective styles of mineralization present are Thorn Suite magmatic rocks. However, the timing of hydrothermal activity is closely related to the late stages of Windy Table volcanic deposition. The lead isotopic compositions presented above indicate that auriferous fluids for high-sulphidation mineral assemblage veins, the Oban polymetallic breccia-hosted mineralization and the Cirque porphyry Cu-Mo, were probably sourced from associated Windy Table Suite intrusive rocks. Additionally, very little fluid-wall rock interaction took place during the deposition of ore minerals.

Timing of Mineralization in Relation to Late Cretaceous Magmatism

The timing of hydrothermal activity relative to magmatism is critical in not only demonstrating the link between ore fluids and causative intrusive phases but also in constraining the physical conditions that existed during the ore forming processes. At the Thorn Property this is particularly important as it helps to constrain the depth of formation of the high-sulphidation mineral assemblage veins. Figures 3-11 and 3-12 provide a comprehensive schematic visual overview of the timing of magmatism vs. hydrothermal activity, as well as the distribution of alteration assemblages, mineralized rocks and magmatic rocks relative to older Triassic and Jurassic rocks and major structures. The earliest stages of Late Cretaceous magmatic activity Thorn Suite) are contained by two U-Pb ages of 90.6 ± 1.1 Ma and 93.3 ± 2.4 provided in Chapter 2 and Mihalynuk *et al.* (2003). Clasts of Stuhini Group and/or Laberge Group rocks as clasts in Oban magmatic hydrothermal breccia constrain its formation to before the deposition of the Windy Table Suite. This is supported by a $^{40}Ar/^{39}Ar$ plateau age of 89.45 ± 0.50 Ma (see above) on hydrothermal sericite in mineralized Oban breccia, which constrains the age of coprecipitated sulphide mineralogy in the crustiform mineral assemblage. This age also constrains Au and Ag mineralization in the Oban breccia, as Au has a strong association with early-forming pyrite and Ag with coprecipitated boulangerite. Exhumation of the Thorn Stock and the Oban breccia is constrained by the age of the Windy Table basal strata, deposited nonconformably onto the Thorn Stock at 85.5 ± 0.7 Ma (Chapter 2).

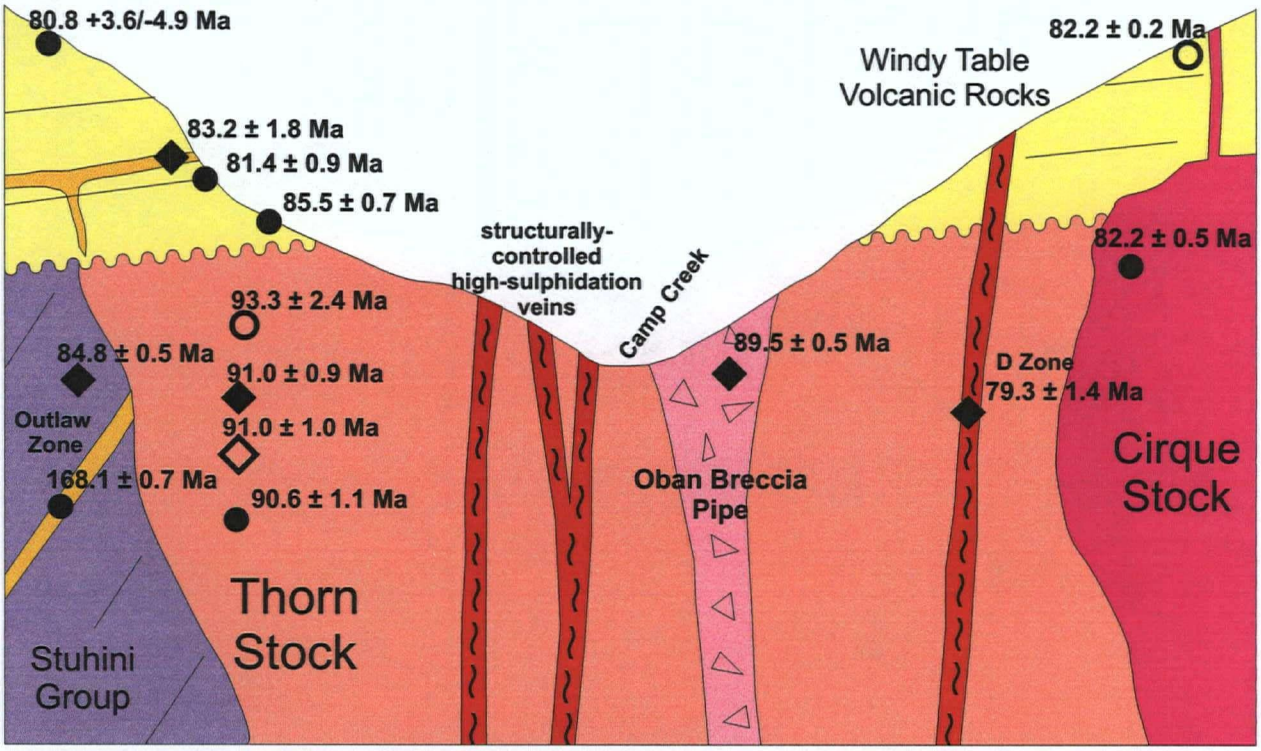

Figure 3-11: Schematic cross section through the Camp Creek corridor showing the main rock units and available geochronology. Black circles (●) are U/Pb results from this study, open circles (O) are U/Pb results from Milhalynuk et al. (2003), black diamonds (◆) are Ar/Ar data from this study and open diamonds (◇) are $^{40}Ar/^{39}Ar$ data from Milhalynuk et al. (2003). Errors are given at 2σ levels.

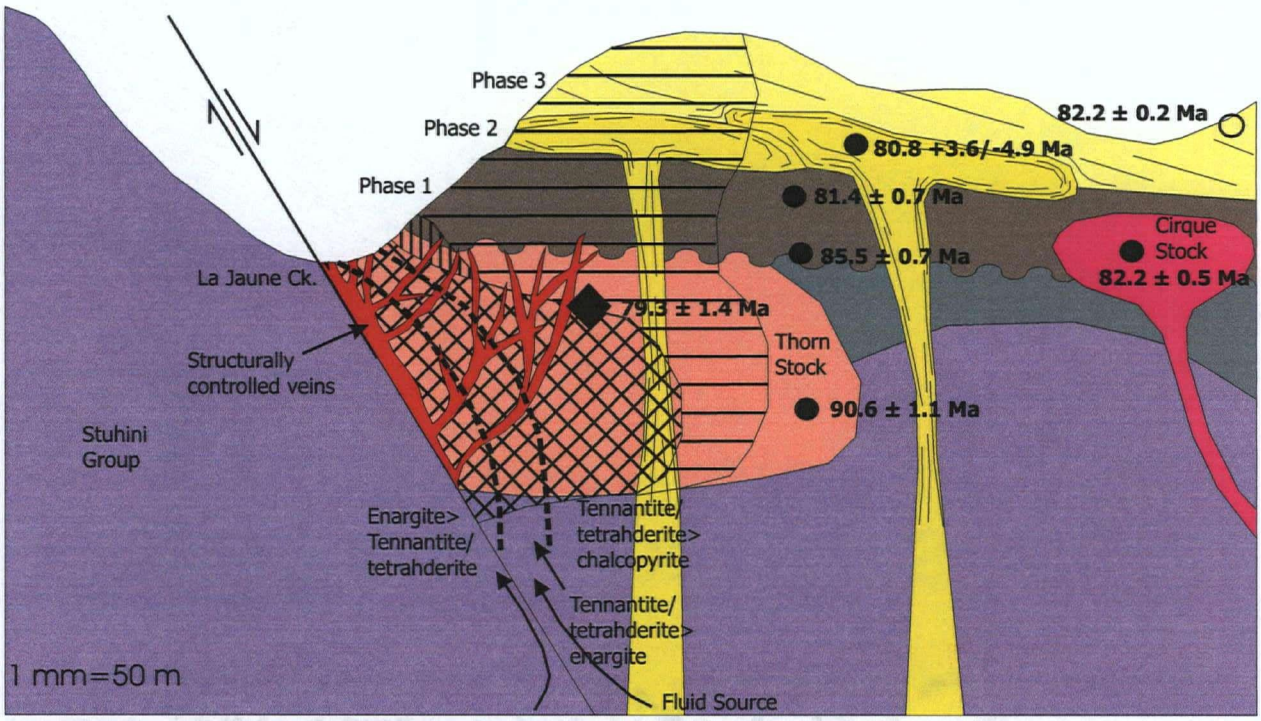

Figure 3-12: Schematic long section of a mineralized corridor along Amarillo Creek. Showing the distribution of alteration types and ore shoots contained within planar altered zones. Cross-hatched area is pyrophyllite+dickite+diaspore alteration, vertical hatching area is dickite+alunite alteration, horizontal hatching is sericite+kaolinite+chlorite alteration. Section is shown to scale in the vertical dimension, at the near surface.

Porphyry Cu-Mo mineralization at the Cirque is constrained to an age maximum of 82.2 ± 0.2 Ma, the age of the host Cirque monzonite. Furthermore, an age on hydrothermal biotite of 81.8 ± 1.1 Ma constrains the age of hydrothermal activity at the Thorn to be roughly coeval with Type 1 Windy Table intrusive rocks. Porphyry style mineralization also extends into the surrounding Windy Table volcanic strata.

Till cover limits the observation of high-sulphidation mineral assemblage veins, disrupting evaluation of their timing relationships to the magmatic rocks of the Thorn and Windy Table Suites. The majority of these veins are hosted in the Thorn Stock, thus limiting their age maximum to that of the Thorn Stock. At the I-Zone, clay alteration and disseminated tetrahedrite extends into Windy Table strata along a steeply-dipping fault, which bounds the Thorn Stock and Windy Table strata at this location. This field relationship further constrains the age maximum to lower members of the Windy Table volcanic strata. The age of sericite alteration associated with enargite-pyrite mineral assemblages at the D-Zone is constrained by a $^{40}Ar/^{39}Ar$ plateau age of 79.3 ± 1.4 Ma (Figure 3-11). This age is younger than and not within error of the uppermost portions of Windy Table volcanic strata, which is tightly constrained by two U-Pb ages to approximately 82 Ma. This geochronologic data suggests that high-sulphidation mineral assemblage veins are closely associated with the waning stages of Windy Table suite magmatism.

Premineralizing Conditions

Premineralizing structures in the Thorn Stock are critical to ore deposition at the Thorn Property. Brittle deformation of the Thorn Stock was likely related to its exhumation and the subsequent apparent normal movement along a fault parallel to La Jaune Creek. The timing of the topographically highest and thickness Windy Table strata constrain the depth of formation for high-sulphidation mineral assemblage veins to a minimum of 1600 m below the paleosurface. Characteristically hot (commonly deep) alteration mineral assemblages of pyrophyllite, dickite and diaspore (Hedenquist *et al.*, 1996) support the concept of the veins forming relatively deep. The minimum of 1600 m places the veins at the Thorn Property to depths somewhere between characteristic depths for typical porphyry and epithermal systems.

Fluid Evolution

Figure 3-12 shows a schematic longsection of a high sulphidation mineral assemblage vein complex in the Thorn Stock, alteration distribution, metal and mineral zonation and predicted fluid pathways. As/Sb and Cu/Zn metal ratios presented above show that higher ratios are concentrated along La Jaune Creek and progressively decrease to the NE and

topographically upwards along the structures. This metal zonation reflects the fluid evolution during hydrothermal alteration and mineralization. For example, higher Cu/Zn and As/Sb ratios are considered to be coincident with either the source area of fluids, hotter temperatures of precipitation or less fluid wall-rock interaction (Einaudi *et al.*, 2003). Higher metal ratios along the La Jaune Creek fault suggest that the fault may have been used as a fluid pathway for auriferous fluids (Figure 3-12).

The metal zonation discussed above is a direct reflection of the ore minerals present. For instance, near La Jaune Creek, enargite is an important phase, with tennantite and tetrahedrite increasing in importance to the NE. Additionally, chalcopyrite abundance increases dramatically in the topographically highest and farthest NE parts of the mineralized structural corridors at the Talisker zone. This mineral evolution is also observed in the paragnetic sequence and suggests that farther away from the source and with time the fluid evolved from high-sulphidation to intermediate sulphidation compositions. This evolution is supported by the paragenesis of alteration minerals, which show a trend from characteristic high-sulphidation and acidic assemblages to mineral assemblages characteristic of neutral pH conditions.

Conclusions

The data presented here provides clear linkages between magmatic rocks of the NW B.C. Late Cretaceous volcanoplutonic belt and hydrothermal mineralization at the Thorn. Furthermore, several distinct pulses of hydrothermal activity are present at the Thorn Property. Most of these appear to be more closely related to the Windy Table Suite rather than the Thorn Suite, which serves as the main host rock at the Thorn Property. Pb isotope compositions of the sulphides are comparable to those of Windy Table Suite intrusions, supporting the concept of Windy Table rocks being sources of auriferous fluids. Additionally, this study supports the conclusions of Childe (1997) whereby there is an overall evolution from less to more radiogenic Pb isotopic compositions over time in the Stikine Terrane.

The structurally controlled veins in Camp Creek contain ore (enargite + pyrite) and alteration minerals (pyrophyllite, diaspore, alunite) characteristic of high-sulphidation/acid sulphate systems. However, the veins formed at a minimum of 1600 m below the paleosurface indicating that these veins precipitated below epithermal depths. The veins appear to have been sourced in the vicinity of La Jaune Creek where high-sulphidation mineral assemblages are most common. Farther away from the fluid source, towards the NE, auriferous fluids evolved from acid and high-sulphidation to neutral and intermediate sulphidation auriferous fluids. Evidence for this is provided by metal, ore mineral and alteration mineral zonations.

Alteration distribution at the Thorn Property does not appear to be a useful exploration guide. Mapped advanced argillic alteration zones do not extend much beyond the spatial limits of mineralized zones. However, widespread sericite, chlorite, smectite alteration is present, but is also a common distal alteration phase for both the Oban breccia and the Cirque porphyry Cu-Mo system. The best exploration guideline to find other Thorn Property styles of mineralization is to locate large bodies of brittly deformed, unreactive rock (i.e. Thorn Stock-like) that are coincident with and/or overlain by Windy Table strata and intrusive rocks.

References

Alldrick, D.J. (1991): Geology and Ore Deposits of the Stewart Mining Camp, British Columbia; *University of British Columbia*, Unpublished Ph.D. thesis, Vancouver, B.C., 347 pages.

Awmack, H.J. (2000): 2000 Geological, Geochemical and Geophysical Report on the Thorn Property; *British Columbia Ministry of Energy and Mines*, Assessment Report #26,433.

Awmack, H.J. (2003): 2002 Geological, Geochemical and Diamond Drilling Report on the Thorn Property; *British Columbia Ministry of Energy and Mines,* Assessment Report #27,120.

Baker, D.E.L. (2003): 2003 Geological, Geochemical and Diamond Drilling Report on the Thorn Property; *British Columbia Ministry of Energy and Mines,* Assessment Report #27,120.

Baker, D.E.L. (2005): 2004 Geological, Geochemical, Geophysical and Diamond Drilling Report on the Thorn Property; *British Columbia Ministry of Energy and Mines,* Assessment Report #unassigned; to be released January, 2006.

Baker, D.E.L. (in prep.): 2005 Geological, Geochemical, Geophysical and Diamond Drilling Report on the Thorn Property; *British Columbia Ministry of Energy and Mines,* Assessment Report #unassigned, to be released January, 2007.

Barton, P.B., Jr., Bethke, P.M. and Toulmin, P., III (1963): Equilibrium in ore deposits; *International Mineralogical Association*, International Mineralogical Association Symposium on the Mineralogy of Sulphides, 3rd General Meeting, Washington, D.C., 1963, Proceedings, pages 171-185.

Barton, P.B. (1970): Sulphide Petrology; *Mineralogical Society of America*, Special Paper 3, pages 187-198.

Bissig, T., Clark, A.H., Lee, J.K.W. and von Quadt, A. (2003): Petrogenetic and Metallogenic Responses to Miocene Slab Flattening: New Constraints from El Indio-Pascua Au-Ag-Cu belt, Chile/Argentina; *Mineralium Deposita,* Volume 38, pages 844-862.

Bultman, T.R. (1979): Geology and tectonic history of the Whitehorse Trough west of Atlin; unpublished Ph.D. thesis, *Yale University,* 284 pages.

Childe, F.C. (1997): Timing and Tectonic Setting of Volcanogenic Massive Sulphide Deposits in British Columbia: Constraints from U-Pb Geochronology, Radiogenic Isotopes and Geochemistry; *The University of British Columbia*, Unpublished Ph.D. thesis, 298 pages.

Einaudi, M.T., Hedenquist, J.W. and Inan, E.E. (2003): Sulphidation State of Fluids in Active and Extinct Hydrothermal Systems: Transitions from Porphyry to Epithermal Environments; *Society of Economic Geologists*, Special Publication 10, pages 285-313.

Geological Survey of Canada (1988): *National Geochemical Reconnaissance 1:250,000 Map Series (Tulsequah)*; Open File 1647.

Hanes, J.A. (1991): K-Ar and $^{40}Ar/^{39}Ar$ geochronology: methods and applications. *In* Short course handbook on applications of radiogenic isotope systems to problems in geology.

Edited by L. Heaman and J.N. Ludden, *Mineralogical Association of Canada*, Short Course Handbook, Vol. 19, pp. 27-57.

Hedenquist, J.W., Arribas, A., Jr. and Reynolds, T.J. (1998): Evolution of an Intrusion-Centered Hydrothermal System: Far Southeast-Lapanto porphyry and epithermal Cu-Au deposits, Philippines; *Economic Geology*, volume 93, pages 373-404.

Hedenquist, J.W., Arribas, A., Jr. and Gonzalez-Urien, E. (2000): Exploration for Epithermal Gold Deposits; *Reviews in Economic Geology*, volume 13, pages 245-277.

Hedenquist, J.W. and White, N.C. (2005): Epithermal Gold-Silver Ore Deposits: Characteristics, Interpretation and Exploration; *Prospectors and Developers Association of Canada*, Short Course notes.

Henley, R.W. and Ellis, A.J. (1983): Geothermal Systems Ancient and Modern: A Geochemical Review; *Earth-Science Reviews*, volume 19, pages 1-50.

Jannas, R.R., Beane, R.E., Ahler, B.A. and Brosnahan, D.R. (1990): Gold and copper mineralization at the El Indio deposit, Chile; *Journal of Geochemical Exploration*, Volume 36, Pages 233-266.

Jannas, R.R. (1995): Reduced and Oxidized High Sulphidation Deposits of the El Indio District, Chile; *Harvard University*, Unpublished Ph.D. thesis, Cambridge, Massachusetts, 421 pages.

Jannas, R.R., Bowers, T.S., Petersen, U. and Beane, R.E. (1990): High-Sulphidation Deposit types in the El Indio district, Chile; *Society of Economic Geologists*, Special Publication 7, Pages 219-266.

Jenks, G. F. and Caspall, F.C. (1971): Error on Choroplethic Maps: definition, measurement, reduction; *Annals of the Association of American Geographers*, volume 61 (2), pages 217-244.

Lang, J.R. and A.. Thompson (2003): Thorn Property, British Columbia, Petrography and SEM Analysis of Eight Polished Thin Sections; *Private report for Rimfire Minerals Corporation and First Au Strategies Corp.*, dated January 17, 2003. *In* D.E.L. Baker (2003): 2003 Geological, Geochemical and Diamond Drilling Report on the Thorn Property.

Lewis, P. (2002): Structural Analysis of Au-Ag-Cu Mineralization in the Camp Creek area, Thorn Property; *Private report for Rimfire Minerals Corporation and First Au Strategies Corp.*, dated July 15, 2002. *In* H.J. Awmack (2003): 2002 Geological, Geochemical and Diamond Drilling Report on the Thorn Property.

Mihalynuk M.G. and Smith, M.T. (1992): Highlights of 1991 mapping in the Atlin-west map area (104N/12); *in* Geological Fieldwork 1991, Grant, B. and Newell, J.H., editors, *B.C. Ministry of Energy Mines and Petroleum Resources,* Paper 1992-1, pages 221-227.

Mihalynuk, M.G. (1999): Geology and Mineral Resources of the Tagish Lake Area, B.C.; *Ministry of Energy and Mines*, Bulletin 105.

Mihalynuk, M.G., J. Mortensen, R. Friedman, A. Panteleyev and H.J. Awmack (2003): Cangold partnership: regional geologic setting and geochronology of high-sulphidation mineralization at the Thorn property. British Columbia; *Ministry of Energy and Mines,* Geofile 2003-10.

Renne, P.R., Swisher, C.C., III, Deino, A.L., Karner, D.B., Owens, T. and DePaolo, D.J. (1998): Intercalibration of standards, absolute ages and uncertainties in $^{40}Ar/^{39}Ar$ dating; *Chemical Geology*, Volume 145 (1-2), Pages 117-152.

Reyes, A.G. (1990): Petrology of Philippine Geothermal Systems and the Application of Alteration Mineralogy; *Journal of Volcanology and Geothermal Research*, volume 43, pages 279-309.

Sawkins, F.J., 1990, Metal Deposits In Relation To Plate Tectonics, 2nd edn.: Berlin, Springer-Verlag, 461 p.

Sillitoe, R.H. (1972): Relation of metal provinces in western Americas to subduction of oceanic lithosphere: *Geological Society of America Bulletin*, v. 83, p. 813–818.

Sillitoe, R.H. (1985): Ore-Related Breccias in Volcanoplutonic Arcs: *Economic Geology*, volume 80, pages 1467–1514.

Simmons, A.T., Tosdal, R.M., Baker, D.E.L., Friedman, R.M. and Ullrich, T.D. (2005): Late Cretaceous Volcano-Plutonic Arcs in Northwestern British Columbia: Implications for Porphyry and Epithermal Deposits; *in* Geological Fieldwork 2004, Grant, B. and Newell, J.M., Editors, *B.C. Ministry of Energy Mines and Petroleum Resources,* Paper RR15, pages 347-360.

Simmons, S.F. and Browne, P.R.L. (2000): Hydrothermal Minerals and Precious Metals in the Broadlands-Ohaaki Geothermal System: Implications for Understanding Low Sulphidation Epithermal Environments; *Economic Geology*, volume 95, pages 971-999.

Smith, M.T. and Mihalynuk, M.G. (1992): Tulsequah Glacier: Maple Leaf (104K); *in* Exploration in British Columbia 1991, *B.C. Ministry of Energy, Mines, and Petroleum Resources*, pages 133-142.

Souther, J.G. (1971): Geology and Mineral Deposits of the Tulsequah map-area, British Columbia; *Geological Survey of Canada,* Memoir 362, 84 pages.

Stacey, J.S. and Kramers, J.D. (1975): Approximation of terrestrial lead isotope evolution by a two-stage model; *Earth and Planetary Science Letters*, Volume 26, pages 207-221.

Sutherland Brown, A., ed., 1976, Porphyry deposits of the Canadian Cordillera; *Canadian Institute of Mining and Metallurgy*, Special Volume 15, 510 p.

Thirlwall, M.F. (2000): Inter-laboratory and other errors in Pb isotope analyses investigated using a ^{207}Pb–^{204}Pb double spike; *Chemical Geology*, Volume 163, Pages 299–322.

Titley, S.R., ed., 1982, Advances In Geology Of The Porphyry Copper Deposits, Southwestern North America: Tucson, University of Arizona Press, 560 p.

Tosdal, R.M., Wooden, J.L. and Bouse, R.M. (1999): Pb Isotopes, Ore Deposits, and Metallogenic Terranes; *Reviews in Economic Geology*, volume 12, pages 1-28.

Walton, G. (1987): Tats Project, 1987 Summary Report; *British Columbia Ministry of Energy and Mines*, Assessment Report #16,726.

Wurst, A.T. (2004): Geology and Genesis of the Mt. Muro Au-Ag Epithermal Deposits, Indonesia; *University of Tasmania*, unpublished Ph.D. thesis, 418 pages.

Chapter 4

Conclusions and Recommendations for Future Research

Conclusions

The geological mapping, geochronology (U-Pb and $^{40}Ar/^{39}Ar$), petrography, geochemistry and Pb isotopic results presented herein define the geological framework of the Thorn Au-Ag-Cu Prospect within the Late Cretaceous volcanoplutonic belt of northwest B.C. The 1:20:000-scale map in Plate 1 summarizes the geology of the Thorn Property. This is the first study to characterize Late Cretaceous continental arc rocks in northern British Columbia in terms of their timing, lithology, petrologic characteristics, and geochemical characteristics. Prior to this thesis only scarce geochronological data on similar-aged continental arc rocks were provided by Mihalynuk (1999) and Mihalynuk *et al.* (2003). A portion of this study was focussed on correlating intrusive and extrusive rocks suites north and south of the Thorn Property in order to define the extent, spatial distribution and regional variations of Late Cretaceous continental arc rocks in northwest B.C. This study characterizes the timing, alteration mineralogy, ore mineralogy, fluid source and fluid evolution of structurally-controlled high-sulphidation mineral assemblage veins at the Thorn Property. Additionally, Late Cretaceous hydrothermal systems are evaluated and characterized. This thesis contributes a base understanding of a previously unrecognized arc and associated hydrothermal alteration, in terms of timing, magmatic evolution and hydrothermal evolution during the Late Cretaceous in the Stikine Terrane of northwest British Columbia.

Geology

The Stikine Terrane formed as a volcanic island arc outboard of western North America and was amalgamated with the Cache Creek and Quesnel Terranes during the early Middle Jurassic (e.g., Monger, 1984; Monger *et al.* 1991; Mihalynuk *et al.* 1994). A subduction zone developed west of the Stikine Terrane producing voluminous continental arc magmas, which comprise the Coast Plutonic Complex. In the area of the Thorn Property arc magmatism began during the Late Cretaceous. These rocks intrude and are emplaced onto the Triassic Stuhini Group and Lower to Middle Jurassic Laberge Group rocks. In the study area these rocks may be broadly divided into Late Cretaceous and Eocene magmatic events. This study focuses on the Late Cretaceous aspect.

Late Cretaceous Magmatic Arc

The Late Cretaceous magmatic arc contains three major components each divided on the basis of geochronology, geochemistry and petrologic characteristics. These units are: 1) the 93 – 87 Ma Thorn Suite intrusive rocks, 2) the 86 - 82 Ma Windy Table Suite intrusive rocks and 3) the 86 - 80 Ma Windy Table Suite volcanic rocks. Age constraints on igneous rocks are provided by 17 U-Pb SHRIMP-RG and 5 U-Pb TIMS ages generated as part of this study.

The Thorn Suite rocks form small stocks and dykes throughout the belt and are volumetrically less important than the younger Windy Table Suite. The rocks are dominantly quartz-plagioclase-biotite porphyritic quartz diorites. The largest known example occurs at the Thorn Property and is named the Thorn Stock. The Thorn Stock was emplaced at shallow levels and was exhumed by at least five million years after it crystallized. The Windy Table volcanic strata were deposited nonconformably onto the Thorn Stock. The Windy Table strata are inferred to been deposited into a paleo-depression, which allowed for their preservation at the Thorn Property. Volcanism at the Thorn is divided into three distinct packages based on time and lithology. The youngest is series of largely pyroclastic rocks, which is overlain by extensive, but variable in thickness, rhyolitic flows. Another thick sequence of pyroclastic rocks overlies the flows. Deposition of the Windy Table volcanic strata end by 82 Ma. Their intrusive equivalents, Windy Table Suite intrusive rocks, are subdivided based on petrologic characteristics, into four distinct types. These are: 1) Type 1 feldspar-biotite porphyritic monzonite to granodiorite, 2) Type 2 hornblende-biotite bearing granophyric granodiorite to monzogranite, 3) Type 3 plagioclase megacrystic monzonite to quartz monzonite and 4) narrow flow-banded aphanitic rhyolitic dykes.

Pre-Windy Table Mineralization

Pre-Windy Table mineralization is restricted to the Oban polymetallic Ag-Pb-Zu-(Cu-Au) breccia. The breccia is magmatic-hydrothermal in nature and a later auriferous fluid sporadically replaced the matrix of the breccia. The dominant ore assemblage includes early crustiform boulangerite and sphalerite with later pyrite. From SEM and available assay information, Ag is associated with boulangerite, while Au is associated with pyrite and is more widespread than Ag. The timing of mineralization is constrained to 89.45 ± 0.50 Ma by an $^{40}Ar/^{39}Ar$ plateau age on sericite, which formed as part of the crustiform assemblage with boulangerite and sphalerite.

Windy Table Mineralization

Windy Table associated hydrothermal systems are divided into four styles: a) Enargite-tetrahedrite veins, b) Porphyry Cu-Mo, c) Skarn and d) Quartz-stibnite-arsenopyrite veins. Emphasis during this study was placed on the enargite vein systems because it is the most important style in terms of grade, tonnage potential, and importance for understanding the potential for Late Cretaceous epithermal Au-Ag-Cu systems in northwestern British Columbia.

The structurally-controlled veins in Camp Creek contain ore (enargite + pyrite) and alteration minerals (pyrophyllite, diaspore, alunite) characteristic of high-sulphidation/acid sulphate systems. However, geologic evidence suggests thatthe veins formed at a minimum of 1600 m below the paleosurface, well below depths for normal high-sulphidation epithermal deposits. The veins appear to have been sourced in the vicinity of La Jaune Creek where high-sulphidation mineral assemblages are most common. Farther away from the fluid source, towards the NE, auriferous fluids evolved from acidic and high-sulphidation to neutral and intermediate-sulphidation auriferous fluids. Evidence for this is provided by metal, ore mineral and alteration mineral zonations. The high sulphidation mineral assemblage veins at the Thorn Property are representative of a typical fluid evolution of magmatic-hydrothermal fluid derived from calc-alkaline plutons. However, veins of this style emplaced at depths greater than epithermal, while common (e.g. Chuiquicamata, Chile, Far Southeast-Lepanto, Philippines), are commonly overlooked during exploration and are not commonly studied.

Lithological Association of High-sulphidation Mineral Assemblage Veins

High importance is placed on the presence of a brittle, competent, non-reactive host rocks to the development of extensive vein systems. This point is well-illustrated at the Catto vein, where a high-sulphidation mineral assemblage vein crosses the Thorn Stock/Stuhini Group contact. At this location, the vein rapidly pinches out in the Stuhini Group rocks. Additionally, the nature of alteration and ore mineralogy abruptly changes from high-sulphidation mineral assemblages to quartz, pyrite and chalcopyrite. The high carbonate content in Stuhini Group rocks neutralizes the acidic, high-sulphidation fluid fluids. This observation indicates that the Stuhini Group rocks are not favourable host rocks for high-sulphidation mineral assemblage styles of mineralization.

Recommendations

The geological architecture provided in this study represents the first step towards a framework for the presence and preservation of hydrothermal alteration and mineralization

related to Late Cretaceous magmatism in the Stikine Terrane of northwestern British Columbia. Additionally, it provides a first order study of the recently recognized Late Cretaceous magmatic rocks and serves as a basis for future studies in the area.

Future geochronological and geological studies should better constrain ages, be it relative or absolute, of the high-sulphidation mineral assemblages veins. Determining the ages of these veins is particularly problematic, because the only K-bearing alteration mineral present is sericite/illite. It is difficult to obtain precise $^{40}Ar/^{39}Ar$ ages from sericite/illite because of problems encountered with Ar-loss due to small grain size and recoil. Nuclear recoil is an artefact of the irradiation process where the production of 39Ar by neutron bombardment of 39K (i.e, 39K(n,p)39Ar reaction) results in sub-μm-scale displacement of the 39Ar within or, at grain boundaries and fast diffusion pathways, out of the mineral. For extremely fine-grained (<5 μm) minerals, a significant amount of 39Ar can be lost during irradiation, resulting in anomalously old ages. Less commonly, recoiling 39Ar from fine-grained minerals can be imbedded in adjacent potassium-poor phases, resulting in complex age spectra. Additionally, one has to be careful to select sericite that is present with the ore minerals of interest. Towards the end of this study, alunite was recognized by PIMA at one location and could be used in future studies to better constrain the absolute age of advanced argillic alteration associated with the high-sulphidation mineral assemblage veins. Emphasis should be placed on the logging of future exploration holes, which continue to be drilled farther to the NE, in the area of the Thorn Stock-Windy Table volcanic rock contact. These holes will provide important information about the nature of the veins when they contact Windy Table strata above an unconformable surface.

Detailed mapping exercises should be carried out to better define Windy Table volcanic strata, to test whether the strata are part of a single eruption or if there are multiple eruptions. Moreover, detailed mapping may give additional insights as to the nature of the Windy Table depositional environment (i.e. caldera collapse, half-grabben fill, post-emplacement fault preserved, etc.).

References

Mihalynuk, M.G., Nelson, J. and Diakow, L. (1994): Cache Creek Terrane entrapment: oroclinal paradox within the Canadian Cordillera; *Tectonics*, Volume 13, pages 575-595.

Mihalynuk, M.G. (1999): Geology and Mineral Resources of the Tagish Lake Area, B.C.; *Ministry of Energy and Mines*, Bulletin 105.

Mihalynuk, M.G., J. Mortensen, R. Friedman, A. Panteleyev and H.J. Awmack (2003): Cangold partnership: regional geologic setting and geochronology of high-sulphidation

mineralization at the Thorn property. British Columbia; *Ministry of Energy and Mines,* Geofile 2003-10.

Monger, J.W.H. (1984): Cordilleran Tectonics: A Canadian Perspective; *Bulletin de la Société Géologique de France*, Series 7, Volume 26, pages 197-324.

Monger, J.W.H., Wheeler, J.O., Tipper, H.W., Gabrielse, H., Harms, T., Struik, L.C., Campbell, R.B., Dodds, C.J., Gehrels, G.E. and O'Brien, J. (1991): Cordilleran Terranes; *in* Geology of the Cordilleran orogen in Canada, Gabrielse, H. and Yorath, C.J. editors, *Geological Survey of Canada*, Geology of Canada, Volume 4, pages 281-327.

Appendix I: Geochronologic Results of intrusive and extrusive rocks and hydrothermal alteration

U-Pb Isotope Dilution Thermal Ionization Mass Spectrometry (ID-TIMS)

Uranium-lead zircon dating of five samples of Late Cretaceous and Jurassic intrusive and extrusive units from the Thorn area in northwest British Columbia was undertaken using conventional ID-TIMS methods in order to establish crystallization ages for the main magmatic events in the region. Coordinates of samples listed below are given in Universal Transverse Mercator (UTM), NAD 87, Zone 8.

Methodology

R.M. Friedman

Zircon was separated from rock samples using conventional crushing, grinding, and Wilfley table techniques, followed by final concentration using heavy liquids and magnetic separations. Mineral fractions for analysis were selected based on grain morphology, quality, size and magnetic susceptibility. All zircon fractions were air abraded prior to dissolution to minimize the effects of post-crystallization Pb-loss, using the technique of Krogh (1982). All mineral separations, geochemical separations and mass spectrometry were done in the Pacific Centre for Isotopic and Geochemical Research in the Department of Earth and Ocean Sciences, University of British Columbia. Samples were dissolved in concentrated HF and HNO_3 in the presence of a mixed $^{233\text{-}235}U$-^{205}Pb tracer. Separation and purification of Pb and U employed ion exchange column techniques modified slightly from those described by Parrish et al. (1987). Pb and U were eluted separately and loaded together on a single Re filament using a phosphoric acid-silica gel emitter. Isotopic ratios were measured using a modified single collector VG-54R thermal ionization mass spectrometer equipped with a Daly photomultiplier. Measurements were done in peak-switching mode on the Daly detector. U and Pb analytical blanks were in the range of 1 pg and 1-5 pg, respectively, during the course of this study. U fractionation was determined directly on individual runs using the $^{233\text{-}235}U$ tracer, and Pb isotopic ratios were corrected for a fractionation of 0.37%/amu for Faraday and Daly runs, respectively, based on replicate analyses of the NBS-981 Pb standard and the values recommended by Thirlwall (2000). All analytical errors were numerically propagated through the entire age calculation using the technique of Roddick (1987). Concordia intercept ages and associated errors were calculated using a modified version the York-II regression model (wherein the York-II errors are multiplied by the MSWD) and the algorithm of Ludwig (1980). All age errors are quoted at 2σ (Ma) and errors for isotopic ratios are quoted at 1σ (%)

Pre-Cretaceous

Sample AS-071a (6490270 mN, 632543 mE): This sample contained a small amount of zircon, most of which were fine-grained (40 μm long axis), clear, colourless elongate prisms. Four fractions were analyzed and all yielded concordant analyses (Table 2-2, Figure 2-6A). Fractions A and B give somewhat older ages than fractions C and D. The best estimate for age of crystallization of the sample is given by the total range of $^{206}Pb/^{238}U$ ages for the concordant and overlapping factions A and B of 168.1 ± 0.7 Ma. Fractions C and D are interpreted to have experienced post crystallization Pb-loss.

Cretaceous

Sample AS-107a (6493090 mN, 631320 mE): This sample contained abundant zircon, most of which were medium grained (150 μm long axis), clear, colourless to pale yellow, stubby crystals. Four fractions were analyzed and all yielded concordant analyses (Table 2-2, Figure 2-6B). Fractions A and C are the most concordant of the fractions and both overlap with each other, while fraction B and D are marginally concordant yielding slightly younger and older ages respectively. The best estimate for age of crystallization of the sample is given by the total range of $^{206}Pb/^{238}U$ ages for the concordant and overlapping factions A and c of 82.2 ± 0.5 Ma. Fraction B has experienced post crystallization Pb-loss while fraction D contains an inherited component.

Sample AS-099a (6491930 mN, 629040 mE): Only a small amount of zircon was recovered form this sample. Most zircons were fine-grained (100 μm long axis), clear, pale yellow needle-like crystals. Fractions C and D yield concordant ages with fraction D being slightly younger and more concordant than fraction C (Table 2-2, Figure 2-6C). Fractions A and B contain significant inherited components. The best estimate for age of crystallization of the sample is given by the lower intercept of a three-point regression of fractions A, B and D of 80.8 +3.6/-4.9 Ma.

Sample AS-060a (6493721 mN, 632438 mE): Three fractions of strongly abraded coarse-grained (300 μm long axis), clear, colourless, elongate zircons were analyzed (Table 2-2, Figure 2-6D). Fraction B contains minor older inherited component, however overlapping and concordant fractions D and C with a total range of $^{206}Pb/^{238}U$ ages of 86.6 ± 0.6 Ma is interpreted as the age of crystallization of this sample.

Sample AS-035a (6492888 mN; 628407 mE): This sample contained abundant zircons, which were fine-grained (80 μm long axis), clear, pale yellow, stubby prisms. Of the three fractions

that were analyzed one (D) was concordant (Table 2-2, Figure 2-6E). Fraction B contains an inherited component, while fraction C has experienced post-crystallization Pb-loss. A precise age was not determined based on this data and was re-analyzed using the SHRIMP-RG (see below), however an age of *ca.* 82 Ma is interpreted for this sample using this data set.

U-Pb Sensitive High Resolution Ion Micro Probe Reverse Geometry (SHRIMP) Zircon Geochronology

Seventeen samples of Triassic, Jurassic, Late Cretaceous and Paleogene age were analyzed using the Stanford-U.S. Geological Survey Sensitive High-mass Resolution Ion MicroProbe-Reverse Geometry (SHRIMP-RG) by a combination of Adam Simmons, Richard Tosdal, Claire Chamberlain and Alan Wainwright. Figure 2-7E shows a duplicate U-Pb zircon sample of AS-035a done using TIMS (Figure 2-6E) in which an age could not be determined due to zircons from different fractions containing inherited zircons from lithic fragments and the fractions also lost lead. This emphasizes the importance of the U-Pb SHRIMP method over the TIMS method in determining ages on samples with possible lithic components, a problem common to pyroclastic rocks, which TIMS cannot resolve because the method does not employ single grain in-situ analyses of zircons. Coordinates of samples listed below are given in Universal Transverse Mercator (UTM), NAD 87, Zone 8.

Methodology

The samples were prepared at the University of British Columbia using the methods outlined for U-Pb TIMS analysis. The populations of zircons obtained from these samples were dated using the SHRIMP-RG at Stanford University, California. The SHRIMP-RG has a reverse geometry design and has improved mass resolution compared to conventional SHRIMP designs (Williams, 1998; Bacon *et al.*, 2000). Bacon *et al.* (2000) summarize the operational conditions for the SHRIMP-RG. Reviews on the ion microprobe technique and data interpretation are provided in Ireland and Williams (2003). Compositions for initial common Pb compositions were based on the measured ^{204}Pb and the model of Cumming and Richards (1975). Zircon and Pb isotope data were reduced using the SQUID program (Ludwig, 2001) and ISOPLOT (Ludwig, 1999). Spot U-Pb analyses are provided in Table 2-1 and are plotted on concordia and weighted mean diagrams in figures 2-4 and 2-5. All errors are given at the 1σ level.

Pre-Cretaceous

Sample 04AS-21 (6479072 mN, 636336 mE): Zircons in this sample were stubby, prismatic and often broken, with abundant dark inclusions. Two of the zircons displayed a dark rounded core

with lighter overgrowth of zircon. All zircons were moderately zoned. No correlation was noted between older and younger ages to core and rims, respectively. Spots AS21-2, AS21-5 and AS-21-6 are interpreted to have undergone post crystallization Pb-loss and are not considered in the statistical analysis. Ignoring these spots yields a weighted mean average of 249.0 ± 6.4 Ma (Table 2-1, Figure 2-5A). Zircon sizes ranged from 75 - 100 μm in the long dimension and 15 - 40 μm in the short dimension.

Sample 04AS-28 (6479202 mN, 668843 mE): Zircons in this sample were coarse-grained, elongate prismatic and often broken. These zircons were not complex, contained no older cores and were strongly zoned. No correlation was noted between older and younger ages to crystal interiors and edges, respectively. Spots AS28-6, 7, 8, 11 and 12 are interpreted to have undergone post crystallization Pb-loss and are not considered in the statistical analysis. Spot AS28-4 is interpreted as containing an inherited component, likely of Stuhini Group affinity and is not considered in the statistical analysis. Ignoring these spots yields a weighted mean average of 219.2 ± 3.5 Ma (Table 2-1, Figure 2-5B). Zircon sizes ranged from 400 - 750 μm in the long dimension and 125 - 450 μm in the short dimension.

Sample 04AS-27 (6472437 mN, 667318 mE): Zircons in this sample were coarse-grained, elongate prismatic and often broken. Core with overgrowth of zircon were noted in approximately half of the zircons and were strongly zoned. The zircons analyzed were extremely well behaved and did not yield multiple age in spite of the noted cores. Machine drift was encountered during this analysis, as seen in the weighted mean diagram, which shows a constantly decreasing age with each analysis. Spot AS27-5 is interpreted to have undergone post crystallization Pb-loss and is not considered in the statistical analysis. Spots AS27-6, 7, 8, 9, 10, 11 and 12 were used for statistical analysis because they form more consistent weighted mean than spot AS27-1, 2, 3 and 4. These spots yield an age of 211 +11/-40 Ma (Table 2-1, Figure 2-5C). Zircon sizes ranged from 350 - 600 μm in the long dimension and 75 - 250 μm in the short dimension.

Cretaceous

Sample 04AS-20 (6486420 mN, 630561 mE): Two populations of zircon were noted in this sample: a) fine-grained, prismatic (~ 15 x 80 μm), light zoned zircons and b) coarse grained (~ 150 x 400 μm), dark, zoned and broken zircons. The sample was taken from a lithic rich tuff and probably reflects the ages of the surrounding Stuhini Group rocks and the crystallization age of the rock. A statistically valid age could not be obtained due to a lack of zircon, however

the concordia plots indicates that the most likely age of this samples is *ca.* 91 Ma (Table 2-1, Figure 2-5D).

Sample 277510 (6492060 mN, 628010 mE): Zircons in this sample were coarse-grained, dark, stubby, prismatic and euhedral crystals. These zircons are not complex, contained no older cores and were strongly zoned. No correlation was noted between older and younger ages to crystal interiors and edges, respectively. Spots AS510-1, 2, 3, 4, 5, 12 and 13 are interpreted to have undergone post crystallization Pb-loss and are not considered in the statistical analysis. Ignoring these spots yields a weighted mean average of 90.6 ± 1.1 Ma (Table 2-1, Figure 2-4A). Zircon sizes ranged from 250 - 500 μm in the long dimension and 50 - 200 μm in the short dimension.

Sample 04AS-12 (6506221 mN, 610885 mE): Zircons in this sample were coarse-grained, dark, stubby, prismatic and euhedral crystals. These zircons are not complex, contained no older cores, were strongly zoned and contained numerous dark inclusions. No correlation was noted between older and younger ages to crystal interiors and edges, respectively. Spots AS12-1 and 9 are interpreted to have undergone post crystallization Pb-loss and are not considered in the statistical analysis. Ignoring these spots yields a weighted mean average of 88.0 ± 0.6 Ma (Table 2-1, Figure 2-5E). Zircon sizes ranged from 400 - 600 μm in the long dimension and 200 - 250 μm in the short dimension.

Sample 04AS-22 (6500947 mN, 638724 mE): Zircons in this sample were fine-grained, light, elongate, prismatic and euhedral crystals. Approximately 25% of the zircons contained older cores and/or were broken. All zircons were strongly zoned. No correlation was noted between older and younger ages to core and rims, respectively. Spots AS22-4, 5, 6, 8, 10, 11 and 12 are interpreted to have undergone post crystallization Pb-loss and are not considered in the statistical analysis. Ignoring these spots yields a weighted mean average of 87.7 ± 1.1 Ma (Table 2-1, Figure 2-5F). Zircon sizes ranged from 75 - 200 μm in the long dimension and 30 - 75 μm in the short dimension.

Sample AS-060 (6493721 mN, 632438 mE): Zircons in this sample were coarse-grained, dark, stubby, prismatic and euhedral crystals. These zircons are not complex, contained no older cores and were strongly zoned. No correlation was noted between older and younger ages to crystal interiors and edges, respectively. Spot AS60-5 is interpreted to have undergone post crystallization Pb-loss and is not considered in the statistical analysis. Spots AS60-1 and 4 are interpreted to contain an inherited component and are not considered in the statistical analysis. Ignoring these spots yields a weighted mean average of 87.6 ± 1.2 Ma (Table 2-1, Figure 2-

4B). Zircon sizes ranged from 250 - 500 μm in the long dimension and 100 - 175 μm in the short dimension.

Sample 04AS-009 (6493530 mN, 627160 mE): Zircons in this sample were fine-grained, light, elongate, prismatic and euhedral crystals. These zircons are not complex, contained no older cores and were strongly zoned. No correlation was noted between older and younger ages to crystal interiors and edges, respectively. Spot 4AS9B-11 is interpreted to have undergone post crystallization Pb-loss and is not considered in the statistical analysis. Spots AS60-1, 8, 10 and 13 are interpreted to contain an inherited component and are not considered in the statistical analysis. Ignoring these spots yields a weighted mean average of 85.5 ± 0.7 Ma (Table 2-1, Figure 2-4C). Zircon sizes ranged from 100 - 200 μm in the long dimension and 30 - 75 μm in the short dimension.

Sample 04AS-25 (6500184 mN, 619202 mE): Zircons in this sample were medium-grained, dark, stubby, prismatic and euhedral crystals containing numerous dark inclusions. These zircons are not complex, contained no older cores and were strongly zoned. No correlation was noted between older and younger ages to crystal interiors and edges, respectively. Spots 4AS525-5 and 8 are interpreted to contain an inherited component and are not considered in the statistical analysis. Ignoring these spots yields a weighted mean average of 85.5 ± 0.7 Ma (Table 2-1, Figure 2-5G). Zircon sizes ranged from 200 - 350 μm in the long dimension and 100 - 200 μm in the short dimension.

Sample 04AS-03 (6491574 mN, 627976 mE): Zircons in this sample were fine-grained, light, stubby, prismatic and euhedral crystals, which were often embayed. These zircons are not complex, contained no older cores and were moderately to weakly zoned. No correlation was noted between older and younger ages to crystal interiors and edges, respectively. Spots AS-03-1, 8, 9, 10, 11, 12 and 13 are interpreted to have undergone post crystallization Pb-loss and are not considered in the statistical analysis. Ignoring these spots yields a weighted mean average of 84.5 ± 2.3 Ma (Table 2-1, Figure 2-4D). However the MSWD and probability are not sufficient enough for this to be a legitimate age. Therefore, this sample is considered to be not interpretable with the data provided during this study. Zircon sizes ranged from 80 - 200 μm in the long dimension and 25 - 75 μm in the short dimension.

Sample AS-086a (6491030 mN, 632794 mE): Zircons in this sample were coarse-grained, dark, stubby, prismatic and euhedral crystals, which were occasionally broken. These zircons are not complex, contained no older cores and were generally not zoned. No correlation was noted between older and younger ages to crystal interiors and edges, respectively. Spot AS86-9 is

interpreted to have undergone post crystallization Pb-loss and is not considered in the statistical analysis. Ignoring these spots yields a weighted mean average of 82.0 ± 0.9 Ma (Table 2-1, Figure 2-4E). Zircons form this sample had two size populations which were 150 - 700 μm and 75 - 150 μm in the long dimension and 200 - 250 μm and 25 - 75 μm in the short dimension.

Sample 04AS-23 (6493563 mN, 647720 mE): Zircons in this sample were fine-grained, light, stubby, prismatic and euhedral crystals. These zircons are not complex, contained no older cores and were moderately zoned. No correlation was noted between older and younger ages to crystal interiors and edges, respectively. Spots AS23-2, 6, 7, 8 and 12 are interpreted to contain an inherited component and are not considered in the statistical analysis. Ignoring these spots yields a weighted mean average of 81.6 ± 0.9 Ma (Table 2-1, Figure 2-5H). Zircon sizes ranged from 80 - 175 μm in the long dimension and 25 - 80 μm in the short dimension.

Sample AS-035a (6492888 mN, 628407 mE): Several populations of zircon were present in this sample, including a) coarse-grained (200 x 100 μm), dark, stubby, prismatic and euhedral crystals, b) fine-grained (70 x 20 μm), light, stubby, prismatic and broken crystals and c) medium-grained (100 x 40 μm), dark, stubby, prismatic, embayed and euhedral crystals. All zircons are not complex, contained no older cores and were zoned. No correlation was noted between older and younger ages to crystal interiors and edges, as well as population types. Spots 35A-4, 8, 9 and 14 are interpreted to have undergone post crystallization Pb-loss and is not considered in the statistical analysis. Spots 35A-5, 7, 10, 16, 19 and 20 are interpreted to contain an inherited component and are not considered in the statistical analysis. Ignoring these spots yields a weighted mean average of 81.4 ± 0.9 Ma (Table 2-1, Figure 2-4F).

Sample 04AS-29 (6478980 mN, 666312 mE): Zircons in this sample were medium-grained, very dark, stubby crystals. Approximately 25% of these zircons contained older cores. No correlation was noted between older and younger ages to cores and rims, respectively. All crystals were strongly zoned. Spot AS29-4 is interpreted to have undergone post crystallization Pb-loss and is not considered in the statistical analysis. Spots AS29-5, 7 and 8 are interpreted to contain an inherited component and are not considered in the statistical analysis. Ignoring these spots yields a weighted mean average of 81.3 ± 0.4 Ma (Table 2-1, Figure 2-5I). Zircon sizes ranged from 150 - 400 μm in the long dimension and 80 - 200 μm in the short dimension.

Post-Cretaceous

Sample 04AS-11 (6506538 mN, 612037 mE): Zircons in this sample were coarse-grained, dark, elongate, euhedral crystals, which contained abundant dark inclusions. These zircons are not complex, contained no older cores and were moderately zoned. No correlation was noted

between older and younger ages to crystal interiors and edges, respectively. Spots 4AS11-1, 3, 5 and 12 are interpreted to have undergone post crystallization Pb-loss and are not considered in the statistical analysis. Spot 4AS11-2 is interpreted to contain an inherited component and is not considered in the statistical analysis. Ignoring these spots yields a weighted mean average of 56.3 ± 0.7 Ma (Table 2-1, Figure 2-5J). Zircon sizes ranged from 200 - 600 μm in the long dimension and 80 - 200 μm in the short dimension.

Sample 04AS-19 (6506461 mN, 622970 mE): Zircons in this sample were coarse-grained, dark, elongate, euhedral crystals, which contained abundant dark inclusions. These zircons are not complex, contained no older cores and were moderately zoned. No correlation was noted between older and younger ages to crystal interiors and edges, respectively. Spots 4AS19-1, 2, 5 and 7 are interpreted to contain an inherited component and are not considered in the statistical analysis. Ignoring these spots yields a weighted mean average of 55.5 ± 0.6 Ma (Table 2-1, Figure 2-5K). Zircon sizes ranged from 200 - 800 μm in the long dimension and 80 - 200 μm in the short dimension.

$^{40}Ar/^{39}Ar$ Geochronology

A total of ten altered samples were analyzed by the $^{40}Ar/^{39}Ar$ method from rocks that were subjected to Late Cretaceous hydrothermal alteration. Four of ten samples did not produce interpretable ages due to either extreme Ar-loss or complications related to particular minerals (e.g. recoil in some sericite samples). All samples were analyzed by Thomas Ullrich at the University of British Columbia.

Each sample was crushed by rubber mallet, while the sample was in a plastic sample bag. Mineral separates were hand-picked, wrapped in aluminium foil and stacked in an irradiation capsule with similar-aged samples and neutron flux monitors (Fish Canyon Tuff sanidine, 28.02 Ma (Renne *et al.*, 1998)).

The samples were irradiated on January 21 and 22, 2004, May 18, 2004 and April 25 to 27, 2005 at the McMaster Nuclear Reactor in Hamilton, Ontario, for 56 MWH, with a neutron flux of approximately $3x10^{16}$ neutrons/cm^2. Analyses (n=42, 57 and 63) of 11, 19 and 18 neutron flux monitor positions, respectively, produced errors of <0.5% in the J value.

The samples were analyzed on April 14 and 15, 2004, October 27 to 29, 2004 and June 5, 2005 at the Pacific Centre for Isotopic and Geochemical Research, University of British Columbia, Vancouver, B.C., Canada. The samples were step-heated at incrementally higher powers in the defocused beam of a 10W CO_2 laser (New Wave Research MIR10) until fused.

The gas evolved from each step was analyzed by a VG5400 mass spectrometer equipped with an ion-counting electron multiplier. All measurements were corrected for total system blank, mass spectrometer sensitivity, mass discrimination, radioactive decay during and subsequent to irradiation, as well as interfering Ar from atmospheric contamination and the irradiation of Ca, Cl and K (Isotope production ratios: $(^{40}Ar/^{39}Ar)$ K=0.0302, $(^{37}Ar/^{39}Ar)$ Ca=1416.4306, $(^{36}Ar/^{39}Ar)$ Ca=0.3952, Ca/K=1.83($^{37}ArCa/^{39}ArK$)). The plateau and correlation ages were calculated using ISOPLOT version 3.09 (Ludwig, 2003). Errors quoted are at the 2-sigma (95% confidence) level are propagated from all sources, except mass spectrometer sensitivity and age of the flux monitor.

The best statistically-justified plateau and plateau age were picked based on the following criteria:

1. Three or more contiguous steps comprising more than 50% of the ^{39}Ar;
2. Probability of fit of the weighted mean age greater than 5%;
3. Slope of the error-weighted line through the plateau ages equals zero at 5% confidence;
4. Ages of the two outermost steps on a plateau are not significantly different from the weighted-mean plateau age (at 1.8σ, six or more steps only);
5. Outermost two steps on either side of a plateau must not have nonzero slopes with the same sign (at 1.8σ, nine or more steps only).

Results of this data are presented above in Table 3-2 and Figure 3-5. There are a number of reasons to explain steps the are deviated from the plateau, including: mineral inclusions, dirty sample (i.e. contains multiple minerals), fluid inclusions, degrees of alteration, Ar-loss/addition at crystal grain boundaries, etc.

Sample THN03-22 (6491914 mN, 628769 mE): The sample submitted contained fine grained white mica with a slight yellow colour. The mica was extracted from massive sulphide of the Oban breccia. Samples analyzed were amalgamations ("chunks") of several white mica. All deviated steps may have included fluid inclusions and/or Ar-addition and/or been partially altered.

Sample Oban (6491907 mN, 628763 mE): The sample submitted was a massive sericite sample, which formed part of the crustiform assemblage of the Oban breccia. The sericite had a slight grey tone and oily to touch. Sericite composition was confirmed by PIMA. Sample was a 1 cm thick crustiform band contained within boulangerite, sphalerite and pyrite. The first step

of the plateau was rejected due to Ar-loss at the crystal grain boundary, while steps 2-5 where rejected due to either fluid inclusions and/or Ar-addition and/or been partially altered

Sample AS-025a (6491624 mE, 627740 mE): The sample submitted contained fine grained white mica with a slight yellow colour. The mica was extracted from massive sulphide of the D-zone vein. Samples analyzed were amalgamations ("chunks") of several white mica. The first step of the plateau was rejected due to Ar-loss at the crystal grain boundary, while the last four steps where rejected because of anomalously high Ca/K, indicating a separate mineral phase other than sericite.

Sample 277540 (6491150 mN, 628070 mE): The sample submitted contained fine grained white mica. The sample was picked form crushed Thorn Stock (in its least altered form) and probably represents sercite replacement of the matrix to the Thorn Stock. The first step of the plateau was rejected due to Ar-loss on the crystal grain edge, while the last two steps where rejected due to either fluid inclusions and/or Ar-addition and/or been partially altered

Sample Cirque (6493088 mN, 631349 mE): The sample submitted contained fine grained dark to honey brown biotite. The mica was picked via tweezers and a knife from samples of potassically altered Cirque Stock in the main zone of porphyry Cu-Mo mineralization. The four steps of the plateau was rejected due to Ar-loss on the crystal grain edge.

Sample Outlaw (6490280 mN, 632690 mE): The sample submitted contained fine grained dark brown biotite.. The sample was picked with tweezers from the light fraction of the sample used for U-Pb TIMS geochronology for sample AS-071a. The two steps of the plateau was rejected due to Ar-loss on the crystal grain edge, while the last two steps where rejected due to either fluid inclusions and/or Ar-addition and/or been partially altered

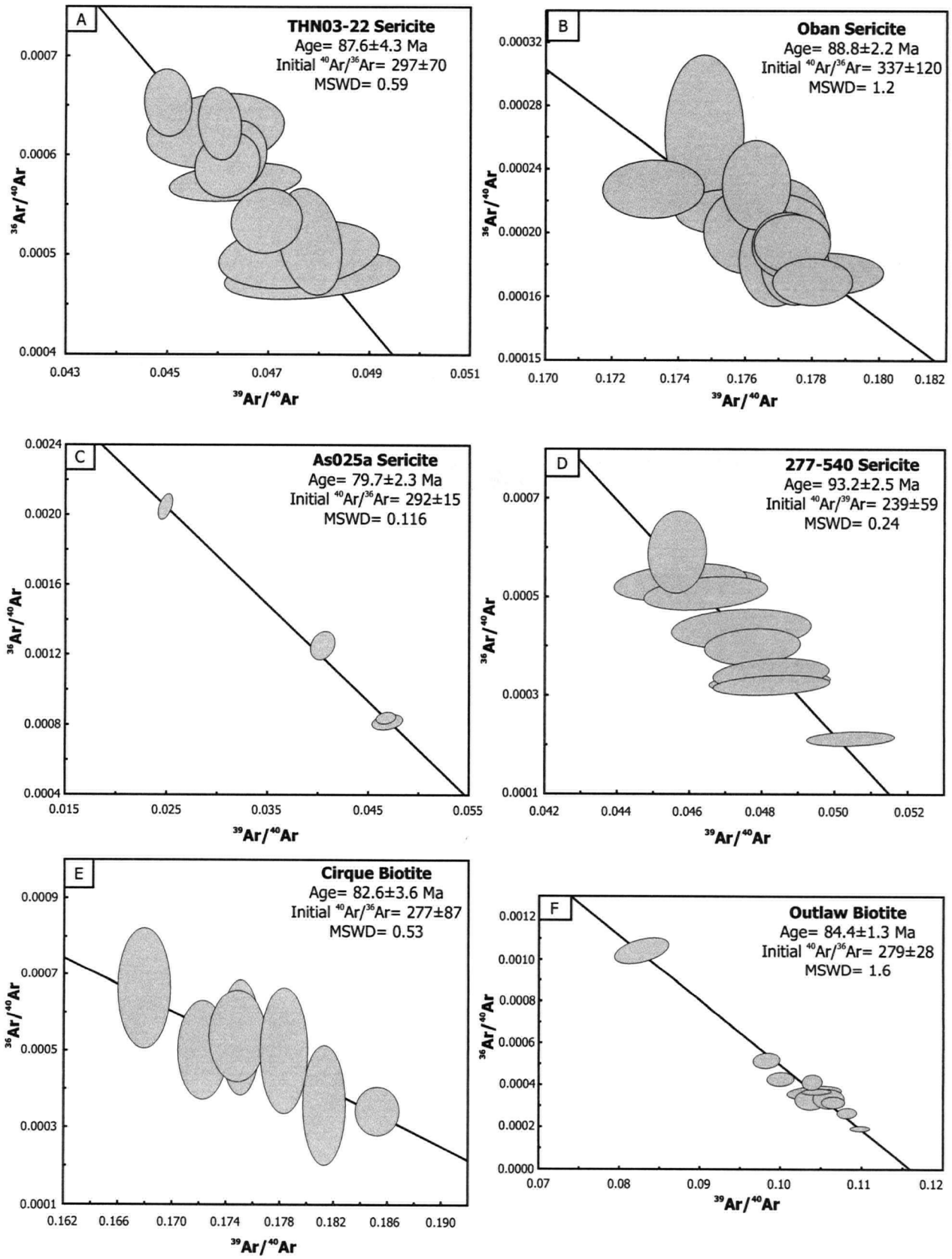

Figure 3-5: $^{40}Ar/^{39}Ar$ geochronology of alteration from the Thorn Property. Inverse isochrons for plateaus given in Chapter 3. Only the steps used for the plateau were considered in the inverse isochrons. Errors in box heights given at 2σ.

$^{40}Ar/^{39}Ar$ samples not used in thesis

Sample AS-017b (6493800 mN, 628290 mE): The sample submitted contained medium to coarse-grained muscovite. The mica was extracted from the rock by knife and tweezers. The first two steps of the plateau are rejected due to Ar-loss. High atmospheric ^{40}Ar.

Sample AS-068e (6492585 mN, 633215 mE): The sample submitted was coarse grained anhedral biotite, which had been slightly chloritized (slight green colour). The mica was extracted from the rock by knife and tweezers. No interpretable age for this sample, but indicates maximum of ~ 83Ma and lost Ar at ~55 Ma, which coincides with the Sloko magmatic event. High atmospheric ^{40}Ar.

Sample AS-068e2 (6492585 mN, 633215 mE): The sample submitted was coarse grained euhedral hornblende, which had been partly chloritized (slight green colour). The mica was extracted from the rock by knife and tweezers. No interpretable age for this sample. Both the plateau and inverse isochron indicate Ar-loss at ~55 Ma, which coincides with the Sloko magmatic event. High atmospheric ^{40}Ar.

Sample Glen (6491990 mN, 628330 mE): The sample submitted contained fine grained white mica with a slight yellow colour. The mica was extracted from massive sulphide of the Jim Beam vein. No interpretable age for this sample. Both the plateau and inverse isochron indicate Ar-loss at ~55 Ma, which coincides with the Sloko magmatic event. High atmospheric ^{40}Ar.

Sample Jim Beam (6492222 mN, 628677 mE): The sample submitted contained fine grained white mica with a slight silvery colour, and mixed with fine grained quartz. The mica was extracted from massive sulphide of the Jim Beam vein. No interpretable age for this sample. Both the plateau and inverse isochron indicate Ar-loss at ~55 Ma, which coincides with the Sloko magmatic event. High atmospheric ^{40}Ar.

Sample Jim Beam (6492222 mN, 628677 mE): The sample submitted contained fine grained white mica with a slight yellow colour. The mica was extracted from massive sulphide of the Jim Beam vein. No interpretable age for this sample. Both the plateau and inverse isochron indicate Ar-loss at ~55 Ma, which coincides with the Sloko magmatic event. High atmospheric ^{40}Ar.

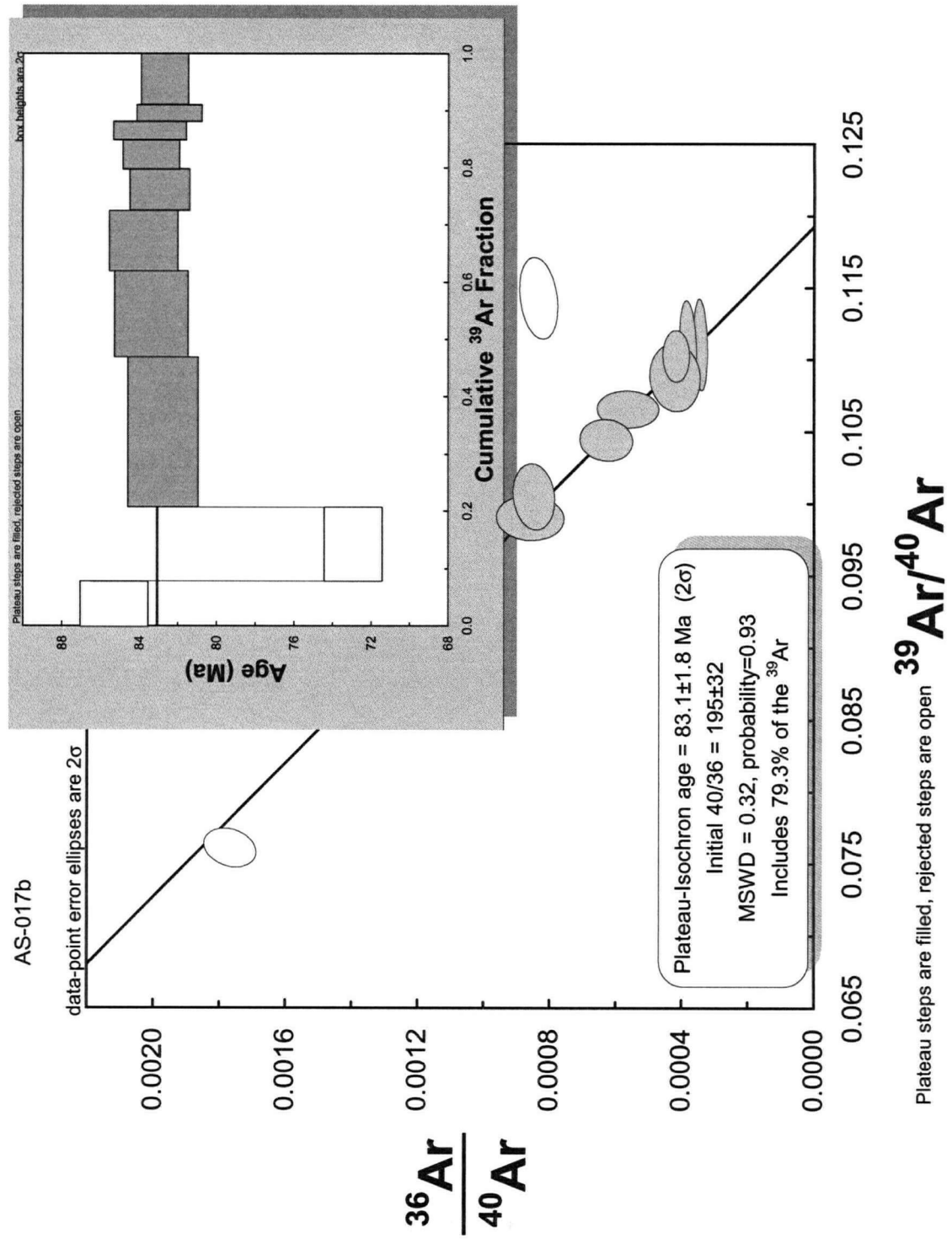

Figure I-2: Plateau and inverse isochron plots from 40Ar/39Ar samples not used in thesis. Sample AS-017b is from euhedral muscovite from a dacite sill in Phase 3 Windy Table volcanic rocks.

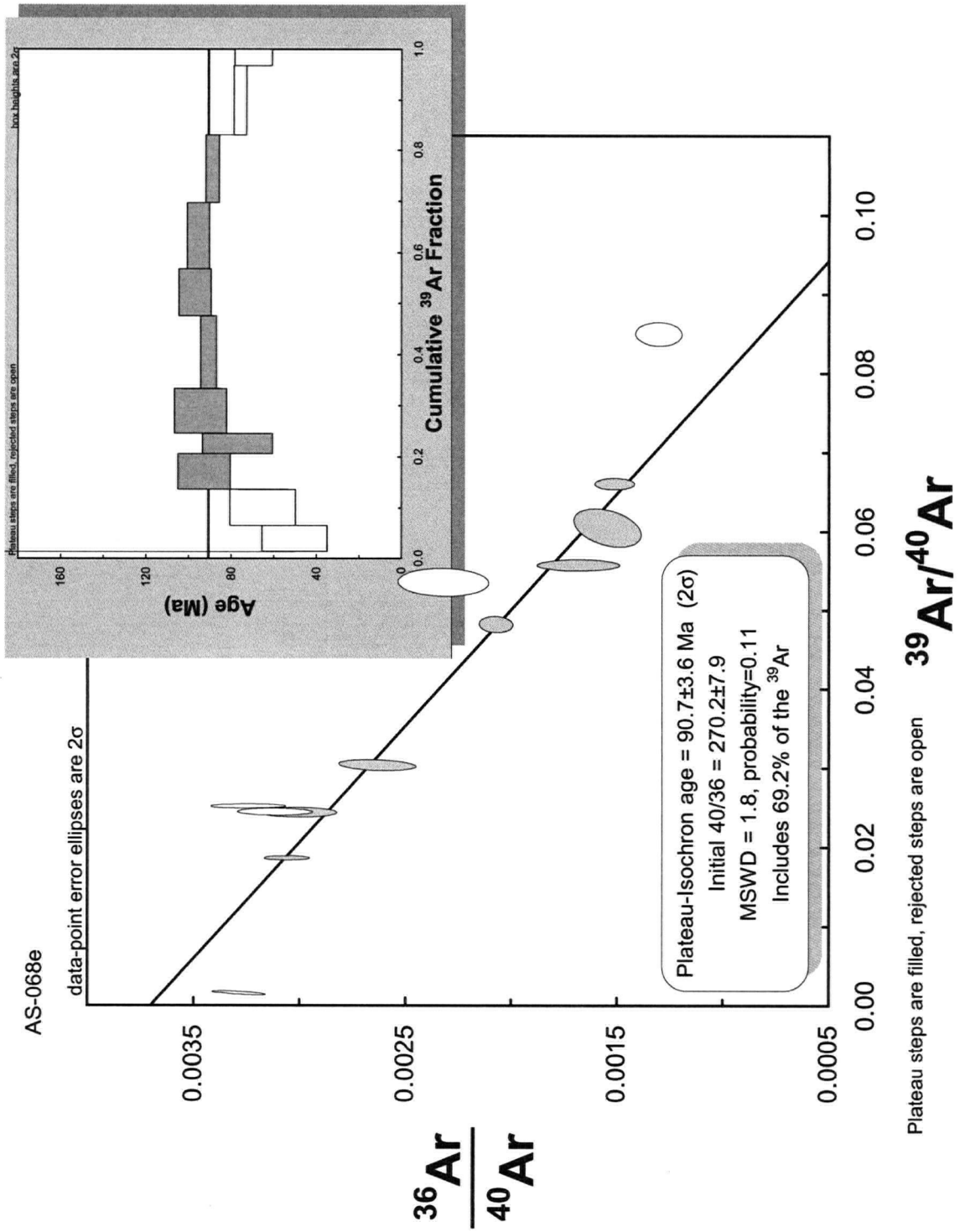

Figure I-2: Plateau and inverse isochron plots from 40Ar/39Ar samples not used in thesis. Sample AS-068e (Bt) is from slightly altered bioitite from Type 2 Windy Table intrusion in the Cirque area.

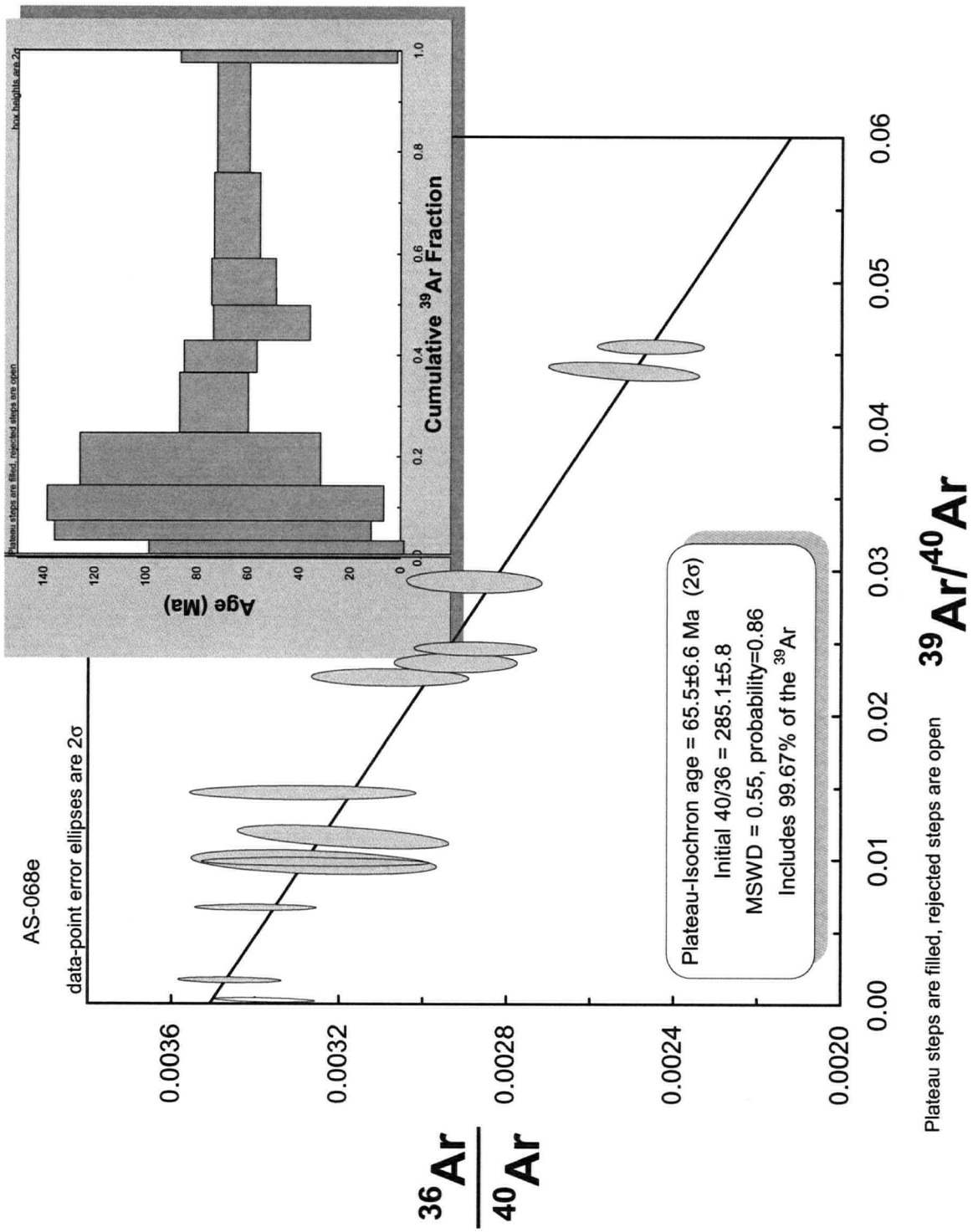

Figure I-2: Plateau and inverse isochron plots from 40Ar/39Ar samples not used in thesis. Sample AS-068e (Hb) is from slightly altered hornblende from Type 2 Windy Table intrusion in the Cirque area.

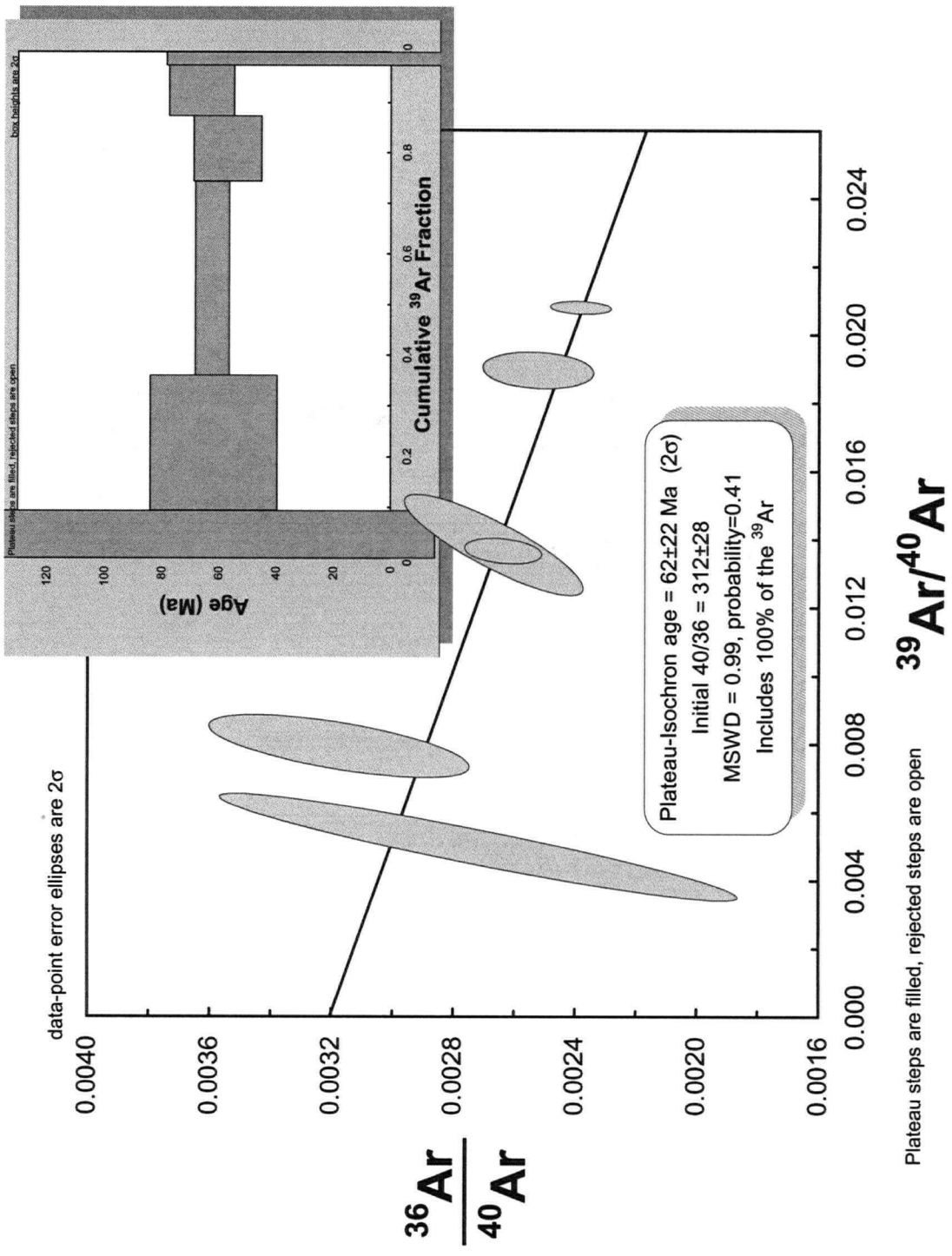

Figure I-2: Plateau and inverse isochron plots from 40Ar/39Ar samples not used in thesis. Sample Glen is fine grained sericite contained within massive sulphide from the Glenlivet high-sulphidation mineral assemblage vein.

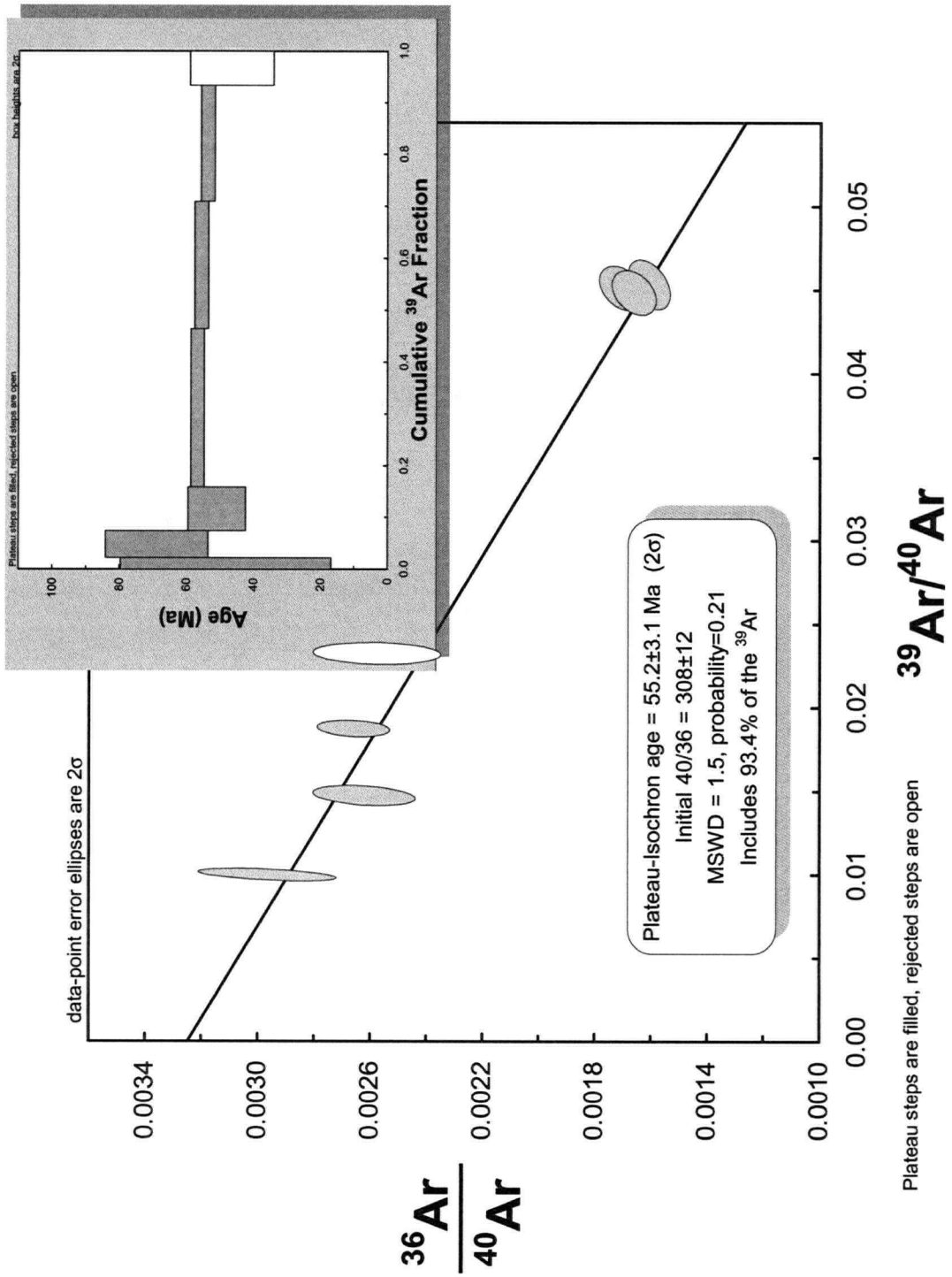

Figure I-2: Plateau and inverse isochron plots from 40Ar/39Ar samples not used in thesis. Sample Jim Beam is fine grained sericite with quartz contained within massive sulphide from the Jim Beam high-sulphidation mineral assemblage vein.

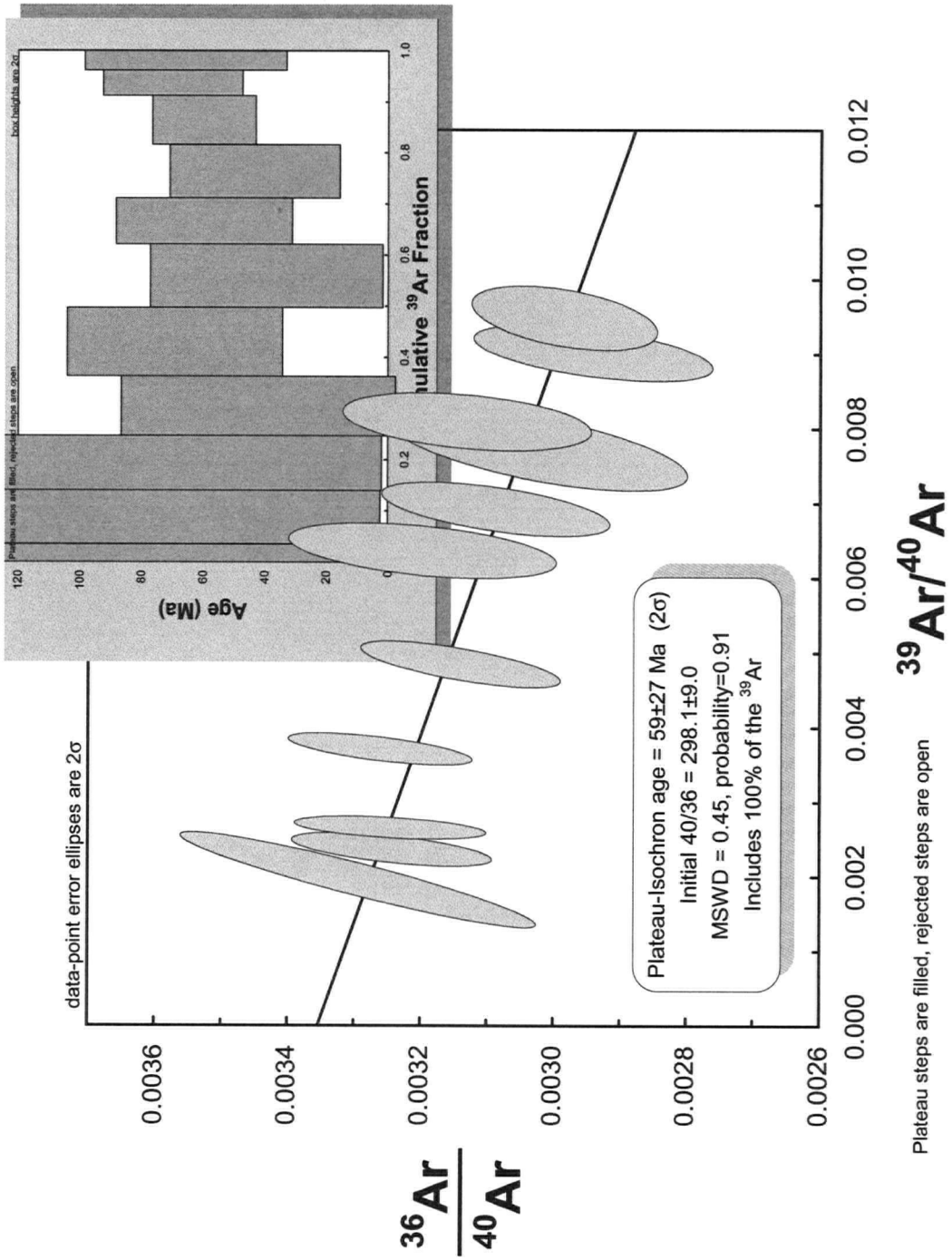

Figure I-2: Plateau and inverse isochron plots from 40Ar/39Ar samples not used in thesis. Sample Jim Beam 2 is fine grained yellowish sericite contained within massive sulphide from the Jim Beam high-sulphidation mineral assemblage vein.

Table I-1: 40Ar/39Ar data from samples not used in the thesis

Laser Power(%)	Isotope Ratios $^{40}Ar/^{39}Ar$	$^{38}Ar/^{39}Ar$	$^{37}Ar/^{39}Ar$	$^{36}Ar/^{39}Ar$	Ca/K	Cl/K	$\%^{40}Ar$ atm	$f^{39}Ar$	$^{40}Ar^*/^{39}ArK$	Age
		Sample=**AS-017b**		Mineral=**Muscovite**						
1.8	13.411±0.014	0.018±0.041	0.003±0.30	0.024±0.035	0.019	0	51.92	7.97	6.301±0.285	62.77±2.79
2	8.939±0.020	0.014±0.031	0.009 0.614	0.008±0.052	0.082	0	24.37	12.78	6.615±0.203	65.84±1.99
2.2	9.130±0.023	0.013±0.032	0.001 0.518	0.004±0.052	0.009	0	11.09	26.23	8.014±0.202	79.46±1.96
2.3	9.182±0.024	0.014±0.042	0.001 0.128	0.004±0.047	0.004	0	10.02	15.02	8.112±0.208	80.41±2.02
2.4	9.418±0.018	0.014±0.040	0.001 0.063	0.005±0.126	0.003	0	12.24	10.59	8.076±0.230	80.06±2.23
2.5	9.689±0.010	0.015±0.031	0.002 0.129	0.006±0.114	0.003	0	16.44	7.23	7.849±0.228	77.86±2.21
2.7	9.982±0.011	0.020±0.042	0.003 0.084	0.007±0.085	0.007	0.001	18.37	5.06	7.821±0.213	77.59±2.06
2.9	10.699±0.012	0.032±0.067	0.005 0.090	0.011±0.080	0.017	0.004	25.12	3.26	7.563±0.279	75.09±2.71
3.2	10.616±0.018	0.052±0.027	0.006 0.129	0.011±0.049	0.027	0.008	24.82	2.91	7.483±0.222	74.30±2.16
4	9.321±0.013	0.090±0.024	0.003 0.191	0.005±0.066	0.02	0.017	12.12	8.96	7.975±0.143	79.08±1.38
Total.Avg.	**9.487±.004**	**.023±0.006**	**.010±.037**	**0.006±0.012**		**.003**		**100**	**8.055±0.039**	**76.07±0.40**
J=0.005619±0.000018										
Volume 39ArK =794.85										
Integrated Date =76.07±0.80										
		Sample=**AS-068e**		Mineral=**Biotite**						
1.8	626.01±0.02	0.535±0.032	0.084±0.55	2.046±0.032	0.556	0.032	96.8	1.45	19.81±14.44	190.3±131.7
1.9	41.009±0.009	0.206±0.029	0.014±0.15	0.133±0.044	0.068	0.039	95.43	5.16	1.784±1.707	17.99±17.13
2	41.807±0.015	0.132±0.039	0.012±0.60	0.130±0.046	0.062	0.022	91.74	7.14	3.342±1.743	33.55±17.34
2.1	54.570±0.012	0.132±0.042	0.017±0.10	0.167±0.030	0.107	0.02	90.11	6.93	5.266±1.404	52.58±13.82
2.2	42.733±0.020	0.116±0.045	0.020±0.09	0.129±0.052	0.104	0.018	88.57	3.92	4.658±1.864	46.60±18.41
2.4	33.750±0.018	0.127±0.036	0.008±0.27	0.089±0.053	0.038	0.022	77.52	8.85	7.381±1.486	73.29±14.46
2.6	21.256±0.018	0.125±0.023	0.007±0.19	0.045±0.034	0.044	0.024	60.86	14.15	8.096±0.439	80.23±4.25
2.8	18.727±0.011	0.128±0.028	0.004±0.74	0.033±0.088	0	0.025	49.35	9.16	9.084±0.863	89.78±8.32
3.1	17.081±0.032	0.129±0.017	0.010±0.17	0.027±0.072	0.067	0.025	45.26	13	9.033±0.790	89.29±7.62
3.5	15.691±0.009	0.123±0.018	0.003±2.55	0.025±0.048	0	0.024	44.33	13.22	8.418±0.353	83.35±3.42
4	12.292±0.015	0.152±0.027	-	0.017±0.062	0	0.031	38.15	13.79	7.270±0.329	72.20±3.20
5	20.741±0.027	0.148±0.049	0.016±0.23	0.051±0.068	0.047	0.029	68.21	3.24	5.921±0.995	59.02±9.76
Total/Avg	**33.18±.003**	**.141±0.004**	**.026±.035**	**0.088±0.007**		**.026**		**100**	**9.054±0.182**	**72.28±1.78**
J =0.005617±0.000020										
Volume 39ArK =216.91										
Integrated Date =72.28±3.55										
		Sample=**AS-068e2**		Mineral=**Hornblende**						
1.8	3495.299±.14	4.373±0.143	0.335±0.16	11.767±0.142	1.313	0.502	99.7	0.33	10.513±93.482	103.45±894.04
1.9	628.75±0.077	2.038±0.081	0.194±0.13	2.178±0.081	0.705	0.376	102.1	0.54	-12.792±17.335	-134.45±189.15
2	154.344±.028	0.634±0.032	0.065±0.12	0.525±0.044	0.382	0.121	100.3	2.65	-0.424 ±5.272	-4.30±53.52
2.1	105.061±.021	0.346±0.045	0.017±2.13	0.343±0.066	0.004	0.062	96.09	3.9	3.960 ±6.475	39.67±64.15
2.3	103.661±.070	0.216±0.084	0.081±0.62	0.338±0.083	0.675	0.032	96.18	6.93	3.859 ±6.982	38.67±69.21
2.5	87.663±0.057	0.182±0.061	0.127±0.25	0.279±0.059	1.139	0.027	94.12	10.49	5.057 ±5.333	50.51±52.52
2.7	41.746±0.015	0.122±0.028	0.037±0.20	0.121±0.042	0.295	0.02	84.76	11.75	6.174±1.456	61.47±14.25
2.9	44.273±0.022	0.193±0.048	0.029±0.17	0.131±0.045	0.176	0.036	86.15	6.3	5.842±1.524	58.22±14.95
3.2	45.991±0.021	0.801±0.028	0.036±0.92	0.142±0.050	0.247	0.175	90.7	6.97	4.088±1.932	40.93±19.13
3.6	35.572±0.021	0.686±0.028	0.022±1.50	0.103±0.045	0.142	0.15	84.75	9.26	5.199±1.267	51.90±2.46
4.2	23.587±0.010	0.611±0.031	0.072±1.17	0.060±0.034	0.643	0.135	74.11	16.79	5.890±0.586	58.69±5.74
5	22.572±0.009	0.659±0.017	0.012±0.15	0.056±0.041	0.081	0.146	72.23	21.68	6.081±0.685	60.57±6.71
6	73.111±0.028	0.408±0.035	0.049±0.15	0.243±0.068	0.205	0.081	96.92	2.42	2.071±4.471	20.86±44.77
Total/Avg	**62.84±.005**	**0.491±.006**	**.214±.036**	**0.195±0.008**		**.143**		**100**	**5.728± 0.470**	**51.16± 4.63**
J =0.005614±0.000024										
Volume 39ArK =122.26										
Integrated Date =51.16±9.25										
		Sample=**Glen**		Mineral=**Hornblende**						
1.8	209.662±.258	0.125±0.229	1.144±0.07	0.580±0.087	1.683	0	79.93	9.41	41.433±53.144	197.82±240.32
2	74.172 0.086	0.053 0.109	0.408 0.032	0.202 0.046	0.652	0	78.45	26.64	15.601 6.401	77.05 30.95
2.2	49.311 0.007	0.039 0.093	0.282 0.015	0.120 0.031	0.353	0	69.95	38.32	14.419 1.108	71.33 5.37
2.4	56.543 0.022	0.041 0.101	0.835 0.024	0.148 0.053	1.482	-	74.14	13.02	13.613 2.165	67.41 10.52
2.8	78.124 0.020	0.070 0.126	1.068 0.021	0.213 0.035	1.271	0.003	77.5	10.03	16.493 1.956	81.36 9.43
3.5	143.759 .047	0.134 0.207	4.057 0.047	0.468 0.077	6.042	0.003	93.53	2.58	8.248 9.081	41.15 44.79
Total/Avg	**74.69±.035**	**0.052±.035**	**.515±.006**	**0.195±0.011**		**.001**		**100**	**14.215± 2.65**	**84.86± 12.78**
J = 0.002797±0.000006										
Volume 39ArK = 19.88										
Integrated Date = 72.6±4.2										

Volumes are 1E-13 cm3 NPT
Neutron flux monitors: 28.02 Ma FCs (Renne et al., 1998)
Isotope production ratios: $(^{40}Ar/^{39}Ar)K=0.0302$, $(^{37}Ar/^{39}Ar)Ca=1416.4306$, $(^{36}Ar/^{39}Ar)Ca=0.3952$, $Ca/K=1.83(^{37}ArCa/^{39}ArK)$.
*=Radiogenic ^{40}Ar

Table I-1: Continued

Laser Power(%)	Isotope Ratios $^{40}Ar/^{39}Ar$	$^{38}Ar/^{39}Ar$	$^{37}Ar/^{39}Ar$	$^{36}Ar/^{39}Ar$	Ca/K	Cl/K	$\%^{40}Ar$ atm	$f^{39}Ar$	$^{40}Ar^*/^{39}ArK$	Age
	Sample=**Jim Beam**			Mineral= **Silvery sericite with quartz**						
1.8	109.273±.017	0.096±0.139	1.210±.020	0.330±0.055	2.054	0.003	87.1	2.25	13.453±5.342	66.64±25.98
2	71.698±0.034	0.068±0.081	0.530±.027	0.192±0.055	0.902	0.004	76.78	5.17	16.104±3.276	79.48±5.82
2.2	55.564±0.022	0.054±0.083	0.320±.024	0.150±0.040	0.463	0.002	77.84	8.53	11.977±1.681	59.45±8.21
2.4	22.457±0.027	0.050±0.077	0.090±.020	0.037±0.035	0.168	0.007	46.25	30.6	11.830±0.619	58.73±3.02
2.7	22.817±0.024	0.053±0.032	0.113±.019	0.039±0.036	0.222	0.007	47.9	24.41	11.595±0.593	57.58±2.90
3	22.714±0.024	0.064±0.026	0.123±.016	0.040±0.036	0.224	0.01	49.2	22.43	11.226±0.599	55.78±2.93
3.4	45.425±0.022	0.069±0.112	0.414±.022	0.120±0.070	0.586	0.007	75.38	6.6	10.689±2.464	53.15±12.07
Total.Avg.	**30.60±.005**	**0.056±.014**	**.179±.004**	**0.063±0.009**		**.006**		**100**	**11.620±0.205**	**58.74± 1.01**
J =0.002797±0.000006										
Volume 39ArK =78.84										
Integrated Date =58.74±2.01										
	Sample=**Jime Beam**			Mineral=**Sericite**						
1.8	528.432±.025	0.391±0.054	2.265±0.02	1.765±0.031	4.201	0.009	97.05	3.5	15.618±12.645	77.14±61.14
2	434.844±.026	0.296±0.045	0.757±.024	1.429±0.034	1.15	0.003	95.56	10.54	19.308±13.738	94.89±65.77
2.1	386.253±.032	0.268±0.067	0.758±.026	1.270±0.038	1.499	0.003	95.62	10.64	16.909±13.232	83.37±63.76
2.2	274.153±.031	0.183±0.106	0.689±.023	0.906±0.029	1.188	-.001	96.05	11.65	10.767±8.486	53.53±41.57
2.3	209.762±.030	0.142±0.053	0.601±.030	0.667±0.032	1.087	0	92.44	13.39	15.731±5.923	77.68±28.63
2.4	159.777±.041	0.117±0.070	0.638±.034	0.518±0.051	0.745	0.001	94.15	12.44	9.200±7.459	45.84±36.69
2.5	148.007±.033	0.110±0.078	0.888±.028	0.464±0.040	1.169	0.001	90.88	8.94	13.190±5.309	65.36±25.84
2.7	126.530±.037	0.096±0.109	0.768±.030	0.402±0.050	1.356	0.001	92.18	10.44	9.656±5.663	48.08±27.82
3	108.645±.031	0.079±0.077	0.822±.032	0.330±0.039	1.303	0	87.76	9.72	12.882±2.786	63.86±13.57
3.4	117.353±.021	0.098±0.065	1.610±.022	0.353±0.040	2.591	0.003	86.45	4.93	15.005±3.751	74.17±18.17
4	137.446±.034	0.125±0.120	2.078±.035	0.425±0.048	3.312	0.005	88.96	3.8	14.280±4.637	70.65±22.50
5	20.741±0.027	0.148±0.049	0.016±0.23	0.051±0.068	0.047	0.029	68.21	3.24	5.921±0.995	59.02±9.76
Total/Avg	**231.3±.005**	**0.159±.013**	**.781±.005**	**0.737±0.007**		**.002**		**100**	**12.481±1.410**	**67.40±6.86**
J =0.002797±0.000006										
Volume 39ArK =26.93										
Integrated Date =66.3±7.8										

Volumes are 1E-13 cm3 NPT
Neutron flux monitors: 28.02 Ma FCs (Renne et al., 1998)
Isotope production ratios: $(^{40}Ar/^{39}Ar)K=0.0302$, $(^{37}Ar/^{39}Ar)Ca=1416.4306$, $(^{36}Ar/^{39}Ar)Ca=0.3952$, $Ca/K=1.83(^{37}ArCa/^{39}ArK)$.
*=Radiogenic 40Ar

References

Bacon, C.R., Persing, J.M., Wooden, J.L. and Ireland, R.R. (2000): Late Pleistocene granodiorite beneath Crater Lake Caldera, Oregon, dated by ion microprobe; *Geology (Boulder)*, Volume 28, Pages 467-470.

Compson, W. (1999): Geologic age by instrumental analysis; the 29th Hallimond Lecture, *Mineralogical Magazine*, Volume 28, Pages 297-311.

Cumming, G.L. and Richards, J.R. (1975): Ore lead isotope ratios in a continuously changing Earth; *Earth and Planetary Science Letters*, Volume 63, Pages 155-171.

Ireland, T.R. and Williams, I.S. (2003): Considerations in zircon geochronology by SIMS; *in* Zircon, Hanchar, J. and Hoskin P. (editors); *Reviews in Mineralogy and Geochemistry*, volume 53, pages 215-241

Krogh, T.E (1982): Improved accuracy of U-Pb zircon ages by the creation of more concordant systems using an air abrasion technique; *Geochimica et Cosmochimica Acta*, Volume 46, Pages 637-649.

Ludwig, K.R. (1980): Calculation of uncertainties of U-Pb isotopic data; *Earth and Planetary Science Letters*, Volume 46, Pages 212-220.

Ludwig, K.R. (1999): ISOPLOT: A plotting ad regression program for radiogenic-isotope data; *U.S. Geological Survey Open File*, Volume 91-445, Page 41.

Ludwig, K.R. (2001): SQUID 1.00, a users manual; *Berkeley Geochronology Center*, Special Publication 2, 17 pages.

Ludwig, K.R. (2003): Isoplot 3.00 A Geochronological Toolkit for Microsoft Excel; *Berkeley Geochronology Centre*, Special Publication Number 4.

Parrish, R., Roddick, J.C., Loveridge, W.D., and Sullivan, R.W. (1987): Uranium-lead analytical techniques at the geochronology laboratory; Geological Survey of Canada. *In* Radiogenic Age and Isotopic Studies, Report 1, *Geological Survey of Canada*, Paper 87-2, Pages 3-7.

Renne, P.R., Swisher, C.C., III, Deino, A.L., Karner, D.B., Owens, T. and DePaolo, D.J. (1998): Intercalibration of standards, absolute ages and uncertainties in $^{40}Ar/^{39}Ar$ dating; *Chemical Geology*, Volume 145 (1-2), Pages 117-152.

Roddick, J.C. (1987): Generalized numerical error analysis with application to geochronology and thermodynamics; *Geochimica et Cosmochimica Acta*, Volume 51, Pages 2129-2135.

Thirlwall, M.F. (2000): Inter-laboratory and other errors in Pb isotope analyses investigated using a ^{207}Pb–^{204}Pb double spike; *Chemical Geology*, Volume 163, Pages 299–322.

Williams, I.S. (1998): U-Th-Pb geochronology by ion microprobe, *in* McKibben, M.A., Shanks, W.C., III and Ridley, W.I. (editors); Applications of micro analytical techniques to understanding mineralizing processes, Volume 7: Reviews in Economic Geology: Socorro, NM, United States, *Society of Economic Geologists*, Pages 1-35.

Appendix II: Sample Description and Locations

The following table is a compilation of field observations recorded during three field seasons in the Thorn area from 2003-2005.

Abbreviations used in table

Common
plag-plagioclase
qtz-quartz
bt-biotite
feld-feldspar
bx-breccia
frags-fragments
pyrr-pyrrhotite
moly-molybdenite
cp-chalcopyrite
aspy-arsenopyrite
py-pyrite
xtals-crystals

Textures: phenocrysts, groundmass
p-porphyritic
a-aphanitic
g-glassy
f-fine <1mm
m-medium
c-coarse >5mm
mvs-massive sulphide
semimvs-semi-massive sulphide
gr-granophyric
g-glassy
r-recrystallized
f-very fine grained

C-coherent
V=volcaniclastic

Alteration
p-propylitic
a-argyllic
aa-advanced argillic
s-silica
ser-sericite
cb-carbonate
cl-chlorite
k-potassic
calc-calc-silicate

Components
x-crystal fragments
l-lithic fragments
lv-volcanic lithic
li-intrusive lithic
p-pumice fragments
f-fiamme

Grain size
a-<2mm
b-2-10mm
c->10mm
fl-fine lapilli 2-34mm
cl-coarse lapilli 34-64mm

Lithofacies
w-welded
ff-flow foliated
fb-flow banded
ps-poorly sorted
fs-fairly sorted
ws-well sorted
ma-massive
xg-not graded
ng-normal graded
cs-clast supported
ms-matrix supported

Composition
dio-diorite
bslt-basalt
rhy-rhyolite
rhydac-rhyodacite
and-andesite
qtzmonz-quartz monzonite
monz-monzonite
grano-granodiorite

bold is for coherent rocks

Table II-1: Rock sample locations and descriptions

Sample	Loaction		Colour	Alteration		C	Texture	Lithofacies	Components/Grain Size	Comp.
	Easting	Northing		Intensity	Type	V	phenocrysts groundmass			
277501	627753	6491795	light tan	3	a-aa	c	p, c plag, qtz, bt- f		a	dio
277502	627751	6491828	buff yellow	3	a	c	p, c plag, qtz, bt- f		a	dio
277503	627751	6491828	yellow-grey	2	p	c	p, c plag, qtz, bt- f		a	dio
277504	627760	6491890	yellow	4	a-aa	c	p, c plag, qtz, bt- f		a	dio
277505	627830	6491880	yellow	3	aa	c	p, c plag, qtz, bt- f		a	dio
277506	627964	6491969	light grey	1	a-p	c	p, c plag, qtz, bt- f		a	dio
277507	627985	6492034	yellow	3	a-aa	c	p, c plag, qtz, bt- f		a	dio
277508	627985	6492034	tan grey	2	a	c	p, c plag, qtz, bt- f		a	dio
277509	627985	6492034	purple grey	1	p	c	p, c plag, qtz, bt- f		a	dio
277510	627985	6492034	grey	1	p	c	p, c plag, qtz, bt- f		a	dio
277512	628720	6492020	grey yellow	4	ser cb	v	clast supported	breccia	sulphide of Oban bx-a	
277513	628720	6492020	dark grey	4	ser cb	v	clast supported	breccia	sulphide of Oban bx-a	
277514	628513	6492161	yellow	5	aa	c	p, c plag, qtz, bt- f		a	dio
277515	628583	6492190	light grey blue	3	a	c	f	ff	c	rhy
277516	628349	6492475	light grey tan	2	a	c	p, c plag, qtz, bt- f		a	dio
277517	628349	6492475	light grey tan	2	a	c	p, c plag, qtz, bt- f		a	dio
277518	628349	6492475	light grey blue	4	a-p	c	p, c plag, qtz, bt- f		a	dio
577519	628349	6492475	light yellow	5	aa	c	p, c plag, qtz, bt- f		a	dio
277520	628349	6492475	light grey tan	3	a-aa	c	p, c plag, qtz, bt- f		a	dio
277521	628349	6492475	grey blue	2	p-a	c	p, c plag, qtz, bt- f		xe (mafic) – a	dio
277522	628349	6492475	grey brown	1	p	c	p, a, f		b	bslt
277523	628349	6492475	grey	2	p-a	c	p, c plag, qtz, bt- f		a	dio
277524	628349	6492475	grey purple	5	aa		mvs		I zone vein	
277525	628680	6492027	light grey	2	p	v	clast supported	breccia	Oban bx-a	
277526	628680	6492027	light grey	2	p	v	clast supported	breccia	Oban bx-a	
277527	628680	6492027	light grey	3	p	v	clast supported	breccia	Oban bx-a	
277528	628680	6492027	light grey	3	p	v	clast supported	breccia	Oban bx-a	
277529	628680	6492027	light grey	2	p	v	clast supported	breccia	Oban bx-a	
277530	628680	6492027	light grey	3	p	v	clast supported	breccia	Oban bx-a	
277531	628680	6492027	light grey	2	p	v	clast supported	breccia	Oban bx-a	
277532	628680	6492027	grey brown	1	p	c	p, f		b	bslt
277533	628680	6492027	yellow	4	ser cb	v	clast supported	breccia	sulphide of Oban bx-a	
277534	628680	6492027	buff tan	4	ser cb	v	clast supported	breccia	sulphide of Oban bx-a	
277535	628680	6492027	buff tan	4	ser cb	v	clast supported	breccia	sulphide of Oban bx-a	
277536	627577	6491891	grey green	2	ser cb cl	v	c bslt fragments - f	ms	lv - a	bslt
277537	627594	6491669	yellow	5	aa	c	p, f plag, qtz, bt - f	ff	a	dio
277538	627594	6491669	yellow	5	aa	c	p, f plag, qtz, bt- f	ff	a	dio
Tamdhu	627639	6491605	dark purple	5	aa		mvs		Tamdhu vein	
277539	627754	6491562	dark purple	5	aa		mvs		D-zone vein	
277540	628077	6491148	grey green	2	p	c	p, f plag, qtz, bt- f		a	dio
277541	628077	6491148	grey green	2	p	c	p, f plag, qtz, bt- f		a	dio
277542	628467	6492069	grey tan	3	a	c	p, f plag, qtz, bt- f		a	dio
277543	628362	6492009	dark purple	5	aa		mvs		F zone vein	

Sample	Loaction		Colour	Alteration		C	Texture	Lithofacies	Components/Grain Size	Comp.
	Easting	Northing		Intensity	Type	V	phenocrysts groundmass			
277544	628353	6492005	light grey tan	3	ser, cb	v	clast supported	breccia	Matrix of Oban bx	
277703a	628319	6491969	dark purple	5	aa	c	mvs		Glenlivet vein	
277703b	628319	6491969	yellow	5	aa	c	p, f plag, qtz, bt- f		a	dio
277703c	628319	6491969	yellow	5	a-aa	c	p, f plag, qtz, bt- f		a	dio
277703d	628319	6491969	pale yellow	5	s-aa	c	p, f plag, qtz, bt- f		a	dio
Glen	628319	6491969	dark purple	5	aa	c	mvs		Glenlivet vein	
AS-016a	628107	6493724	light grey	2	p	v	p, m, qtz, feldspar - f	fb		rhy
AS-017a	628245	6493850	light grey	1	p	v	c, rhy frags - f	ps	x = feld, lv	rhydac
AS-017b	628285	6493793	grey green	2	p	c	p = feld - f		c	dac
AS-018a	628365	6493855	dark green	1	p	c	a		c	bslt
AS-018b	628424	6493873	grey green	1	p	v	c, rhy frags - f	w, ps	x = feld, lv, f	dac
AS-020a	628581	6493708	dark grey	1	p	c	p = feld - f		c	dac
AS-021a	628733	6492108	light grey	3	a-p	c	a	fb	c	rhy
277546	628733	6492108	light grey	3	a-p	c	a	fb	c	rhy
AS-021b	628602	6491639	light grey	3	ser, cb, cl	v	clast supported	breccia	Matrix of Oban bx	
AS-022a	628720	6492073	tan	4	ser, cb	v	clast supported	breccia	Matrix of Oban bx	
AS-023a	628624	6491945	tan, yellow	4	ser	v	clast supported	breccia	Matrix of Oban bx	
AS-024a	628696	6491952	dark green	1	p	c	a		c	bslt
277547	628696	6491952	dark green	1	p	c	a		c	bslt
AS-025a	627740	6491624	dark purple	5	aa	c	mvs		D-zone vein	
277548	627740	6491624	dark purple	5	aa	c	mvs		D-zone vein	
AS-026a	637872	6491599	light yellow	5	aa	c	p, f plag, qtz, bt- f		a	dio
AS-028a	628688	6490701	pink	1	cb		marble in shear zone			
AS-028b	628688	6490701	white	4	s		quartz barite vein			
AS-031a	628581	6490763	dark green	2	ser, cl	v	m = fragments - f	ws, ng, cs	lv, ls – c	bslt
AS-032a	628362	6492505	pale yellow	4	a-aa	c	p, f plag, qtz, bt- f		a	dio
AS-033a	628380	6492616	grey green	4	a	v	c angular frags -r	ps	lv, a	and
AS-034a	628359	6492680	green	4	p-a	v	c angular frags -r	ps	x = plag, lv, a	and
AS-035a	628407	6492888	light grey	1	p	v	c- f	w, ps, ms	p, f	dac
277549	628407	6492888	light grey	1	p	v	c- f	w, ps, ms	p, f, fl	dac
AS-041a	629355	6491678	light grey	1	p	v	c lithic frags- f	w, ps, ms	lv, p, f, cl	dac
AS-042a	629556	6491573	dark green	1	p	c	a		c	bslt
AS-043a	628686	6492093	tan, yellow	4	ser	v	clast supported	breccia	pyrite in Oban bx	
AS-044a	628663	6492235	dark purple	5	aa	c	mvs		F zone vein	
AS-044b	628661	6492206	dark purple	5	aa	c	mvs		Jim Beam vein	
AS-045a	631757	6495262	grey tan	2	ser-p	v	f = feld - f	fs, ms	lc, li, fl	dac
AS-049a	631000	6495421	dark grey	1	p	v	c - f	xg, ps	al	?and?
AS-049b	631000	6495421	tan	2	p	v	f = feld - f	ng, ws	lc, li, fl	dac
AS-050a	630357	6495179	blue grey	1	p	v	c lithic frags- f	w, ps, ms	lv, p, f, cl	and-dac
AS-051a	630182	6495105	grey	1	p	v	c - f	w, ps, ms	p, f, lv, cl	dac
AS-052a	630152	6494655	light grey	2	p	c	a	fb	c	rhy
AS-054a	632308	6494226	light grey	4	p-a	c	a	fb	c	rhy
AS-055a	632225	6494027	grey	2	p	v	c = lithic frags - f	ma, ms	lv	and-dac
AS-056a	631946	6493800	light grey	1	p	c	p = qtz - f			rhy

Sample	Loaction		Colour	Alteration		C	Texture	Lithofacies	Components/Grain Size	Comp.
	Easting	Northing		Intensity	Type	V	phenocrysts groundmass			
AS-058a	632265	6493649	light grey	3	ser	c	a	fb	c	dac
AS-060a	632438	6493721	grey yellow	2	p-a	c	p, c plag, qtz, bt- f		a	dio
AS-TAL-01	632922	6492675	pale pink	4	k	c	p, m plag, bt- f		a, w/ moly veins	qtzmonz
AS-TAL-01	632922	6492675	pale pink	4	k	c	p, m plag, bt- f		a	qtzmonz
ASMOR-01	632662	6492956	white & grey	2	s	v	g, f	ws	ash	rhy
AS-061a	632839	6493958	grey	3	p-a	c	p, c plag, qtz, bt- f		a	dio
AS-061b	632839	6493958	grey	3	p, cb	c	p, c plag, qtz, bt- f		a	dio
AS-062a	632514	6494108	dark grey	3	s	v	c feld xtals, f, g	ps, xg, ms	x=feld, ash	?rhy?
AS-062b	632571	6494103	light grey pink	3	k, s	v	c feld xtals, f, g	ps, xg, ms	x=feld, ash	rhy
AS-063a	632016	6492722	pale pink	4	k	c	p, m plag, bt- f		a, w/ moly veins	qtzmonz
AS-063b	632016	6492722	pink	5	k	c	p, m plag, bt- f		a	qtzmonz
AS-063c	632016	6492722	pink	5	k	c	p, m plag, bt- f		a, w/ moly veins	qtzmonz
AS-064a	632105	6492695	grey green	1	p	c	gr, c		a	grano
AS-065a	632750	6493272	pale pink	3	k	c	p, c plag, bt- f		a	qtzmonz
AS-066a	631396	6491856	grey green	1	p	c	gr, c		a	grano
AS-067a	633081	6492544	dark grey	3	s, p	v	f,?r?	ps, xg	ash	dac
AS-067b	633081	6492544	grey yellow	2	p-a	c	p, c plag, qtz, bt- f		a	dio
AS-068a	633215	6492585	dark green	1	p	c	a		c	bslt
AS-068b	633215	6492585	grey green	3	p-s	c	gr, c		a	grano
AS-068c	633215	6492585	white	5	s				cb, qtz, cp, aspy vein	
AS-068d	633215	6492585	white	5	s				cb, qtz, cp, aspy vein	
AS-068e	633215	6492585	grey green	1	p	c	gr, c		a	grano
AS-068f	633215	6492585	white	5	s				cb, qtz, cp, aspy vein	
AS-070a	632611	6489824	dark green	2	cb, p	v	a, f	ma	X = plag	and
AS-070b	632611	6489824	light red	5	s				cb, qtz, py vein	
AS-071a	632543	6490270	light grey	4	ser, s	c	a	fb		rhydac
AS-071b	632543	6490270	pink grey	2	calc	v	c- round clasts - f	ws, wg, cs	lv	and
AS-071c	632543	6490270	pink grey	2	calc	v	c- round clasts - f	ws, wg, cs	lv, w/qtz, py veins	and
AS-071d	632543	6490270	pink grey	3	s, calc	v	f - f	wg	lv	and
ASFloat-01	632491	6490197	pink grey	1	s	v	c- round clasts - f	ws, wg, cs	lv	and
AS-072a	632920	6490402	light grey	2	s	v	a	ff		?rhy?
AS-TAL-02	633008	6490905	light grey pink	2	calc		r=coarse calcite			limestone
AS-075a	632498	6489769	dark green	2	cb	v	a, f	ma	X = plag	and
AS-078a	632226	6489894	dark green	4	cb	v	a, f	ma	X = plag	and
AS-078b	632226	6489894	light red	5	s				cb, qtz, cp vein	
AS-078c	632226	6489894	light red	5	s		open space		cb, qtz, cp vein	
AS-078d	632226	6489894	light red	5	s		open space		cb, qtz, cp vein	
AS-078e	632226	6489894	light red	5	s		sheeted		cb, qtz, cp vein	
AS-078f	632226	6489894	light red	5	s		open space		cb, qtz, cp vein	
277052	632226	6489894	light red	5	s		open space		cb, qtz, cp vein	
AS-079a	632226	6490126	pink grey	4	s, calc	v	f, semimvs - f	wg	lv, py, pyrr, cp	and
277053	632226	6490126	pink grey	4	s, calc	v	f, semimvs - f	wg	lv, py, pyrr, cp	and
AS-080a	632136	6490269	pink grey	3	s, calc	v	f - f	ms, wg	lv	and
AS-082a	632948	6490277	light grey	4	ser, s	c	a	fb		rhydac

Sample	Loaction		Colour	Alteration		C	Texture	Lithofacies	Components/Grain Size	Comp.
	Easting	Northing		Intensity	Type	V	phenocrysts groundmass			
AS-083a	633019	6490604	light grey pink	2	calc		r=coarse calcite			limestone
277054	633019	6490604	light grey pink	2	calc		r=coarse calcite			limestone
AS-085a	632866	6491084	light grey pink	5	calc		r=coarse calcite			limestone
AS-086a	632794	6491030	grey green	1	p	c	gr, c		a	grano
AS-088a	632387	6490483	pink grey	2	s, calc	v	f - f	ms, wg	lv	and
AS-090a	631986	6490270	white	5	s				qtz, aspy vein	
AS-091a	631908	6490293	pink grey	3	s, calc	v	f - f	ms, wg	Lv	and
AS-092a	631532	6490426	grey green	3	p-ser	c	gr, c		A	grano
AS-092b	631532	6490426	pink grey	4	s, calc	v	f, semimvs - f	wg	lv, py, pyyh, cp	and
AS-092c	631532	6490426	dark grey	4	s, calc	v	f, semimvs - f	wg	lv, py, pyyh, cp	and
AS-094a	630430	6490800	light grey pink	5	calc		r=coarse calcite			limestone
AS-098a	629527	6492169	white	5	s-cb				cb, qtz, cp, aspy vein	
AS-099a	629252	6491922	light grey	2	p	v	p, m, qtz, feldspar - f	fb		rhy
AS-104a	631157	6492900	grey	4	s	v	a, f	ma	x = plag	and-dac
AS-105a	631157	6492900	grey	4	s	v	a, f	ma	x = plag, w/ moly vein	and-dac
AS-106a	631025	6493471	light grey	2	p	v	p, m, qtz, feldspar - f	fb	w/ moly veins	rhy
AS-107a	631316	6493092	grey pink	2	k	c	p, m plag, bt- f		a	qtzmonz
AS-107b	631281	6493143	pink	5	k	c	p, m plag, bt- f		a	qtzmonz
04AS009	627160	6493530	dark grey	2	p-ser	v	g, f	w, ps	x=plag, l, p, f	dac-and
4AS11	612037	6506538	grey	1	p	c	p, c plag, qtz- f		a	dio
4AS12	610885	6506221	buff grey	2	p	c	p, c plag, qtz, bt- f		a	dio
4AS19	622970	6506461	grey	1	p	c	p, c plag, qtz- f		a	dio
4AS25	619202	6500184	grey	1	p	c	p, c plag, qtz- f		a	monz
THN03-22	628769	6491914	grey yellow	5	ser	v	clast supported	breccia	sulphide of Oban bx-a	
04AS03	627980	6491570	light grey	2	p-a	c	p, m plag, bt- f		a	qtzmonz
Cirque	631347	6491915	grey pink	2	k	c	p, m plag, bt- f		a	qtzmonz
Oban	628741	6491915	grey yellow	5	ser	v	clast supported	breccia	sulphide of Oban bx-a	
4AS13	611490	6506410	light grey	2	ser	v	c - g, f	ps, ma, ms	x=qtz, feld, p	dac-rhy

Appendix III: Geochemistry Analytical Methods

Collection, Crushing and Analytical Methods

Twenty-seven intrusive rock samples (2 from Jurassic rocks, 18 from Cretaceous rocks and 7 from Palaeogene rocks) and 18 volcanic rock samples (4 from Triassic rocks and 14 from Cretaceous rocks) from the Thorn area were collected during property and regional mapping and from drill core for geochemical analysis. All samples are from outcrops and where possible the least altered samples were collected. Results of these data are presented in Table 2-3 above.

Samples were prepared for processing by cutting away weathered edges with a diamond embedded saw and were sent to ALS-Chemex Laboratory Services Ltd. in North Vancouver, Canada. The samples were then crushed and pulverized to approximately 150 mesh in tungsten-carbide. Tantalum contamination during tungsten-carbide crushing is problematic and therefore all samples processed by this method likely have excess Ta. Thus all Ta values are viewed suspect and were not used in geochemical analysis. In addition, because of the tungsten-carbide grinding media, tungsten and cobalt may have been carried over to the samples. Typical ranges of contamination for granite range between 30 and 300 ppm for tungsten and between 10 and 30 ppm for cobalt (www.alschemex.com).

All samples were analyzed for major, trace and rare earth-element abundances. Major element analyses were determined on fused disks by X-ray fluorescence (XRF). Reposted Fe_2O_3 (T) is a measure of the total iron in the sample assuming all iron is ferric. Ferrous iron (FeO) was determined by Wilson Titration method. Trace and rare-earth elements were prepared by dissolving the rock powders in nitric, perchloric and/or hydrofluoric acids, followed by lithium metaborate fusion. The solutions were then analyzed by inductively coupled plasma mass-spectrometry (ICP-MS). Detection limits for major, trace and rare-earth elements are listed in Table III-1.

Duplicates and Standards

Duplicate analysis for MDRU reference samples PA-1 (Granodiorite from the Coast Plutonic Complex), MBX-1 (the MBX pluton from the Central Interior B.C.) and WP-1 (Watts Point Dacite from the Coast Plutonic Complex) were submitted as unknowns to test for analytical precisions and accuracy. Duplicate analyses of these samples are precise and are within three standard deviations of the mean values from previous analyzes (Table III-2).

Table III-1: Detection limits for major, trace and rare-earth elements at ALS-Chemex Labs.

Element	Method	Lower Limit (ppm)	Upper Limit (ppm)
Ag	ICP-MS	1	1000
Ba	ICP-MS	0.5	10000
Ce	ICP-MS	0.5	10000
Co	ICP-MS	0.5	10000
Cr	ICP-MS	10	10000
Cs	ICP-MS	0.1	10000
Cu	ICP-MS	5	10000
Dy	ICP-MS	0.1	1000
Er	ICP-MS	0.1	1000
Eu	ICP-MS	0.1	1000
Ga	ICP-MS	1	1000
Gd	ICP-MS	0.1	1000
Hf	ICP-MS	1	1000
Ho	ICP-MS	0.1	10000
La	ICP-MS	0.5	1000
Lu	ICP-MS	0.1	10000
Mo	ICP-MS	2	1000
Nb	ICP-MS	1	10000
Nd	ICP-MS	0.5	10000
Ni	ICP-MS	5	10000
Pb	ICP-MS	5	10000
Pr	ICP-MS	0.1	10000
Rb	ICP-MS	0.2	1000
Sm	ICP-MS	0.1	10000
Sn	ICP-MS	1	1000
Sr	ICP-MS	0.1	10000
Ta	ICP-MS	0.5	10000
Tb	ICP-MS	0.1	1000
Th	ICP-MS	1	1000
Tl	ICP-MS	0.5	1000
Tm	ICP-MS	0.1	1000
U	ICP-MS	0.5	1000
V	ICP-MS	5	10000
W	ICP-MS	1	10000
Y	ICP-MS	0.5	1000
Yb	ICP-MS	0.1	1000
Zn	ICP-MS	5	10000
Zr	ICP-MS	0.5	10000

Element	Method	Lower Limit (%)	Upper Limit (%)
Al	XRF	0.01	100
Ba	XRF	0.01	100
Ca	XRF	0.01	100
Cr	XRF	0.01	100
Fe (T)	XRF	0.01	100
K	XRF	0.01	100
Mg	XRF	0.01	100
Mn	XRF	0.01	100
Na	XRF	0.01	100
P	XRF	0.01	100
Si	XRF	0.01	100
Sr	XRF	0.01	100
Ti	XRF	0.01	100
LOI	XRF	0.01	100
FeO	titration	0.01	100

Table III-2: Mean values and duplicate analyses of standards P1, MBX-1 and WP-1.

	P1 (n=5)* *mean*	std deviation	P1-A	P1-B	MBX-1 (n=20)* *mean*	std deviation	MBX-1-A	MBX-1-B
Major element oxides (wt. %)								
SiO_2	70.96	0.17	70.61	70.2	57.80	0.54	57.93	57.4
TiO_2	0.38	0.00	0.40	0.37	0.50	0.02	0.49	0.47
Al_2O_3	14.10	0.06	14.27	14.10	17.60	0.24	17.28	17.15
Fe_2O_3T	3.90	0.00	3.79	3.71	4.00	0.05	3.84	3.84
FeO	2.34	0.08	2.25	-	1.90	0.06	2.06	-
MnO	0.08	0.00	0.08	0.07	0.08	0.00	0.07	0.06
MgO	1.11	0.01	1.04	1.08	2.06	0.04	1.99	2.09
CaO	3.49	0.02	3.44	3.41	3.82	0.07	3.69	3.69
Na_2O	3.80	0.00	3.59	3.78	5.19	0.10	4.82	5.16
K_2O	2.12	0.01	2.00	2.02	4.64	0.18	4.67	4.68
P_2O_5	0.08	0.00	0.08	0.07	0.25	0.00	0.23	0.24
TOTAL	100.56	0.22	99.85	99.5	99.49	0.77	98.72	98.8
Trace and rare earth element concentrations (ppm)								
Ag	0.30	0.00	<1	<1	-	-	<1	<1
Ba	724.00	8.00	745	811	789.91	61.21	701	790
Ce	28.00	1.26	25.2	24.1	26.23	2.16	24.1	25.9
Co	6.20	0.40	6.8	8	7.13	2.05	6.3	8.2
Cs	1.22	0.10	1.1	1.3	2.90	0.67	2.5	2.7
Cu	15.50	5.50	7	12	361.39	51.25	364	460
Dy	3.30	0.15	3.0	3	-	-	2.3	2.7
Er	2.10	0.09	2.0	2	-	-	1.5	1.6
Eu	0.80	0.03	0.7	0.7	0.88	0.15	0.7	0.9
Ga	15.00	1.10	14	16	-	-	19	22
Gd	3.10	0.10	2.8	3	-	-	2.4	2.7
Hf	3.76	0.14	4	4	2.36	0.40	2	2
Ho	0.70	0.04	0.6	0.7	-	-	0.5	0.5
La	13.20	0.40	13.0	13.6	14.26	1.00	13.4	14.2
Lu	0.40	0.01	0.4	0.3	0.23	0.03	0.3	0.2
Nb	3.78	0.17	3	4	-	-	9	11
Nd	13.00	0.63	11.5	13	11.74	1.43	11.1	11.6
Ni	-	-	7	11	11.38	2.55	10	13
Pb	10.20	1.47	11	11	1.30	0.82	6	5
Pr	3.40	0.10	2.9	2.9	-	-	2.7	2.7
Rb	50.40	3.14	45.2	52.1	78.00	2.55	79.7	88.3
Sm	2.90	0.12	2.6	2.5	2.37	0.41	2.2	2.6
Sn	2.44	0.88	2	2	-	-	1	2
Sr	256.00	4.90	220	238	513.00	68.90	498	532
Ta	0.30	0.01	<0.5	<0.5	0.57	0.18	0.5	0.6
Tb	0.50	0.02	0.5	0.5	0.28	0.10	0.4	0.4
Th	4.38	0.21	4	5	2.86	0.22	3	4
Tl	0.31	0.02	<0.5	<0.5	-	-	<0.5	<0.5
Tm	0.40	0.01	0.3	0.3	-	-	0.2	0.2
U	1.48	0.07	1.4	1.4	0.71	0.17	0.6	0.7
V	58.20	0.40	61	69	169.18	14.43	172	196
Y	22.80	0.75	19.0	21.2	11.75	5.99	14.2	16.2
Yb	2.50	0.15	2.1	2.1	1.46	0.24	1.5	1.6
Zn	44.00	0.89	41	42	35.98	7.20	28	30
Zr	126.00	10.20	122.0	123.5	108.4	14.07	79.7	81.3

P1 and MBX-1 are MDRU reference materials

Mean values of P1 and MBX-1 are based on the average of 5 and 20 previous repeat analyses, respectively

A and B are duplicate analyses of the standards that were analysed to test for precision

Table III-2: Continued

	WP-1 (n=5)* *mean*	std deviation	WP-1-A	WP-1-B
Majors (wt. %)				
SiO_2	65.06	0.12	64.54	64.5
TiO_2	0.50	0.00	0.51	0.49
Al_2O_3	16.38	0.10	16.63	16.40
Fe_2O_3T	4.52	0.04	4.43	4.35
FeO	2.56	0.10	2.57	-
MnO	0.08	0.00	0.09	0.07
MgO	2.70	0.01	2.62	2.72
CaO	5.05	0.02	5.02	4.93
Na_2O	4.30	0.00	4.02	4.29
K_2O	1.64	0.01	1.54	1.56
P_2O_5	0.18	0.00	0.17	0.17
TOTAL	100.62	0.20	99.88	99.9
Trace and rare earth elements (ppm)				
Ag	0.15	0.05	<1	<1
Ba	582.00	23.15	608	661
Ce	28.25	0.50	28.3	31.8
Co	11.80	0.98	12.2	14.4
Cs	0.45	0.01	0.4	0.5
Cu	16.20	0.98	14	19
Dy	2.43	0.05	2.3	2.4
Er	1.33	0.05	1.3	1.4
Eu	0.92	0.02	0.8	0.9
Ga	19.00	0.89	18	20
Gd	2.98	0.10	2.7	2.9
Hf	3.32	0.16	3	3
Ho	0.49	0.01	0.5	0.5
La	13.25	0.50	14.2	13.9
Lu	0.23	0.01	0.2	0.2
Nb	4.04	0.14	4	4
Nd	15.00	0.00	14.3	14.9
Ni	44.80	1.17	45	58
Pb	7.20	0.40	8	10
Pr	3.68	0.10	3.5	3.3
Rb	23.00	0.63	21.7	23.5
Sm	3.30	0.08	3.0	3
Sn	1.58	0.37	2	2
Sr	724.00	4.90	715	742
Ta	0.22	0.01	<0.5	<0.5
Tb	0.44	0.02	0.4	0.4
Th	2.08	0.07	2	2
Tl	0.15	0.01	<0.5	<0.5
Tm	0.21	0.01	0.2	0.2
U	0.83	0.04	0.8	0.8
V	82.40	1.36	90	100
Y	15.20	0.75	13.0	14.2
Yb	1.45	0.06	1.2	1.3
Zn	58.60	1.36	54	56
Zr	112.00	4.00	110.5	107

WP-1 is an MDRU standard
Mean value of WP-1 is based on the average of 5 previous repeat analyses
A and B are duplicate analyses of the standards that were analysed to test for precision

Appendix IV: Geological Fieldwork Publications

LATE CRETACEOUS VOLCANO-PLUTONIC ARCS IN NORTHWESTERN BRITISH COLUMBIA: IMPLICATIONS FOR PORPHYRY AND EPITHERMAL DEPOSITS

A.T. Simmons[1], R.M. Tosdal[1], Baker, D.E.L.[2], R.M. Friedman[1] and T.D. Ullrich[1]

KEYWORDS: *Epithermal Deposits, Volcanic Rocks, Plutonic Rocks, Late Cretaceous, Tulsequah area, Thorn Property area, Regional Geology, Windy Table Suite Magmatic Rocks, Rocks to Riches Program*

INTRODUCTION

Porphyry Cu and epithermal deposits are spatially and temporally related to specific volcanic and plutonic rocks emplaced during the formation of long-lived magmatic arcs formed along convergent plate boundaries (e.g. Sillitoe, 1972, 1997; Sutherland-Brown, 1976; Titley, 1982; Sawkins, 1990; Bissig et al. 2003). Recognizing the presence, types of deposits, and age of the mineralized volcanoplutonic complexes in under-explored terranes is an important step toward identifying the metallogenic potential of a terrane as a means to aid exploration. Historically in British Columbia, porphyry Cu deposits have dominated exploration and mining actively (e.g. Highland Valley, Gibraltar, Afton, Copper Mountain, Galore Creek) In contrast, epithermal deposits have until recently (e.g. Toodoggone district deposits) remained largely underexplored because of their low preservation potential coupled with the Mesozoic age of most of the convergent margin arcs in the western Canadian Cordillera. For example, the known porphyry Cu and several epithermal deposits in British Columbia are associated with Jurassic arcs, with the Cretaceous arc seemingly of less interest from a metallogenic viewpoint.

The Cretaceous arc in British Columbia is represented prinicipally by the Coast Plutonic belt located along the west coast and in adjacent Alaska. It can be divided into a series of magmatic belts with no obvious time-space distribution based on current data (Brew and Morell, 1983; Barker et al. 1986). In northern BC in the Taku River area, however, work by the British Columbia Geological Survey identified a series of Late Cretaceous volcanic and subvolcanic plutonic rocks that form a belt on the eastern margin of the Coast Plutonic Belt where it intrudes the Stikine Terrane (e.g. Mihalynuk 1999). This belt extends from at least the Golden Bear Mine (Oliver, 1996) in the southeast to the Surprise Lake Batholith in the northwest (Mihalynuk 1999). The known or inferred Late Cretaceous volcanoplutonic complexes are varying eroded, are spaced 10 to 20 kms apart, and have associated hydrothermally altered rocks (Souther, 1971; Mihalynuk, 1999; Simmons et al., 2003). Porphyry Cu-Mo, Au-Ag-Cu veins, breccia-hosted Ag-Au-Pb-Zn, and Zn skarn are recognized.

In 2003 a research project was initiated by the Mineral Deposit Research Unit (MDRU) at the University of British Columbia (UBC) to investigate Late Cretaceous volcanoplutonic complexes in the Taku River area of the Stikine Terrane, northwestern B.C. A goal of the project sought to evaluate the mineralization potential along the belt, with emphasis placed upon epithermal types of deposit because of their high value and low tonnage. Work reported herein is drawn on fieldwork in 2004 and data from a M.Sc. thesis at UBC by Adam Simmons on the Thorn Property, which is located within the Late Cretaceous volcanoplutonic belt. Particular emphasis is placed on presenting the timing and known or inferred relationships between mineralizing types and magmatic rocks. The goal is to establish a framework from which better exploration strategies in northern BC can be developed. Funding for the project derives in part from the Rocks to Riches program, which is administered by the BC and Yukon Chamber of Mines, and from the Natural Sciences and Engineering Research Council of Canada (NSERC) through an Industrial Post-Gradute Fellowship to Adam Simmons and a Discovery Grant to Richard Tosdal. [2]

Fieldwork in the 2004 field season had two main goals. Firstly, regional mapping was carried out in the Taku River area aimed at refining the current understanding of Late Cretaceous magmatic rocks in this region, defining the magmatic evolution and investigating the geological setting of mineralization associated with these magmatic rocks. Approximately 7 weeks of mapping and sampling was carried out over an area from the Thorn Property

[1]-MINERAL DEPOSIT RESEARCH UNIT (MDRU), DEPARTMENT OF EARTH AND OCEAN SCIENCES, THE UNIVERSITY OF BRITISH COLUMBIA, VANCOUVER, B.C.

[2] EQUITY ENGINEERING LTD., VANCOUVER, B.C.

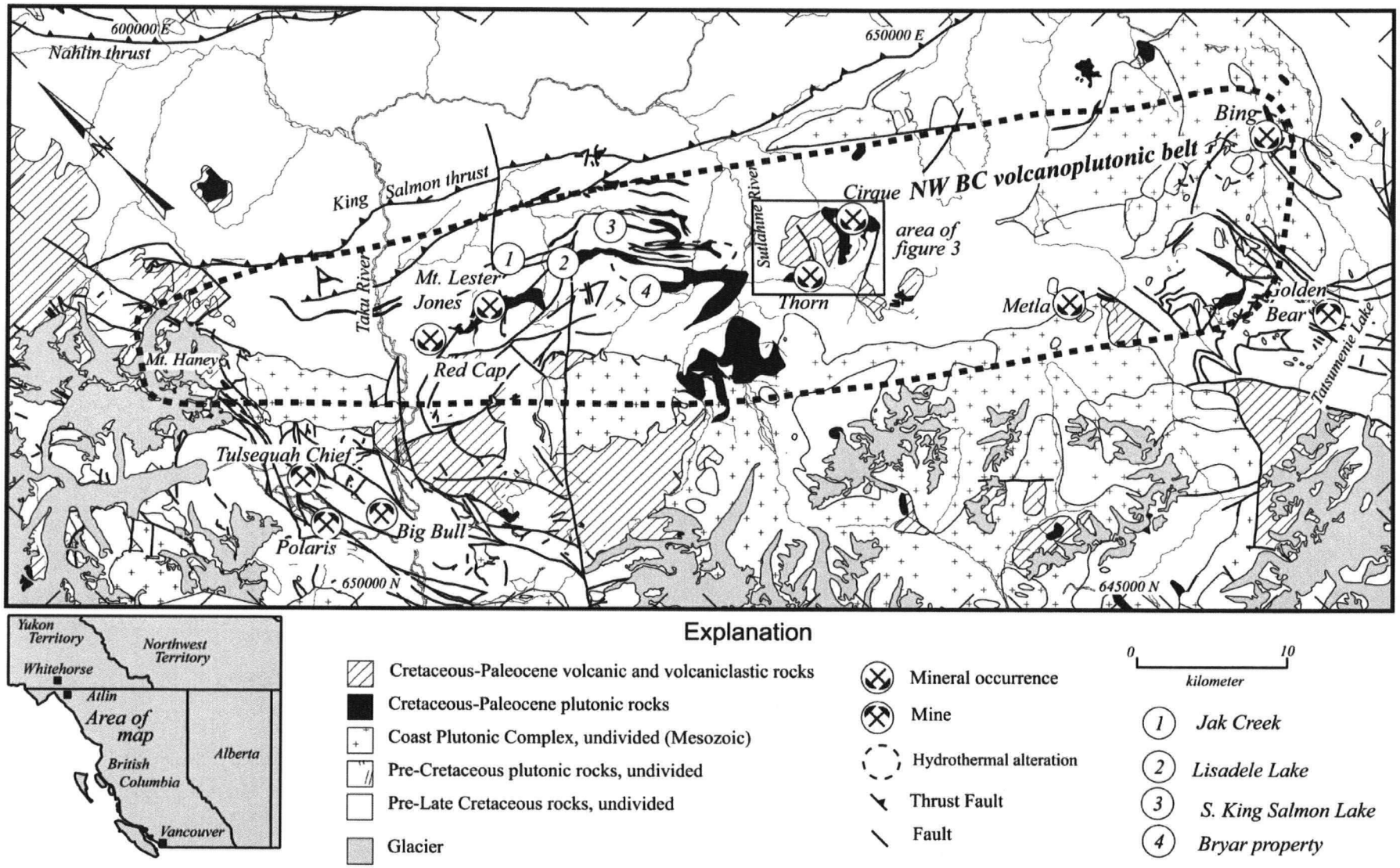

Figure 1. Simplified geologic map of Cretaceous belt of volcanoplutonic complexes and associated hydrothermal system. Belt stretches from Mount Haney in the northwest to perhaps the Bing property near the Golden Bear mine in the southeast. Note that map is tilted 45° to northwest. Base geology from the British Columbia Department of Energy and Mines (http://www.em.gov.bc.ca/MIning/Geolsurv/Publications/catalog/bcgeolmap.htm#2003-17) with location of mines and prospects from Souther (1981) and Minfile.

in the southeast to Mount Lester Jones in the northeast. Secondly, a regional investigation of mineralized occurrences along this belt aimed to define their petrogenesis, timing history and fluid chemistry. The goals are to establish source of fluids for the mineralizing types and linking them to particular magmatic events along the belt. Effort was devoted to determining their relative timing in the field, and collecting samples for absolute timing relationships using U-Pb and $^{40}Ar/^{39}Ar$ geochronology. Approximately 12 days was devoted to the regional reconnaissance study. Preliminary results this study are presented herein.

2004 FIELD MAPPING STUDIES IN THE TAKU RIVER AREA

During the 2004 field season, mapping in the Taku River area was concentrated on five areas between the Thorn Property and the Taku River (Figure 1). These areas were selected based on mineral potential as inferred from Regional Geochemical Survey data and favourable geology interpreted from the geologic map of Souther (1971) and publicly available assessment reports. Rocks in the study area are variably deformed Triassic and Jurassic volcanic and clastic sedimentary rocks, which have been intruded by granitic rocks and overlain by dacitic rocks. The igneous rocks range in age from 168Ma to 55Ma (Table 1). The spatial and temporal distribution of the magmatic rocks are not well understood, however the majority of the magmatic rocks located in the volcanoplutonic belt are constrained between the ages of 93Ma and 81Ma (Mihalynuk et al. 2003; this study).

Pre-Cretaceous Stikine Terrane Supracrustal Rocks

Mapping during the 2004 field season identified three dominant rock units of the Stikine volcanic arc in the Taku River area. These are the Upper Triassic Stuhini Group volcanic and sedimentary rocks including the Upper Triassic Sinwa Formation sedimentary rocks. The Lower to Middle Jurassic clastic sedimentary rocks of Laberge Group unconformably overlie the Triassic rocks (Figure 2). All sedimentary rocks are weakly to strongly altered and variably deformed. Alteration is limited to rocks adjacent to younger magmatic rocks. North-northwest verging, open to close folds and post-accretionary normal faults deform the sedimentary rocks. These rocks are only briefly described below.

STUHINI GROUP

Stuhini Group strata form a northwesterly trending belt from the Golden Bear Mine area to the Tulsequah area where the strata were named by Kerr (1948) after Stuhini Creek. These strata continue to the north through the Tagish Lake area (Mihalynuk, 1999) and are correlative to the Lewis River Group further north (Wheeler, 1961 and Hart et al. 1989).

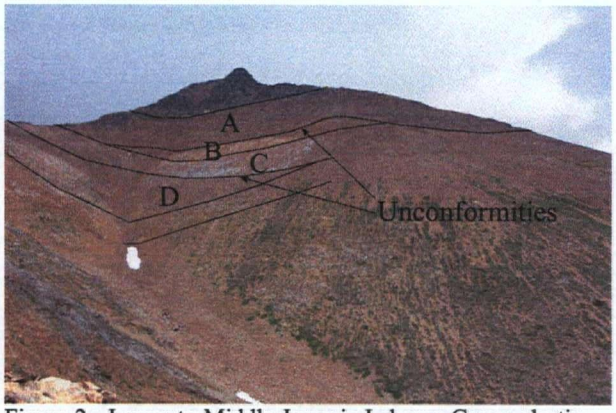

Figure 2. Lower to Middle Jurassic Laberge Group clastic sedimentary rocks (A) unconformably overlie Upper Triassic Sinwa Formation clastic sedimentary rocks (B) and limestone (C), which unconformably overlie Stuhini Group clastic sedimentary rocks at the Thorn Property.

A wide range of rock types including basic to intermediate subalkaline flows, pyroclastic rocks and related sedimentary rocks characterize the Stuhini Group (Mihalynuk 1999). The Stuhini Group may be divided in the study area into a sequence dominated by sub-marine volcanic rocks and a sequence dominated by clastic sedimentary rocks and lesser carbonate rocks. Near the Thorn Property (Figure 3), submarine mafic volcanic strata are overlain by sedimentary strata (Simmons, 2003; Baker, 2003) and are similar to the section described by Mihalynuk (1999) at Willison Bay. However, north of the Thorn Property, in the Mt. Lester Jones area, this subdivision is not evident. Mihalynuk (1999) attributes the lack of stratigraphic continuation to major lateral facies variations, deposition on surfaces with major paleotopographic relief, and disruption by later faults.

SINWA FORMATION

The Sinwa Formation is considered to be the top of the Stuhini Group. The strata can be traced discontinuously throughout the map area (Souther, 1971), and serves as a local marker horizon between the upper Triassic Stuhini Group strata and lower to middle Jurassic Laberge Group. Where exposed, Sinwa Formation ranges in thickness from 5-20m and unconformably overlies Stuhini Group clastic sedimentary rocks (Figure 2). To the north, in the Tagish Lake area, Mihalynuk (1995a, b) did not

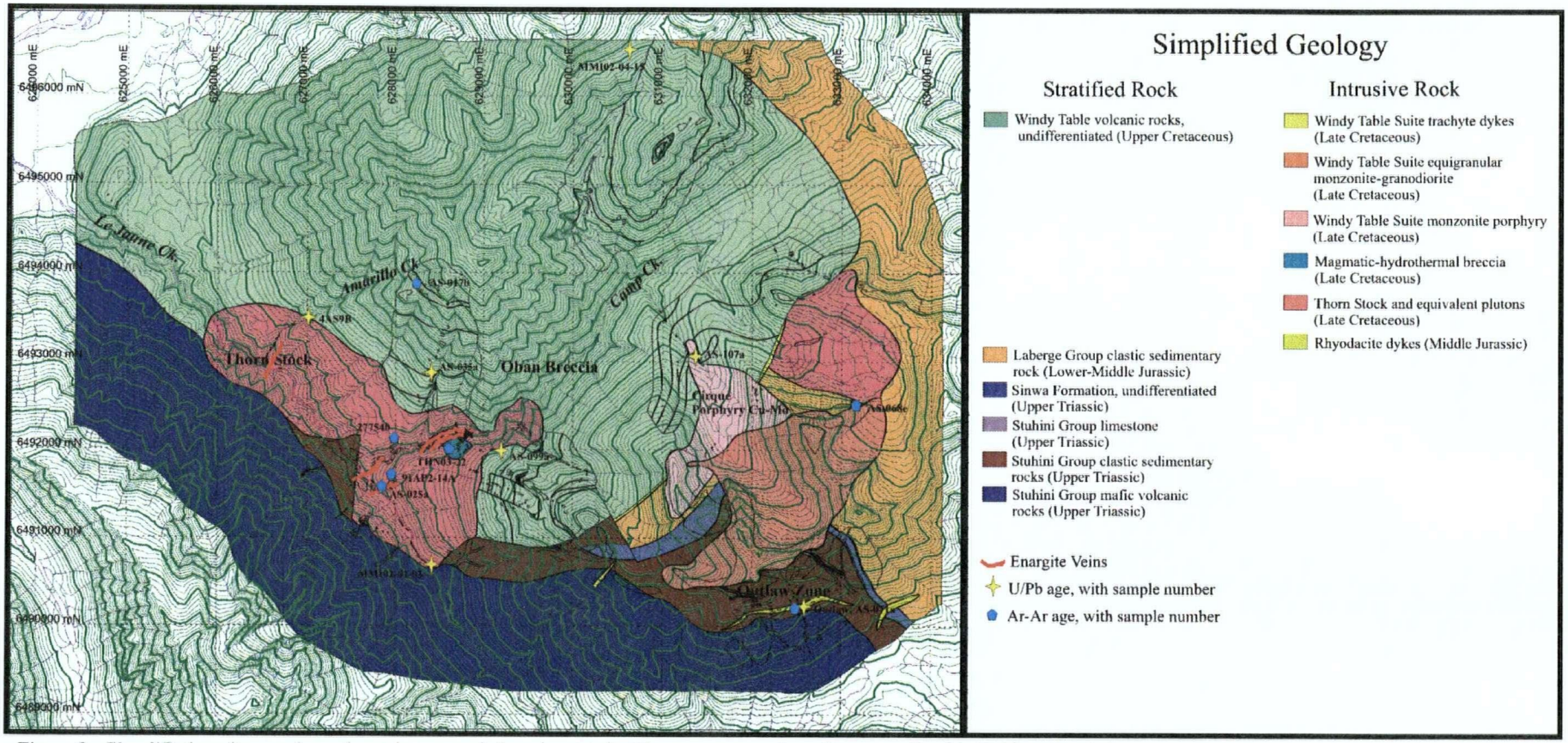

Figure 3. Simplified geology and geochronology sample locations at the Thorn property. Samples are outlined in Table 1 (see below). Map is modified from Baker, 2003.

separate the different sedimentary rock sequences due to poor lateral continuation.

The Sinwa Formation has two main rock types, 1) limestone and 2) overlying clastic sedimentary rocks. Dolomitization, skarnification and recrystalization of limestone is common. In the study area, a boulder conglomerate containing volcanic and intrusive rocks may be correlative to "Limestone Boulder Conglomerate (UTSl)" of Mihalynuk (1999), which separates Upper Triassic Stuhini Group strata from Pliensbachian argillites of the Laberge Group in the Kirtland and Moon Lake areas, north of the study area. Farther north in the Whitehorse area, sandstone and wacke are described as the clastic sedimentary rock associated with the boundary between Stuhini and Laberge Group strata (Wheeler, 1961, Hart and Radloff, 1990).

LABERGE GROUP

The Laberge Group extends from the Dease Lake area in the south to the Yukon in the north, well outside the NW B.C. volcanoplutonic belt on Figure 1. These strata are thought to be an overlap assemblage linking terranes by the Early Jurassic (Wheeler et al. 1991, Mihalynuk 1999).

The Laberge Group is the major of unit in the study area. Souther (1971) estimated the thickness of the Laberge Group to be 3100m, athough others estimated the thickness to be as much as 5000m (e.g. Bultman 1979). Typical rocks include boulder to cobble conglomerate (mafic volcanic clasts > intrusive clasts and intrusive clasts > mafic volcanic clasts), immature sandstones and siltstones, wackes, and argillites. Correlating individual suquences from Mt. Lester Jones to the Thorn Property area is difficult due to quick lateral facies changes and lack of marker horizons.

Cretaceous (81-85Ma) Volcanic and Sedimentary Rocks

Cretaceous subaerial volcanic and sedimentary rocks are rare but important strata throughout the study area. Plutonic equivalents of these strata are more common (see below). In the map area, these strata form three volcanic centers at Lisadele Lake, the Thorn Property and the Metla Property. Each are separated by some 10-20km. Together, these volcanic and plutonic rocks are part of a northwesterly trending magmatic belt with associated hydrothermal alteration and sulphide minerals.

Historically, these strata were mapped as Tertiary Sloko Group volcanic rocks (*ca.* 55Ma) by Souther (1971) in the Tulsequah map area. However, Mihalynuk (2003) reported a U/Pb age of 82.8±0.6Ma (MMI02-01-03, Table 1) from a rhyolite breccia on the Thorn Property (Figure 3), which suggests that the Sloko Group mapped by Souther (1971) includes significant late Cretaceous volcanic rocks. Subsequent mapping and U/Pb geochronology (Summarized in Table 1) has confirmed the ages and extended the belt of late Cretaceous volcanic rocks north and south of the Thorn Property. These rocks are considered correlative to the Windy Table Suite volcanic rocks described by Mihalynuk (1999) in the Tagish Lake area.

The best-preserved section of these strata is located at the Thorn Property. Here, approximately 1800m of subaerial volcanic and related sedimentary rocks are preserved. The Thorn volcanic sequence is characterized by flat-lying strata, except around the margins, where the contact between older strata and Late Cretaceous volcanic rocks is steeply faulted causing local rotation and tilting of volcanic stratigraphy. This faulted margin is continuous along the eastern contact and forms a curvilinear trace across the geologic map (Figure 3). In one location, the original stratigraphic contact between the volcanic rocks and older rocks is preserved (Figure 4). Here, the 93Ma quartz-feldspar-biotite porphyrytic diorite of the Thorn Stock (Mihalynuk, 2003) is overlain by boulder conglomerate composed of rounded clasts of porphyry diorite (see below). The section through the Late Cretaceous volcanic rocks and unit descriptions are outlined below.

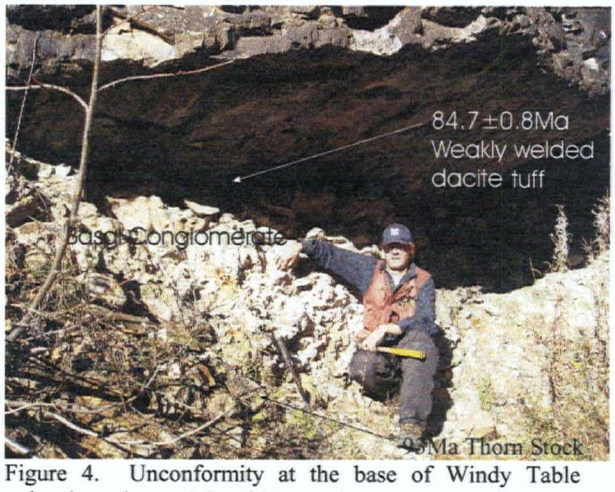

Figure 4. Unconformity at the base of Windy Table volcanic rocks: a 1-5m thick basal conglomerate separates 93Ma Thorn Stock (base of photo) from 85Ma subaerial volcanic rocks (top of photo). Note: Sample 4AS9B (Table 1) was collected from the weakly welded tuff above conglomerate in this photo.

THORN STRATIGRAPHIC SECTION THROUGH WINDY TABLE VOLCANIC ROCKS

Table 1. Preliminary U/Pb and $^{40}Ar/^{39}Ar$ geochronology of magmatic and mineralized rocks, preliminary results. * beside sample numbers indicate ages from Mihalynuk et al. (2003), all other samples from this study. All ages are given with errors at 2σ. 13 U/Pb samples and 8 $^{40}Ar/^{39}Ar$ samples still in progress.

Sample	Northing	Easting	Description	Interpreted Age (Ma)	Method (Mineral)
U/Pb					
Thorn Area					
AS-099a	6491930	629040	Rhyolite flow, fine grained, aphanitic	80.8+3.6/-4.9	U/Pb TIMS (Zircon)
AS-035a	6492888	628407	Trachyte flow, feldsparpheric, feldspar phenocrystic	81.1±1.5	U/Pb SHRIMP-RG (Zircon)
AS-107a	6493090	631320	Cirque monzonite, feldspar porphyritic	82.2±0.2	U/Pb TIMS (Zircon)
MMI02-04-15 *	6496260	630090	Sutlahine Rhyolite Breccia	82.8±0.6	U/Pb TIMS (Zircon)
4AS9B	6493530	627160	Weakly welded crystal tuff, feldsparpheric, <1% xenocrystic	84.7±0.8	U/Pb SHRIMP-RG (Zircon)
MMI02-01-03 *	6490890	628200	Thorn Stock; Bt-Hbld-Qtz-feldspar porphyritic diorite-qtz diorite	93.3±2.4	U/Pb TIMS (Zircon)
AS-071a	6490270	632543	Fine grained aphanitic rhyodacite dyke	168.1±0.7	U/Pb TIMS (Zircon)
Mt Lester Jones Area					
4AS11	6506538	612037	Bt-Hbld-feldspar porphyritic diorite	55.3±0.8	U/Pb SHRIMP-RG (Zircon)
MMI94-45-6 *	6510100	605100	Mt. Lester Jones Porphyry	83.8±0.2	U/Pb TIMS (Zircon)
MMI94-9-4 *	6513150	698800	Red Cap Porphyry	87.3±0.9	U/Pb TIMS (Zircon)
Ar-Ar (Cooling)					
Thorn Area					
AS-017b	6493800	628290	Trachyandesite sill, intruding Windy Table volcanic rocks	83.1±1.8	$^{40}Ar/^{39}Ar$ (Muscovite)
AS-068e	6492585	633215	Equigranular monzonite bearing biotite and hornblende	90.7±3.6	$^{40}Ar/^{39}Ar$ (Biotite)
Ar-Ar (Alteration)					
Thorn Area					
AS-025a	6491624	627740	In vein sericite from B-zone qtz-enargite-tetrahedrite-pyrite vein	79.3±1.4	$^{40}Ar/^{39}Ar$ Sericite
Outlaw	6490280	627650	Sericite adjacent to arsenopyrite from AS-071a	84.8±0.5	$^{40}Ar/^{39}Ar$ Biotite
THN03-22	6491914	628769	In vein sericite from Oban Breccia-Thorn Property	87.7±0.6	$^{40}Ar/^{39}Ar$ Sericite
277540	6491150	628070	Sericite from "unaltered" Thorn Stock	91.0±0.9	$^{40}Ar/^{39}Ar$ Sericite
91AP2-14A *	6491640	627650	f.g. sericite/illite from Thorn Stock	91.0±1.0	$^{40}Ar/^{39}Ar$ Sericite

Note: Abreviations used Sensitive High Resolution Ion Micro Probe Reverse Geometry (SHRIMP-RG), Thermal Ionization Mass Spectrometer (TIMS, Biotite (Bt), Horneblende (Hbld), Quartz (Qtz), fine-grained (f.g.)

The basal contact of the Windy Table Volcanic Rocks crops out for several tens of meters in Amarillo Creek at the Thorn Property (Fig. 4). Here, the basal contact is a monomictic clast-supported, cobble to boulder conglomerate. Clasts are typically rounded and composed of quartz-feldspar-biotite porphyrytic diorite to quartz diorite, likely of Thorn Stock affinity. The conglomerate matrix is made up of coarse to fine sand-sized detritus, chiefly composed of coarse sand-sized diorite, rounded quartz, and subrounded feldspar, which has been replaced by sericite.

Above the basal conglomerate is an 80m succession composed dominantly of dacitic to andesitic lapilli tuffs with lesser flows and volcaniclastic rocks. Individual beds do not extend for more than 10's meters along strike due to rapid lateral facies changes and lack of marker horizons. Tuffs are unwelded to weakly welded. In Amarillo Creek, a 15-80cm lithic poor, weakly welded dacitic crystal tuff directly overlies the basal conglomerate. This tuff has a U/Pb SHRIMP-RG zircon age of 84.7±0.8Ma (4AS9B, Table 1). This age marks the onset of Windy Table volcanism in the study area.

Stratigraphically above the tuff-dominated strata is a 120m section of volcaniclastic-dominated strata with lesser tuffs. Individual beds are poorly sorted, can be difficult to distinguish, and are laterally discontinuous. Typically, clasts are volcanic rocks with lesser sedimentary rocks and intrusive rocks. Clasts are subrounded to rounded, and range in size from boulder to fine sand.

A 360m-section dominated by dacitic lapilli tuff overlies the volcaniclatic rocks. This section is similar to the lowermost sequence of tuffs. Approximately 15m above the volcaniclastic sequence is a 5m thick feldspar phenocrystic trachyte flow which returned an U-Pb zircon age of 81.1±1.5Ma (AS-035a, Table 1).

Stratigraphically above the tuff and volcaniclastic dominated sequence is a 340m thick

section of flows, domes, and intrusive rocks. At the headwaters of Amarillo Creek is series of vertical dykes, which are inferred to be feeders to the extrusive lavas, as well as domes. Here, the domes and dykes are flow foliated Foliation is generally flat-lying, but is locally intensely folded (syn-magmatic) and steeply dipping in the feeder dykes. Overall, the lava-dominated section is characterized by fine-grained, dacitic feldspar phyric units at the base that upsection become coarser grained quartz-feldspar phenocrystic rhyolite flows. Minor tuffs and volcaniclatsic rocks are intercalated with the lavas. A ^{40}Ar-^{39}Ar age on coarse muscovite of 83.1±1.8Ma (AS-017b, Table1) was obtained from a trachyandesite sill intruding the strata about 215m up from the base of this sequance.

Poorly outcropping volcanic and volcaniclastic strata compose another 900m that extends to the current top of the volcanic sequence. Close to the top of the volcanic sequence, Mihalynuk (2003) reported an U-Pb (zircon) age of 82.8±0.6Ma (MMI02-04-15, Table 1) for a rhyolite breccia.

The available geochronology from the Windy Table Volcanic Rocks implies that some 1600 m of volcanic and volcaniclastic rocks may have been deposited within as much as 3 to 4 million years. However, it is also important to point out that the time range could be significantly less as the uncertainties on the ages overlap throughout the sequence suggesting that there could have been very rapid deposition of most of the volcanic sequence. Implicit in the thickness, similar aged volcanic facies is that the volcanic section at the Thorn is a remanent of a volcanic center.

Intrusive Rocks

Three main periods of plutonism have been recognized in the study area. The oldest is represented by minor 168Ma intrusive rocks. The major period for the purposes of this study is represented by 81-92 Ma late Cretaceous subvolcanic intrusive rocks. The youngest event consists of early Tertiary magmatism related to the Sloko volcanism. The younger period of plutonism is rare in the study are and has only been recorded at one location north of Lisadele Lake (Figure 1), but it is also reported near the Golden Bear Mine (Brown and Hamilton, 2000).

PRE-LATE CRETACEOUS INTRUSIVE ROCKS

A 168.1±0.7Ma (AS-071a, Table 1) intrusion has only been recognized in one location at the Thorn Property. This intrusion is a 3-5m wide, fine-grained, aphanitic rhyodacite dyke intrude into Stuhini Group sedimentary rocks at the Outlaw prospect (Figure 3). Previously, it has been informally suggested that these dykes may have been the source of the mineralizing fluids at the Outlaw, However hydrothermal biotite from the same rock (Outlaw, Table 1) yield minimum ages of 84.8±0.5Ma (includes 84.3% of the ^{39}Ar with an inverse isochron age of 85.4±1.3Ma and initial $^{40}Ar/^{36}Ar$ of 279±28).. This suggests that the dykes and their margins simply focused younger hydrothermal fluids.

Jurassic plutons are common in the Coast Batholith where they in part form the Fourth of July Plutonic Suite of Mihalynuk (1999). They are abt known within the study area. The 168.1±0.7Ma age of intrusive rock at the Outlaw is, furthermore, not a common age for Jurassic magmatism regionally. However, some cooling ages from Fourth of July Plutonic Suite are as young as 165Ma (M. Mihalynuk, 2004 pers. comm.), which suggests the potential for plutonic rocks of similar age lying to the west of the study area.

LATE-CRETACEOUS INTRUSIVE ROCKS

Late Cretaceous subvolcanic plutons are widespread throughout the study area (Figure 1). Known intrusive rocks of this age extend from as far north as Mt. Lester Jones to as far south as the Thorn Property. Rocks of similar composition and texture were mapped and collected for geochronology between the Golden Bear mine and the Thorn Property in an attempt to extent the volcanoplutonic belt. These southern rocks are as yet undated, and thus their precise relationship to the northern rocks is unknown.

The best understood portion of the belt is at the Thorn Property where two pulses of magmatic activity are evident. The older of the two is represented by the quartz-feldspar-biotite porphyrytic diorite and quartz diorite of the Thorn Stock. This stock is unconformably overlain by *ca.* 85 to 82Ma Windy Table volcanic rocks and intruded by similar-age Windy Table Plutonic suite rocks.

93Ma Intrusive Rocks

Plutonic rock of known 93-Ma age are regionally rare. Known examples of this are at the Thorn Property (Mihalynuk 2003), Jack Peak and Racine Lake (Mihalynuk 1999). During the 2004 field season several small Thorn Stock-like intusive rocks were mapped and sampled between Golden Bear mine and Tulsequah mine. However, assigning plutonic rocks to particular periods of magmatic activity is difficult as similar lithologies are known to intrude as part of the Tertiary Sloko magmatic epoch

(Mihalynuk 1999). In the study area, only one age has been reported in this time period. Mihalynuk (2003) reports a U/Pb zircon age of 93.3±2.4Ma for the Thorn Stock. The Thorn Stock the largest known example and covers a 3.5 by 1.5 km area.

The 93-Ma intrusions are best illustrated by the Thorn Stock. The stock is a quartz-feldspar-biotite porphyrytic diorite to quartz diotire. Marginal phases are fine-grained feldspar phyric and flow-banded. Hydrous phases are biotite and lesser horneblende. Common accessory minerals include magnetite and apatite. These rocks are pervasively chlorite- and sericite-altered altered.

Windy Table Suite

Windy Table plutonic rocks are the most common in the map area (Fig. 2). Three different compositional types of intrusions are mapped. The most common is a biotite-bearing, porphyrytic monzonite that contains conspicuous feldspar phenocrysts. These rocks have associated hydrothermal systems through the region. Examples include the 83.8±0.2Ma (MMI94-45-6, Table 1) Mount Lester Jones Porphyry (Mihalynuk 2003), the 87.3±0.9Ma (MMI94-9-4) Red Cap Porphyry (Mihalynuk 2003) and the 82.2±0.2Ma (AS-107a, Table 1) Cirque Monzonite (Simmons et al. 2003). A second type of intrusion is a biotite-hornblende-bearing, medium-grained, equigranular, monzonite to granodiorite. None of this compositional types have yet been dated, however, in the Cirque at the Thorn Property these intrusions intrudes the Cirque Monzonite, and are thus presumably of Late Cretaceous age. Other examples of this intrusive suite were mapped in the Bryar area and Lisadele Lake area (Figure 1).

The least prevalent intrusive suite are fine-grained, aphanitic trachytic dykes, which crop out on the Thorn Property. These rocks could represent subvolcanic equivalents or feeders to the trachytic flows in the Windy Table Volcanic Rocks.

55Ma POST-CRETACEOUS INTRUSIVE ROCKS

Souther (1971) mapped abundant early Tertiary Sloko plutonic rocks in the study. Between this study and Mihalynuk (2003), only one location is known where unequivocal Sloko plutonic rocks crop out. A feldspar-biotite porphyrytic diorite was mapped in the Lisadele Lake area, where it intrudes into Laberge Group clastic sedimentary rocks. This rock returned a U/Pb zircon age of 55.3±0.8Ma (4AS11, Table 1). The petrologic similarity of this rock and the Thorn Stock make it very difficult to unequivocally distinguish the two rock suites.

GEOCHEMICAL STUDIES-PRELIMINARY RESULTS

Geochemical studies of magmatic rocks along the belt have concentrated around the Thorn Property where the geochronologic framework permits placing the compositional groups into distinct time packages. The goals of this study are to geochemically characterize the different rocks units, place constraints on the paleotectonic environment and note any changes in chemistry as the magmatic arc evolved through time. Major, trace and rare earth element data are available from 23 representative samples of all intrusive rocks and Late Cretaceous subaerial volcanic rocks in the Thorn Property area. An additional 18 regional samples are in preparation or have not yet been analyzed. Preliminary interpretations are plotted in Figure 5. It is important to note that the rocks from the Thorn Property were sampled in close proximity to mineralized hydrothermal systems and thus have been altered to varying degrees, thus limiting the usefulness of the major elements to characterize geochemical composition or tectonic environment in which these rocks were emplaced.

Middle Jurassic intrusive rocks are distinct geochemically from the Cretaceous intrusive and extrusive rocks. In general, the Jurassic intrusions have within plate affinity and tend to be more mafic and alkaline than younger intrusions (Figure 5a,c-d). These intrusions are characterized by a relative enrichment in light rare earth (LREE) and heavy rare earth elements (HREE), a shallow rare earth pattern decreasing toward the HREE's and a sharp negative Eu anomaly (Figure 5e). Unfractionated HREE patterns such as those exhibited by Middle Jurassic intrusions suggest that there was no garnet or honrneblende in the residuum and likely represent a deep magma signature.

The 93Ma intrusive rocks are not obviously distinct chemically from other Late Cretaceous intrusive rocks. However, the 93Ma rocks tend to have lower SiO2 contents than other intrusive rocks. They also have a slight tholeiitic affinity compared to other intrusive rocks (Figure 5). The REE pattern exhibits unfractionated HREE and a minor negative Eu anomaly (Figure 5). The HREE pattern can be explained by either increased pressure at the melt generation site, leaving garnet as the stable phase in the residuum (e.g. Kay & Abruzzi 1996; Bissig et al. 2003) or by an increased amount of water in the magma leading to hornblende fractionation and HREE depleted melts (e.g. Haschke et al. 2001; Bissig et al. 2003). The small Eu depletion can be explained by oxidized conditions in the magma or a plagioclase-free residuum.

Windy Table suite intrusive rocks exhibit much the same chemistry as 93Ma intrusive rocks, with

only minor chemical differences. For example, Windy Table intrusive rocks tend to have a broader compositional range from andesite to trachyte whereas the 93Ma intrusive rocks are mainly dacite to andesite. The Windy Table intrusive rocks also have a slightly more calc-alkaline affinity. Most samples exhibit unfractionated HREE and a minor negative Eu anomaly, similar to 93Ma intrusions. Two samples display an overall depletion of REE and an increased negative Eu anomaly. These samples are Windy Table suite trachyte dykes, which tend to be more altered (sericite-silica-pyrite); this can explain the abnormal chemistry.

Windy Table suite volcanic rocks have wide array of compositions ranging from trachyte to andesite. On the Rb vs. Y+Nb plot, three sample have a within plate affinity. These samples are lithic-bearing pyroclastic rocks, which may reflect the chemistry of lithic fragments from older strata, and intrusive rocks. In general, the REE signature is similar to that of their intrusive equivalents, with the exception of a slightly wider spread in HREE. The wider spread and abnormal samples can be explained by the lithic fragment chemistry.

Magmatic rocks that fall within the Late Cretaceous time constraint generally have similar compositions. These similarities make it difficult to distinguish fundamental chemical characteristics between the ~93Ma and ~83Ma pulses of magmatism. More work is required on determining differences in REE and immobile element ratios between these rocks.

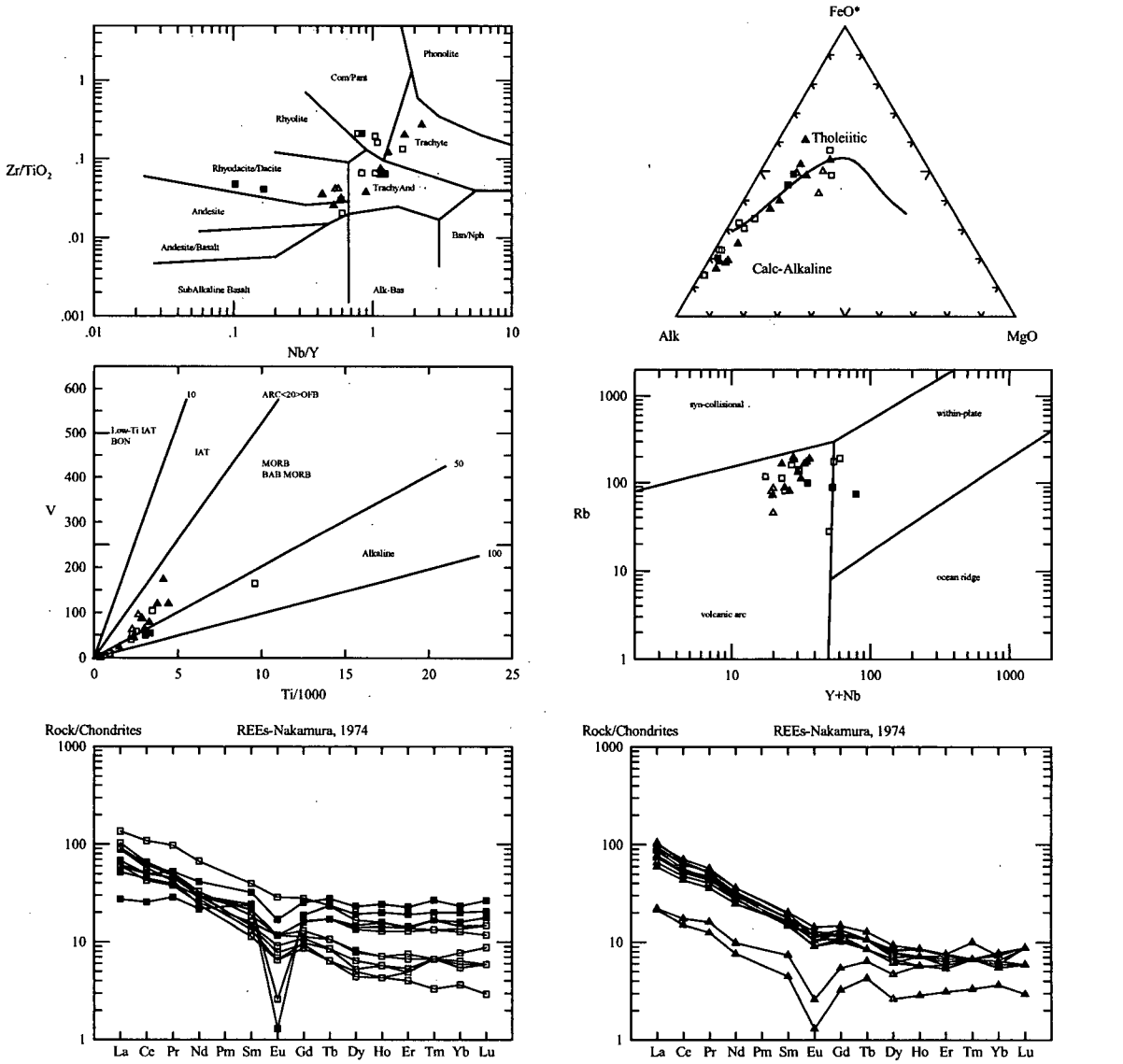

Figure 5. Geochemical discriminant and chondrite-normalized REE abundance diagrams for volcanic and subvolcanic intrusive rocks from the Thorn Property and surrounding area. Closed squares represent Jurassic intrusive rocks, open squares represent Windy Table suite felsic tuffaceous and flow rocks, closed triangles represent Windy Table suite sub-volcanic intrusive rocks and open triangles represent *ca.* 93 Ma Thorn Stock and Thorn Stock-like diorite-quartz diorite intrusions.

CHARACTERISTICS OF MAGMATIC-HYDROTHERMAL ALTERATION SPATIALLY AND TEMPORALLY ASSOCIATED WITH LATE CRETACEOUS MAGMATIC ROCKS

Magmatic-related hydrothermal alteration and sulfide-bearing rocks are common throughout the study area. Six styles of mineralization are associated with the Late Cretaceous volcano-plutonic belt: 1) Quartz-pyrite-enargite-tetrahedrite veins formed in the transition zone between deeper porphyry environment and the shallower epithermal environment; 2) Breccia-hosted Ag-Pb-Zn-(Au-Cu)-bearing sulfides, 3) Porphyry Cu-Mo, 4) Quartz-arsenopyrite±sphalerite-galena veins and disseminations, 5) Skarn and Carbonate replacement and, 6) Sedimentary rock-hosted or Carlin-like mineralization.

Quartz-pyrite-enargite veins are known only at the Thorn Property. There, the veins are hosted in syn-mineralizing normal faults (Lewis, 2002) within the 93Ma Thorn stock. The veins are not found outside of the Thorn Stock. Ore mineralogy includes pyrite, enargite, tetrahedrite/tennantite, with lesser sphalerite, galena, cassiterite and rare native gold and argentite. Veins are typically enveloped by a narrow 50cm-3m zone of pyrophyllite-sericite alteration in a wider zone (5-100m) of intense sericite-clay-pyrite alteration. These zones are flanked by weak clay-sericite-chlorite alteration grading out into chlorite with lesser sericite altered country rock. Pyrophyllite alteration suggest that the mineralizing system is hot and probably within the leached-cap of a porphyry Cu to epithermal system.

The retriction of the veins to the Thorn Stock suggests a genetic link between the veins and the host rocks. Support for this conclusion was provided by Mihalynuk (2003) who reported a $^{40}Ar/^{39}Ar$ age on sericite from intensely altered Thorn Stock of 91.0±1.0Ma. However, attempts to confirm this age have resulted in conflicting data. As part of this study, a $^{40}Ar/^{39}Ar$ age on sericite enclosed in enargite from a different location on the Thorn Property resulted in a minimum age of 79.3±1.4Ma (includes 84.4% of the ^{39}Ar with an inverse isochron age of 79.7±2.3Ma and initial $^{40}Ar/^{36}Ar$ of 292±15). It is unclear at this time what the age discrepancy means.

Breccia-hosted Ag-Pb-Zn-(Au-Cu) mineralization occurs at the Metla and Thorn properties, and presumably at other unknoun locations as several unmineralized breccia pipes were mapped during the 2004 field season in the Lisadele Lake area. The breccia-hosted prospects are characterized by clast-supported, rounded pebble-boulder breccia, where the ore minerals have replaced a fine-grained rock(?) matrix (Figure 6). Ore mineralogy includes pyrite, sphalerite and boulangerite with lesser chalcopyrite. At the Thorn property, sulphosalt is a more dominant phase, whereas at the Metla there are only trace amount of sulphosalt and chalcopyrite. At the Thorn, dickite(?) occurs are narrow massive zones replacing the matrix of the breccia, this narrow dickite-dominated alteration is flanked by moderately sericite-clay-pyrite alteration grading to sericite-chlorite alteration. Sericite from the mineralized matrix, enclosed in pyrite-sphalerite-boulangerite mineralization from the Thorn Property yields an age of 87.7±0.6Ma (includes 81.8% of the ^{39}Ar with an inverse isochron age of 87.6.7±4.3Ma and initial $^{40}Ar/^{36}Ar$ of 297±70), suggesting that it may associated with a hydrothermal system produced by the 93Ma suite of intrusions.

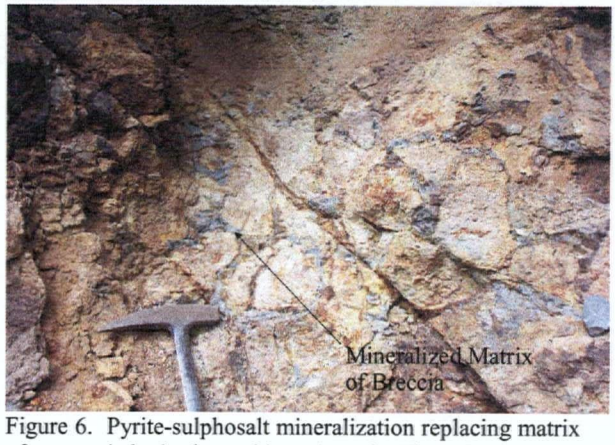

Figure 6. Pyrite-sulphosalt mineralization replacing matrix of magmatic hydrothermal breccia at the Thorn Property.

Porphyry Cu-Mo deposits are the most widespread magmatic-hydrothermal mineralizing type in the study area. Feldspar porphyrytic monzonite is the most common host rock for porphyry Cu-Mo mineralization in the belt. Mineralization is characterized by thin (1mm-8cm) structurally controlled vein sets. Ore mineralization occurs as both disseminations in the host rock and in the vein sets. Vein mineralogy includes quartz-pyrite-chalcopyrite-molybdenite with lesser feldspar and rare sulphosalt. Where veining is most intense biotite-clay alteration dominates and is flanked by a broader zone of chlorite alteration. U/Pb geochronology (zircon) at the Thorn Property on the Cirque monzonite gives an age maximum for porphyry Cu-Mo mineralization of 82.2±0.2Ma.

Like the porphyry Cu-Mo mineralization, quartz-arsenopyrite veins and disseminations are also widespread. These veins were encountered from the Outlaw showing to the Red Cap showing, west of Mt. Lester Jones. At the Red Cap, thin, massive vein swarms are hosted in shears along the contact between porphyrytic dykes and altered Stuhini Group volcanic and sedimentary rocks. Typical vein

mineralogy includes pyrite, arsenopyrite, galena, and sphalerite with lesser chalcopyrite and molybdenite in a quartz-carbonate matrix. During the 2004 field season previously unknown zones with this style of mineralization were mapped in the Jak, South King Salmon Lake and Bryar areas. Alteration is characterized by narrow zones (10's of meters) of pervasive silica-sericite-clay (±biotite) alteration grading outwards into chlorite clay alteration. At the Outlaw showing on the Thorn Property, hydrothermal biotite adjacent to arsenopyrite was dated at 84.8±0.5Ma (includes 84.3% of the ^{39}Ar with an inverse isochron age of 85.4±1.3Ma and initial $^{40}Ar/^{36}Ar$ of 279±28).

Skarn and carbonate replacement mineralization is common throughout the study area; however, limestone beds in the region are only thin (maximum of approximately 10m) limiting the potential for skarn deposits. Examples can be found at the Bungee showing on the Thorn property, in the Bryar area and South King Salmon Lake area. 2-8m wide discontinuous lenses of massive and semi-massive pyrhhotite-sphalerite with lesser galena and rare chalcopyrite characterize these deposits. Typical skarn calc-silicate minerals including diopside and garnet increase in abundance towards the mineralized zone. The lack of precious metals makes these less attractive exploration targets.

Carlin-like mineralization is rare in the area. However, Oliver (1996) suggests that Golden Bear mineralization is similar to that at the Carlin trend (see also Brown and Hamilton, 2000). There are no plutons in the immediate area of Golden Bear mine, however, a $^{40}Ar/^{39}Ar$ age was produced from hydrothermal sericite of 83.9±1.2Ma (Oliver, 1996) suggesting that the mineralizing fluids at Golden Bear may be derived from rocks of the Late Cretaceous volcanoplutonic belt.

DISCUSSION AND PRELIMINARY CONCLUSIONS

Although still in its infancy, preliminary results from this project give new insights into the nature, timing and distribution of magmatic rocks in the area south of the Taku river, northern Stikinia and their timing relationship to known magmatic-hydrothermal mineralization in the region. Mapping in the 2004 field season extended the late Cretaceous volcano-plutonic belt identified by Mihalynuk (2003) and Simmons (2003) north and south of its previously known limits. Furthermore, the late Cretaceous belt may be divided into two distinct pulses of magmatic activity: an 87-94 Ma pulse of largely diorite porphyries and an 80-85 Ma pulse of sub-aerial volcanic rocks and co-magmatic subvolcanic intrusive rocks. It is not well understood which of these pulses of magmatism have more prospective hydrothermal systems associated with them. However, preliminary ages, as part of this study, from known magmatic-hydrothermal alteration along the belt suggests that the late Cretaceous subvolcanic intrusions have associated hydrothermal systems spanning at least 79 Ma to 91 Ma.

An important step in exploring for magmatic-hydrothermal deposits is to understand the timing and spatial relationships between hyrdothermally altered rocks and the magmatic host and source rocks. At the Thorn property, $^{40}Ar/^{39}Ar$ ages on sericite from enargite veins suggest that hydrothermal alteration associated with these veins may be linked to younger Windy Table (81-85Ma) magmatism. However, Mihalynuk (2003) suggests that sericite alteration associated with enargite veins is 91 Ma and may be associated with the older magmatic pulse. The discrepancy in ages is not understood at this time. Also at the Thorn property, sericite from breccia-hosted Ag-Pb-Zn-(Au-Cu) mineralization suggest that hydrothermal alteration may be linked to the 87-94 Ma magmatic pulse. At the Cirque showing on the Thorn property the timing of porphyry Cu-Mo mineralization is constrained to a minimum by the host *ca.* 82 Ma monzonite. A Pb isotope study is underway to help determine which magmatic pulse is most likely to be the source of fluids for mineralized veins.

Enargite veins have been a recent focus for exploration along the belt. Pyrophyllite alteration related to enargite veins at the Thorn property suggest that these veins formed in a hot and deep(?) environment, possibly at the porphyry-epithermal transitional depth beneath the leached cap. Fluid inclusion work is currently underway to constrain depth and temperature of ore mineral deposition in these veins. Here the veins are exposed only along syn-mineralizing normal faults in the porphyry diorite Thorn stock and are not known to crop out in younger strata or intrusive rocks. Historically late Cretaceous volcanic strata in the study area have been sporadically explored. Age dates at the Thorn property suggest that Windy Table volcanic rocks overlap in time with alteration associated with Au-Ag-Cu bearing enargite veins, leaving the possibility that the volcanic strata may host epithermal deposits topographically above the porphyry-epithermal transitional depths. Mapping during the 2004 field season identified similar volcanic stratigraphy north of the Thorn property indicating that more chronologically favourable strata may be found along the late Cretaceous volcano-plutonic belt.

ACKNOWLEDGMENTS

Norm Graham of Discovery Helicopters provided excellent and timely helicopter service during the summer, without whoms help, this project would not have progressed as planned. Tom Bond of Lake Else Air also provided excellent helicopter service. We thank Helen Smith for making life operate as normal while in the field. Jim Mortensen for valuable input geochronology and tectonics of magmatic rocks in the Cordillera. Mitch Mihalynuk has provided valuable information about the stratigraphy and geology of the northern Stikine Terrane, discussions about the timing of magmatic activity and hydrothermal alteration have been extremely valuable. Rimfire Minerals Corp. and Equity Engineering Ltd. provided logistical support for much of this project. Dave Tupper of Solomon Resources Ltd. for allowing sampling on the Metla Property. We also thank Shane Ebert who provided excellent insights about porphyry-epithermal mineralization and alteration in the field. Gayle McCreery, Brett McKay and Tim Sullivan provided outstanding company in the field.

REFERENCES

Arribas Jr., A., Hedenquist, J.W., Itaya, T., Okada, T., Concepción, R.A. and Garcia Jr., J.S. (1995): Contemporaneous Formation of Adjacent Porphyry and Epithermal Cu-Au Deposits over 300 ka in Northern Luzon, Philippines; *Geology,* Volume 23, Number 24, pages 337-340.

Awmack, H.J. (2003): 2002 Geological, Geochemical and Diamond Drilling Report on the Thorn Property; *British Columbia Ministry of Energy and Mines,* Assessment Report #27,120.

Baker, D.E.L. (2003): 2003 Geological, Geochemical and Diamond Drilling Report on the Thorn Property; *British Columbia Ministry of Energy and Mines,* Assessment Report #27,120.

Barker, F., Arth, J.G. and Stern, T. W. (1986): Evolution of the Coast batholith along the Skagway traverse, Alaska and British Columbia; *American Mineralogist,* Volume 71, pages 632-643.

Bissig, T., Clark, A.H., Lee, J.K.W. and von Quadt, A. (2003): Petrogenetic and Metallogenic Responses to Miocene Slab Flattening: New Constraints from El Indio-Pascua Au-Ag-Cu belt, Chile/Argentina; *Mineralium Deposita,* Volume 38, pages 844-862.

Brew, D.A. and Morrell, R.P. (1983): Intrusive rocks and Plutonic Belts of southeastern Alaska; *Geological Society of America,* Memoir 159, pages 171-193.

Bultman, T.R. (1979): Geology and tectonic history of the Whitehorse Trough west of Atlin; unpublished Ph.D. thesis, *Yale University,* 284 pages.

Brown, D. and Hamilton, A., 2000, The golded Bear mine: Carlin-type sediment-hosted, dissememinated gold deposit in northwestern British Columbia, *in* Cluer, J.K., Price, J.G., Struhsacker, E.M., Hardyman, R.F., and Morris, C.L., eds., Geology and Ore Deposits 2000: The Great Basin and Beyond: Geological Society of Nevada Symposium Proceeds, May 15-18, 2000, p. 1002-1020.

Hart, C.J.R., Pelletier, K.S., Hunt, J. and Fingland, M. (1989): Geological map of Carcross (105D/2) and part of Robinson (105D/7) map areas; *Indian and Northern Affairs Canada,* Open File Map 1989-1.

Hart, C.J.R. and Radloff, J.K. (1990): Geology of the Whitehorse, Alligator Lake, Fenwick Creek, Carcross and part of the Robinson map areas (105D/11, 6, 3, 2 & 7), Yukon Territory; *Indian and Northern Affiars Canada,* Open File 1990-4, 113 pages and 4 map sheets.

Haschke, M., Günther, A. , Siebel, W., Scheuber, E. and Reutter, K-J. (2001): Magma Source Variations of late Cretaceous-late Eocene magmatic rocks of the Chilean Precordillera (21.5-26°S): due to vaiable water fugasity or crustal thickening? poster on http://sfb267.goeinf.fu-berlin.de/web/de/poster/posterb.asp

Kay, S.M. and Abbruzzi, J.M. (1996): Magmatic Evidence for for Neogene Lithoshperic Evolution of the Central Andean "flat slab" between 30 and 32°S. *Tectonophysics,* Volume 259, pages 15-28.

Kay, S.M. and Mpodozis, C. (2001): Central Andean Ore Deposits linked to Evolving Shallow Subduction Systems and Thickening Crust; GSA Today, Volume 11 (3), pages 4-9.

Kay, S.M., Mpodozis, C., Ramos, V.A. and Munizaga, F. (1991): Magma Source Variations for mid-late Tertiary Magmatic Rocks associated with a shallowing subduction zone and thickening crust in the central Andes (28-33°S). In: Harmon R.S., Rapela, C. (eds) Andean Magmatism and its tectonic setting; *Geological Society of America Special Paper 265,* Littleton, Colorado, pages 113-137.

Kerr, F.A. (1948): Taku River map area, British Columbia; *Geological Survey of Canada,* Memoir 248.

Lewis, P. (2002): Structural Analysis of Au-Ag-Cu Mineralization in the Camp Creek area, Thorn Property; *Private report for Rimfire Minerals Corporation and First Au Strategies Corp.,* dated July 15, 2002. *In* H.J. Awmack (2003): 2002 Geological, Geochemical and Diamond Drilling Report on the Thorn Property.

Mihalynuk, M.G., Meldrum, D., Sears, W.A. and Johannson, G.G. (1995a): Geology of the Stuhini Creek Area (104K/11); *in* Geological Fieldwork 1994, Grant, B. and Newell, J.M., Editors, *B.C. Ministry of Energy Mines and Petroleum Resources,* Paper 1995-1, pages 321-342.

Mihalynuk, M.G., Meldrum, D., Sears, W.A. and Johannson, G.G., Madu, B.E., Vance, S., Tipper, H.W. and Monger, J.W.H. (1995b): Geology and Lithogeochemistry of the Stuhini Creek Area (104K/11), *B.C. Ministry of Energy Mines and Petroleum Resources,* Open File 1995-5.

Mihalynuk, M.G. (1999): Geology and Mineral Resources of the Tagish Lake Area, B.C.; *Ministry of Energy and Mines*, Bulletin 105.

Mihalynuk, M.G., J. Mortensen, R. Friedman, A. Panteleyev and H.J. Awmack (2003): Cangold

partnership: regional geologic setting and geochronology of high sulphidation mineralization at the Thorn property. British Columbia; *Ministry of Energy and Mines,* Geofile 2003-10.

Oliver, J. L. (1996): Geology of Stikine Assemblage Rocks in the Bearskin (Muddy) and Tatsamenie Lake District, 104K/1 and 104K/8, Northwestern British Columbia, Canada and Characteristics of Gold Mineralization, Golden Bear Mine: Northwestern British Columbia: *Queen's University*, Unpublished Ph.D. thesis, 242 pages.

Panteleyev, A. (1996): Epithermal Au-Ag: Low Sulphidation in *Select Mineral Deposit Profiles, Volume 2-Metallic Deposits,* Lefebure, D.V. and Höy, T. (eds), British Columbia Ministry of Employment and Investment, Open File 1996-13, Pages 41-44.

Sawkins, F.J., 1990, Metal deposits in relation to plate tectonics, 2nd edn.: Berlin, Springer-Verlag, 461 p.

Sillitoe, R.H., 1972, Relation of metal provinces in western Americas to subduction of oceanic lithosphere: Geological Society of America Bulletin, v. 83, p. 813–818.

Sillitoe, R.H. (1976): Andean Mineralization: A Model for the Metallogeny of Convergent Margins; *Geological Association of Canada, Special Paper no. 14,* Toronto, pages 59-100.

Simmons, A., Tosdal, R., Baker, D. and Baknes, M. (2003): Geologic Framework of the Thorn Epithermal Deposit, Northwestern, B.C.; Poster Abstract for the Mineral Exploration Roundup, *British Columbia & Yukon Chamber of Mines.*

Sillitoe, R.H., 1988, Epochs of intrusion-related copper mineralization in the Andes: Journal of South American Earth Sciences, v. 1, p. 89–108.

Souther, J.G. (1971): Geology and Mineral Deposits of the Tulsequah map-area, British Columbia; *Geological Survey of Canada,* Memoir 362, 84 pages.

Sutherland Brown, A., ed., 1976, Porphyry deposits of the Canadian Cordillera: Canadian Institute of Mining and Metallurgy, Special Volume 15, 510 p.

Titley, S.R., ed., 1982, Advances in geology of the porphyry copper deposits, southwestern North America: Tucson, University of Arizona Press, 560 p.

Wheeler, J.O. (1961): Whitehorse map-area, Yukon Territory, (105D); *Geological Survey of Canada,* Memoir 312, 156 pages.

Wheeler, J.O., Brookfield, A.J., Gabrielse, H., Monger, J.W.H., Tipper, H.W. and Woodsworth, G.J. (1991): Terrane map of the Canadian Cordillera; *Geological Survey of Canada,* Map 1713A, scale 1:2 000 000.